APROXIMACIONES ÓMICAS Y GENÓMICA FUNCIONAL PARA LA VALIDACIÓN DE BLANCOS MOLECULARES DE POTENCIALES AGENTES ANTICHAGÁSICOS

Mag. María Florencia Mosquillo Aranda

Directora:

Dra. Leticia Pérez Díaz

Tesis de Doctorado en Ciencias Biológicas

PEDECIBA Biología

Sección Genómica Funcional

Facultad de Ciencias, Universidad de la República

Diciembre 2022

Tabla de contenidos

1 Resumen

El protozoario patógeno *Trypanosoma cruzi* es el agente etiológico de la enfermedad de Chagas, la cual afecta a las poblaciones más vulnerables de América Latina. Esta enfermedad está clasificada por la Organización Mundial de la Salud como una de las 20 enfermedades tropicales desatendidas a nivel mundial, caracterizada por la falta de vacunas y una farmacoterapia adecuada, así como por una baja inversión histórica por parte de la industria farmacéutica. A más de 100 años del descubrimiento de esta enfermedad, los fármacos empleados en la actualidad presentan limitaciones, contraindicaciones y efectos secundarios que disminuyen la efectividad y la continuidad del tratamiento, por lo que existe una necesidad urgente de desarrollar nuevos medicamentos. Los complejos basados en metales han demostrado ser un enfoque prometedor contra las enfermedades parasitarias y este estudio tiene como objetivo lograr avances en la búsqueda de compuestos eficaces. En el presente trabajo se caracterizan tres nuevos compuestos basados en metales con actividad tripanocida, nombrados $V^{IV}O$(5Brsal)(aminofén), Pd-dppf-mpo y Pt-dppf-mpo. Con el fin de dilucidar los mecanismos por los que actúan, se aplicaron herramientas ómicas para determinar los efectos a nivel metalómico, transcriptómico y proteómico. La combinación de la información ómica permitió generar modelos de acción y seleccionar varios candidatos a blancos moleculares. Una de las vías estudiadas como posible blanco de acción es la de la síntesis del ergosterol, cuyo producto final al tratar los parásitos con los compuestos de paladio y platino, disminuye de forma significativa con respecto a parásitos sin tratar, demostrando que la vía se encuentra efectivamente afectada. Para validar algunos candidatos a blancos moleculares identificados en la vía, se trabajó en una estrategia de ganancia de función, mediante la generación de parásitos sobreexpresantes. Particularmente, se sobreexpresaron las enzimas fosfomevalonato quinasa (PMK) y lanosterol 14-α demetilasa (CYP51), porque cumplían con criterios de elegibilidad como ser enzimas esenciales para la sobrevida del parásito, expresarse a lo largo de todo el ciclo de vida del mismo, no estar presentes o ser muy diferentes a su ortólogo mamífero o ser altamente drogables. De esta manera, se validó que estos prometedores compuestos actúan particularmente sobre la enzima CYP51 disminuyendo los niveles del producto final de la vía del ergosterol y se continúa trabajando en la validación de más blancos moleculares.

La financiación necesaria para la realización de este posgrado, se obtuvo de los siguientes programas y proyectos:

- Programa de Desarrollo de las Ciencias Básicas (PEDECIBA) Área Biología.
- Programa de Iniciación a la Investigación de la Comisión Sectorial de Investigación Científica (CSIC).
- Proyecto Fondo María Viñas de la Agencia Nacional de Investigación e Innovación (ANII).
- Beca de Apoyo a Docentes para estudios de posgrado en la UdelaR de la Comisión Académica de Posgrados (CAP).
- Beca de apoyo para la Finalización de Estudios de Posgrados en la UdelaR de CAP.

2 Introducción y antecedentes

2.1 *Trypanosoma cruzi*

2.1.1 Generalidades

El protozoario ***Trypanosoma cruzi*** es el agente etiológico de la Enfermedad de Chagas. Es un organismo unicelular flagelado, perteneciente a la Clase *Zoomastigophora*, Órden *Kinetoplastidiae*, Familia *Trypanosomatidae*, Género *Trypanosoma*, Subgénero *Schizotrypanum*a. Las cepas de *T. cruzi* son heterogéneas en la mayoría de las características biológicas tanto en modelos experimentales *in vitro* como *in vivo*: cada cepa muestra propiedades distintas en términos de infectividad, tropismo tisular, actividad metabólica, expresión enzimática y niveles variables de susceptibilidad a fármacos *in vitro* y resistencia natural (Bermudez, 2016). Se ha sugerido que la diversidad genética del parásito puede influir en la evolución de la infección, la presentación clínica y el resultado del tratamiento durante la enfermedad (Zingales, 2014). Sin embargo, una revisión sistemática no logró encontrar asociaciones estadísticamente significativas entre el genotipo de *T. cruzi* y el resultado clínico crónico, riesgo de transmisión vertical, reactivación y brotes de transmisión oral (Messenger, 2015).

Dentro de la especie *T. cruzi,* según el genotipado se reconocen actualmente siete linajes genéticos distintos o **unidades de tipificación discretas** (*Discrete Typing Units* o DTU), denominados formalmente TcI a TcVI y TcBat (Vela, 2021). Las DTUs difieren ampliamente en su distribución geográfica y nicho ecológico (Breniere, 2016). En una breve descripción, TcI presenta alta diversidad genética, tiene la distribución geográfica más amplia y predomina tanto en el ciclo selvático como en el doméstico. TcII tiene baja diversidad genética, se relaciona mayoritariamente con ciclos domésticos en las regiones al sur de la Amazonía, y es extremadamente raro en el norte y América Central. TcIII y TcIV rara vez se muestrean y se asocian principalmente con ciclos de transmisión selvática. TcV y TcVI, las DTU más recientes resultantes de la hibridación entre cepas de los tipos TcII y TcIII o TcIV, están claramente asociadas con ciclos de transmisión doméstica. En Perú, Bolivia y el norte de Chile, TcV es la DTU más común, mientras que en Argentina y Paraguay se pueden encontrar tanto TcV como TcVI (Breniere, 2016). TcBat, compuesto por cepas aisladas inicialmente de murciélagos, se identificó como un DTU independiente (Lima, 2015), que se encuentra más relacionado con TcI que con otras DTU, y en el año 2014 fue registrada la primera infección humana con TcBat en una niña de 5 años en el noroeste de Colombia (Ramirez, 2014).

Estructuralmente, este protozoario exhibe ciertas características particulares, las cuales se esquematizan en la Figura 1. Una característica peculiar es la presencia de una sola **mitocondria** que se extiende a lo largo de todo el cuerpo celular. El genoma mitocondrial se

encuentra compactado en una zona especializada, denominada **kinetoplasto**, el cual puede llegar a representar hasta el 25% del ADN total del parásito. Presenta dos tipos de ADN circular concatenados entre sí, los maxicírculos y los minicírculos. Los maxicírculos son equivalentes al genoma mitocondrial de otros eucariotas, mientras que los minicírculos son mucho más cortos (rara vez superan los 2 kb) y codifican los ARN guía (ARNg) necesarios para modificar la mayoría de los transcritos provenientes de maxicírculos, en un proceso conocido como edición o *editing* (Aphasizhev, 2014; Read, 2016). Durante el *editing*, se producen inserciones y eliminaciones de residuos de uridina en sitios específicos en los ARN diana después de la transcripción para obtener transcritos maduros (Simpson, 2003). Los maxicírculos presentan regiones repetitivas, por lo que su tamaño ha sido subestimado con secuenciaciones de lecturas cortas (estimados en hasta 28 kb). Recientemente, usando secuenciación de lecturas largas (*long-read sequencing*), estas regiones repetitivas pudieron analizarse correctamente, encontrando que las longitudes reales oscilan entre 35 y 50 kb (Berna, 2021). Las regiones codificantes de los maxicírculos conservan el orden de los genes entre los tripanosomátidos, e incluyen genes que codifican miembros de la cadena respiratoria, como la NADH deshidrogenasa (subunidades 1–5, 7–9), citocromo c oxidasa (subunidades I-III), citocromo b y ATPasa, y los marcos de lectura abiertos de función desconocida *murf* y *cr* (Berna, 2021).

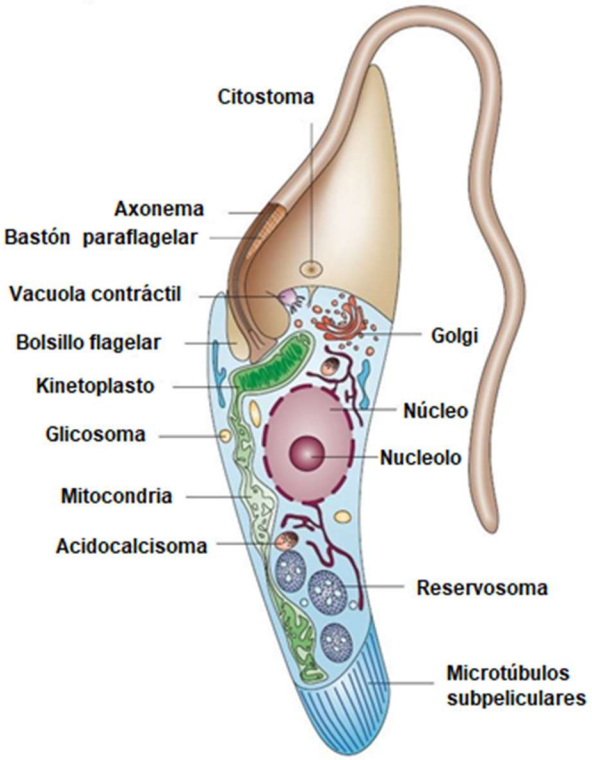

Figura 1. Representación esquemática de *T. cruzi*. Se señalan las principales estructuras en un corte longitudinal de un epimastigota. Extraído y modificado de (Docampo, 2005).

En estos parásitos, el **núcleo** presenta una organización estructural semejante al de las células eucariotas típicas. Tiene un tamaño cercano a los 2,5 µm de diámetro y contiene un nucleolo centralizado (Schenkman, 2011). Presenta una membrana nuclear típica provista de poros y la cromatina condensada dispersa a lo largo del nucleoplasma (Elias, 2001). Los cromosomas son difíciles de distinguir ya que durante el ciclo celular la cromatina no se condensa (Schenkman, 2011).

Poseen un **flagelo** que presenta una estructura típica de nueve pares de dobletes de microtúbulos periféricos y un par central (Portman, 2010). Emerge de una invaginación llamada bolsillo flagelar y es responsable de la movilidad durante ciertos estadios de su ciclo de vida. Una de las peculiaridades de los kinetoplastideos, compartida con *Euglenida*, es la presencia de una estructura adicional, el bastón paraflagelar (*paraflagellar rod* o PFR), un complejo trilaminar unido a los microtúbulos axonemales del flagelo (Lander, 2015). Una proteína peculiar de los tripanosomas es una glicoproteína inmunodominante, localizada en la unión entre el flagelo y el cuerpo celular que se denomina GP72 en *T. cruzi* o FLA1 en *T. brucei,* y es esencial para la fijación flagelar en ambos casos (LaCount, 2002).

Una característica distintiva de los tripanosomátidos es la compartimentación de la glicólisis en organelos especializados denominados **glicosomas** (Hannaert, 2003; Moyersoen, 2004)**.** Los glicosomas tienen un importante rol en la adaptación metabólica del parásito a los diferentes entornos a los que se expone durante su ciclo de vida. La glicólisis se organiza de tal forma que las siete enzimas que convierten la glucosa en 3-fosfoglicerato están dentro del glicosoma, mientras que las últimas tres se ubican en el citosol (Michels, 2000).

Otros organelos particulares, descritos por primera vez en tripanosomátidos, y caracterizados en más detalle en esta familia, son los **acidocalcisomas**. Estos organelos cumplen funciones de almacenamiento de calcio, magnesio, sodio, potasio, zinc, hierro, pirofosfato inorgánico, así como en la homeostasis del pH y la osmorregulación (Docampo, 2005), participando en estrecha asociación con la **vacuola contráctil**. La vacuola contráctil es una estructura formada por varios túbulos conectados a una vacuola central localizada cerca del bolsillo flagelar. Estudios de estrés osmótico en *T. cruzi* demostraron que contribuye a la regulación del volumen celular bajo estrés hiposmótico (Rohloff, 2008), y también ha sido demostrado que alberga un transportador de poliamina que puede ser traslocado a la membrana plasmática cuando el medio de incubación es deficiente en poliaminas (Hasne, 2010).

Otra estructura distintiva son los **reservosomas**, donde son dirigidas las macromoléculas endocitadas. Una de las principales moléculas obtenidas del medio extracelular es el transportador de hierro transferrina; los iones de hierro son esenciales para la replicación del ADN, la defensa antioxidante, la respiración mitocondrial y también para la síntesis de la base

modificada “J” (Taylor, 2010). Después de la internalización, la transferrina se dirige a los reservosomas, donde es almacenada junto con proteasas lisosomales como la cruzipaína, la principal cisteína proteasa de este parásito (Batista, 2015).

2.1.2 Ciclo de vida

T. cruzi tiene un ciclo de vida digenético, variando entre estadios infecciosos y no infecciosos, así como replicativos y no replicativos, que alternan entre los insectos vectores conocidos como vinchucas (triatominos hematófagos) y los hospedadores mamíferos (Tyler K.M., 2003). Cuando un insecto vector está infectado, en el intestino medio se encuentra la forma **epimastigota**, la cual es no infectiva y replicativa. Al avanzar por el intestino posterior hacia la ampolla rectal, éstos reciben menos nutrientes y se diferencian al estadio **tripomastigota metacíclico**, infectivo y no replicativo. Esta forma infectiva del parásito se libera con las heces de los insectos, durante o inmediatamente después de la ingesta de sangre por parte de la vinchuca. La proximidad de las heces con la zona de succión proporciona una vía de entrada adecuada para el parásito, el cual puede penetrar en el huésped mamífero invadiendo una amplia gama de tipos de células nucleadas (Rassi, 2010a). Una vez dentro del hospedero, los parásitos son ingeridos por macrófagos e internalizados en la célula mediante vacuolas endocíticas conocidas como vacuolas parasitóforas. Luego de la acidificación del medio, y a medida que los tripomastigotas metacíclicos comienzan a diferenciarse, se secreta la proteína lítica TcTox que en conjunto con la actividad trans-sialidasa lleva a la ruptura gradual de la vacuola parasitófora y a la liberación de los parásitos en el citoplasma de la célula infectada. Una vez dentro, los parásitos disminuyen su tamaño, entre otros cambios morfológicos, culminando en la formación de **amastigotas** replicativos que se replican por fisión binaria en el citoplasma de la célula infectada por 4 a 5 días, ocupando la mayor parte del volumen citoplasmático. Los amastigotas se diferencian luego en **tripomastigotas sanguíneos** que son liberados a la sangre tras la lisis celular, lo que les permite migrar a través del sistema linfático y el torrente sanguíneo para infectar nuevas células (Tyler K.M., 2003), y en ese recorrido pueden ser ingeridos por un insecto en una nueva ingesta de sangre, perpetuando así el ciclo de vida (Figura 2).

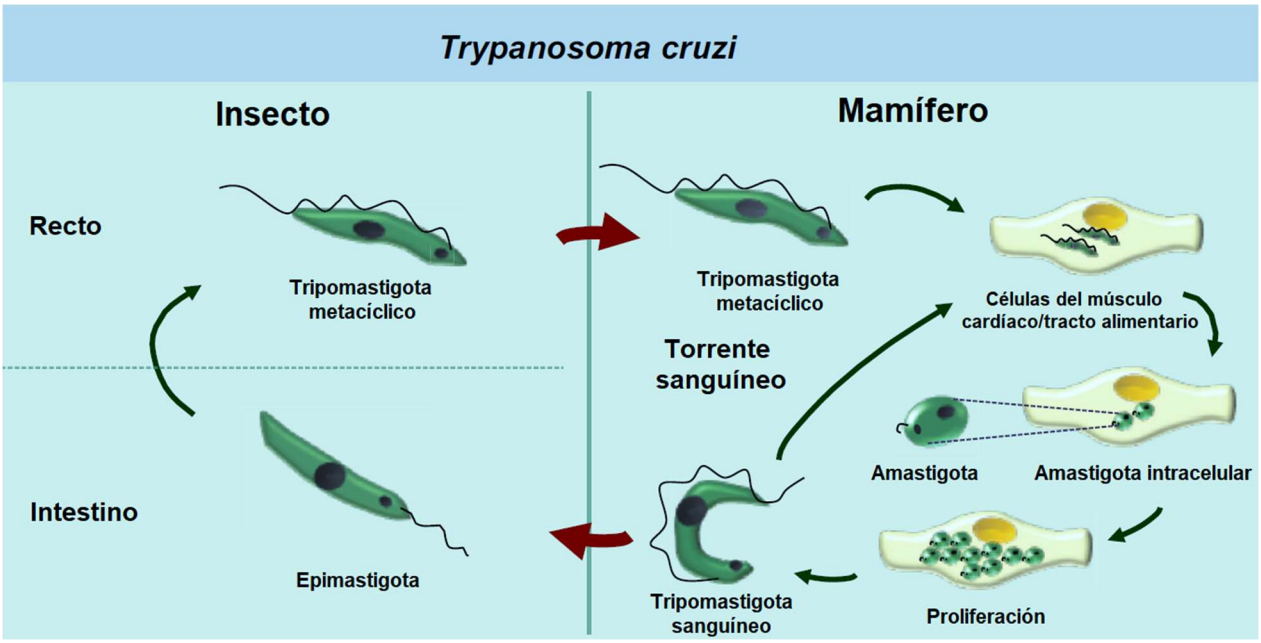

Figura 2. Ciclo de vida de *T. cruzi*. Se observan los diferentes estadios que alternan en los hospederos triatomino y mamífero. Extraído y modificado de (Brennand, 2012).

Durante el proceso de transición de una etapa del ciclo de vida a otra, el parásito exhibe profundos cambios metabólicos y morfológicos como forma celular, tamaño, posición de núcleo y kinetoplasto, longitud del flagelo, entre otros (Tyler K.M., 2003). Las principales características de cada estadio se describen a continuación. Los **epimastigotas** tienen un flagelo anclado cerca del centro del cuerpo del parásito. El kinetoplasto se ubica anterior al núcleo y tiene forma de disco. Los epimastigotas miden de 10 a 20 µm de largo, pero crecen otros 10 µm a medida que viajan por el intestino del insecto donde se transforman en tripomastigotas metacíclicos. Este estadio puede mantenerse de forma axénica en condiciones de laboratorio. Los **tripomastigotas metacíclicos** tienen el núcleo cercano a la parte posterior de su cuerpo, el cual aparece como un organelo elongado con alto contenido de heterocromatina y carente de nucleolo. Tienen además, un flagelo libre anclado a una membrana ondulante en el cuerpo y el kinetoplasto tiene una ubicación posterior al núcleo. Estos tripomastigotas tienen un tamaño aproximado de 20 µm de largo y 3 µm de diámetro. Por su parte, los **amastigotas** son intracelulares, de forma oval o redondeada, no tienen flagelo protuberante y el kinetoplasto se encuentra anterior al núcleo. Pueden alcanzar un tamaño de entre 3 y 5 µm de largo. Este estadio puede mantenerse mediante un modelo axénico en el laboratorio, o mediante cultivos que requieren la infección *in vitro* de células de mamíferos. Finalmente, los **tripomastigotas sanguíneos** están expuestos a las moléculas efectoras del sistema inmune del huésped, incluyendo anticuerpos específicos. Estas formas celulares expresan en su superficie múltiples miembros de una gran familia de moléculas, las más caracterizadas son las mucinas y las trans-sialidasas, asociadas a protección y evasión del sistema inmune del hospedero (da Fonseca, 2019). Si bien los tripomastigotas metacíclicos y

los sanguíneos son bastante similares morfológicamente, existen diferencias a nivel de su biología molecular que permiten su identificación, así como de la expresión de proteínas de superficie (Minning, 2009). Un modelo de tripomastigotas celulares puede obtenerse en el laboratorio por infección de células de mamíferos, luego de haber proliferado intracelularmente como amastigotas que se diferencian a este nuevo estadio.

2.1.3 Características del genoma

Estos organismos presentan una inusual organización del genoma, ya que los genes que codifican para proteínas se disponen en *tándem* en grupos direccionales con polaridad de hebra, conocidos como **unidades de transcripción policistrónica** (*Polycistronic Transcription Units* o PTU) y se transcriben como largos policistrones de 10–100 genes, los cuales, a diferencia de los operones bacterianos, en su mayoría no están relacionados funcionalmente entre sí (Clayton, 2019). Las PTU se encuentran separadas por secuencias cortas de unas pocas kilobases llamadas **regiones de cambio de hebra** (*Strand-Swith Regions* o SSR), donde el sentido de la transcripción diverge o converge (Macias, 2016). Los sitios de cambio de hebra divergente se consideran sitios de inicio de la transcripción y los sitios de cambio de hebra convergente se consideran sitios de terminación de la transcripción (Lima, 2021; Siegel, 2009). Los CDS y los snoARN se transcriben mediante la ARN polimerasa II, mientras que los ARNt, 5S ARNr y snARN se transcriben mediante la ARN polimerasa III, y los ARN ribosomales grandes son transcritos por la ARN polimerasa I (Lima, 2021).

Una característica distintiva de los tripanosomátidos es la **ausencia de intrones**. Sin embargo, existen algunas excepciones documentadas: el gen de la poliA polimerasa (PAP) de *T. cruzi* y *T. brucei* presenta intrones (Mair, 2000), así como el gen que codifica para el ARN de transferencia de la tirosina (ARNt-Tyr) (Padilla-Mejia, 2009). Además, estudios de RNA-Seq en *T. brucei* permitieron la confirmación experimental de un intrón presente en el gen de la proteína helicasa (Siegel, 2010).

En el año 2005 fue publicada la secuenciación del genoma de referencia de *T. cruzi* correspondiente a la cepa **CL Brener** (DTU TcVI), la cual es un genoma híbrido que comprende dos haplotipos divergentes: Esmeraldo-like (TcII) y non-Esmeraldo-like (TcIII). El genoma haploide de la cepa CL Brener totaliza 67 Mb distribuidas en aproximadamente 28 cromosomas y se estima que contiene 12000 genes que codifican para proteínas, casi 2000 genes para ARNs (tARN, rARN, slARN, snARN, snoARN y srpARN) y más de 3500 pseudogenes (El-Sayed, 2005a). En un trabajo adicional se incluyó a otros dos tripanosomátidos relacionados, el causante de la Tripanosomiasis africana, *Trypanosoma brucei* y uno de los agentes etiológicos de la leishmaniasis, *Leishmania major*, conocidos en conjunto como TriTryps (El-Sayed, 2005b).

Las secuencias genómicas de otras cepas de *T. cruzi* han sido reportadas desde esta publicación inicial, utilizando nuevas tecnologías de secuenciación, como Roche 454, Illumina, PacBio y Nanopore (Herreros-Cabello, 2020). La complejidad intrínseca del genoma de este parásito por la abundancia de secuencias repetitivas y genes organizados en *tándem*, ha impedido sistemáticamente el ensamblaje y la anotación de genomas de alta calidad. En el año 2018 fue publicado el genoma de dos cepas de *T. cruzi*: TCC y Dm28c, obtenidos mediante la tecnología PacBio (Berna, 2018). La secuenciación de lecturas largas demuestra una mejora significativa en la calidad del ensamblaje del genoma y la anotación disponible para este parásito, lo que implica estimaciones más precisas de los tamaños del genoma, números de copias de genes y distribución de secuencias repetitivas.

El análisis del genoma de la cepa Dm28c revela aspectos únicos en la arquitectura genómica de *T. cruzi*, como la compartimentación del genoma en regiones de diferente composición de bases y una distribución sesgada de genes (Berna, 2018). El genoma de *T. cruzi* está compartimentado en dos regiones claramente definidas: un 'compartimento central' compuesto por genes conservados e hipotéticamente conservados, es decir, genes que codifican proteínas con una función conocida denominada y genes sin una función asignada pero presentes en más de una especie de tripanosomátidos, y un 'compartimento disruptivo' no sinténico, compuesto por las familias multigénicas TS, MASP y mucinas. Por otro lado, las familias multigénicas GP63, DGF1 y RHS tienen una distribución dispersa en el genoma, estando presentes en ambos compartimentos, que a su vez pueden organizarse como distribución única o en arreglos en *tándem*. Dado que el compartimento central corresponde a los bloques sinténicos descritos anteriormente en *T. brucei* y *L. major* (El-Sayed, 2005b), y el compartimento disruptivo está compuesto principalmente por genes específicos de especie o género, este último puede considerarse como un región reciente del genoma. Un análisis de composición de bases demuestra que el compartimento disruptivo exhibe constantemente un contenido de GC más alto que el compartimento central. Por su parte, las regiones SSR muestran picos de GC que indican algún tipo de composicion particular, cuyo estudio debe profundizarse (Berna, 2018).

2.1.4 Expresión génica y regulación

Los nuevos transcritos requieren ciertas modificaciones para convertirse en un ARN mensajero (ARNm) maduro. Una de ellas es la adición de una estructura que consiste en una 7-metilguanosina (m^7G), denominada caperuza, casquete o CAP, en el extremo 5′. La adición de esta estructura CAP al ARNm se realiza co-transcripcionalmente de forma particular en los tripanosomas, debido a que la transcripción es policistrónica y los extremos 5′ de los ARNm no son directamente accesibles para las enzimas que la añaden (Kramer, 2021). La caperuza se

agrega a los transcritos primarios mediante un proceso denominado ***trans-splicing***, el cual adiciona además una secuencia de ARN de 39 nucleótidos al extremo 5', conocida como "*spliced leader*" o "SL" o "miniexón" (Michaeli, 2011; Preusser, 2012). Este se transcribe por separado de un arreglo en *tandem* de aproximadamente 100 genes de ARN SL, cada copia con su propio promotor, siendo estos los únicos promotores canónicos de ARN Polimerasa II identificados en tripanosomas (Gilinger, 2001; Srivastava, 2018). La adición del miniexón se produce en un sitio consenso constituido por un dinucleótido AG localizado corriente arriba del codón de iniciación de cada gen, a distancias variables, y generalmente está precedido por un tracto de polipirimidinas (Siegel, 2010). Una característica particular de los tripanosomas es que la CAP está fuertemente metilada, los primeros cuatro nucleótidos transcritos (AACU) tienen metilaciones en la posición 2'-O de la ribosa y hay metilaciones adicionales en las bases de la primera y la cuarta posición (Bangs, 1992). La metilación de la CAP es esencial para el *trans-splicing* y la metilación de la ribosa es necesaria para una traducción eficiente en tripanosomátidos (Zamudio, 2009; Zeiner, 2003).

El proceso de **poliadenilación** también ocurre co-transcripcionalmente y es similar al resto de los eucariotas superiores (Clayton, 2019). En el mismo participa una endonucleasa de restricción específica que corta el pre-mensajero en su extremo 3' y la enzima poli(A) polimerasa que incorpora adenosinas a expensas de ATP. Sin embargo, el reconocimiento del sitio poli(A) no es convencional, en lugar de reconocer elementos *cis* específicos en el ARNm, el sitio de poliadenilación está estrictamente determinado por la posición del tracto de polipirimidina que señala el *trans-splicing* del gen corriente abajo (Matthews, 1994). El sitio de poliadenilación en *T. brucei* se encuentra a una distancia de entre 70–140 nt corriente arriba del tracto de polipirimidinas (Benz, 2005) y a una distancia de 500 nt en *Leishmania*, con una fuerte preferencia por un residuo A (Smith, 2008). La razón probable de este inusual reconocimiento de sitios poli(A) es el acoplamiento estricto del *trans-splicing* con la poliadenilación del transcrito corriente arriba (Kramer, 2021). Las principales características del procesamiento de ARNm en tripanosomátidos se esquematizan en la Figura 3.

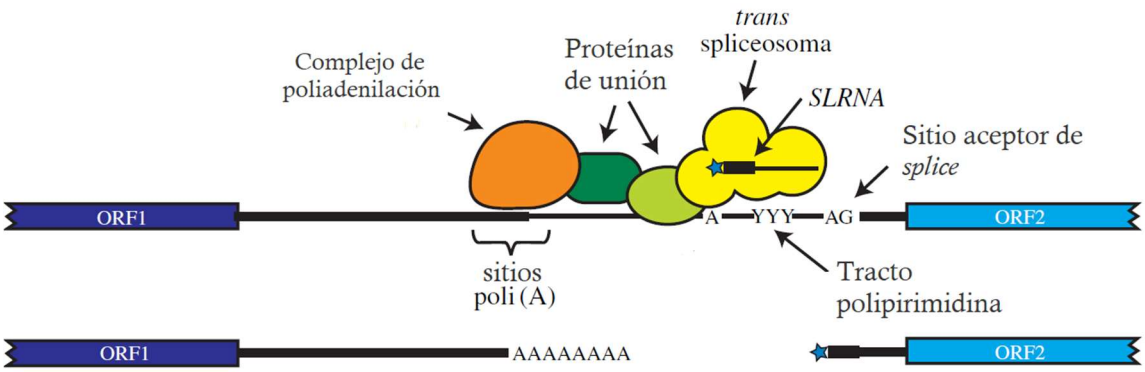

Figura 3. Procesamiento de ARNm. Se muestra la región entre dos marcos de lectura abiertos diferentes, ORF1 y ORF2. La distancia entre el tracto de polipirimidina y el sitio de poliadenilación varía entre los tripanosomátidos. Se desconoce la naturaleza de la interacción entre los complejos de poliadenilación y *splicing*; se muestran proteínas de enlace hipotéticas, pero la interacción podría ser directa. Se observa el sitio consenso constituido por un dinucleótido AG, donde se produce la adición del miniexón. Modificado de (Clayton, 2019).

Se ha observado que los tripanosomas carecen de un punto de control que evite que los ARNm sin procesar comiencen a exportarse del núcleo al citosol, por lo que este proceso puede comenzar co-transcripcionalmente. Mediante ensayos de hibridación *in situ* se ha evidenciado la exportación de ARNm antes de que el extremo 3' haya sido completamente sintetizado (Goos, 2019). Es importante destacar que la exportación co-transcripcional sucede con alrededor de la mitad de los transcritos largos, que abandonan el núcleo mientras aún están siendo procesados (la mayoría como dicistrones), probablemente porque pueden alcanzar un poro nuclear mientras están siendo transcritos. Se desconoce si existe un punto de control que impida la finalización de la exportación de ARNm si estos no están procesados (por ejemplo, reconociendo la ausencia de una cola de poli(A) y/o factores asociados) (Kramer, 2021). Por otro lado, ha sido postulado como mecanismo de regulación, la localización diferencial de los mensajeros en la célula y que la compartimentación nuclear contribuye al control de la expresión génica estadio-específica en *T. cruzi* (Pastro, 2017). Los mensajeros que no son requeridos en un estadio particular no son procesados eficientemente y se acumulan en el núcleo como forma de impedir su traducción, siendo los mensajeros con productos altamente requeridos, procesados y acumulados en el citoplasma, probablemente debido a un aumento de su vida media, garantizando así su traducción. Se desconoce aún si esta distribución diferencial de ARNm se logra mediante retención nuclear o a un decaimiento diferencial citoplasma-núcleo del ARNm (Pastro, 2017).

La iniciación de la traducción en eucariotas por lo general comienza con la unión en la CAP 5' del factor de iniciación eIF4E, el cual recluta eIF4G, que a su vez recluta a la helicasa eiF4A1. Los kinetoplastos tienen un repertorio inusualmente grande de eIF4E (numerados de 1-6) y de eIF4G (de 1-5); eIF4E3, eIF4E4, eIF4E5 y eIF4E6 parecen ser eIF4E 'clásicos', ya que

cada uno interactúa con al menos un eIF4G (Clayton, 2019). Mientras tanto, otros factores, incluidos eIF2 y eIF3, se adicionan durante el ensamblaje del complejo 43S, que contiene un ARNt cargado con la metionina inicial, unido a la subunidad ribosomal 40S. La interacción de eIF4G asociado a la CAP, con eIF3 recluta el complejo 43S al ARNm, formando el complejo 48S. Este complejo es el que escanea hasta el codón de iniciación, donde se une la subunidad 60S (Shirokikh, 2018), y queda ensamblado para iniciar la fase de elongación de la síntesis proteica. En procariotas y eucariotas, las tasas de elongación de la traducción están fuertemente influenciadas por la composición de codones, y se ha demostrado en tripanosomátidos, que el sesgo de codones influye en la traducción y la abundancia de ARNm, tendiendo los codones subóptimos a producir menos ARN y menos proteína (de Freitas Nascimento, 2018; Jeacock, 2018).

Debido a la organización genómica y a que todos los precursores de ARN policistrónico se transcriben a tasas similares, se ha propuesto que la regulación de la expresión de genes ocurre básicamente a nivel post-transcripcional (Clayton, 2019). La ausencia de elementos canónicos conservados como promotores de la ARN polimerasa II apoya el hecho que una ausencia de regulación del inicio de la transcripción (Gomez, 2010; Kramer, 2021). En consecuencia, los tripanosomas se basan en procesos post-transcripcionales como estabilidad del ARNm, eficiencia traduccional y modificación postraduccional para coordinar transiciones de desarrollo y otras respuestas adaptativas (Li, 2016). En este sentido, estudios transcriptómicos en tripanosomátidos a lo largo del ciclo de vida, han encontrado diferencias relativas de transcripto en estado estacionario, incluso en los genes individuales que pertenecen a una misma unidad policistrónica (Akopyants, 2004; Li, 2016; Minning, 2009).

Las modificaciones de la cromatina también juegan un importante rol en la expresión génica, ya que los inicios y finales de la transcripción de las unidades de transcripción policistrónica, en sitios divergentes de cambio de hebra, están marcados de forma epigenética por variantes de histonas e histonas modificadas post-traduccionalmente (Respuela, 2008; Siegel, 2009; Thomas, 2009). También se han evidenciado algunas estrategias por parte del parásito para aumentar el nivel de expresión de ciertos genes en tripanosomátidos, como el aumento del número de copias del gen de interés en el genoma, resultando en arreglos de repetidos en *tándem* para ciertos genes de alta expresión (Iantorno, 2017).

Por otro lado, se han identificado factores que actúan en *trans*, principalmente a nivel de proteínas de unión al ARN (*RNA-binding proteins* o RBP) (Alves, 2016; Clayton, 2016) e interaccionan con secuencias en *cis*, principalmente localizadas en las regiones no traducidas de los mensajeros (*Untranslated region* o UTR) (De Gaudenzi, 2013). Se ha demostrado que las

RBP establecen interacciones con grupos de ARNs que comparten elementos en *cis*, definiendo grupos co-regulados de mensajeros que podrían cumplir funciones relacionadas (Noe, 2008).

También se ha enfatizado en el estudio del rol de la eficiencia traduccional de los ARNm, como forma de regular la abundancia proteica en los tripanosomátidos (da Silva Augusto, 2015; Smircich, 2015). Las regiones no traducidas en el extremo 5' (5' UTR) son importantes en los procesos de control traduccional, existiendo mecanismos específicos como la presencia de pequeños marcos abiertos de lectura corriente arriba de la secuencia codificante principal, conocidos como *upstream* ORF o uORF (Radio, 2020). El inicio traduccional a partir del uORF da lugar a un marco abierto de lectura que solapa, o bien, termina antes del codón de inicio del CDS principal. En la mayoría de los genes que contienen uORF la eficiencia traduccional disminuye, si bien existe evidencia de algunos genes con eficiencia traduccional aumentada (Chen, 2010; Radio, 2020).

2.2 Enfermedad de Chagas

La enfermedad de Chagas o tripanosomiasis americana es una zoonosis potencialmente letal que afecta principalmente a la población rural y marginada de Latinoamérica, cuyo agente etiológico es el parásito protozoario *Trypanosoma cruzi*. Esta enfermedad debe su nombre al médico brasileño Carlos Justiniano Ribeiro das Chagas, quien la describió en 1909 cuando trabajaba en el Instituto Oswaldo Cruz de Río de Janeiro (Chagas, 1909). Está clasificada por la Organización Mundial de la Salud (OMS) como una "enfermedad tropical desatendida" (***Neglected Tropical Diseases*** o NTD). Este es un conjunto heterogéneo, integrado actualmente por 20 enfermedades y grupos de afecciones con la característica particular de que impactan en las comunidades más empobrecidas y la inversión para su tratamiento o prevención ha sido históricamente baja. En el año 2021 la OMS emitió una hoja de ruta para estas enfermedades, con foco en su control y eliminación para el año 2030 (OMS, 2021b). Particularmente para la enfermedad de Chagas, el objetivo es eliminarla como problema de salud pública y que en un 37% de los países afectados se logre interrumpir el contagio por las cuatro vías de transmisión (vectorial, transfusión, transplante y vertical), con una cobertura de tratamiento antiparasitario del 75% de la población elegible.

Esta enfermedad constituye un importante problema de salud pública con una gran carga económica, estimada en U$S 600 millones anuales en cuidados de la salud (Lascano, 2020). Es endémica en 21 países de América Latina y se estima que entre 6 y 7 millones de personas en todo el mundo están infectadas por el parásito, que se transmite principalmente a los humanos por insectos triatominos que funcionan como vectores, conocidos como vinchucas. Sin embargo,

el número de casos notificados ha aumentado en Estados Unidos, Canadá, muchos países europeos y algunos países del Pacífico Occidental. Estos casos notificados en países no endémicos se deben principalmente a la migración de la población latinoamericana al resto del mundo (Park, 2017; Salvador, 2014; Schmunis, 2010), abriendo un camino para otras vías de transmisión también consideradas de importancia epidemiológica como la transfusión de sangre o el trasplante de órganos (Bermudez, 2016; Coura, 2015). Otras formas de transmisión incluyen la vía vertical, de madre infectada a su hijo, por vía oral mediante ingestión de alimentos contaminados, y en menor medida accidentes laborales. Se estima que actualmente hay 30.000 casos nuevos anuales por todas las vías de transmisión, 12.000 muertes anuales y cerca de 70 millones de personas que viven en áreas expuestas al Chagas y están en riesgo de contraer la enfermedad (OPS, 2022).

La enfermedad presenta dos fases clínicas: una fase aguda inicial corta y una fase crónica. Entre ellas puede darse una fase denominada indeterminada, en la cual el paciente puede estar un período de 10-30 años sin diagnóstico o tratamiento, dado que no desarrolla síntomas (Perez-Molina, 2018). La **fase aguda** se caracteriza por una gran cantidad de parásitos que circulan en la sangre, una duración de 4 a 8 semanas y es en la mayoría de los casos asintomática y normalmente no se diagnostica, sin embargo, se pueden observar manifestaciones sintomáticas como fiebre prolongada, cefalea, mialgia, linfadenitis, hepatomegalia y esplenomegalia, entre otros, y causar la muerte de un ~5% de los pacientes, principalmente en inmunodeprimidos y niños (Vela, 2021). Después de la fase aguda, los pacientes infectados entran en una **fase crónica**, en la cual disminuyen la parasitemia en sangre, ya que los parásitos viven intracelularmente, principalmente en cardiomiocitos y células del músculo digestivo, por lo que un 30-40% de los pacientes inicialmente asintomáticos pueden desarrollar manifestaciones clínicas que incluyen arritmias e insuficiencia cardíaca progresiva, y con menor frecuencia, se desarrolla una forma digestiva de la enfermedad, con la generación de megaórganos, como megaesófago o megacolon, además de alteraciones neurológicas o mixtas que pueden conducir hasta la muerte del paciente (Rassi, 2010b).

2.2.1 Estado actual del tratamiento

A pesar de ser una enfermedad que supera ampliamente los 100 años desde su descubrimiento, los fármacos que se emplean actualmente son los mismos de hace 50 años, cuando fueron aprobados en la década del ‘70. El tratamiento actual se basa en el uso de dos compuestos nitroaromáticos de amplio espectro, **Nifurtimox** desarrollado por Bayer y registrado en 1967, y **Benznidazol**, registrado por Roche en 1971, cuya eficacia ha sido cuestionada dada su alta toxicidad y su controversial eficacia en la fase crónica de la enfermedad (Ribeiro, 2020).

En el caso del Benznidazol sólo dos estudios con 6 y 14 adultos bastaron para su aprobación, con una dosis definida en base a cultivos de epimastigotas y una duración del tratamiento que continúa en discusión (Kratz, 2018). La eficacia del Nifurtimox (NFX) y el Benznidazol (BZN) es variable y depende de la etapa de la enfermedad, la dosis del fármaco, la edad de los pacientes, y la cepa o genotipo de *T. cruzi* infectante.

Actualmente estos tratamientos están indicados para la fase aguda, incluidos los recién nacidos o lactantes con transmisión vertical, para la reactivación de la infección debido a inmunosupresión, la fase crónica en pacientes de hasta 18 años, y mujeres en edad fértil con infección por *T. cruzi* (se recomienda la anticoncepción durante el tratamiento) (Kratz, 2018). Asimismo, desde el 2002 la OMS ha establecido el consenso de que se debe ofrecer tratamiento a los adultos con Enfermedad de Chagas Crónica (individuos con serología positiva) (OMS, 2002).

El BZN es el fármaco más utilizado para el tratamiento de la enfermedad. Es un nitroimidazol antimicrobiano oral de amplio espectro que tiene actividad contra bacterias y varios parásitos. Ha demostrado eficacia frente a cepas de *T. cruzi* en varios modelos animales *in vivo* (Chatelain, 2015; Chatelain, 2018; Francisco, 2016; Romanha, 2010). Los estudios de tiempo de muerte indican que el efecto tripanocida de BZN es dependiente tanto del tiempo como de la concentración del fármaco (Canavaci, 2010; Moraes, 2014). Usando múltiples cepas de *T. cruzi*, se demostró un efecto tripanocida con un 100% de eliminación de parásitos, una tasa superior a la de otros complejos, como los inhibidores de la biosíntesis de ergosterol (Moraes, 2014).

El BZN es un profármaco, que requiere activación por las enzimas nitroreductasas del parásito que lo reducen, iniciando una cascada de reacciones que conducen a la formación de metabolitos altamente reactivos (Hall, 2012). Se cree que la principal enzima del parásito involucrada en la activación de BZN es la nitroreductasa de tipo 1. Los metabolitos de BZN resultantes, como el dialdehído glioxal, son altamente reactivos y se unen a macromoléculas del parásito, formando aductos con proteínas, ADN, ARN y moléculas pequeñas, que interrumpen el metabolismo de *T. cruzi* y lo conducen a la muerte celular (Hall, 2012). Sin embargo, utilizando un enfoque metabolómico para evaluar el mecanismo de acción de BZN, Trochine y cols. propuso que la unión covalente de BZN con tioles de bajo peso molecular también como ocurre con los tioles proteicos, es la causa principal de la toxicidad del fármaco contra *T. cruzi*, en lugar de la generación de glioxal (Trochine, 2014). Esto sugiere que BZN actúa de manera compleja y aún quedan algunas incertidumbres sobre su mecanismo de acción.

Las reacciones adversas a medicamentos más comúnmente observadas asociadas con el uso de BZN incluyen erupción y prurito, dolor de cabeza, mialgia y malestar gastrointestinal.

Reacciones cutáneas aparecen característicamente entre 7 y 12 días después del inicio del tratamiento. También se han reportado menos frecuentemente hepatitis asociada a fármacos, leucopenia, neuropatía periférica e hipersensibilidad grave a fármacos (síndrome Stevens-Johnson y otras reacciones con síntomas sistémicos) (Lascano, 2020).

Al igual que con el BZN, para el NFX también hay considerable falta de conocimiento sobre muchos aspectos de su farmacocinética, efectividad y metabolismo. Se cree que el mecanismo de acción de NFX es la generación de radicales nitro-anión, después de la activación por las nitroreductasas del parásito en presencia de oxígeno. Esto conduce a la producción de radicales que dañan los componentes vitales de *T. cruzi*, bloqueando la síntesis de ADN y acelerando la degradación del ADN y del ARN (Bartel, 2010).

Las reacciones adversas a medicamentos más frecuentemente observadas con el tratamiento de NFX son anorexia y pérdida de peso, irritabilidad, somnolencia y otros síntomas del sistema nervioso; depresión, neuropatía periférica y síntomas psiquiátricos han sido informados (Rodriques Coura, 2002). También se asocia con exantema, prurito y hepatitis asociada a fármacos, pero con menos frecuencia que el BZN (Villar, 2014). Las reacciones adversas asociadas a ambos medicamentos parecen mucho más comunes y graves en adultos y generalmente leves en niños, incluidos los recién nacidos (Berenstein, 2021). Ambos fármacos están contraindicados durante el embarazo en la mayoría de los protocolos de tratamiento clínico, principalmente debido a evidencia limitada sobre la seguridad en etapa de gestación. Por lo general, estos medicamentos no se recomiendan en pacientes con insuficiencia renal o hepática, principalmente a la falta de datos de seguridad, y el NFX también está contraindicado en personas con antecedentes de trastornos neurológicos o psiquiátricos (OMS, 2021a).

2.2.2 Reposicionamiento y búsqueda de fármacos

En los últimos años se ha propuesto el reposicionamiento de fármacos que puedan ser potencialmente eficaces para actuar sobre distintos blancos moleculares en el parásito. Este enfoque de reposicionamiento es ventajoso en términos de costos y disminución de tiempos requeridos para el proceso en comparación con el desarrollo de nuevos medicamentos, especialmente en enfermedades desatendidas, ya que los medicamentos reposicionados ya tienen evaluado su perfil toxicológico y farmacocinético cuando se utilizan en su objetivo terapéutico anterior (Alberca, 2016).

Una de las vías más estudiada es la de biosíntesis del ergosterol, tanto por su importancia en la supervivencia del parásito como por la disponibilidad de múltiples medicamentos que ya están en el mercado (fármacos antimicóticos azólicos) que podría reposicionarse fácilmente para

ensayos clínicos (Ribeiro, 2020; Scarim, 2018; Simoes-Silva, 2019; Watson, 2019). Hasta el momento, el alopurinol y algunos azoles se han estudiado en ensayos clínicos, estudios observacionales e informes de casos. El fármaco alopurinol ha demostrado ser útil en combinación con NFX y BZN en ensayos pequeños, pero la evidencia aún es insuficiente (Mazzeti, 2019; Perez-Mazliah, 2013; Rassi, 2007). Algunos azoles reposicionables prometedores como la monoterapia con ketoconazol, ravuconazol o posaconazol no han demostrado ser eficaces para el tratamiento de la infección crónica por *T. cruzi* (Brener, 1993; Molina, 2014; Torrico, 2018) y la combinación de posaconazol y BZN no proporciona una ventaja adicional de eficacia o seguridad sobre la monoterapia con BZN (Morillo, 2017; Villalta, 2019). Particularmente, se comparó posaconazol en dosis altas y bajas con placebo y los resultados de la investigación concluyeron que tiene una actividad antitripanosómica aceptable, pero también un aumento significativo en el fracaso del tratamiento en comparación con el grupo BZN (Molina, 2014). Otro ensayo aleatorizado controlado con placebo en adultos probó E1224, un profármaco de ravuconazol, en diferentes regímenes de dosificación combinado a BZN versus placebo, y encontró que el grupo E1224+BZN mostró un efecto supresor transitorio sobre la eliminación del parásito, mientras que BZN mostró una eficacia temprana y sostenida hasta los 12 meses de seguimiento. Este efecto transitorio se demostró sólo en el subgrupo de dosis alta, mientras que los niveles de parásitos en los grupos de E1224 de dosis baja y corta regresaron gradualmente a los niveles de placebo (Torrico, 2018). Por su parte, el fexinidazol es un fármaco previamente reposicionado para la infección por *Trypanosoma brucei gambiense* (tripanosomiasis africana) después de demostrar su eficacia en un ensayo controlado aleatorio (Mesu, 2018). Además, la seguridad y la farmacocinética del fexinidazol se han estudiado adecuadamente en humanos, lo que demuestra que la administración oral es segura y bien tolerada (Bahia, 2014; Deeks, 2019; Watson, 2019). Considerando que este fármaco es eficaz para eliminar *T. cruzi* en estudios preclínicos, se está llevando a cabo un ensayo aleatorizado, doble ciego y controlado con placebo en curso en Argentina, Bolivia y España para evaluar su eficacia en el tratamiento de esta enfermedad (NCT02498782) (Lascano, 2020).

En cuanto a estudios preclínicos, han sido identificados objetivos interesantes para la acción de los fármacos, como la cruzipaína (cisteína proteasa lisosomal del parásito), el citocromo B, el sistema de tripanotiona reductasa, las ciclofilinas, el N-miristoiloma, las anhidrasas carbónicas y el receptor de glutamato NMDA (Santos Souza, 2019; Villalta, 2019). Sin embargo, ninguno de estos potenciales blancos moleculares tiene fármacos en ensayos clínicos aún. Alternativamente, algunos compuestos naturales también se han estudiado para determinar su actividad anti-tripanosomátida, como los extractos de microalgas (Veas, 2020), veneno de avispa (Freire, 2020), cumarinas (Soares, 2019), extractos de vernonieae de América del Sur (Sosa, 2020), curcumina (Hernandez, 2018) y resveratrol (Vilar-Pereira, 2016). El uso de compuestos

naturales para tratar enfermedades conocidas podría conducir a recursos costo-beneficio efectivos, considerando que muchos de estos compuestos no están sujetos a restricciones de patentes y pueden estar ampliamente disponibles. Sin embargo, se deben realizar pruebas clínicas formales antes de que se utilice cualquiera de estos compuestos en los pacientes, y los costos cada vez mayores del desarrollo de fármacos y los ensayos clínicos en humanos dificulta que muchas moléculas nuevas estén en el mercado en un futuro previsible (Ribeiro, 2020). A pesar de la abundancia relativa de candidatos moleculares preclínicos y fármacos reposicionables potenciales, actualmente no hay nuevas clases de fármacos en proceso de desarrollo clínico para la enfermedad de Chagas, y BZN y NFX siguen siendo los únicos dos medicamentos disponibles para el tratamiento con datos clínicos que respaldan su uso.

2.2.3 Principales genes candidatos a blancos moleculares de fármacos

Los criterios de selección para determinar blancos apropiados, incluyen esencialidad, selectividad y drogabilidad (Osorio-Mendez, 2018). La **esencialidad** refiere a la evidencia química y genética de que el blanco es indispensable para el crecimiento o sobrevida del parásito. Para validar esto es necesario demostrar que la disrupción o deleción de ese gen causa la muerte celular. En tripanosomátidos los estudios de esencialidad de los genes son usualmente realizados en *T. brucei* mediante ensayos de interferencia de ARN (RNAi), pero este sistema no es funcional en *T. cruzi* (Kolev, 2011), por lo que la principal estrategia empleada ha sido el *knock-out* de genes (Burle-Caldas Gde, 2015) o recientemente CRISPR-Cas9 (Lander, 2015). En esta estrategia, el gen endógeno es reemplazado por un marcador de selección usando recombinación homóloga. Se presentan desafíos adicionales cuando hay más de una copia de un gen, ya que varios reemplazos son requeridos para obtener mutantes nulos, sin embargo se han podido deletar familias génicas mediante CRISPR-Cas9 (Burle-Caldas, 2022; Santi, 2022). Además, debe considerarse que *T. cruzi* es un organismo diploide y en algunas circunstancias, es posible que sólo una copia de un gen esencial sea suficiente para el parásito (haplosuficiencia). Por otro lado, la deleción de genes esenciales puede conducir a células inviables, entonces los mutantes nulos no pueden ser seleccionados para analizar el fenotipo resultante. En esos casos, se puede introducir una copia inducible o transitoria del gen, antes de su reemplazo en el genoma (Jones, 2018). Un aspecto a tener en cuenta es que la esencialidad debe ser evaluada en una etapa relevante del desarrollo del parásito. Estos ensayos se realizan en epimastigotas, por lo que para evaluar otros estadios es necesario diferenciar los parásitos editados genéticamente. Todas estas dificultades del modelo, han llevado a que sólo 16 genes estén verificados como genes esenciales a través de experimentos de genética reversa en *T. cruzi* (Osorio-Mendez, 2018). La **selectividad** refiere a que el compuesto químico tenga efectos sobre el blanco molecular del parásito y no sobre los genes o proteínas homólogas del hospedero. La selectividad puede ser difícil de

alcanzar especialmente para blancos que pertenecen a grandes familias relacionadas estructural y funcionalmente, por lo que son preferibles los blancos presentes en el parásito y ausentes en el hospedero. En su defecto, son convenientes los que presenten baja homología. Para alcanzar este objetivo es necesario contar con información estructural tanto de las proteínas de hospedadores, como del parásito. Aún no alcanzan a 300 las estructuras de proteínas de *T. cruzi* depositadas en el Protein Data Bank, lo cual evidencia una necesidad urgente de información estructural. La **drogabilidad** describe la habilidad de una proteína de unirse a una molécula química, la cual modula su función de forma específica. Las proteínas drogables deben tener una estructura con atributos fisicoquímicos que permitan la unión de un complejo (Sosa, 2018). La drogabilidad de un blanco usualmente es estimada por comparación con homólogos de otros organismos que han sido exitosamente blanco de acción de otros complejos específicos. Otra manera de determinar la drogabilidad es por el desarrollo de algoritmos matemáticos, que usan información estructural sobre los sitios de unión de las proteínas, para estimar su potencial como blanco molecular. Tal es el caso de la base de datos TDR Target, la cual recopila información de múltiples fuentes y estudios publicados que incluyen esencialidad, información funcional y estructural, clasificación de vías, e información de los compuestos que los emplean como blancos (Uran Landaburu, 2020).

La búsqueda de blancos moleculares en *T. cruzi* se ha centrado en procesos biológicos y vías metabólicas importantes para la sobrevida del parásito, los cuales incluyen principalmente la vía glucolítica, procesamiento degradativo de péptidos y proteínas, biosíntesis *de novo* de nucleótidos de pirimidina, salvataje de purinas y vías metabólicas de los nucleótidos, biosíntesis de esteroles, y daño por estrés oxidativo. A continuación, se describe brevemente la importancia de cada vía metabólica y qué candidatos relevantes han sido explorados hasta ahora.

1. Vía glucolítica: triosafosfato isomerasa (TIM)

La glucólisis juega un rol central en el metabolismo energético, por lo que se considera una vía esencial tanto en procariotas como en eucariotas. TIM es un homodímero que cataliza reversiblemente la interconversión entre D-gliceraldehído 3-fosfato y dihidroxiacetona fosfato, en la quinta reacción de la vía glucolítica mediante una reacción de isomerización, la cual no requiere ningún cofactor o ion metálico (Alvarez, 2014; Zarate-Perez, 2008).

TIM está presente tanto en humanos como en *T. cruzi*, y en general, los residuos involucrados en el sitio activo de la TIM del parásito son casi idénticos a los de la isoforma humana (Kurkcuoglu, 2011). Sin embargo, en la TIM de *T. cruzi* los residuos que forman la región de interfaz del dímero están menos conservados, presentando en *T. cruzi* una secuencia de aminoácidos y una conformación específicas (Olivares-Illana, 2007). La interfaz está más apretada en la isoforma humana que en la isoforma del parásito, es decir, menos accesible. La

accesibilidad de la interfaz en la isoforma del parásito ha marcado esta región como un sitio objetivo para los estudios de diseño de fármacos, mediante inactivación selectiva de la enzima parasitaria perturbando los contactos entre las subunidades (Kurkcuoglu, 2011).

2. Procesamiento degradativo de péptidos y proteínas: cruzipaína

La principal cisteín-proteasa de *T. cruzi* es la cruzipaína, también conocida como cruzaína. La cruzipaína es una peptidasa que pertenece a la familia de las papaínas y que se expresa durante todas las etapas de desarrollo del ciclo de vida y es esencial para varios procesos fisiológicos del parásito, como nutrición, evasión de la respuesta inmunitaria del huésped e invasión de las células del huésped (Beltran-Hortelano, 2020). Las cisteín-proteasas son una clase de enzimas que juegan un papel importante en el procesamiento degradativo de péptidos y proteínas (Martinez-Mayorga, 2015). Al igual que otras cisteín-proteasas, la cruzipaína se expresa inicialmente como un zimógeno inactivo, que sufre una autoactivación dependiente del pH, la temperatura y la concentración para transformarse en la enzima activa (Barbosa da Silva, 2019).

El sitio activo de la cruzipaína de *T. cruzi* se divide en siete subsitios que se unen a los aminoácidos peptídicos, con varios residuos que no se conservan, lo que admite la posibilidad de diseñar inhibidores específicos que se unen a esos residuos no conservados. En este sentido, múltiples estudios han demostrado que su inhibición bloquea la replicación y diferenciación del parásito *in vitro* e *in vivo*, incluso reduciendo la carga parasitaria en modelos murinos (Durrant, 2010; Ferreira, 2017).

3. Biosíntesis *de novo* de nucleótidos de pirimidina: dihidroorotato deshidrogenasa (DHODH)

La biosíntesis de pirimidinas para el suministro de precursores para la síntesis de ARN y ADN, glicoproteínas y lípidos de membrana, se lleva a cabo por vías *de novo* y de salvataje. En *T. cruzi* el equilibrio entre estas actividades varía en las diferentes etapas del desarrollo del parásito, siendo los amastigotas esencialmente dependientes de la biosíntesis *de novo* de pirimidinas *in vivo* (Annoura, 2005; Nara, 2005). La vía *de novo* comprende seis reacciones enzimáticas secuenciales, en las que DHODH participa en el cuarto paso y es la única reacción redox en esta cascada enzimática. Esta flavoenzima cataliza la oxidación de (S)-dihidroorotato a orotato en un ciclo catalítico que consta de dos semirreacciones. La primera mitad de la reacción puede ocurrir a través de un mecanismo concertado en el que el dihidroorotato se oxida a orotato y se combina con la reducción de los cofactores del mononucleótido de flavina (FMN) tanto en *T. cruzi* como en humanos. En la segunda mitad de la reacción, el fumarato se reduce a succinato en el parásito, y la ubiquinona a ubiquinol en humanos, y el cofactor FMN reducido se reoxida (Inaoka, 2017; Takashima, 2002).

Según la homología de secuencia de aminoácidos, los DHODH de diferentes organismos se han clasificado en dos familias, la familia 1 y la familia 2, que a su vez de dividen en subfamilias, que son diversas en su capacidad de aceptar electrones, sitios activos y localización subcelular. Dado que presentan un sitio activo pequeño, con un bucle altamente flexible, y una alta conservación entre las isoformas de *T. cruzi* y la humana de los residuos que forman el bolsillo de sitio activo, la dificultad de diseño ha sido evidente y ha impedido avanzar en el uso de esta enzima como blanco de acción (Cheleski, 2010; Inaoka, 2016).

4. Salvataje de purinas y vías metabólicas de nucleótidos: dihidrofolato reductasa-timidilato sintasa (DHFR-TS)

Los tripanosomátidos son auxótrofos del folato, nutriente esencial para los organismos vivos. El folato en su forma reducida es un precursor de los cofactores que se requieren para la síntesis de timidilatos, nucleótidos de purina, metioninas, serinas y glicinas necesarias para la síntesis de ADN, ARN y proteínas (Senkovich, 2005). La biosíntesis de nucleótidos se diferencia en los tripanosomátidos porque son incapaces de sintetizar purinas *de novo*, por lo que dependen de vías de salvataje de purinas que les permitan adquirir y procesar purinas del huésped para satisfacer sus necesidades (Bouton, 2021).

La DHFR es una enzima ubicua, que juega un papel central en el metabolismo nucleotídico y la síntesis de ADN en *T. cruzi*, y es un blanco conocido y exitoso en química médica en tratamientos anticancerígenos, antibacterianos y antipalúdicos (Chitnumsub, 2009; McGuire, 2003). En la mayoría de los organismos, DHFR y TS existen como enzimas monofuncionales separadas, sin embargo, en *T. cruzi* se presentan como una proteína homodimérica bifuncional, con el dominio timidilato sintasa (TS) ubicado en el extremo C-terminal. La estructura general de DHFR-TS es muy flexible, y el dominio DHFR se encuentra en el extremo N-terminal, separado del dominio TS por un conector peptídico que varía en tamaño (Senkovich, 2009).

El sitio activo de DHFR fue estudiado en *T. cruzi* y en su contraparte de humano, y su comparación revela diferencias en dos residuos de carga positiva presentes en el sitio activo en la DHFR del parásito, que cambian por residuos de carga negativa en la enzima humana, y se ha postulado que la diferencia de cargas podría ser ventajosa para el desarrollo de inhibidores selectivos (Senkovich, 2009; Zuccotto, 1998). También están descritos cambios que pueden ser relevantes, tanto en la forma de diferentes sub-bolsillos de unión, como en el dominio DHFR parasitario, el cual parece tener propiedades más hidrofóbicas que el dominio DHFR humano (Senkovich, 2009).

Por otro lado, el dominio TS de *T. cruzi* es altamente homólogo al TS humano. Hay una notable participación de hojas plegadas β y es precisamente el empaquetamiento de las láminas

beta de dos subunidades lo que constituye las principales interacciones en el ensamblaje de los dímeros en las enzimas TS monofuncionales, así como en el caso de las enzimas bifuncionales DHFR-TS. El sitio activo de TS del parásito está formado por residuos de ambas subunidades del dímero (Senkovich, 2009).

DHFR-TS es una enzima dependiente de nicotinamida adenina dinucleótido fosfato (NADPH), que participa en reacciones consecutivas en la síntesis *de novo* de dTMP. TS cataliza la conversión de los sustratos monofosfato de desoxiuridina (dUMP) y 5,10-metilentetrahidrofolato a los productos monofosfato de timidina (dTMP) y dihidrofolato (H_2F), mientras que DHFR es responsable del paso posterior de regeneración de tetrahidrofolato (H_4F) por la reducción de H_2F (Pez, 2003; Sienkiewicz, 2008). La inhibición de DHFR o TS impide la biosíntesis de ADN, lo que lleva a la muerte celular, lo que convierte a esta enzima bifuncional en un objetivo importante de la investigación en fármacos antifolatos.

5. Daño por estrés oxidativo: tripanotiona reductasa (TR) y superóxido dismutasa (Fe-SOD)

TR es una flavoenzima dependiente de NADPH que protege a los parásitos contra el daño oxidativo mediado por el sistema inmunitario del huésped mamífero. TR participa en el metabolismo del parásito al reducir el grupo disulfuro del tripanotión, manteniéndolo en su estado reducido para conservar la homeostasis redox. Sin embargo, esta enzima no es exclusiva del parásito. Los mamíferos están protegidos del estrés oxidativo por una enzima homóloga llamada glutatión reductasa (GR), que tiene características similares en términos de propiedades físicas y químicas, así como de mecanismo y estructura (Beltran-Hortelano, 2017).

Ambas enzimas están compuestas por dos homodímeros y están organizadas y subdivididas en cuatro dominios: un dominio de unión a FAD (dominio I), un dominio de unión a NADPH (dominio II), un dominio central (dominio III) y un dominio de interfaz (dominio IV). Ambos tienen una estructura general muy conservada, incluido su sitio activo. Solo cinco residuos ubicados en la hendidura del sitio activo de la GR humana son diferentes en la TR de *T. cruzi*, permitiendo estas sustituciones que las dos enzimas tengan una especificidad exclusiva hacia sus respectivos sustratos, y que la TR se considere un objetivo potencial debido a sus propiedades estéricas y electrostáticas (Beltran-Hortelano, 2017).

Las superóxido dismutasas (SOD) son un grupo primordial y conservado de enzimas que contienen metales, y proporcionan a todos los organismos aeróbicos una defensa contra el daño oxidativo. Estas enzimas actúan como captadores de intermediarios tóxicos del oxígeno, como el anión superóxido o los radicales hidroxilo, que se producen en la reducción de oxígeno durante la respiración mitocondrial. Las SOD eliminan el exceso de radicales libres de oxígeno mediante un proceso de dismutación en peróxido de hidrógeno (Beltran-Hortelano, 2022). En base a sus

grupos protésicos, se han descrito cuatro isoformas de SOD: hierro (Fe-SOD), cobre/zinc (Cu/Zn-SOD), manganeso (Mn-SOD) y níquel (Ni-SOD). Específicamente, las Fe-SOD son de gran interés por su presencia en tripanosomátidos y su ausencia en mamíferos, lo que convierte a este tipo de SOD en un objetivo potencial para diseñar y desarrollar nuevos candidatos efectivos contra la enfermedad.

Las dos isoformas principales de Fe-SOD de *T. cruzi* (una citosólica y otra mitocondrial) y las enzimas homólogas de Cu/Zn y Mn-SOD humanas fueron estudiadas, y la comparación de sus sitios activos demuestra que, aunque la estructura general está muy conservada y sus sitios activos son muy similares, las Fe-SOD de *T. cruzi* muestran diferencias relevantes que pueden utilizarse para el diseño de inhibidores específicos (Beltran-Hortelano, 2022). Se propone que la interacción entre un ligando y los residuos cercanos al sitio activo pueden inducir una modulación en el potencial de reducción del hierro, provocando su desplazamiento y, por tanto, la perturbación y posible inhibición de las Fe-SOD del parásito (Beltran-Hortelano, 2022; Martin-Escolano, 2018; Paucar, 2019).

6. Biosíntesis de esterol: lanosterol 14α-Demetilasa (CYP51)

El ergosterol es necesario para la estabilización de la membrana celular, la determinación de su permeabilidad y fluidez, y la modulación de la actividad de las enzimas unidas a membrana y los canales iónicos, lo que significa que el ergosterol es necesario para la formación de membranas viables y para diferentes procesos reguladores que son esenciales para el crecimiento del parásito, desarrollo y división. Los protozoos como *T. cruzi* no pueden acumular ergosterol, por ello, el bloqueo de la producción de ergosterol se considera letal para el parásito (Buckner, 2012; Lepesheva, 2007a). CYP51 es una hemoproteína conservada que forma parte de la superfamilia del citocromo P450. Esta enzima actúa en la etapa posterior a la formación del escualeno en la ruta de biosíntesis de esteroles y cataliza la eliminación monooxidativa en tres pasos del grupo 14α-metilo de los precursores de esteroles ciclados.

CYP51 es una enzima ubicua en *T. cruzi,* pudiendo ser localizada en las membranas de los glicosomas, el retículo endoplasmático y las mitocondrias, lo que sugiere la posibilidad de una localización multi-organelo de la ruta biosintética de esteroles en el parásito. La razón de esta amplia distribución subcelular de la vía no está del todo clara, pero podría respaldar las múltiples funciones reguladoras de los esteroles endógenos en tripanosomátidos (Lepesheva, 2011a; Lepesheva, 2011b). CYP51, como todos los citocromos P450, contiene un cofactor hemo (protoporfirina IX), donde el hierro en su posición de coordinación axial está unido al lado proximal de la proteína a través de un ligando tiolato derivado de cisteína. Esta coordinación hierro-cisteína permite la reacción de catálisis de CYP51, que incluye tres pasos consecutivos de monooxigenación (Hargrove, 2018). Un rasgo característico de CYP51 es la falta de cambios

conformacionales en la cavidad del sitio activo tras la unión de inhibidores, lo que convierte a esta enzima en un objetivo atractivo para el diseño de fármacos basados en estructura (Lepesheva, 2007b). A pesar de que varios residuos son idénticos en todos los miembros conocidos de la familia CYP51, lo que permite que estas enzimas conserven su función catalítica, se ha descrito que 22 de los 47 residuos que forman una cavidad en la CYP51 parasitaria son diferentes de los residuos correspondientes en la contraparte humana (Lepesheva, 2011a), lo cual representa una oportunidad en el desarrollo racional de fármacos.

2.3 Antecedentes

2.3.1 Complejos metálicos como potenciales agentes antichagásicos

El desarrollo de nuevos agentes antiparasitarios eficaces contra la enfermedad de Chagas se ha convertido en un importante objetivo y una necesidad. En las últimas décadas, el campo de la química inorgánica medicinal ha demostrado su capacidad para desarrollar fármacos prospectivos basados en metales para el tratamiento de diversas enfermedades (Pessoa, 2015; Rodriguez Arce, 2015; Willsky, 2011). El cisplatino es quizás el fármaco a base de metales más conocido. Este fármaco induce la muerte de células cancerosas después de su interacción con el ADN (Crul, 2002). En la búsqueda de nuevas herramientas terapéuticas, los complejos metálicos apuntan a combinar la actividad de ligandos que actúan como agentes antitripanosomátidos con metales farmacológicamente activos. Dado que los complejos metálicos podrían actuar como agentes antiproliferativos a través de múltiples mecanismos de acción por combinación de las acciones farmacológicas del metal y el ligando, su uso en el área de las NTD aparece como un nuevo enfoque prometedor (Navarro, 2010; Rivas, 2021).

En nuestro país, el Grupo de Química Inorgánica Medicinal (GQIM) de la Facultad de Química ha generado un gran número de compuestos metálicos bioactivos por medio de dos estrategias de diseño básicas o por combinación de ambas: la coordinación de iones metálicos de importancia farmacológica (Ru, Pt, Pd, V, Au, Cu, Ni, Co, Mn) a ligandos orgánicos bioactivos contra *T. cruzi*, y la coordinación de iones metálicos de importancia biológica, a ligandos intercalantes del ADN para obtener complejos con esta biomolécula como blanco de acción. El desarrollo racional de estos complejos, así como sus evaluaciones biológicas han dado lugar a más de 40 trabajos científicos en los últimos 10 años.

Recientemente, el vanadio ha surgido como un metal con un potencial notable para usos médicos en compuestos antitumorales y potenciadores de la insulina (Rehder, 2012; Thompson, 2009) y se han dedicado algunos esfuerzos al desarrollo de agentes prospectivos de vanadio contra enfermedades parasitarias desatendidas (Benitez, 2011). Particularmente, el GQIM diseñó compuestos de oxidovanadio (IV) que incluyen ligandos de la 1,10-fenantrolina con capacidad de intercalación de ADN (Fernandez, 2013a; Fernandez, 2013b). En particular, de una familia de 32 complejos estructuralmente relacionados, se destacó el derivado **[V^{IV}O(5Brsal)(aminofén)]** donde, 5 Brsal representa 5-bromosalicilaldehído semicarbazona, y aminofén es 5-amino-1,10-fenantrolina (Figura 4 A). Durante el ensayo de estabilidad en solución mediante EPR y NMR, se observó una oxidación parcial que conduce a una nueva especie después del desplazamiento del heteroligando de aminofén. Se demostró que esta nueva especie no es activa en *T. cruzi*, y el aminofén desplazado tiene un valor de IC_{50} veinte veces más alto en epimastigotas de la cepa Tulahuen 2 y una selectividad 97 veces menor que la especie original, confirmando que el

compuesto $V^{IV}O$ (5Brsal)(aminofén) inicial intacto es efectivamente la especie activa (Fernandez, 2013b).

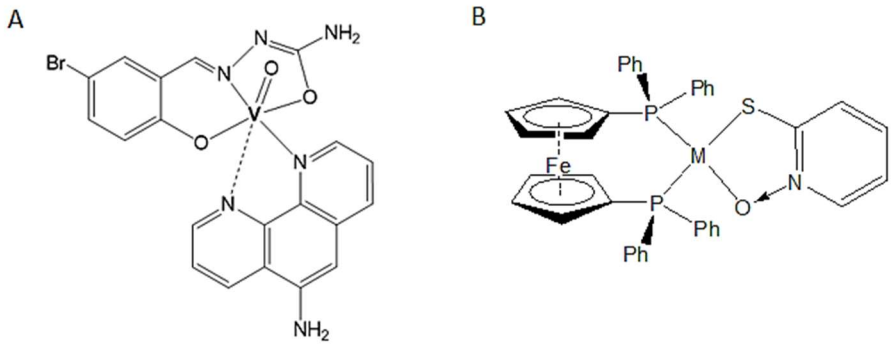

Figura 4. Compuestos metálicos sintetizados como agentes anti-tripanosomátidos. A. Compuesto de vanadio: $V^{IV}O$(5Brsal)(aminofén)**. B.** Compuestos organometálicos: M-dppf-mpo, donde el metal central es Pd (Pd-dppf-mpo) o Pt (Pt-dppf-mpo).

En colaboración con el GQIM, y en el marco de mi maestría, hemos estudiado el efecto biológico de novedosos compuestos basados en paladio y platino sintetizados como agentes anti-tripanosomátidos (Rodriguez Arce, 2015). En la última serie de compuestos, de fórmula global **$[M^{II}$(dppf)(mpo)]**, el centro metálico M corresponde a un átomo de Pd o Pt, que se coordina *cis*-trapezoidal casi plano con dos ligandos bidentados: un 1,1'-bis(difenilfosfino) ferroceno (dppf) y un piridin-2-tiolato-1-óxido (mpo) (Figura 4). Estos ligandos combinan la actividad antitripanosomátida del mpo, junto con una mejor permeabilidad de la membrana debido al dppf. Los nombres simplificados de estos complejos son **Pd-dppf-mpo** y **Pt-dppf-mpo**. Ambos complejos demostraron ser estables en solución, particularmente en medio biológico (Gambino, 2017).

El desarrollo de nuevos metalofármacos contra *T. cruzi* continúa siendo un campo emergente, y los enfoques ómicos de alto rendimiento pueden resultar buenos aliados para proporcionar información detallada sobre el mecanismo de acción de los nuevos compuestos basados en metales. La identificación de objetivos moleculares y la comprensión del modo de acción de los fármacos candidatos son necesarios para su desarrollo clínico (Wang, 2020; Wang, 2019).

Los estudios ómicos se refieren a un análisis integral y, por lo general, utilizan enfoques analíticos e informáticos avanzados de alto rendimiento para estudiar los roles, las relaciones y las acciones de varios tipos de moléculas en las células de un organismo. La combinación de varios campos, como la genómica, la proteómica, la transcriptómica, la metabolómica y la metalómica, permite la identificación de múltiples dianas moleculares y vías metabólicas

parasitarias afectadas por fármacos antiparasitarios potenciales. La metalómica es un área emergente, particularmente relevante para la química inorgánica biológica, que se ocupa de las interacciones y asociaciones funcionales de metales con biomoléculas, evolucionando como el campo científico destinado a determinar la identidad, cantidad y localización de especies de metales en una célula o un organismo (Callejon-Leblic, 2019; Lopez-Barea, 2006; Olivier, 2019; Singh, 2018).

Varias iniciativas relevantes que combinan metalómica, transcriptómica y proteómica, se han implementado con éxito en los últimos años para dilucidar los aspectos mecanísticos de la acción de los fármacos anticancerígenos basados en metales a nivel celular. Los grupos pioneros de Keppler y Gerner utilizaron recientemente un enfoque multiómico para dilucidar el modo de acción del fármaco de rutenio, KP1339, en un estudio clínico (Neuditschko, 2021). La identificación de proteínas ribosomales y el factor de transcripción GTF2I como interactores potenciales del agente Ru(III), indicó la alteración ribosómica y la inducción de estrés en el retículo endoplásmico como parte del modo de acción del fármaco (Neuditschko, 2021). Con respecto a otros grupos de quimioterapéuticos, un enfoque multiómico se ha utilizado para estudiar el modo de acción de fármacos a base de bismuto, utilizados en clínica para el tratamiento de la infección estomacal por *Helicobacter pylori* (Li, 2019). Sin embargo, el uso de aplicaciones ómicas sigue siendo un campo poco explorado para quimioterápicos desarrollados para actuar contra la enfermedad de Chagas. En este trabajo, se pretende avanzar y generar conocimiento en esta área a partir de la aplicación de metalómica, transcriptómica y proteómica para el estudio de nuevos complejos metálicos sintetizados en el país.

2.3.2 Estudio del compuesto Pt-dppf-mpo

En el marco de mi tesis de Maestría, se profundizó en el estudio del efecto del complejo Pt-dppf-mpo contra *T. cruzi*. Fue determinado un valor de IC_{50} de 60 ± 3 nM sobre epimastigotas de la cepa CL Brener, con un valor de Índice de Selectividad (IS: IC_{50} células mamífero/IC_{50} *T. cruzi*) asociado de 85, de acuerdo con el valor de IC_{50} reportado para células VERO de 5,1 ± 3,3 µM (Rodríguez Arce, 2015). Los principales resultados de ensayos *in vitro* y metalómicos se resumen a continuación. Los ensayos celulares *in vitro* mostraron cambios morfológicos, particularmente, se observa una disminución significativa de parásitos con morfología normal al incubarlos con concentraciones equivalentes a 1, 5 y 10 veces el IC_{50} calculado, adquiriendo los parásitos morfología redondeada y pérdida de movilidad, incluso luego de 6 horas de incubación. Para determinar el tipo de muerte celular inducido fue empleada una marcación con Anexina V (AV), la cual tiene una alta afinidad por la fosfatidilserina expuesta en las membranas celulares en los procesos de apoptosis y Ioduro de propidio (IP), el cual se une a ácidos nucleicos liberados

en células necróticas. Durante las primeras 6 horas, en parásitos tratados con 1x y 5x IC_{50}, no se observa un aumento significativo del marcado con AV y/o IP, pero sí comienza a evidenciarse en parásitos incubados con 10x IC_{50}. La inducción necrótica (AV^+/IP^+) se hace más evidente luego de 24 horas de tratamiento con 10x IC_{50}, donde se observa una doble marcación en un 10,6% de la población total. En este caso, la inducción de la necrosis no parece estar precedida por un mecanismo de apoptosis temprana, dado que no se observan parásitos AV^+/IP^- incluso luego de tiempos cortos de incubación (3 y 6 horas), descartando que la doble marcación observada a 24 horas corresponda a una apoptosis tardía. Fueron estudiadas también las variaciones de potencial de membrana mitocondrial usando el colorante catiónico JC-1, un compuesto lipofílico que en células saludables se acumula de manera dependiente del potencial de membrana (Δψm) en las mitocondrias, generando J-agregados, mientras que, en células apoptóticas o no saludables, cuando ocurren cambios en el potencial de membrana, se genera un cambio en la fluorescencia ya que el colorante se encuentra como monómero. La disminución de la tasa de fluorescencia J-agregado/monómero es indicativa de un Δψm mitocondrial comprometido. Luego de 6 horas de incubación la tasa de fluorescencia cae un 45% ($P < 0.05$) al incubar parásitos con 10x IC_{50}. A las 24 horas, la tasa de fluorescencia se reduce de forma estadísticamente significativa en todas las concentraciones ensayadas (1x, 5x y 10x IC_{50}) entre un 28 y un 52% en comparación con los parásitos control sin tratar.

En cuanto a los ensayos metalómicos, fueron analizados el índice de captura, su asociación con macromoléculas y su capacidad de actuar como agente tripanocida o tripanostático. El porcentaje de compuesto incorporado fue analizado mediante un ensayo de espectrometría de absorción atómica electrotérmica midiendo el elemento Pt. Luego de 24 horas, la incorporación por parte de los parásitos fue de un 75%, 48% y 19% cuando fueron incubados con concentraciones equivalentes al 1x, 5x y 10x IC_{50}, respectivamente. La incorporación de metal aumenta de forma lineal hasta las 6 horas de incubación, cuando se estabiliza, observándose una tasa de ingreso en aumento conforme se agrega mayor concentración de compuesto. Para los ensayos de asociación a macromoléculas (ADN, ARN, proteínas solubles e insolubles) se cuantificó el elemento Pt en cada fracción obtenida a partir de parásitos tratados. En las muestras de proteínas solubles y de ARN la cantidad de metal asociado no supera el 7% para 5x y 10x IC_{50}. Por su parte, se detectó en promedio un 21% del platino total asociado a proteínas insolubles para ambas concentraciones. Finalmente, la asociación preferencial del compuesto se da con el ADN, con un promedio de 66%. Los porcentajes de asociación para el tratamiento con 5x o 10x IC_{50} no presentaron diferencias estadísticamente significativas, lo cual sugiere que la asociación del compuesto con las macromoléculas del parásito es independiente de su concentración. Finalmente, fueron cuantificados en cada fracción los moles de los metales Pt y Fe, y pudo

determinarse una relación estequiométrica de 1:1, sugiriendo que el complejo que ingresa al parásito y alcanza a las distintas macromoléculas se encuentra íntegro (Tabla 1).

Tabla 1. Cuantificación mediante espectrometría de absorción atómica electrotérmica de los metales Pt y Fe que componen el compuesto Pt-dppf-mpo.

Macromolécula	Pt (moles)	Fe (moles)	Estequiometría
Proteínas Insolubles 5x IC_{50}	8,3E-11	8,0E-11	1,0
Proteínas Insolubles 10x IC_{50}	9,2E-11	9,5E-11	1,0
Proteínas Solubles 5x IC_{50}	3,6E-10	3,2E-10	1,1
Proteínas Solubles 10x IC_{50}	7,1E-10	7,2E-10	1,0
ADN 5x IC_{50}	6,8E-12	7,7E-12	0,9
ADN 10x IC_{50}	1,6E-11	1,6E-11	1,0
ARN 5x IC_{50}	1,7E-12	2,1E-12	0,8
ARN 10x IC_{50}	2,2E-12	2,6E-12	0,9

El efecto tripanostático o tripanocida de un compuesto se determina usualmente en experimentos de "lavado", en los cuales los cultivos de parásitos son expuestos por un período de tiempo breve a un compuesto (4 horas), lavados y transferidos a un medio fresco libre de compuesto, donde su crecimiento y recuperación son monitoreados durante un período de observación (72 horas). Los parásitos tratados con Pt-dppf-mpo en una concentración equivalente al valor IC_{50}, mostraron un crecimiento normal similar al de los parásitos control no tratados, sin embargo, los parásitos tratados durante 4 horas con 5x IC_{50}, reanudaron su crecimiento aproximadamente un 10% más lento que los parásitos control, y los tratados con 10x IC_{50} perdieron su capacidad de reanudar el crecimiento, incluso después de 72 horas de observación. La literatura recomienda caracterizar la capacidad tripanocida o tripanostática en referencia al valor de IC_{50} y a los tiempos de incubación y observación. En este caso, *T. cruzi* expuesto a Pt-dppf-mpo a una concentración de 1x y 5x IC_{50} por 4 horas luego de un período de observación de 72 horas actúa como un agente tripanostático. Por su parte, *T. cruzi* expuesto a Pt-dppf-mpo a una concentración de 10x IC_{50} por 4 horas luego de un período de observación de 72 horas no recupera su crecimiento, determinando que Pt-dppf-mpo es un compuesto tripanocida bajo esas condiciones de experimentación.

Por otro lado, fue estudiado el efecto de la incubación en el proceso de infección por tripomastigotas, y en la persistencia de amastigotas intracelulares, con el objetivo de obtener una caracterización celular global del efecto de este compuesto sobre *T. cruzi*. En el primer caso, tripomastigotas celulares fueron pretratados con 1x, 5x y 10x el valor IC_{50} determinado para epimastigotas durante 30 minutos y se utilizaron para infectar células VERO. El porcentaje de células infectadas en los experimentos control (sin pretratar) fue de 55% y 87% después de 24 y 48 horas, respectivamente. Un número de células infectadas significativamente menor ($p < 0.001$)

fue observado para parásitos pretratados con 10x IC_{50} luego 24 horas de infección. A las 48 horas, la disminución en el número de células infectadas fue más evidente, siendo significativa para todas las concentraciones empleadas (1x, 5x y 10x IC_{50}), lo que sugiere que la inhibición de la infección es dependiente de la dosis. En cuanto a la presencia de amastigotas, una reducción en el número de amastigotas por célula fue observada para concentraciones correspondientes a 5x y 10x IC_{50} incluso después de 24 horas de incubación, siendo este efecto más evidente a las 48 horas, cuando en todas las concentraciones ensayadas se observó una disminución en número de amastigotas por célula de forma estadísticamente significativa ($p < 0.001$) y de manera dosis dependiente. Este hallazgo sugiere que la preincubación de tripomastigotas celulares con Pt-dppf-mpo no afecta sólo el proceso de infección, sino también la replicación de estos parásitos tratados dentro de la célula. Para evaluar la persistencia del parásito en un proceso de infección establecido, monocapas de células VERO ya infectadas en ausencia de compuesto, fueron tratadas con concentraciones de Pt-dppf-mpo correspondientes a 1x, 5x y 10x IC_{50} y se determinó el número de amastigotas por célula. En este caso, fue observada una disminución significativa en el número parásitos por célula cuando se usaron concentraciones correspondiente a 5x y 10x IC_{50} después de 24 horas de tratamiento. Esta reducción en el número de amastigotas fue más marcada después de 48 horas después de la incubación ($p < 0.001$). Este hallazgo sugiere que el compuesto es capaz de alcanzar parásitos intracelulares y reducir su número de manera dosis dependiente, ya sea por inducción de muerte celular o alteraciones en el proceso de proliferación.

Los resultados obtenidos para el compuesto Pt-dppf-mpo fueron publicados al finalizar mi maestría, en el año 2018 en la revista científica Chemical Biology & Drug Design, en el artículo titulado "*Trypanosoma cruzi* biochemical changes and cell death induced by an organometallic platinum-based compound" (Mosquillo, 2018).

3 Hipótesis y objetivos

4.1 Hipótesis

El análisis del metaloma, el transcriptoma y el proteoma de parásitos tratados permite identificar y seleccionar posibles blancos moleculares de nuevos compuestos potencialmente antichagásicos. La sobreexpresión de blancos seleccionados es una estrategia adecuada para verificar su participación en la respuesta a nuevos compuestos químicos.

4.2 Objetivo general

Estudiar los procesos afectados por potenciales compuestos antichagásicos en el metaloma, transcriptoma y proteoma de *T. cruzi* con el fin de identificar genes o vías metabólicas candidatas a ser blancos de acción de estos compuestos y validarlos mediante genómica funcional.

4.3 Objetivos específicos

I) Analizar el efecto del compuesto metálicos de vanadio, **$V^{IV}O$(5Brsal)(aminofén)**, a través del análisis del metaloma, transcriptoma y proteoma de parásitos tratados en comparación con parásitos control sin tratar (Capítulo I).

II) Analizar el efecto del compuesto metálico de paladio, **Pd-dppf-mpo,** a través del análisis del metaloma de parásitos tratados (Capítulo II).

III) Analizar el efecto de los compuestos de paladio y platino, **Pd-ddpf-mpo** y **Pt-ddpf-mpo**, a través del análisis del metaloma, transcriptoma y proteoma de parásitos tratados con los compuestos metálicos y analizar la información de forma comparativa (Capítulo III).

IV) Seleccionar a partir de los datos ómicos de los compuestos de paladio y platino posibles candidatos a blancos moleculares y validarlos analizando comparativamente su efecto en poblaciones sobreexpresantes (Capítulo IV).

4 Capítulo I. Análisis ómicos para el estudio del compuesto $V^{IV}O$(5Brsal)(aminofén)

En la búsqueda de moléculas biológicamente activas contra *T. cruzi*, el grupo de Química Inorgánica Medicinal diseñó una familia de 37 compuestos relacionados estructuralmente basados en oxidovanadio(IV). El compuesto destacado de esa serie es $V^{IV}O$(5Brsal)(aminofén) y el objetivo de este trabajo se centra en evaluar los efectos celulares y el mecanismo de acción por el cual ejerce su efecto antiproliferativo contra *T. cruzi*. Este compuesto presenta un valor de IC_{50} de 3,76 ± 0,08 µM en epimastigotas de la cepa CL Brener. Los ensayos de recuperación han revelado un efecto tripanostático, acompañado de alteraciones en la forma y motilidad celular. El análisis del mecanismo de muerte celular permite descartar la participación de un mecanismo basado en apoptosis temprana o necrosis a las concentraciones y tiempos ensayados. Mediante determinaciones de vanadio se dedujo una captación mayoritariamente asociada a la fracción insoluble, incluyendo principalmente membranas y proteínas de membrana, con baja asociación a los ácidos nucleicos. En concordancia, no se detectaron cambios drásticos en el transcriptoma del parásito después de 6 h de tratamiento. Por otro lado, fue empleada una aproximación proteómica para identificar proteínas afectadas y los pasos metabólicos en los que están involucradas. Las proteínas totales de parásitos tratados y control fueron aisladas y separadas en fracción soluble e insoluble (proteínas de membrana) y analizadas mediante espectrometría de masas (Servicio de la Unidad de Bioquímica y Proteómica Analíticas del Institut Pasteur de Montevideo). Fueron seleccionadas para su estudio las proteínas únicas y las expresadas diferencialmente en forma significativa (filtradas por FDR ≤ 0,05). Este análisis proteómico revela la modulación de proteínas involucradas en diferentes procesos, como el metabolismo energético y redox, sistemas de transporte, vías de desintoxicación, síntesis de proteínas ribosomales y proteínas del proteasoma. A nivel global, los resultados aquí presentados constituyen una contribución para comprender el mecanismo de acción de este potencial fármaco para el tratamiento de la enfermedad de Chagas.

Los resultados de los análisis celulares y ómicos del compuesto $V^{IV}O$(5Brsal)(aminofén) fueron publicados en el artículo titulado “High throughput approaches to unravel the mechanism of action of a new vanadium-based compound against *Trypanosoma cruzi*” publicado en la revista Bioinorganic Chemistry and Applications. El trabajo completo representa el primer estudio que aporta conocimientos sobre metalómica, proteómica y transcriptómica de un agente prospectivo a base de metal contra *T. cruzi*, y ha recibido por ello el Premio a Mejor Artículo del año 2020 de la Editorial Hindawi.

Hindawi
Bioinorganic Chemistry and Applications
Volume 2020, Article ID 1634270, 10 pages
https://doi.org/10.1155/2020/1634270

Research Article

High Throughput Approaches to Unravel the Mechanism of Action of a New Vanadium-Based Compound against *Trypanosoma cruzi*

M. Florencia Mosquillo,[1] Pablo Smircich,[1,2] Analía Lima,[3] Sergio A. Gehrke,[4,5] Gonzalo Scalese,[6] Ignacio Machado,[7] Dinorah Gambino,[6] Beatriz Garat,[1] and Leticia Pérez-Díaz[1]

[1]*Laboratorio de Interacciones Moleculares, Facultad de Ciencias, Universidad de la República, Montevideo, Uruguay*
[2]*Departamento de Genómica, Instituto de Investigaciones Biológicas Clemente Estable, Montevideo, Uruguay*
[3]*Unidad de Bioquímica y Proteómica Analíticas, Institut Pasteur de Montevideo, Montevideo, Uruguay*
[4]*Biotecnos, Technology and Science, Montevideo, Uruguay*
[5]*Department of Biotechnology, Catholic University of Murcia, Murcia, Spain*
[6]*Área Química Inorgánica, Facultad de Química, Universidad de la República, Montevideo, Uruguay*
[7]*Área Química Analítica, Facultad de Química, Universidad de la República, Montevideo, Uruguay*

Correspondence should be addressed to Beatriz Garat; bgarat@fcien.edu.uy and Leticia Pérez-Díaz; lperez@fcien.edu.uy

Received 2 August 2019; Accepted 3 January 2020; Published 11 April 2020

Academic Editor: Anastasios Keramidas

Treatment for Chagas disease, a parasitosis caused by *Trypanosoma cruzi*, has always been based on two drugs, nifurtimox and benznidazole, despite the toxic side effects described after prolonged prescription. In this work, we study a new prospective antitrypanosomal drug based on vanadium, here named $V^{IV}O$(5Brsal)(aminophen). We found a good IC_{50} value, (3.76 ± 0.08) μM, on CL Brener epimastigotes. The analysis of cell death mechanism allowed us to rule out the implication of a mechanism based on early apoptosis or necrosis. Recovery assays revealed a trypanostatic effect, accompanied by cell shape and motility alterations. An uptake mostly associated with the insoluble fraction of the parasites was deduced through vanadium determinations. Concordantly, no drastic changes of the parasite transcriptome were detected after 6 h of treatment. Instead, proteomic analysis uncovered the modulation of proteins involved in different processes such as energy and redox metabolism, transport systems, detoxifying pathways, ribosomal protein synthesis, and proteasome protein degradation. Overall, the results here presented lead us to propose that $V^{IV}O$(5Brsal)(aminophen) exerts a trypanostatic effect on *T. cruzi* affecting parasite insoluble proteins.

1. Introduction

Chagas disease is caused by the protozoan parasite *Trypanosoma cruzi* that is mainly transmitted to the mammalian host by blood-sucking triatomine bugs. It can also be congenitally transmitted, from infected mother to child, through blood transfusion and organ transplantation or by ingestion of contaminated food. Currently, there are around 8 million infected people, 10,000 annual deaths, and approximately 25 million people living in risk zones, mainly rural regions of Latin America [1]. Chagas disease remains the most important parasitic disease in this region and is recognized by the World Health Organization as one of the 20 Neglected Tropical Diseases. Although Chagas disease is endemic in Latin America, it has been getting increased attention due to its dissemination to nonendemic countries (USA, Canada, Spain, Australia, and Japan, among others) [2]. The emigration from Latin America of

unknowingly infected people and the lack of controls of blood transfusion and organ transplants may have constituted the reason for the disease spreading.

Current chemotherapy is based on two almost 50-year-old drugs: benznidazole and nifurtimox. Both show severe side effects, controversial efficacy in chronic phase, and drug resistance development in some regions. Therefore, new less toxic and more effective drugs are needed. Although many natural and synthetic compounds have been assayed for activity against *T. cruzi*, only a few of them have advanced to clinical trials but were unsuccessful [1, 3, 4]. In the last decades, the inorganic medicinal chemistry field has demonstrated its capacity to develop prospective metal-based drugs for the treatment of parasitic diseases [5–11]. Since then, vanadium has emerged as a metal with remarkable potential for medical uses in insulin-enhancing and antitumor compounds [12–14]. Recently, some efforts have been dedicated to the development of vanadium prospective agents against neglected parasitic diseases [7, 15].

Looking for activity against *T. cruzi*, our group designed oxidovanadium (IV)-based compounds including polypyridyl ligands (NN) with DNA intercalating capacity [16–23]. In particular, a family of 37 structurally related [$V^{IV}O$(L-2H)(NN)] complexes, including semicarbazones of salicylaldehyde derivatives as coligands *L*, has turned out to be promising based on its submicromolar half-maximal inhibitory concentration (IC_{50}) range and high selectivity in comparison to mammalian cells. Among them, the 5-bromosalicylaldehyde semicarbazone derivative, [$V^{IV}O$(L-2H)(NN)], where *L* is 5-bromosalicylaldehyde semicarbazone and NN is 5-amino-1,10-phenanthroline, here named $V^{IV}O$(5Brsal)(aminophen) for simplicity (Figure 1), stood out, showing an IC_{50} value of 0.27 μM on *T. cruzi* (Tulahuen 2 strain epimastigotes) and a selectivity of 185 using J774 macrophages [20].

The stability in solution of $V^{IV}O$(5Brsal)(aminophen) towards solvolysis and/or oxidation was previously studied by electron paramagnetic resonance (EPR) and V-51 nuclear magnetic resonance (NMR) [20]. Only a partial oxidation leading to [$V^{V}O_2$(5Brsal-2H)(solvent)], after displacement of the aminophen heteroligand, was observed. This new V(V) species was demonstrated to be nonactive on *T. cruzi*, and free aminophen showed a twenty-time higher IC_{50} value on the parasite than the original $V^{IV}O$(5Brsal)(aminophen) species [19, 20]. In addition, $V^{IV}O$(5Brsal)(aminophen) showed a 97-fold higher selectivity than aminophen [20]. Therefore, the intact initial $V^{IV}O$(5Brsal)(aminophen) compound was considered as the active species.

Here we studied the mode of action of this vanadium compound as a prospective agent against *T. cruzi* (CL Brener strain). We analyzed the cell death mechanism involved and parasite recovery response. In addition, the amount of the vanadium uptaken by the parasite and its association with parasite macromolecules were determined. Finally, proteomics and transcriptomics strategies were undertaken to identify putative pathways or possible molecular targets affected. To our knowledge, this is the first *omics* study of these characteristics performed on a metal-based prospective agent against *T. cruzi*.

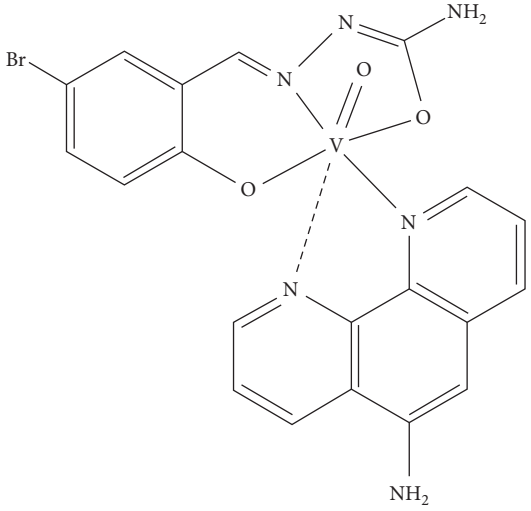

Figure 1: Molecular formula of $V^{IV}O$(5Brsal)(aminophen).

2. Materials and Methods

2.1. Reagents and $V^{IV}O$(5Brsal)(Aminophen) Synthesis. The 5-bromosalicylaldehyde semicarbazone ligand was synthesized and characterized as previously reported from an equimolar mixture of 5-bromosalicylaldehyde and semicarbazide [24]. For the synthesis of the [$V^{IV}O$(L-2H)(NN)] complex, a suspension in ethanol, previously purged with nitrogen, 0.375 mmol of *L*, 0.375 mmol of 5-amine-1,10-phenanthroline, and 0.375 mmol of [$V^{IV}O(acac)_2$], where acac denotes acetylacetonate, was heated at reflux under nitrogen for 4 h, and the reddish brown solid formed was filtered off, washed with ethanol and diethyl ether, and characterized by C, H, and N elemental analyses and by Fourier-transform infrared (FTIR) and EPR spectroscopies as previously reported [20, 22].

2.2. Parasites and Cell Culture. *T. cruzi* epimastigotes (CL Brener strain) were maintained at 28°C in the Brain Heart Infusion (BHI) medium supplemented with 10% fetal bovine serum and passed every three days.

2.3. Determination of In Vitro Anti-Trypanosoma cruzi Activity. Anti-*T. cruzi* activity was determined following a previously reported method [25–27]. Briefly, an 11.25 mM $V^{IV}O$(5Brsal)(aminophen) solution was prepared in dimethyl sulfoxide (DMSO). Epimastigotes were counted using the Neubauer chamber, and 1×10^6 parasites/mL were incubated in a 96-well plate in 200 μL BHI containing up to 16 μM $V^{IV}O$(5Brsal)(aminophen). Initial parasite density at time 0 (A_0) and parasite proliferation after five days of incubation (A_5) were determined by absorbance at 595 nm. Inhibition of proliferation was calculated considering the proliferation of control parasites incubated with the DMSO vehicle alone, by the following equation: %parasite proliferation=$(A_5-A_0)/(A_{5c}-A_{0c}) \times 0100$, where A_{5c} and A_{0c} correspond to the optic density of control cultures on day 5 and 0, respectively. In all cases, DMSO never exceeded a final

concentration of 0.04%. A dose-response curve was constructed and the IC_{50} value was determined using GraphPad Prism version 6.00 for Windows (GraphPad Software). The results are presented as averages ± SD (standard deviation) of six independent biological replicates.

2.4. Cell Death Mechanism. Cell death mechanism analysis was performed using the Dead Cell Apoptosis Kit (Thermo Fisher Scientific). Parasites were incubated for 24 h with 1x, 5x, and 10x IC_{50} of $V^{IV}O$(5Brsal)(aminophen), harvested by centrifugation, washed with phosphate-buffered saline (PBS), and incubated for 15 min with 5 mg/mL Alexa Fluor® 488 annexin V (AV) and 10 mg/mL propidium iodide (PI), followed by dual-parameter analysis using an Accuri C6 (BD Bioscience) flow cytometer. For AV and PI detection, a 533/30 nm signal detector (FL1) and a 670 nm long pass signal detector (FL3) were used, respectively. Two independent experiments were performed in duplicate for each $V^{IV}O$(5Brsal)(aminophen) concentration, and 10,000 events were acquired in each one. Data were analyzed using BD CSampler software (BD Bioscience). Nontreated parasites were used as a control. For apoptosis and necrosis positive control, parasites were treated for 2.5 h with H_2O_2 50 μM and 100 μM, respectively.

2.5. Live/Dead Assay. Cell viability was assessed with Calcein AM (CA) and propidium iodide (PI) (Thermo Fisher Scientific). Nontreated parasites and compound-treated parasites were harvested by centrifugation after 24 h of incubation and resuspended in 0.1 mL 1x PBS containing 0.1 mM of CA and 10 mg/mL of PI. Samples were incubated for 60 min at RT and immediately analyzed by flow cytometry with a 533/30 nm filter (FL1) for CA and a 670 nm long pass filter (FL3) for PI. The fluorescence intensity of two independent experiments was acquired for 10,000 events, and the data were analyzed using BD CSampler software (BD Bioscience).

2.6. Morphology Analysis. For scanning electron microscopy, 1×10^6 parasites in exponential growth phase, untreated or treated for 6 h with 5x IC_{50} of $V^{IV}O$(5Brsal)(aminophen), were washed with PBS and fixed with 4% paraformaldehyde. The samples were then subjected to dehydration with increasing concentration of acetone (30–100%) and gold-coated in the Metallizer Sputter Coater SCD050/LEICA. After metallization, samples were observed in a scanning electron microscope (Philips XL30, Eindhoven).

2.7. Recovery Assays. Recovery assays of *T. cruzi* epimastigotes were performed as previously described [25, 28]. Epimastigotes were incubated for 4 h with 1x, 5x, and 10x IC_{50} of $V^{IV}O$(5Brsal)(aminophen) and washed with and transferred to fresh compound-free BHI. Parasite proliferation was followed at 595 nm in a Thermo Scientific Varioskan® Flash Multimode for 24, 48, and 72 h. To calculate relative proliferation, untreated control parasites were used.

2.8. $V^{IV}O$(5Brsal)(Aminophen) Uptake Determination and Macromolecule Association Analysis. Vanadium uptake was determined by incubating the parasites with $V^{IV}O$(5Brsal)(aminophen) followed by electrothermal atomic absorption spectrometry in a Thermo iCE 3500 spectrophotometer (Thermo Fisher Scientific). Epimastigotes (1×10^7 parasites/mL) were incubated for 24 h with 1, 5, and 10x IC_{50} of the vanadium compound. At the indicated time points, 8×10^7 parasites were collected by centrifugation, washed once, and resuspended in PBS for vanadium quantification. Noninternalized vanadium in the supernatant was also determined. Two independent experiments were performed for each of the three concentrations evaluated.

To determine the association of vanadium with nucleic acids (~~3 ×10^7~~ parasites), 4×10^7 Wizard®GenomicDNAPurificationKit(Promega) and TRIzol Reagent (Life Technologies) for DNA and RNA isolation, respectively, were used. For protein analyses, parasites (4×10^7) were resuspended in 1 mL of Parasite Lysis Buffer containing 10 mM Tris-Cl pH 7.5, 1 mM EDTA, 1% CHAPS, 10% glycerol, 0.5% Triton, and Complete™ProteaseInhibitorCocktail(Roche); stirred 30 min at 4°C; and centrifuged at 4°C for 1 h at 20,000g to separate soluble from insoluble fraction. The associated vanadium was then determined in each fraction. Two independent experiments were performed for all analytical determinations and for each sample, and two vanadium determinations were performed in each one.

2.9. Transcriptome and Proteomic Analysis. Total RNA was isolated from parasites (1×10^9), untreated and treated with 5x IC_{50} $V^{IV}O$(5Brsal)(aminophen) during 6 h, using TRIzol (Life Technologies) reagent following the manufacturer's instructions (three independent replicas for each one). PoliA + RNA pair-end sequencing was performed at Macrogen using Illumina TruSeq™ RNA Sample Preparation Kit v2 and HiSeq 2500 (http://www.macrogen.com). Trimmomatic [29] was used to obtain good quality sequence reads that were mapped to the *T. cruzi* genome (version 29, http://tritrypdb.org) using Bowtie 2 in very sensitive mode [30]. The number of sequence reads per gene was determined using htseq-count [31]. Differentially expressed genes were determined using the DESeq2 package [32].

Total proteins from parasites (1×10^9), untreated and treated with 5x IC_{50} $V^{IV}O$(5Brsal)(aminophen) during 6 h, were isolated by incubation with lysis buffer (7 M urea, 2 M thiourea, 4% CHAPS) for 30 min at 4°C, centrifuged at 4°C for 1 h at 20,000g to separate soluble from insoluble fractions, and analyzed by LC tandem-mass spectrometry (LC-MS/MS) (three independent replicas). Briefly, 20 μg of each sample was resolved in precast 4%–12% gradient gels (NuPAGE, MES System, Invitrogen). Each lane was cut and processed for mass spectrometry analysis according to previously reported protocols [33]. Peptide samples were fractionated into a nano-HPLC system (EASY-nLC 1000, Thermo Scientific) equipped with a reverse-phase column (PepMap™, RSLC, C18, 2 m, 100 Å, 50 mm × 15 cm, Thermo

Scientific) using a gradient from 50% to 100% of 0.1% formic acid in acetonitrile at a flow rate of 250 nL/min. Peptide analysis was performed in a LTQ Velos nano-ESI linear ion trap instrument (Thermo Scientific) operated in data dependent acquisition mode (top 10) with a dynamic exclusion list of 45 s. Data analysis was carried out using PatternLab for Proteomics software (version 4.0.0.84). Raw files were searched against a target-decoy database generated from *Trypanosoma cruzi* (strain CL Brener) sequences downloaded from UniProt (http://www.uniprot.org), applying the following parameters: trypsin as proteolytic enzyme with full specificity, methionine oxidation as variable modification, cysteine carbamidomethylation as fixed modification, and 800 ppm of tolerance from the measured precursor *m/z*. PatternLab's Approximately Area Proportional Venn Diagram and T-Fold modules were used to quantitatively analyze data [34–36].

2.10. Real-Time PCR. Quantitative RT-PCR (qRT-PCR) using SensiFAST SYBR Hi-ROX Kit (Bioline) was performed on 10 ng/μL of cDNA obtained from RNA of each transcriptome biological replica using random primers and Superscript II (Life Technologies). Specific primers were designed with the OligoPerfect Primer Designer tool from Thermo Fisher Scientific (https://www.thermofisher.com). The threonyl-tRNA synthetase gene was used as an internal amplification control, since its transcript level does not present variations between treated and control parasites according to the obtained transcriptomic data. The reactions were carried out containing the primers in a final concentration of 0.4 μM with an annealing temperature of 60°C in a StepOnePlus Real-Time PCR System. All reactions were performed in duplicate. The data obtained were processed with StepOnePlus™ software v2.3, and the determination of the relative values of RNA was performed by the $2^{-\Delta\Delta CT}$ method [37].

3. Results

3.1. Growth Inhibition Mechanisms of $V^{IV}O$(5Brsal)-(Aminophen) in T. cruzi Epimastigotes. As a first step to study the antiproliferative mechanism of action of $V^{IV}O$(5Brsal)-(aminophen) on *T. cruzi* epimastigotes, we analyzed the growth inhibition curve and determined the IC_{50}, (3.76 ± 0.08) μM, in CL Brener strain (Figure 2).

Parasites were grown at 28°C for 5 days in BHI with the indicated concentrations of $V^{IV}O$(5Brsal)(aminophen). Each point represents the mean of six independent experiments with the associated standard error.

To find out if cell death mechanisms such as early apoptosis or necrosis/late apoptosis were involved, we performed flow cytometry analysis with the fluorescent hallmark probes AV and PI as described previously [25–27]. The absence of AV and/or PI positive cells after incubation with either 1x, 5x, or 10x IC_{50} for 24 h suggests that neither apoptosis nor necrosis processes were triggered by the $V^{IV}O$(5Brsal)(aminophen) treatment (Figure 3(a)). Similar results were obtained for 6 and 12 h of incubation. To determine whether treated parasites were dead or growth arrested, a live/dead assay was performed using fluorescent Calcein AM. As shown in Figure 3(b), the cell esterase activity was not affected (with 1x IC_{50}) or slightly decreased (with 5x and 10x IC_{50}). In addition, no drastic morphological changes in VIVO(5Brsal)(aminophen) treated parasites could be observed by scanning electron microscopy when using 5x IC_{50} (Figure 3(c)). However, a tendency to have shortened cell bodies and a clear loss of motility (not shown) was observed.

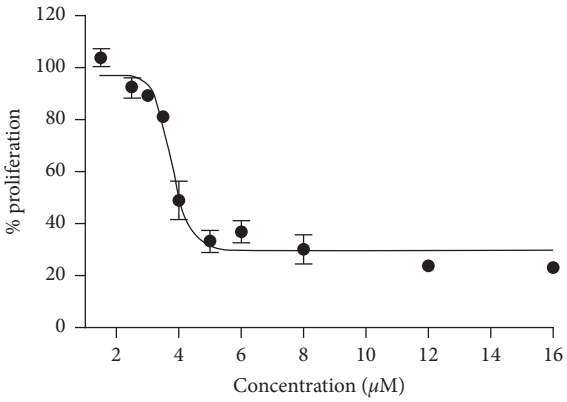

Figure 2: Effect of $V^{IV}O$(5Brsal)(aminophen) on T. *cruzi* epimastigotes proliferation.

Considering that these results prove that classical cell death mechanisms are not involved in the parasite growth inhibition of $V^{IV}O$(5Brsal)(aminophen), we investigated the existence of a trypanostatic effect through the recovery assay described by Kessler [28]. After an incubation period, enough to induce cell death mechanisms, similar parasite growth recovery profiles were observed for untreated and treated parasites at all the concentrations tested (Figure 4). This result confirms a trypanostatic mechanism of action for the $V^{IV}O$(5Brsal)(aminophen) since the parasite's growth is inhibited in presence of the compound, but parasites can resume growth in its absence.

3.2. Vanadium Uptake in T. cruzi Epimastigotes Treated with $V^{IV}O$(5Brsal)(Aminophen). In order to advance towards understanding the molecular mechanism of the trypanostatic action, we estimated the amount of vanadium uptaken by the parasites. As shown in Figure 5(a), parasites exhibit a dose dependent vanadium uptake with values of 0.50, 1.18, and 3.51 nmol for 1x, 5x, and 10x IC_{50} of $V^{IV}O$(5Brsal)(aminophen), respectively. It is worth noting that the parasite uptake only reaches on average the 2.4% of the vanadium present in the incubation mixture (total vanadium: 15 nmol for 1x IC_{50}). This low uptake hampers the analysis of a detailed subcellular distribution of the vanadium associated with the parasites.

Considering the capacity of the ligand to intercalate within nucleic acids [19], the distinctive association with the parasite DNA and RNA was analyzed. Despite the low values of vanadium associated with the parasite nucleic acids

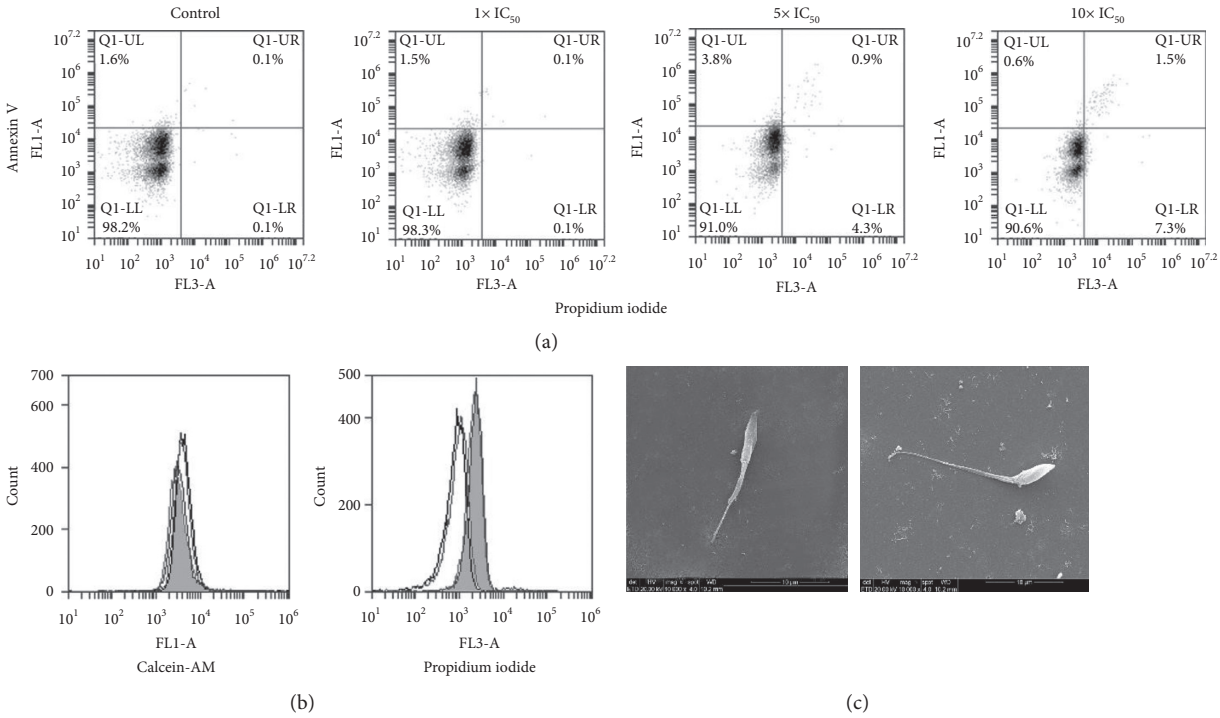

Figure 3: Cell death mechanism and morphological analysis of $V^{IV}O$(5Brsal)(aminophen) treated T. *cruzi* epimastigotes. (a) Flow cytometry analysis of parasites, untreated (control) and treated with $V^{IV}O$(5Brsal)(aminophen) for 24 h at the indicated concentrations (1x IC_{50}, 5x IC_{50}, and 10x IC_{50}), labeled with annexin V and propidium iodide. Dot plots represent unlabeled parasites (lower left square), early apoptotic annexin V labeled parasites (upper left square), and late apoptotic/necrotic annexin V/propidium iodide double labeled parasites (upper right square). (b) Flow cytometry analysis of parasites, untreated (black line) and incubated with the vanadium-based compound for 24 h at 1x IC_{50} (gray line), 5x IC_{50} (solid filled black line), and 10x IC_{50} (solid filled gray line), labeled with Calcein AM (left panel) and with propidium iodide (right panel). (c) Scanning electron microscopy image of a representative control untreated parasite (left image) and epimastigotes treated with 5x IC_{50} of $V^{IV}O$(5Brsal)(aminophen) for 6 h. Images were obtained with a Philips XL30 scanning electron microscope (magnification of 10,000 x.)

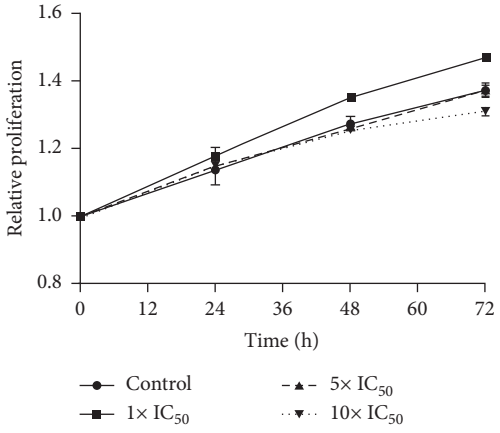

Figure 4: Recovery experiment of T. *cruzi* epimastigotes treated with $V^{IV}O$(5Brsal)(aminophen). The growth of parasites exposed for 4 h to 0, 1x, 5x, and 10x IC_{50} $V^{IV}O$(5Brsal)(aminophen) after compound removal was followed by optic density measures (595 nm) at the indicated time points. Proliferation was determined relative to time zero. Each experiment was performed in triplicate, and the mean and standard deviation were represented for each point.

(8.9×10^{-5} μg V/μg DNA and 6.46×10^{-6} μg V/μg RNA), a favored association with DNA was observed (Figure 5(b)).

Nonetheless, using a simple fractionation approach, a preferred association of the metal with the insoluble fraction (more than 90% of the uptaken vanadium) was observed (Figure 5(c)). This result suggests that $V^{IV}O$(5Brsal)(aminophen) could be interacting with membrane associated proteins.

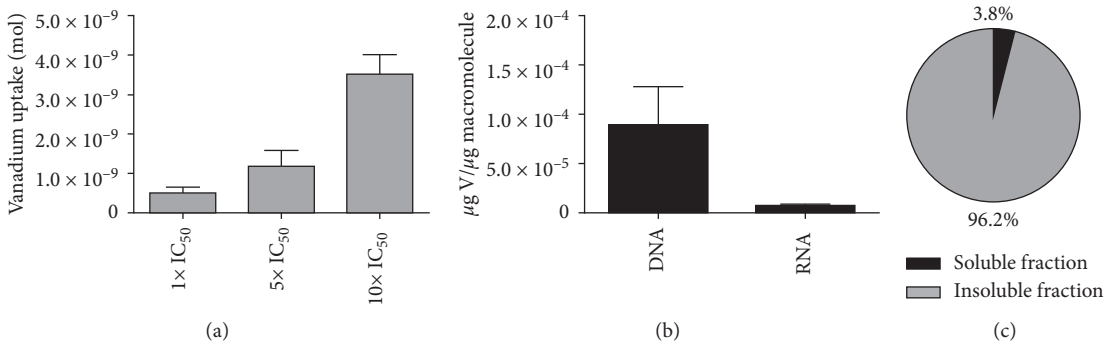

FIGURE 5: Uptake and macromolecule association of $V^{IV}O$(5Brsal)(aminophen) in T. *cruzi* epimastigotes. (a) Amount of vanadium strongly bound and/or uptaken by compound-treated parasites. Parasites were incubated with 3.76 μM (1x IC_{50}), ~~11.28~~ μM (5x IC_{50}), and 37.6 μM (10x IC_{50}) of $V^{IV}O$(5Brsal)(aminophen), and incorporated vanadium was determined through electrothermal atomic absorption spectrometry. (b) Percentage of total vanadium associated with DNA, RNA. (c) Determination of total vanadium associated with soluble and insoluble fraction. Vanadium amounts were determined through electrothermal atomic absorption spectrometry after 6 h of incubation with 5x IC_{50}. The average of two independent experiments is presented with its associated standard deviation. 18.8 μM

3.3. Early Omic Response of T. cruzi Epimastigotes to $V^{IV}O$(5Brsal)(Aminophen) Treatment. To identify key molecules as well as possible pathways involved in the mode of action of the $V^{IV}O$(5Brsal)(aminophen), we studied the main omic changes induced in parasites by the incubation with 5x IC_{50} $V^{IV}O$(5Brsal)(aminophen) for 6 h. We selected a relative short time of incubation to study only the early response triggered specifically by the compound, thus avoiding the incidence of general late or/and indirect mechanisms.

For the analysis of transcriptomic changes, three independent biological replicates were sequenced for each condition, and at least 7 million paired-end sequence reads were mapped to the reference *T. cruzi* genome using Bowtie 2 (Table S1). A very good correlation was observed for the replicates (Pearson correlation coefficient $p > 0.99$). The comparative transcriptomic analysis revealed minimal changes on mRNA steady state levels upon treatment. Indeed, from a total of 10,951 mapped transcripts, less than 100 transcripts (0.008%) were differentially expressed, considering a false discovery rate of 0.01. As expected, most of them (47%) codify for hypothetical proteins with no known function or functional information or domains.

Furthermore, only 2 differentially expressed transcripts (encoding for hypothetical proteins) showed a fold change greater than 1.5 (Table S2). qRT-PCR was performed on some genes to confirm transcriptomic data (Figure S1). An excellent correlation between both approaches (transcriptomic and qRT-PCR) for the selected set of genes (R Pearson 0.97) was obtained. For the analysis of proteomic changes, a shotgun strategy was assayed to separately identify the soluble and insoluble protein changes due to the vanadium compound incubation.

The proteomic analysis of insoluble protein fraction revealed a total of 248 overrepresented and 110 underrepresented insoluble proteins in the $V^{IV}O$(5Brsal)(aminophen) parasites compared with control untreated parasites (Table S3). Cytochrome P450 (TcCLB.506945.190) appears to be the most downregulated insoluble protein. Interestingly this protein has been involved in mediating detoxification processes (Table S3). Among the top overrepresented insoluble proteins, we found two acetyltransferases which constitute component of the pyruvate dehydrogenase complex (TcCLB.509717.20, TcCLB.510105.170) and a Glutathione-S-transferase/glutaredoxin (TcCLB.506443.70). Some reductases (TcCLB.506821.210, TcCLB.510819.4), oxidoreductases (TcCLB.507049.60, TcCLB.506485.80), and hydrolases (TcCLB.503399.20, TcCLB.506931.10, TcCLB.506747.30) also appeared overrepresented in the insoluble protein fraction of treated parasites as well as several ribosomal proteins (Table S3).

Regarding the soluble proteins, 122 appeared underrepresented with 105 of them only present in the untreated controls. Remarkably we found some ATP binding cassette transporters (ABC transporters: TcCLB.506925.530, TcCLB.510943.80, TcCLB.507099.80), with the latter two involved in drug expulsion mechanism [38]. Besides, the abundance of some other proteins related to detoxification processes was also modified (Figure 6). In addition, KEGG pathway analysis revealed that the $V^{IV}O$(5Brsal)(aminophen) treatment affects regulatory processes of protein expression, since the abundance of proteins involved in spliceosome, biosynthesis of amino acids (Gly, Ser, Thr, and His), aminoacyl-tRNA biosynthesis, ribosomes, and proteasome appears to be altered (Table S4). It is interesting to mention that proteasome proteins were also overrepresented among the insoluble proteins (Table S3). Finally, energetic metabolism seems to be also affected by $V^{IV}O$(5Brsal)(aminophen) treatment, as the abundance of many proteins related to carbon metabolism processes, such as citrate cycle, glycolysis, gluconeogenesis, pentose phosphate pathway, pyruvate metabolism, and oxidative phosphorylation, is modified (Table S4).

4. Discussion

The aim of this work was to evaluate the cellular and molecular mechanism of action of a new vanadium-based compound in *T. cruzi*. Proliferation assays revealed an IC_{50} value of (3.76 ± 0.08) μM, similar to the one of the reference drug nifurtimox,

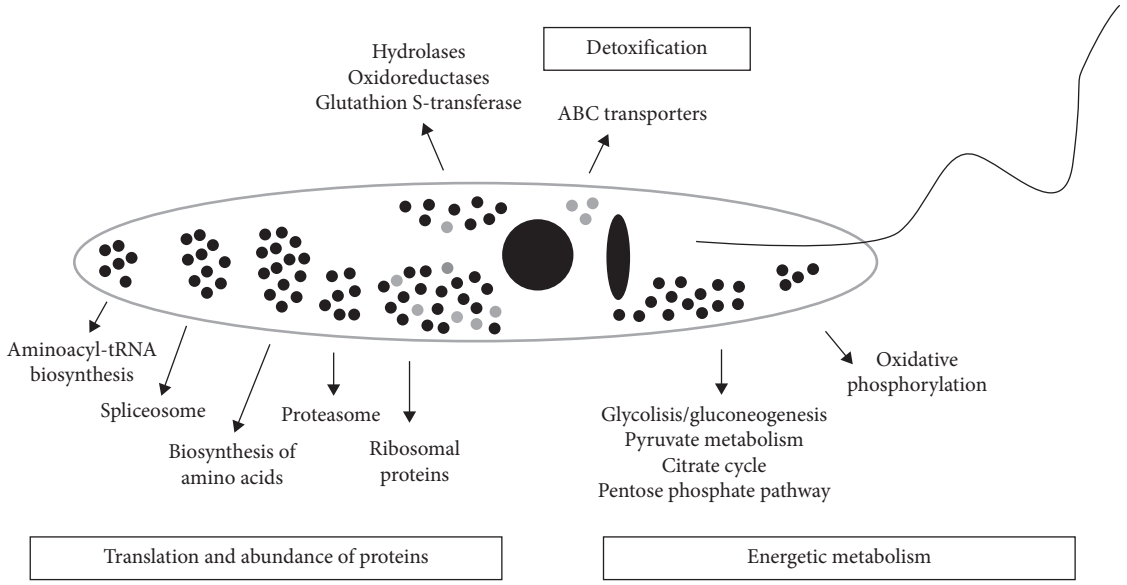

FIGURE 6: Schematic representation of protein abundance changes in (T). *cruzi* epimastigotes treated with $V^{IV}O$(5Brsal)(aminophen). Proteins are grouped based on KEGG pathways distribution. Black and gray dots indicate proteins that appear overrepresented and underrepresented in $V^{IV}O$(5Brsal)(aminophen) treated vs. untreated parasites, respectively.

(2.8 ± 0.2) μM [25, 26]. Thus, $V^{IV}O$(5Brsal)(aminophen) can be visualized as a promising antiproliferative compound.

T. cruzi. It is worth noting that complete inhibition is not achieved with the assayed compound concentrations (Figure 2). To understand this issue, we decided to investigate the mode of action of this compound more deeply.

Regarding the mechanism of inhibition of parasite growth, negative AV and PI labeling revealed that neither apoptosis nor necrosis is involved. Moreover, the slight decrease of the metabolic activity, deduced from the esterase analysis, as well as the absence of the characteristic drastic morphological changes, such as cell membrane rupture or cell body increase [38], suggests a growth arrest phenomenon rather than the involvement of another cell death mechanism. Conversely, a trypanostatic mode of action of $V^{IV}O$(5Brsal)(aminophen) on *T. cruzi* was confirmed by recovery assays.

Though the percentage of the compound uptaken by the parasites (less than 2.4% of the total vanadium used for incubation) is similar to that obtained for other well-known metallic antiproliferative compounds such as cisplatin (3%), oxaliplatin (1%), or pyrodach-2 (0.1%) in three different human cell lines [39], it is notably lower than the ones obtained for other metal-based compounds (more than 20%) in *T. cruzi* epimastigotes [25, 26]. Nonetheless, the low $V^{IV}O$(5Brsal)(aminophen) uptake is enough to exert the antiparasitic effect. Although this vanadium-based compound series has been designed including an intercalating molecule, and its *in vitro* DNA association has been reported [19], in the current *in vivo* assays only vanadium traces associated with nucleic acids could be detected. Anyway, this low amount could be enough to affect DNA replication accounting for the cytostatic effect observed in the recovery assays. On the other hand, a striking association with the insoluble fraction (90%) was found. It is worth mentioning that this fraction mainly contains membrane associated proteins but also includes lipids and diverse functional groups in posttranslationally modified proteins.

High throughput analyses have been only recently implemented to analyze the mechanisms involved in kinetoplastid drug resistance and the mode of action of drugs [40, 41]. Aiming to deepen the study of the molecular mechanism of action of $V^{IV}O$(5Brsal)(aminophen) on *T. cruzi*, we undertook the omics analysis of early altered transcripts and proteins because of the treatment of parasites with this novel compound. Transcriptomic analysis revealed a few differentially expressed transcripts (less than 100, being less than 1%) with low levels of up- or down-regulation (most of them have $\log_2$ Fold change < 0.5), which may be in accordance with the low *in vivo* association of vanadium with the parasite nucleic acids. Nonetheless, the importance of these changes must not be underestimated. For example, a very tiny modification in the expression of a given regulatory protein could result in a global effect in the parasite if it participates in key metabolic pathways. The low effect of vanadium compound on the parasite transcriptome can be explained by its preferred *in vivo* association with the insoluble fraction rather than with nucleic acids (Figure 5). On the other hand, we found that 14% of the total identified proteins (523 out of 3,638) were differentially abundant after treatment, most of them in the insoluble protein fraction (68%) (Figure S2). The number of 3,638 total proteins detected is in good agreement with previous *T. cruzi* proteomics analysis, which has reported the identification of 2,784 [42] and 4,920 proteins [43]. Proteomics has only been employed in Chagas disease chemotherapy studies to analyze the mode of action of naphthoimidazoles with 30 differentially abundant proteins detected in epimastigotes [44] and 61 in trypomastigotes [45]. Conversely, our results reflect a

pleiotropic molecular effect of $V^{IV}O$(5Brsal)(aminophen). Many of the differentially expressed proteins in the insoluble fraction have been reported to be involved in mediating detoxification processes. Among them Cytochrome P450 is worth noting, whose diminished abundance in treated parasites may explain the lack of an effective detoxification response [46]. Other interesting proteins that appear differentially expressed include acetyltransferases, reductases, and hydrolases. While the involvement of transferases, oxidases, reductases, or hydrolases in the modification of internalized compound has been reported [47, 48], these results suggest a major role of $V^{IV}O$(5Brsal)(aminophen) driving to early energy and redox metabolic disorders. Since many ribosomal proteins were differentially expressed in treated parasites (Table S3), despite the minimal association of the compound with mRNA (Figure 5), we can speculate that the translation process could be affected. Among the diminished soluble proteins, we found transporters of the ABC family whose role in drug expulsion mechanisms has been previously proposed [49]. In this way, the compound elimination could be reduced, thus allowing prolonging its trypanostatic effect. Besides, in our proteomic analysis, proteasome proteins appear overrepresented in treated parasites in both soluble and insoluble protein fractions. The proteasome has recently been studied as the target of promising drugs for malaria, leishmaniasis, Chagas disease, and sleeping sickness [50, 51].

It is tempting to speculate that the possible direct inhibition of proteasome by $V^{IV}O$(5Brsal)(aminophen) could lead to an increase in proteasome protein production to hamper the compound effect. The overrepresented proteasome proteins could be also explained by the existence of extensive protein modifications requiring a more active proteasome to degrade them.

Altogether, the data here presented support the idea of a main mode of action of $V^{IV}O$(5Brsal)(aminophen) through the modification of the abundance of numerous parasite proteins. While the altered protein content driven by the $V^{IV}O$(5Brsal)(aminophen) may be due to its direct association with the protein targets promoting their degradation or stabilization, the compound may be also specifically affecting proteins involved in the protein production and degradation processes, thus expanding the effect.

5. Conclusion

In conclusion, this work provides a thorough description of the cellular and molecular responses of *T. cruzi* epimastigotes to a prospective new vanadium-based antiparasitic compound. Interestingly, the very good IC_{50} value determined for $V^{IV}O$(5Brsal)(aminophen) is reached through a trypanostatic mode of action, moderately affecting cell shape and motility. The parasite early response to this compound displays no drastic changes in mRNA levels. Nonetheless, proteomic analysis revealed a wide effect on protein abundance identifying specific proteins potentially involved in this massive response and in the drug metabolism. The combined use of omic approaches allowed us to identify the affected processes that drive a very good inhibition of parasite growth even at the very low uptake levels detected. Globally, the results here presented constitute a contribution to understand the mechanism of action of this potential drug for the treatment of Chagas disease. Furthermore, they contribute an insight into metallomics, proteomics, and transcriptomics of metal-based antitrypanosomal compounds, encouraging this incipient research area.

Data Availability

The transcriptomic and proteomic data used to support the findings of this study are included within the supplementary information files; raw data can also be obtained by emailing the corresponding author.

Conflicts of Interest

The authors declare that they have no conflicts of interest.

Acknowledgments

This work was supported by Agencia Nacional de Investigación e Innovación (ANII) (grant number ANII FMV_1_2014_1_103957 and POS_FMV_2015_1_1005183) and Programa de Desarrollo de las Ciencias Básicas, Uruguay.

Supplementary Materials

Figure S1: validation of transcriptomic data of selected genes with qRT-PCR. The expression of random selected modified transcripts from transcriptome data list was analyzed by qRT-PCR comparing untreated and treated parasites, and expression values ($\log_2$ FC RT-PCR) were plotted against transcriptomic data ($\log_2$ FC transcriptomic). Figure S2: determination of differentially abundant proteins in *T. cruzi* epimastigotes treated with $V^{IV}O$(5Brsal)(aminophen). Soluble (A) and insoluble (B) proteins from untreated (control) and treated parasites were analyzed. The figure shows a Volcano plot generated with the T-Fold module from PatternLab for Proteomics. Proteins detected in at least 4 replicates of all conditions were indicated as individual dots and plotted accordingly to the p value ($\log_2$ (p value)) and fold change ($\log_2$ (fold change)). Black dots represent proteins that do not satisfy neither the fold change nor the statistics criteria for differential expression and thus are considered unchanged between conditions. Dark gray represents proteins that do satisfy the fold change but not the statistic criteria for differential expression. Light gray dots represent low abundant proteins satisfying both fold change and q value criteria for differential expression but not considered for further analysis due to the low number of spectral counts. Finally, white dots correspond to proteins satisfying all statistical filters and represent the differentially expressed proteins between strains. For details about proteins corresponding to white dots, see supplemental Table S3. Table S1: row data stats from transcriptome analysis of control untreated parasites and $V^{IV}O$(5Brsal)(aminophen) treated parasites. Table S2: list of differentially expressed genes

from transcriptome analysis. The upregulated and downregulated transcripts in $V^{IV}O$(5Brsal)(aminophen) treated parasites with respect to control untreated parasites are shown. Table S3: list of differentially expressed proteins from proteomic analysis. The upregulated and downregulated soluble and insoluble proteins in $V^{IV}O$(5Brsal)(aminophen) treated parasites with respect to control untreated parasites are shown in different tabs. Table S4: KEGG enrichment analysis of metabolic pathways using the STRING database for modified proteins in $V^{IV}O$(5Brsal)(aminophen) treated parasites. (*Supplementary Materials*)

References

[1] World Health Organization, 2019, http://www.who.int/chagas/en/.

[2] F. Salvador, B. Trevióo, E. Sulleiro et al., "Trypanosoma cruzi infection in a non-endemic country: epidemiological and clinical profile," *Clinical Microbiology and Infection*, vol. 20, no. 7, pp. 706–712, 2014.

[3] T. A. Houweling, H. E. Karim-Kos, M. C. Kulik et al., "Socioeconomic inequalities in neglected tropical diseases: a systematic review," *PLOS Neglected Tropical Diseases*, vol. 10, no. 5, Article ID e0004546, 2016.

[4] R. Paucar, E. Moreno-Viguri, and S. Pérez-Silanes, "Challenges in chagas disease drug discovery: a review," *Current Medicinal Chemistry*, vol. 23, no. 28, pp. 3154–3170, 2016.

[5] R. W. Brown and C. J. T. Hyland, "Medicinal organometallic chemistry–an emerging strategy for the treatment of neglected tropical diseases," *Medicinal Chemistry Communications*, vol. 6, no. 7, pp. 1230–1243, 2015.

[6] M. B. Camarada, C. Echeverria, and R. Ramirez-Tagle, "Medicinal organometallic compounds with anti-chagasic activity," *Medicinal Chemistry Communications*, vol. 7, no. 7, pp. 1307–1315, 2016.

[7] J. Costa Pessoa, S. Etcheverry, and D. Gambino, "Vanadium compounds in medicine," *Coordination Chemistry Reviews*, vol. 301-302, pp. 24–48, 2015.

[8] D. Gambino and L. Otero, "Design of prospective antiparasitic metal-based compounds including selected organometallic cores," *Inorganica Chimica Acta*, vol. 472, pp. 58–75, 2018.

[9] M. Navarro, C. Gabbiani, L. Messori, and D. Gambino, "Metal-based drugs for malaria, trypanosomiasis and leishmaniasis: recent achievements and perspectives," *Drug Discovery Today*, vol. 15, no. 23-24, pp. 1070–1078, 2010.

[10] A. Tahghighi, "Importance of metal complexes for development of potential leishmanicidal agents," *Journal of Organometallic Chemistry*, vol. 770, pp. 51–60, 2014.

[11] D. Gambino and L. Otero, "Perspectives on what ruthenium-based compounds could offer in the development of potential antiparasitic drugs," *Inorganica Chimica Acta*, vol. 393, pp. 103–114, 2012.

[12] D. Rehder, "The potentiality of vanadium in medicinal applications," *Future Medicinal Chemistry*, vol. 4, no. 14, pp. 1823–1837, 2012.

[13] K. H. Thompson, J. Lichter, C. LeBel, M. C. Scaife, J. H. McNeill, and C. Orvig, "Vanadium treatment of type 2 diabetes: a view to the future," *Journal of Inorganic Biochemistry*, vol. 103, no. 4, Article ID 554558, 2009.

[14] G. R. Willsky, L.-H. Chi, M. Godzala 3rd et al., "Anti-diabetic effects of a series of vanadium dipicolinate complexes in rats with streptozotocin-induced diabetes," *Coordination Chemistry Reviews*, vol. 255, no. 19-20, pp. 2258–2269, 2011.

[15] D. Gambino, "Potentiality of vanadium compounds as antiparasitic agents," *Coordination Chemistry Reviews*, vol. 255, no. 19-20, pp. 2193–2203, 2011.

[16] J. Benítez, L. Becco, I. Correia et al., "Vanadium polypyridyl compounds as potential antiparasitic and antitumoral agents: new achievements," *Journal of Inorganic Biochemistry*, vol. 105, no. 2, pp. 303–312, 2011.

[17] J. Benitez, I. Correia, L. Becco et al., "Searching for vanadium-based prospective agents against trypanosoma cruzi: oxidovanadium (IV) compounds with phenanthroline derivatives as ligands," *Zeitschrift für anorganische und allgemeine Chemie*, vol. 639, no. 8-9, pp. 1417–1425, 2013.

[18] J. Benítez, L. Guggeri, I. Tomaz et al., "Design of vanadium mixed-ligand complexes as potential anti-protozoa agents," *Journal of Inorganic Biochemistry*, vol. 103, no. 4, pp. 609–616, 2009.

[19] M. Fernández, L. Becco, I. Correia et al., "Oxidovanadium (IV) and dioxidovanadium (V) complexes of tridentate salicylaldehyde semicarbazones: searching for prospective antitrypanosomal agents," *Journal of Inorganic Biochemistry*, vol. 127, pp. 150–160, 2013.

[20] M. Fernández, J. Varela, I. Correia et al., "A new series of heteroleptic oxidovanadium (IV) compounds with phenanthroline-derived co-ligands: selective Trypanosoma cruzi growth inhibitors," *Dalton Transactions*, vol. 42, no. 33, pp. 11900–11911, 2013.

[21] I. Machado, M. Fernández, L. Becco et al., "New metal complexes of NNO tridentate ligands: effect of metal center and co-ligand on biological activity," *Inorganica Chimica Acta*, vol. 420, 2014.

[22] G. Scalese, J. Benítez, S. Rostán et al., "Expanding the family of heteroleptic oxidovanadium (IV) compounds with salicylaldehyde semicarbazones and polypyridyl ligands showing anti-*Trypanosoma cruzi* activity," *Journal of Inorganic Biochemistry*, vol. 147, pp. 116–125, 2015.

[23] G. Scalese, M. F. Mosquillo, S. Rostán et al., "Heteroleptic oxidovanadium (IV) complexes of 2-hydroxynaphtylaldimine and polypyridyl ligands against *Trypanosoma cruzi* and prostate cancer cells," *Journal of Inorganic Biochemistry*, vol. 175, pp. 154–166, 2017.

[24] P. Noblia, M. Vieites, B. S. Parajon-Costa et al., "Vanadium (V) complexes with salicylaldehyde semicarbazone derivatives bearing in vitro anti-tumor activity toward kidney tumor cells (TK-10): crystal structure of [VVO2 (5-bromosalicylaldehyde semicarbazone)]," *Journal of Inorganic Biochemistry*, vol. 99, pp. 443–451, 2005.

[25] M. F. Mosquillo, L. Bilbao, F. Hernández et al., "Effect of a new anti-T. cruzi metallic compound based on Palladium," *BioMetals*, vol. 31, no. 6, pp. 961–974, 2018.

[26] M. F. Mosquillo, L. Bilbao, F. Hernández et al., "Trypanosoma cruzibiochemical changes and cell death induced by an organometallic platinum-based compound," *Chemical Biology & Drug Design*, vol. 92, no. 3, pp. 1657–1669, 2018.

[27] E. Rodríguez Arce, M. F. Mosquillo, L. Pérez-Díaz et al., "Aromatic amine N-oxide organometallic compounds: searching for prospective agents against infectious diseases," *Dalton Transactions*, vol. 44, no. 32, pp. 14453–14464, 2015.

[28] R. L. S. Kessler, M. J. Soares, C. M. Probst, and M. A. Krieger, "*Trypanosoma cruzi* response to sterol biosynthesis inhibitors: morphophysiological alterations leading to cell death," *PLoS One*, vol. 8, Article ID e55497, 2013.

[29] A. M. Bolger, M. Lohse, and B. Usadel, "Trimmomatic: a flexible trimmer for Illumina sequence data," *Bioinformatics*, vol. 30, no. 15, pp. 2114–2120, 2014.

[30] B. Langmead and S. L. Salzberg, "Fast gapped-read alignment with Bowtie 2," *Nature Methods*, vol. 9, no. 4, pp. 357–359, 2012.

[31] S. Anders, P. T. Pyl, and W. Huber, "HTSeq–a Python framework to work with high-throughput sequencing data," *Bioinformatics*, vol. 31, no. 2, pp. 166–169, 2015.

[32] M. I. H. Love, W. Huber, and S. Anders, "Moderated estimation of fold change and dispersion for RNA-seq data with DESeq2," *Genome Biology*, vol. 15, no. 12, p. 550, 2014.

[33] J. Rossello, A. Lima, M. Gil et al., "The EAL-domain protein FcsR regulates flagella, chemotaxis and type III secretion system in *Pseudomonas aeruginosa* by a phosphodiesterase independent mechanism," *Scientific Reports*, vol. 7, no. 1, p. 10281, 2017.

[34] P. C. Carvalho, J. S. Fischer, T. Xu, J. R. Yates, and V. C. Barbosa, "PatternLab: from mass spectra to label-free differential shotgun proteomics," *Current Protocols in Bioinformatics*, vol. 40, no. 1, 2012.

[35] P. C. Carvalho, D. B. Lima, F. V. Leprevost et al., "Integrated analysis of shotgun proteomic data with PatternLab for proteomics 4.0," *Nature Protocols*, vol. 11, no. 1, pp. 102–117, 2016.

[36] P. C. Carvalho, J. R. Yates 3rd, and V. C. Barbosa, "Improving the TFold test for differential shotgun proteomics," *Bioinformatics*, vol. 28, no. 12, pp. 1652–1654, 2012.

[37] K. J. Livak and T. D. Schmittgen, "Analysis of relative Gene expression data using real-time quantitative PCR and the 2 (-delta delta C(T)) method," *Methods*, vol. 25, no. 4, pp. 402–408, 2001.

[38] W. Chaabane, S. D. User, M. El-Gazzah et al., "Autophagy, apoptosis, mitoptosis and necrosis: interdependence between those pathways and effects on cancer," *Archivum Immunologiae et Therapiae Experimentalis*, vol. 61, no. 1, pp. 43–58, 2013.

[39] M. Corte-Rodriguez, M. Espina, L. M. Sierra et al., "Quantitative evaluation of cellular uptake, DNA incorporation and adduct formation in cisplatin sensitive and resistant cell lines: comparison of different Pt containing drugs," *Biochemical Pharmacology*, vol. 98, no. 1, pp. 69–77, 2015.

[40] P. Garcia-Huertas, A. M. Mejia-Jaramillo, C. R. Machado, A. C. Guimaraes, and O. Triana-Chavez, "Prostaglandin F2 alpha synthase in *Trypanosoma cruzi* plays critical roles in oxidative stress and susceptibility to benznidazole," *Royal Society Open Science*, vol. 4, no. 9, Article ID 170773, 2017.

[41] A. Verma, V. Bhandari, D. K. Deep et al., "Transcriptome profiling identifies genes/pathways associated with experimental resistance to paromomycin in Leishmania donovani," *International Journal for Parasitology: Drugs and Drug Resistance*, vol. 7, no. 3, pp. 370–377, 2017.

[42] J. A. Atwood 3rd, D. B. Weatherly, T. A. Minning et al., "The *Trypanosoma cruzi* proteome," *Science*, vol. 309, no. 5733, pp. 473–476, 2005.

[43] L. M. F. de Godoy, F. K. Marchini, D. P. Pavoni et al., "Quantitative proteomics of *Trypanosoma cruzi* during metacyclogenesis," *Proteomics*, vol. 12, no. 17, pp. 2694–2703, 2012.

[44] R. F. S. Menna-Barreto, D. G. Beghini, A. T. S. Ferreira, A. V. Pinto, S. L. De Castro, and J. Perales, "A proteomic analysis of the mechanism of action of naphthoimidazoles in *Trypanosoma cruzi* epimastigotes in vitro," *Journal of Proteomics*, vol. 73, no. 12, pp. 2306–2315, 2010.

[45] G. V. Brunoro, V. M. Faca, M. A. Caminha et al., "Differential gel electrophoresis (dige) evaluation of naphthoimidazoles mode of action: a study in *trypanosoma cruzi* bloodstream trypomastigotes," *PLoS Negl Trop Dis*, vol. 10, no. 8, Article ID e0004951, 2016.

[46] L. Koreny, R. Sobotka, J. Kovarova et al., "Aerobic kinetoplastid flagellate Phytomonas does not require heme for viability," *Proceedings of the National Academy of Sciences*, vol. 109, no. 10, pp. 3808–3813, 2012.

[47] A. F. Francisco, S. Jayawardhana, M. D. Lewis et al., "Nitroheterocyclic drugs cure experimental *Trypanosoma cruzi* infections more effectively in the chronic stage than in the acute stage," *Scientific Reports*, vol. 6, no. 1, Article ID 35351, 2016.

[48] I. Pena, M. Pilar Manzano, J. Cantizani et al., "New compound sets identified from high throughput phenotypic screening against three kinetoplastid parasites: an open resource," *Scientific Reports*, vol. 5, no. 1, p. 8771, 2015.

[49] B. Zingales, R. G. A. Araujo, M. Moreno et al., "A novel ABCG-like transporter of *Trypanosoma cruzi* is involved in natural resistance to benznidazole," *Memórias Do Instituto Oswaldo Cruz*, vol. 110, no. 3, pp. 433–444, 2015.

[50] S. Khare, A. S. Nagle, A. Biggart et al., "Proteasome inhibition for treatment of leishmaniasis, Chagas disease and sleeping sickness," *Nature*, vol. 537, no. 7619, pp. 229–233, 2016.

[51] H. Li, A. J. O'Donoghue, W. A. van der Linden et al., "Structure- and function-based design of Plasmodium-selective proteasome inhibitors," *Nature*, vol. 530, no. 7589, pp. 233–236, 2016.

Dear Dr. Mosquillo,

At Hindawi, we place the researcher at the heart of everything we do. We understand that your research journal doesn't stop at the point of publication, and we want to continue to recognize the hard work and achievements of the research community.

What is the Article of the Year Award?

We are therefore delighted to introduce Hindawi's **Article of the Year Award**. We asked our Chief Editors to select original research or review articles published in 2020 which they consider to be exciting and impactful, as well as representative of their journal's research community and its current or future directions.

Article of the Year 2020

We are proud to announce that the winner of the inaugural Article of the Year Award for *Bioinorganic Chemistry and Applications* is:

> High Throughput Approaches to Unravel the Mechanism of Action of a New Vanadium-Based Compound against Trypanosoma cruzi

Dr. Francesco Paolo Fanizzi selected this article for the following reason(s):

> "Following sound bioinorganic chemistry studies on the topic, the article describes a wealth of well-performed biological investigations aimed at understanding the mechanism of action of a Vanadium-based antitrypanosomal drug. The used approach may be of general interest for knowledge advancement in the field and as a methodological example."

To celebrate their outstanding contribution, the authors of the winning article have been rewarded with an article processing charge (APC) waiver on their next submission to the journal.

Please join us in congratulating the authors on their fantastic achievement. We encourage you to read this article yourself to discover why the Chief Editor selected it as the winner.

5 Capítulo II. Análisis metalómico y celular para el estudio del compuesto Pd-dppf-mpo

En este trabajo nos hemos centrado en el análisis del efecto del compuesto Pd-dppf-mpo en la biología celular del parásito. Para este compuesto fue determinado un valor de IC_{50} de 0,30 ± 0,03 µM sobre epimastigotas de la cepa CL Brener y un valor de Índice de selectividad de 83 con respecto al valor de IC_{50} previamente reportado para células VERO. Se observa que el compuesto ofrece capacidad tripanocida a 5 y 10x IC_{50} luego de sólo 4 horas de incubación, ya que los parásitos no son capaces de retomar su proliferación en un medio libre de compuesto. Los datos metalómicos muestran que con esas concentraciones se observa una incorporación de entre 12 y 16% en los parásitos y una asociación preferencial con el ADN, mediante medidas directas de Pd por espectrometría de absorción atómica electrotérmica. La estructura del compuesto incluye un átomo de hierro (dppf), que guarda una relación estequiométrica de 1:1 con el elemento Pd. La cuantificación simultánea del Fe y el metal central Pd por espectroscopía de absorción atómica corrobora esta relación estequiométrica, verificando una alta estabilidad de los compuestos en el medio biológico y la integridad del compuesto al ingresar a los parásitos o al asociarse a macromoléculas. Mediante microscopía electrónica de barrido se observa la disminución del cuerpo celular en parásitos tratados 5 y 10x IC_{50} luego de 6 horas de incubación. Los análisis de citometría de flujo demuestran la inducción de necrosis luego de 24 horas de tratamiento a altas concentraciones, y se verifica que el mecanismo no afecta la función mitocondrial mediante el uso de una sonda que sensa su potencial de membrana. Este compuesto es capaz de afectar el proceso de infección y la persistencia de la misma en monocapas de células de mamíferos. En primer lugar, se demuestra que disminuye de forma significativa el número de células infectadas por tripomastigotas celulares cuando estos son incubados apenas 30 minutos con el compuesto, y se reduce el número de amastigotas intracelulares. Por su parte, fue demostrada también su capacidad de disminuir el número de amastigotas en una infección ya establecida, por lo que el compuesto es capaz de alcanzar a los parásitos intracelulares y disminuir su número mediante un proceso no dilucidado, que puede ser por muerte celular o inhibición de la proliferación. Globalmente, los resultados aquí presentados demuestran que este compuesto podría ser un potencial compuesto antichagásico, por lo que resulta fundamental profundizar en su estudio.

Los resultados del efecto biológico del compuesto Pd-dppf-mpo se encuentran recopilados en el artículo titulado “Effect of a new anti-*T. cruzi* metallic compound based on palladium” publicado en la revista Biometals en el año 2018.

Biometals
https://doi.org/10.1007/s10534-018-0140-4

Effect of a new anti-*T. cruzi* metallic compound based on palladium

M. Florencia Mosquillo · Lucía Bilbao · Fabricio Hernández · Ignacio Machado · Dinorah Gambino · Beatriz Garat · Leticia Pérez-Díaz

Received: 14 June 2018 / Accepted: 21 August 2018

Abstract Chagas disease is a neglected tropical disease caused by the protozoan parasite *Trypanosoma cruzi*. It is estimated that 6 million people are infected in Latin America. Current treatment is not effective due to the severe side effects and the limited efficacy towards the chronic phase of the disease. Considering the growing need for specific anti-*Trypanosoma cruzi* drugs, organometallic Pt and Pd based compounds were previously synthesized. Although the Pt-based compound effects on *T. cruzi* death have been reported, no mechanism of action has been proposed for the Pd-based analogous compound. In this work, we determined excellent to very good values of IC_{50} and SI. To analyze the compound mode of action, we measured Pd uptake and its association to the macromolecules of the parasite by electrothermal atomic absorption spectrometry. We found a poor uptake, which reaches only 16% after 24 h of incubation using $10\times$ IC_{50}, being the scarce incorporated metal preferentially associated to DNA. However, this compound has a trypanocidal effect, leading to morphological changes such as shortening of the parasite cell body and inducing necrosis after 24 h of treatment. Furthermore, this compound impairs the parasite development in the host both at the trypomastigote infection process and the intracellular amastigotes replication. In conclusion, our findings support that Pd-dppf-mpo compound constitutes a promising anti-*T. cruzi* compound effective against the chronic phase of the disease.

Keywords *Trypanosoma cruzi* · Pd-based compound · Cell death mechanism · Morphological changes

M. F. Mosquillo · L. Bilbao · F. Hernández · B. Garat · L. Pérez-Díaz (✉)
Laboratorio de Interacciones Moleculares, Facultad de Ciencias, Universidad de la República, Iguá 4225, 11400 Montevideo, Uruguay
e-mail: lperez@fcien.edu.uy

I. Machado
Área de Química Analítica, Facultad de Química, Universidad de la República, Montevideo, Uruguay

D. Gambino
Área de Química Inorgánica, Facultad de Química, Universidad de la República, Gral. Flores 2124, 11800 Montevideo, Uruguay

Introduction

Chagas disease, also known as Human American trypanosomiasis, is a tropical parasitic illness caused by the infection with the protozoan parasite *Trypanosoma cruzi*. This debilitating illness constitutes an important public health problem with a high economic burden. It is endemic in 21 Latin American countries and about 6–7 million people worldwide are estimated to be infected by the parasite which is

Published online: 26 September 2018

mainly transmitted to humans by insect vector bites (WHO 2016). However, the number of reported cases has been increasing in the United States of America, Canada, many European and some Western Pacific countries. These reported cases in non-endemic countries are rising mainly due to population migration from Latin America to the rest of the world (Munoz et al. 2009; Salvador et al. 2014; Schmunis and Yadon 2010; Traina et al. 2017) opening the way for other transmission routes also considered of epidemiological importance such as blood transfusion or organ transplantations (Bermudez et al. 2016; Coura 2015).

Trypanosoma cruzi has a complex life cycle, with infective and non-infective, as well as replicative and non-replicative developmental stages alternating between insect vectors (blood-sucking triatomine bugs) and mammalian hosts (Tyler and Engman 2001). Non-replicative metacyclic trypomastigotes in the insect feces are phagocyted by macrophages in the mammal host where they differentiate into replicative intracellular amastigotes. The amastigotes multiply inside the cell by binary fission until they differentiate into trypomastigotes which are released to the bloodstream after cell lysis being able to infect new cells or to be taken by an insect in a bloodmeal.

The disease occurs in two phases: a short initial acute phase and a chronic phase. The acute phase is characterized by a high number of parasites circulating in the blood. This phase is in most cases asymptomatic and normally goes undiagnosed, but sometimes can be accompanied by fever, headache and even death specially in immunosuppressed patients and children. After the acute phase, infected patients enter in a chronic phase where parasites are hidden intracellularly mainly in cardiomyocytes and cells of digestive muscle producing cardiac arrhythmias and progressive heart failure, and less frequently, the digestive form of the disease (Rassi et al. 2010; WHO 2016).

This morbid illness is considered one of the Neglected Tropical Diseases because no effective treatment is available neither exists an effective vaccine (Hotez et al. 2007). Chemotherapy is currently the only method available to treat infected people. Until now, only two old nitro-heterocyclic drugs have been used empirically for treatment of infected patients: Nifurtimox and Benznidazol (Salomon 2012). However, drawbacks such as the inefficacy of these treatments specially in the acute phase and the severe associated side effects specially in immunosuppressed patients and children have been pointed out (Viotti et al. 2009). In this context the development of therapies based in new drugs remains challenging.

Some new drug candidates have been tested including napthoquinones, diamidines, nitroimidazoles as well as vanadium and ruthenium complexes. Nevertheless, the quality of most assessed compounds was poor and often associated with potential or demonstrated toxicity (Buckner and Navabi 2010; Demoro et al. 2013; Silva et al. 2010; Soeiro Mde and de Castro 2011). Clinical studies have also been performed to evaluate the efficacy of benznidazole and two ergosterol biosynthesis inhibitors, posaconazole and ravuconazole in chronic patients as potential drugs, on the basis of murine model data (Molina et al. 2014) as well as in humans (Morillo et al. 2017). However, posaconazole failed to provide significant reduction in circulating parasites in clinical trials being long-term ineffective in asymptomatic *T. cruzi* carriers, and other triazoles like ravuconazole were not superior to benznidazole (Urbina 2010). Moreover, no advantages were observed with combined therapy (posaconazole and benznidazole) *versus* benznidazole monotherapy. Therefore, there is an urgent need for safe and efficacious drug treatments for Chagas disease.

In previous work, two organometallic compounds based on platinum and palladium, 1,1′-bis(diphenylphosphino) ferrocene pyridine-2-thiolate-1-oxide Pt(II) hexafluorophosphate, Pt-dppf-mpo, and 1,1′-bis(diphenylphosphino) ferrocene pyridine-2-thiolate-1-oxide Pd(II) hexafluorophosphate, Pd-dppf-mpo, were synthesized and characterized (Rodriguez Arce et al. 2015). In both compounds, the Pd(II) and Pt(II) central ions are in a nearly planar trapezoidal *cis*-coordination bound to the pyridine-2-thiolate-1-oxide (mpo) and to the 1,1′-bis(diphenylphosphino)ferrocene molecules, both acting as bidentate ligands (Fig. 1). The Pt based compound induced parasite necrosis and esterase activity rise, showing an excellent anti-trypanosomal activity even in the intracellular stage of the parasite with low cytotoxicity for cultured mammal cells (Mosquillo et al. 2018). Regarding the Pd-dppf-mpo compound, although previous analyses have shown an antitrypanosomal activity in Dm28c *T. cruzi* cultures with low IC_{50} values and an impairment of the parasite fumarate reductase activity (Rodriguez Arce et al.

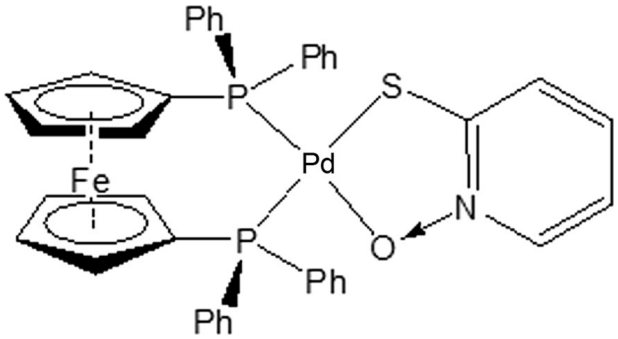

Fig. 1 Organometallic compound, 1,1′-bis(diphenylphosphino) ferrocene pyridine-2-thiolate-1-oxide Pd(II) hexafluorophosphate (Pd-dppf-mpo)

2015), the mechanism of action underlying its antiproliferative effect against *T. cruzi* and the type of death induced remained unexplored.

In this work, we focused on the analysis of the effect of Pd-dppf-mpo compound in the parasite cell biology using the CL Brener *T. cruzi* reference strain. We firstly determined the IC_{50} and the SI value comparing with mammalian cells. We then analyzed the metal uptake percentage in epimastigotes as well as its differential association with different macromolecules inside the parasite. In addition, the morphological changes of treated parasites and the induced cell death mechanism were evaluated. Finally, we studied the effect of the Pd compound in the trypomastigote infection process as well as in the persistence of intracellular amastigotes. Overall, results here presented led to propose this palladium-based compound as a highly promising anti-*Trypanosoma cruzi* agent with low IC_{50} values for intracellular as well as for the insect stage form of the parasite.

Materials and methods

Drugs and dilutions

Compound 1,1′-bis(diphenylphosphino) ferrocene pyridine-2-thiolate-1-oxide Pd(II) hexafluorophosphate was synthetized and purified as previously reported (Rodriguez Arce et al. 2015), dissolved in DMSO (Sigma) prior to use, and then diluted in culture medium. The final concentration of DMSO was less than 0.4% in all experiments.

Parasites and VERO cells culture

Epimastigote forms of *Trypanosoma cruzi* strain CL Brener were maintained in culture in mid-exponential growth phase (2×10^7 parasites/mL). Cultures were diluted 1/10 with fresh BHI medium (Oxoid) supplemented with 10% heat inactivated fetal bovine serum, penicillin (100 units/mL) and streptomycin (100 µg/mL) every 3 days and maintained at 28 °C.

VERO cells were maintained in RPMI medium (Gibco) supplemented with 10% heat inactivated fetal bovine serum, penicillin (100 units/mL) and streptomycin (100 µg/mL) at 37 °C in a humidified 5% CO_2 incubator. Confluent cells were PBS washed, trypsinized, diluted and re-plated for maintenance.

For trypomastigote and amastigote recovery, late stationary phase epimastigotes were used to infect VERO cells. After 6–7 days post-infection, cellular trypomastigotes were obtained from the supernatant. Cell derived trypomastigotes were used to infect 50% confluent VERO cells in a 10:1 rate. In this case, cell derived trypomastigotes were recover from the supernatant after 96 h post infection. Intracellular amastigotes were evaluated 24–48 h post infection.

Antiproliferative activity of Pd-dppf-mpo in vitro

Trypanosoma cruzi epimastigote cultures were set up with an initial concentration of 5×10^6 parasites/mL and incubated with growing concentrations of palladium derived compound solubilized in DMSO. To assess cell proliferation, cell density was monitored at 595 nm at time 0 (A_{0p}) and 5 days post incubation (A_p). All measures were normalized to control population at day 0 (A_{c0}) and at day 5 (A_{c5}). Control parasites were incubated with 0.4% DMSO, corresponding to the highest DMSO concentration of the well. The percentage of parasite proliferation was calculated as: $(A_p - A_{0p})/(A_c - A_{0c}) \times 100$. This assay was independently performed six times. The inhibitory concentration of the drug required to reduce parasite proliferation by 50% (IC_{50}) was calculated by nonlinear regression analysis using GraphPad Prism version 6.00 for Windows, GraphPad Software, La Jolla California USA, www.graphpad.com.

For infection analysis, cell derived trypomastigotes were preincubated for 30 min with Pd based compound in concentrations corresponding to 1×, 5× and 10× the IC_{50} value calculated for epimastigotes.

Immediately, pre-treated parasites were used to infect semiconfluent VERO cells in presence of the Pd-dppf-mpo compound. After 24 and 48 h post infection, cells were washed with 1× phosphate-buffered saline (PBS), fixed with 4% paraformaldehyde, and DAPI stained. The percentage of infected cells over total cells, as well as the number of amastigotes per cell was counted for each Pd-dppf-mpo concentration tested and normalized against control untreated parasites. At least 500 cells were counted in each of two independent infections with trypomastigotes pre-treated with 1×, 5× and 10× the IC_{50} value.

For infection persistence analysis, already infected VERO cells were incubated with Pd based compound in concentrations corresponding to 1×, 5× and 10× the IC_{50} value calculated for epimastigotes. After 24 and 48 h post compound incubation, cells were PBS washed, fixed with 4% paraformaldehyde, and DAPI stained. The number of amastigotes per cell was counted for each Pd-dppf-mpo concentration tested and normalized against control untreated infected cells. At least 500 cells were counted in each of two independent experiments.

A given compound is considered as trypanocide if after 4 h of drug treatment, parasites are unable to resume growth when transferred to drug-free medium. Otherwise, the compound is considered trypanostatic. Epimastigotes cultured at a cell density of 1×10^6 parasites/mL, were incubated with 1×, 5× and 10× the IC_{50} value of Pd-dppf-mpo compound (0.3, 1.5 and 3 μM) for 4 h. After drug incubation, parasites were collected by centrifugation at 2000×*g* for 10 min, washed with fresh BHI medium and transferred to fresh, drug-free BHI medium. Relative growth was obtained by determining the ratio between the cell density at 595 nm in drug incubated cultures and cell density in control cultures by absorbance measures at 595 nm for 24, 48 and 72 h.

Uptake and macromolecules association

To determine the uptake percentage of palladium compound, parasites at a density of 1×10^7 parasite/mL were incubated in the presence of 1×, 5× and 10× the IC_{50} value of Pd-dppf-mpo compound. Parasites were collected at the indicated time points between 0 and 24 h. Each sample (8×10^7 total parasites) was centrifugated at 1000×*g* for 10 min and the pellet was washed with PBS and resuspended in the same buffer. Pellet containing incubated parasites and supernatant containing uncaptured compound were analyzed by electrothermal atomic absorption spectrometry in a spectrophotometer Thermo iCE 3500 (Thermo Fisher Scientific). The uptake percentage of palladium in the parasites was determined according to the following equation: % entry = [P]/[P] + [S], where [P] is palladium concentration in pellet, [S] is palladium concentration in supernatant and [P] + [S] is total concentration of metal incorporated into the experiment (supernatant plus pellet). Two independent experiments at 6 different time points were assayed for each Pd-dppf-mpo concentration: 1×, 5× and 10× IC_{50}. The palladium compound Pd-dppf-mpo (Fig. 1) shows an equimolar amount of Pd and Fe (present in the ferrocene moiety). Therefore, to verify that this palladium species remained intact when being taken up by the parasite, the amount of Fe taken up by the cells was simultaneously measured by atomic absorption spectroscopy. A stoichiometric relationship of Fe to Pd should be observed.

Palladium association with DNA, RNA, soluble and insoluble proteins was analyzed using mid exponential phase parasites incubated with 1×, 5× and 10× the IC_{50} calculated value. After 6 h of incubation, ~~3×10^7~~ parasites were collected for DNA isolation 4x 10^7 using Wizard® Genomic DNA Purification Kit (Promega). Total RNA was isolated using TRIzol Reagent (Life Technologies) starting from 4×10^7 parasites. For protein isolation, 4×10^7 parasites were resuspended in 1 mL of Parasite Lysis Buffer containing Tris–Cl 10 mM pH 7.5, EDTA 1 mM, CHAPS 1%, glycerol 10%, Triton 0.5%, and Complete™ Protease Inhibitor Cocktail (Roche). After 30 min of stirring on ice, the lysate was centrifugated for 1 h at 4 °C at 20,000 g. The soluble proteins were isolated from the supernatant and the insoluble ones from the pellet, which were resuspended in 0.5 mL of PBS for further analysis. Two independent experiments were performed for all palladium analytical determinations, duplicates were made. The samples were analyzed by electrothermal atomic absorption spectrometry in a Thermo iCE 3500 spectrophotometer (Thermo Fisher Scientific).

Morphology analysis

For the observation of morphological changes in epimastigotes, after treatment with 1×, 5× and 10×

the calculated IC_{50} value, 1×10^6 parasites were examined in culture using a microscope coupled to a Canon PowerShot A95 digital camera. Images were processed with Adobe Photoshop CS2 software to improve brightness and contrast. Parasites were classified as normal or rounded. At least 200 parasites were counted per experiment in two independent assays.

For scanning electron microscopy 1×10^6 parasites in exponential growth phase were washed with PBS and fixed with 4% paraformaldehyde. The samples were then subjected to dehydration with increasing concentration of acetone (30–100%) and gold coated in the metallizer Sputter Coater SCD050/LEICA. After metallization, samples were observed in a scanning electron microscopy (Philips XL30, Eindhoven, The Netherlands).

Flow cytometric analysis of cell death mechanism

Flow cytometry experiments were performed in a BD Accuri C6 flow cytometer (BD Biosciences). Cell death mechanism analysis was evaluated using Alexa Fluor® 488 Annexin V/Dead Cell Apoptosis Kit (Thermo Fisher Scientific) following manufacturer instructions. Dual parameter analysis was performed using a 533/30 nm signal detector (FL1) for annexin V (AV) and a 670 nm long pass for propidium iodide (PI) emission signal detector (FL3). 10,000 events were acquired for two independent samples, and recorded data was analyzed using BD CSampler software (BD Bioscience). Debries were gated out according to light scatter measurements (forward and side scatter). Non-treated parasites were used as control.

Cell viability was assessed with Calcein AM (CA) probe and PI (Thermo Fisher Scientific). Pd-dppf-mpo treated and untreated control parasites were incubated for 60 min with CA 0.1 mM and PI 10 mg/mL at RT. Dual parameter analysis was performed using a 533/30 nm band-pass filter (FL1) for CA and a 670 nm band-pass filter (FL3) for PI. Two independent samples were assayed for each condition and 10,000 events were acquired per experiment.

Changes in mitochondrial membrane potential ($\Delta\psi m$) were performed using the cationic carbocyanine dye JC-1 (Molecular Probes). Pd-dppf-mpo treated and control untreated parasites were washed with 0.1 M PBS and incubated with JC-1 dye at a final concentration of 6 μM. Parasites were kept in the dark for 20 min at RT, washed twice in 0.1 M PBS and evaluated by flow cytometry to detect the aggregated form of JC-1 with a band-pass filter of 590 nm (FL2) and the fluorescence of monomeric form of JC-1 with a 533/30 nm band-pass filter (FL1). Data was analyzed with BD CSampler™ software (BD). Two independent experiments were acquired for 10,000 events each one. The ratio between red/green fluorescence intensities (590 nm/530 nm) was analyzed through fluorescence measures in a Varioskan Flash Spectral Scanning (Thermo Scientific) at 590 and 530 nm. Three replicates for two independent experiments were performed in Pd based compound treated parasites and control untreated parasites labeled with JC-1 probe as indicated previously.

Results and discussion

Pd-dppf-mpo constitutes a dose dependent trypanocydal agent of *T. cruzi* epimastigote

With the aim to study the effect of Pd-dppf-mpo compound in the proliferation of *T. cruzi* epimastigotes of the CL Brener reference strain, we sought to firstly determine its IC_{50} value. Incubation of mid-exponential growth phase epimastigotes with increasing amounts of Pd-dppf-mpo compound (from 0.2 to 0.7 μM) resulted in a concentration-dependent proliferation inhibition (Fig. 2a). The IC_{50} calculated at 5 days was estimated in 0.30 ± 0.03 μM (Fig. 2a). This value is almost two times lower than the IC_{50} reported for the Dm28c strain (0.64 ± 0.03 μM) (Rodriguez Arce et al. 2015) suggesting that CL Brener, which belongs to a different genetic lineage (type VI), is a more susceptible strain than the type I Dm28c strain. It is well known that genetic diversity can explain the different clinical manifestations of the illness, different tissue tropisms, virulence and differences in morbidity and mortality as well as different susceptibility to different drugs (Macedo et al. 2004; Manoel-Caetano Fda and Silva 2007).

Based on the IC_{50} value previously reported for this compound in VERO cells (24.5 ± 12.2 μM) (Rodriguez Arce et al. 2015), a selectivity index (SI) of 83 could be calculated for the CL Brener strain. Comparing with the reference drug Nifurtimox in the CL Brener strain, which exhibit an IC_{50} value of

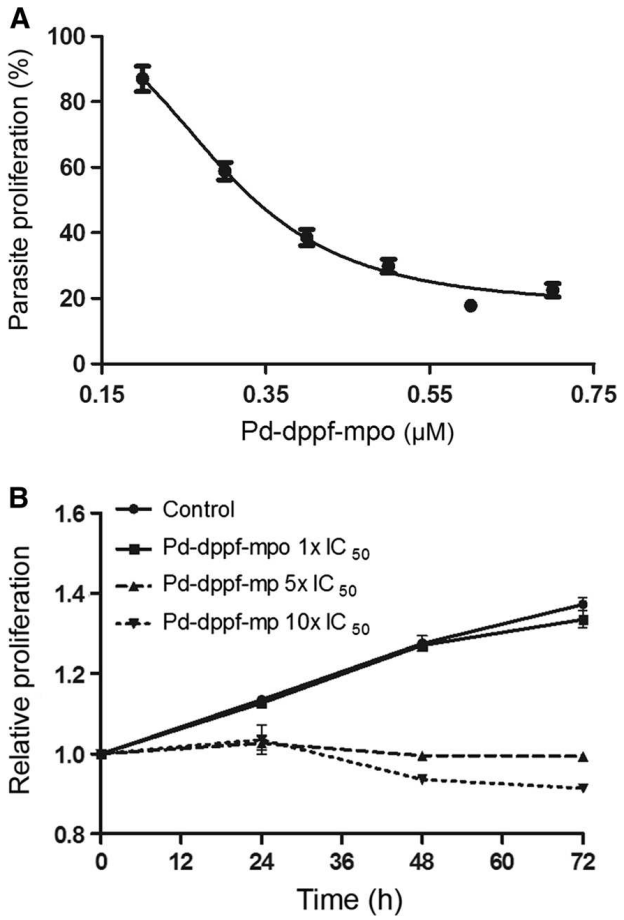

Fig. 2 Antiproliferative effect of Pd-dppf-mpo in *T. cruzi* epimastigotes. **a** Proliferation inhibition curve of cultured *T. cruzi* CL Brener epimastigotes exposed to different concentrations of Pd-dppf-mpo. The IC_{50} value was calculated from the dose–response by nonlinear regression analysis using GraphPad Prism software (GraphPad Prism version 6.00 for Windows, GraphPad Software, La Jolla California USA). Each experiment was performed six times and the mean and standard deviation for each point are represented. **b** Recovery experiments using *T. cruzi* CL Brener epimastigotes exposed for 4 h to Pd-dppf-mpo concentrations corresponding to 1×, 5× and 10× the calculated IC_{50} value and control untreated epimastigotes. After compound removal by successive washes, the subsequent growth of the parasites was followed by optic density measures at 595 nm at the indicated time points. Each experiment was performed in triplicates and the mean and standard deviation is represented for each point

2.76 ± 0.19 μM (Mosquillo et al. 2018) and a SI value of 115 (Fernandez et al. 2013), Pd-dppf-mpo may constitute a good candidate for an antiparasitic new drug.

To discriminate between a trypanostatic or a trypanocide effect of the Pd-dppf-mpo compound, parasite recovery following treatment for the time required for the activation of the programmed cell death pathways (Kessler et al. 2013) were performed. After removing the compound by washing, growth recovery was evaluated transferring treated parasites to a fresh free drug medium. Parasites treated with Pd-dppf-mpo concentrations corresponding to 1× the IC_{50} value, showed a normal growth, similar to the one of untreated control parasites. However, after treatment with 5× and 10× the IC_{50} value, parasites lost their ability to resume growth, even after 48 h of culture (Fig. 2b). This result suggests a trypanocidal effect of Pd-dppf-mpo, which is dependent on

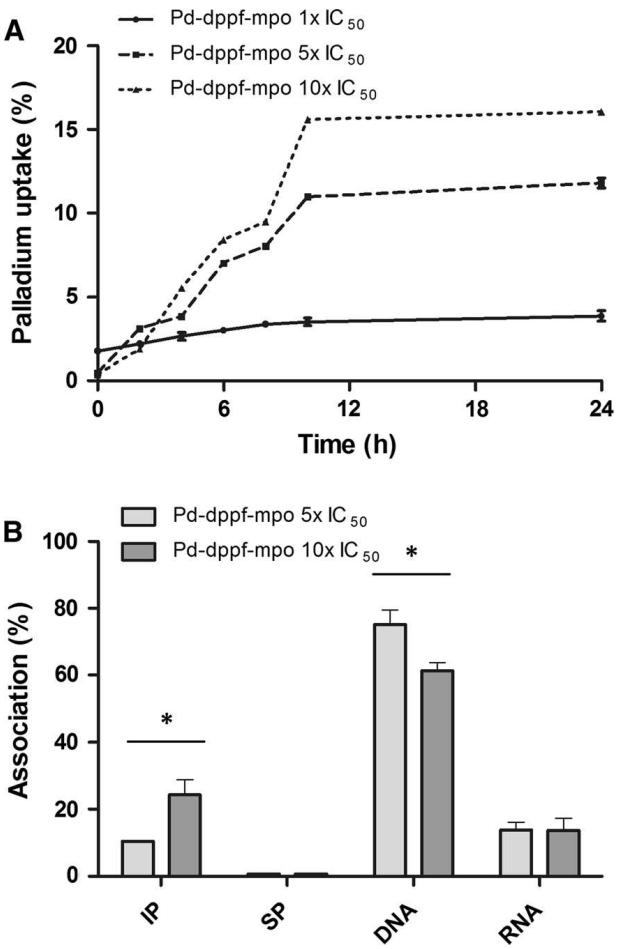

Fig. 3 Pd-dppf-mpo uptake in cultured *T. cruzi* epimastigotes and association with macromolecules. **a** Parasites were incubated with different concentrations of Pd-dppf-mpo (1× IC_{50}, 5× IC_{50} and 10× IC_{50}). Palladium concentration was determined through electrothermal atomic absorption spectrometry at the indicated time points. Two independent experiments were performed and the average for each time is presented. **b** Percentage of palladium associated to the different isolated macromolecules. After 6 h of incubation with 5× and 10× IC_{50}, the average and SD of independent duplicates of metal determinations in DNA, RNA, soluble (SP) and insoluble (IP) protein fractions are shown. ANOVA test: *P value < 0.05

Table 1 Fe and Pd dosification in macromolecules

Macromolecule	Pd (moles)	Fe (moles)	Stoichiometric ratio
Insoluble proteins 5× IC_{50}	4.8E−10	4.7E−10	1.02
Insoluble proteins 10× IC_{50}	1.5E−09	1.4E−09	1.07
Soluble proteins 5× IC_{50}	5.7E−10	5.7E−10	1.00
Soluble proteins 10× IC_{50}	1.1E−09	1.1E−09	1.03
DNA 5× IC_{50}	1.3E−10	1.3E−10	1.00
DNA 10× IC_{50}	1.7E−10	1.8E−10	0.97
RNA 5× IC_{50}	5.0E−11	4.9E−11	1.03
RNA 10× IC_{50}	6.1E−11	6.6E−11	0.92

The average of two independent experiments is shown for each sample in which Pd and Fe were determined independently. The stoichiometric ratio was calculated between these elements

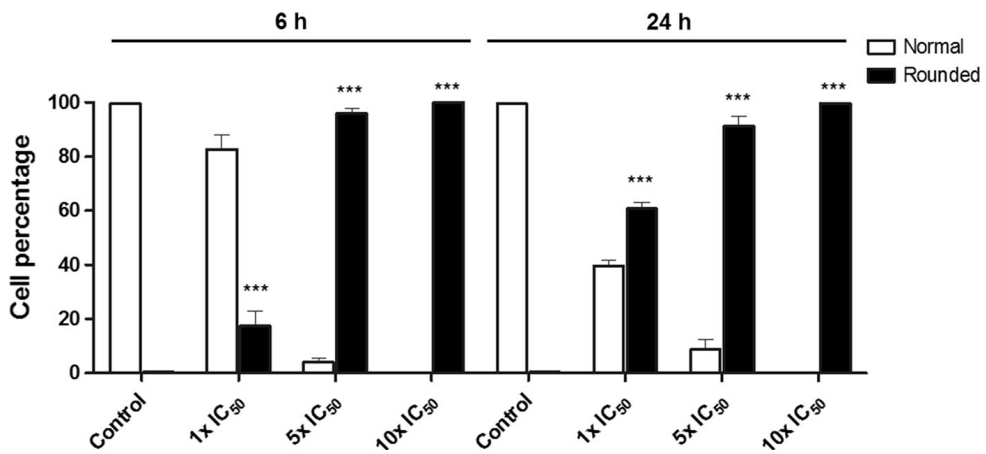

Fig. 4 Pd-dppf-mpo treatment induces morphological changes in *T. cruzi* epimastigotes. Control untreated parasites and parasites treated with the palladium compound 1×, 5× and 10× IC_{50} were analyzed by optic microscopy in culture and classified as normal or rounded after 6 or 24 h of treatment. At least 200 parasites were counted in two independent biological replica and the results are shown as average ± SD for each morphology

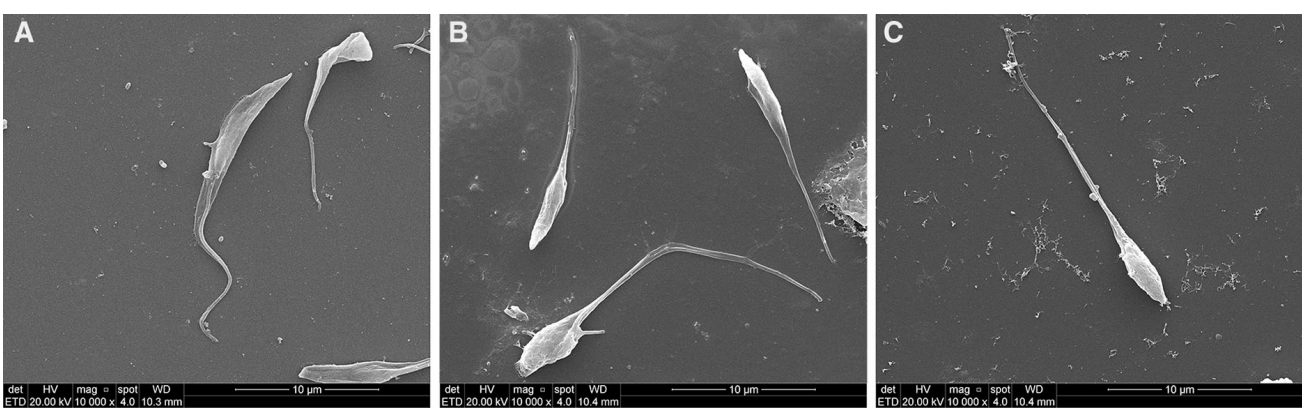

Fig. 5 Ultrastructural effects of Pd-dppf-mpo on *T. cruzi* epimastigotes. Representative images obtained by scanning electron microscopy of control untreated parasites (**a**) and parasites treated with the palladium compound 5× IC_{50} for 6 h (**b**, **c**)

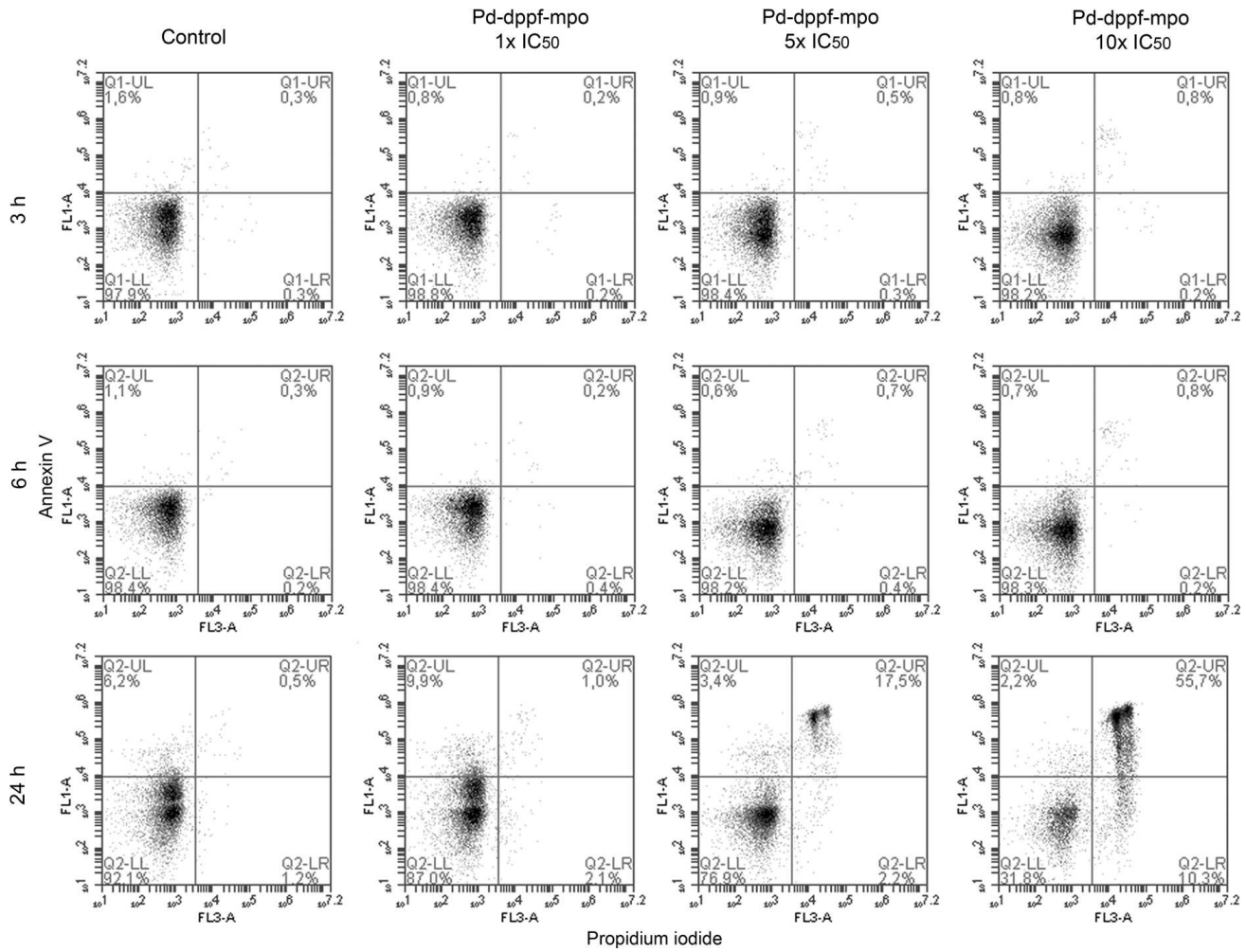

Fig. 6 Analysis of *T. cruzi* epimastigote death mechanism driven by Pd-dppf-mpo. Control untreated parasites as well as Pd-dppf-mpo treated parasites were co-stained with AV and PI to analyze phosphatidylserine exposure and membrane integrity respectively. Parasites were incubated with 1×, 5× and 10× the calculated IC_{50} value for 3, 6 and 24 h. Experiments were performed in duplicates and 10,000 events were acquired in the gated region previously identified as corresponding to epimastigotes in a BD Accuri C6 (BD Biosciences)

compound concentration, leading to the activation of a non-return cell death mechanism.

Pd-dppf-mpo constitutes a dose dependent trypanocydal agent of *T. cruzi* epimastigote with preferred DNA association

In order to determine the palladium uptake, epimastigotes were incubated with Pd-dppf-mpo compound and the amount of palladium strongly bound to and/or taken up by the parasites (not removable by washing) as well as the palladium remaining in the culture medium were determined by atomic absorption spectroscopy. The results of two independent experiments incubating the parasites with increasing amounts of total palladium are shown in Fig. 3a. When using 1× IC_{50} of compound concentration, the metal incorporation percentage increased slowly until 8 h post-incubation and then remained almost constant. After 24 h of incubation, the amount of incorporated palladium reached almost 4% of the initial amount of Pd-dppf-mpo added to the system. The percentage of metal uptake when using higher metal compound concentration corresponding to 5× (1.5 μM) and 10× IC_{50} (3.0 μM) reached almost 12% and 16% of the total Pd compound added, respectively (Fig. 3a).

To analyze the distribution of the metallic compound in the parasite, its association with macromolecules of different nature was evaluated by electrothermal atomic absorption spectrometry

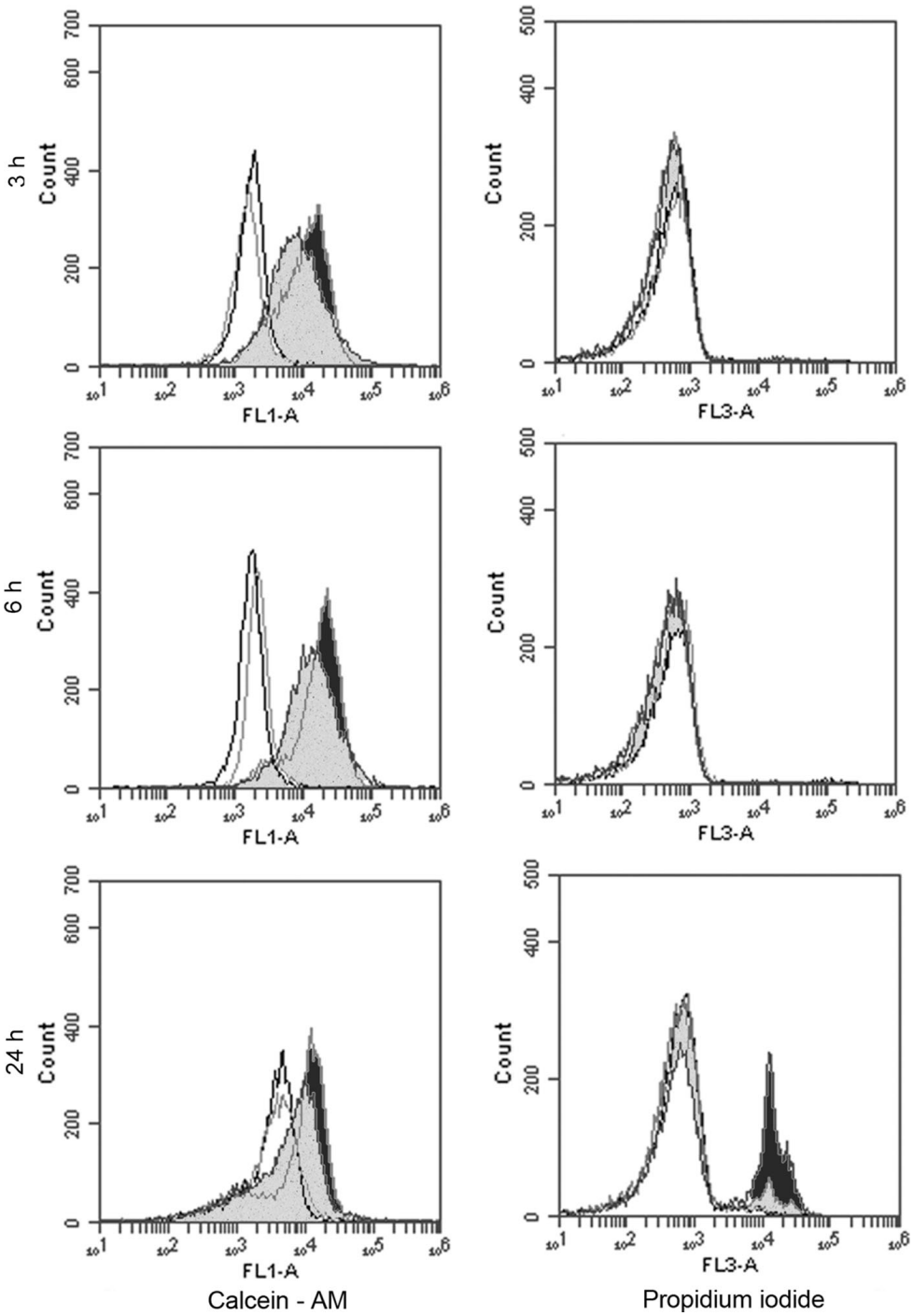

Fig. 7 Analysis of *T. cruzi* epimastigote cell viability during Pd-dppf-mpo treatment. Cell viability was assessed with Calcein AM (CA) probe and PI. Parasites were incubated with 1× IC_{50} (gray lines), 5× IC_{50} (solid pattern line) and 10× IC_{50} (striped pattern line) of Pd-dppf-mpo for 3, 6 and 24 h and labeled with the indicated probes. Untreated parasites were used as control (black lines). All parasites were analyzed by flow cytometry in an Accuri C6 (BD Bioscience). Histograms represent fluorescence intensities of labeled parasites corresponding to one of two experiments performed

(Fig. 3b). While, the amount of associated metal with soluble proteins does not exceed 1% of the captured Pd for both the IC_{50} assayed, the association with insoluble proteins increased from 10 to 24% using 5× and 10× IC_{50}, respectively. On the other hand, approximately 14% of the incorporated palladium is associated with RNA fractions when incubating either with 5× and 10× IC_{50}. But, the preferential association of the compound was observed for the DNA fraction, which show a 61 and 75% of total captured palladium for treatments with 5× and 10× IC_{50}, respectively. The results here presented are in good agreement with previous findings, where complexes with the same ligand but based on a different metal (platinum) exhibit a similar pattern of association (Mosquillo et al. 2018). DNA has been considered

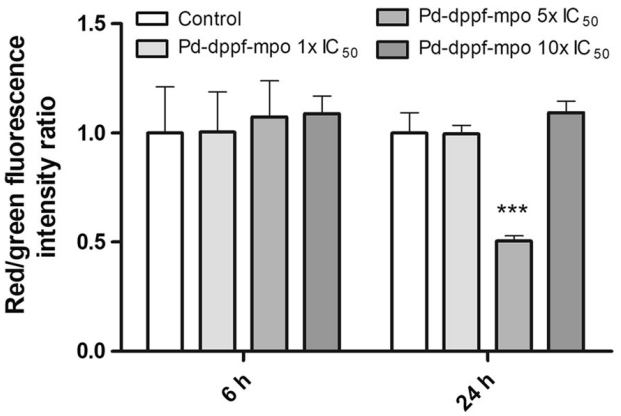

Fig. 8 Evaluation of *T. cruzi* epimastigote mitochondrial membrane integrity during Pd-dppf-mpo treatment. The mitochondrial membrane integrity was evaluated using the lipophilic fluorescence cation dye JC-1 probe. Quantitative analysis of JC-1 dye accumulation was analyzed by fluorescence intensities measures in a Varioskan Flash Spectral Scanning at 590 and 530 nm. Bars represent red/green fluorescence intensity ratio (590/530 nm) after parasite incubation with the palladium compound at 1×, 5× and 10× IC_{50} and control untreated parasites (white bars). Six measures were performed corresponding to two independent experiment, each one with three independent replicates (n = 6). ANOVA test: ***$P < 0.001$

an important target for drug design since this interaction may potentially interfere with gene expression and DNA replication, worsen parasite cell growth and division.

To evaluate if the whole unchanged Pd-dppf-mpo complex is the species taken up by the parasites, Fe uptake (present in the dppf ligand, see Fig. 1) was simultaneously quantified in the same fractions. We found a 1:1 stoichiometric relation between Fe and Pd in each fraction indicating that the compound captured by the macromolecules is the unchanged Pd-dppf-mpo complex (Table 1).

Pd-dppf-mpo causes epimastigote cell shortening

Light microscopy analysis showed that the exposure of *T. cruzi* epimastigotes to 1×, 5× and 10× IC_{50} of Pd-dppf-mpo induced a gradual swelling that leads to parasites with shortened cell bodies as concentration and incubation time increase, even with low concentrations of the compound (Fig. 4). To further analyze the induced morphological changes after 6 h of incubation at 5× IC_{50} scanning electron microscopy was performed. Interestingly, flagella appeared longer in treated parasites compared with control untreated parasites. The increase in flagellum length could not be accounted for an overall increase itself but rather by the reduced size of the cell body, suggesting that Pd-dppf-mpo incubation caused cell body shortening (Fig. 5).

Pd-dppf-mpo induces epimastigote necrosis at high concentration and long incubation periods

Since the incubation with the palladium compound induced morphological changes in the parasites leading to cell death, with no ability to resume growth in a dose dependent manner, we decided to analyze the cell death mechanism involved. For this purpose, we quantified both, the internalization of the vital dye PI and the externalization of phosphatidylserine using AV probe, by flow cytometry. Since plasma membrane rupture is a hallmark of necrotic cell death (Zhang et al. 2018) PI positive cells represent necrotic population. Besides, exposed phosphatidylserine constitutes a hallmark of apoptotic cells and since AV binds phosphatidylserine only when it is exposed to the outer membrane (Fadok et al. 1998), AV positive cells represent early apoptotic population. Double labelling corresponds to late apoptotic/necrotic cells.

As shown in Fig. 6, no cell death mechanism was evidenced with 6 h of compound incubation. Only after 24 h of incubation with 5× and 10× the IC_{50} value, a late apoptotic/necrotic phenotype was evidenced for more than 50% of the treated parasite population, with no evidence of early apoptosis, even at shorter incubation times or at lower Pd-dppf-mpo concentration.

Since other death mechanisms different from apoptosis and necrosis could be present in the unlabeled cells, we also used the CA cell vitality marker followed by flow cytometry analysis to evaluate intracellular esterase activity. Unexpectedly, parasites incubated with 5× and 10× IC_{50}, display an increase in the fluorescence intensity compared to untreated control parasites, even after only 3 h of incubation. This result indicates, not only that the parasites are not dead by another mechanism, but also that treated parasites have an augmented esterase activity, perhaps due to a burst of a defense mechanism against the Pd compound (Fig. 7). No PI labeling differences were observed using 1× IC_{50} for 3 and 6 h, confirming cell membrane integrity of parasites incubated. However, a subpopulation of PI positive parasites can be observed for 5× and 10× IC_{50} at

24 h of incubation. This PI positive population represent the necrotic population previously observed with AV/PI labeling (Fig. 6).

To assess mitochondrial activity, we used the lipophilic fluorescence cation dye JC-1 probe that evaluates mitochondrial membrane integrity. JC-1 is a carbocyanine dye that exists as a monomer at low concentration yielding green color, when the concentration of JC-1 accumulates inside the mitochondria red aggregates are formed. These characteristics make JC-1 a sensitive marker for mitochondrial membrane potential which can be monitored through the red/-green fluorescence ratio. As shown in Fig. 8, changes in mitochondrial potential were only observed for parasites treated with 5× IC_{50} of the Pd-dppf-mpo for 24 h (Fig. 8). No mitochondrial depolarization was observed when incubating parasites for 24 h with 10× the IC_{50} value indicating the involvement of a mitochondrion independent mechanism at high Pd-dppf-mpo concentration.

Pd-dppf-mpo inhibits the trypomastigote infection process and the intracellular amastigotes replication

The infection capacity of cell-derived trypomastigotes pretreated for 30 min with Pd-dppf-mpo was assayed in VERO cells in culture. The number of infected cells were compared with control experiments using untreated cell-derived trypomastigotes. The percentage of infected cells in control experiments were more than 80% after 24 and 48 h (Fig. 9). As seen in

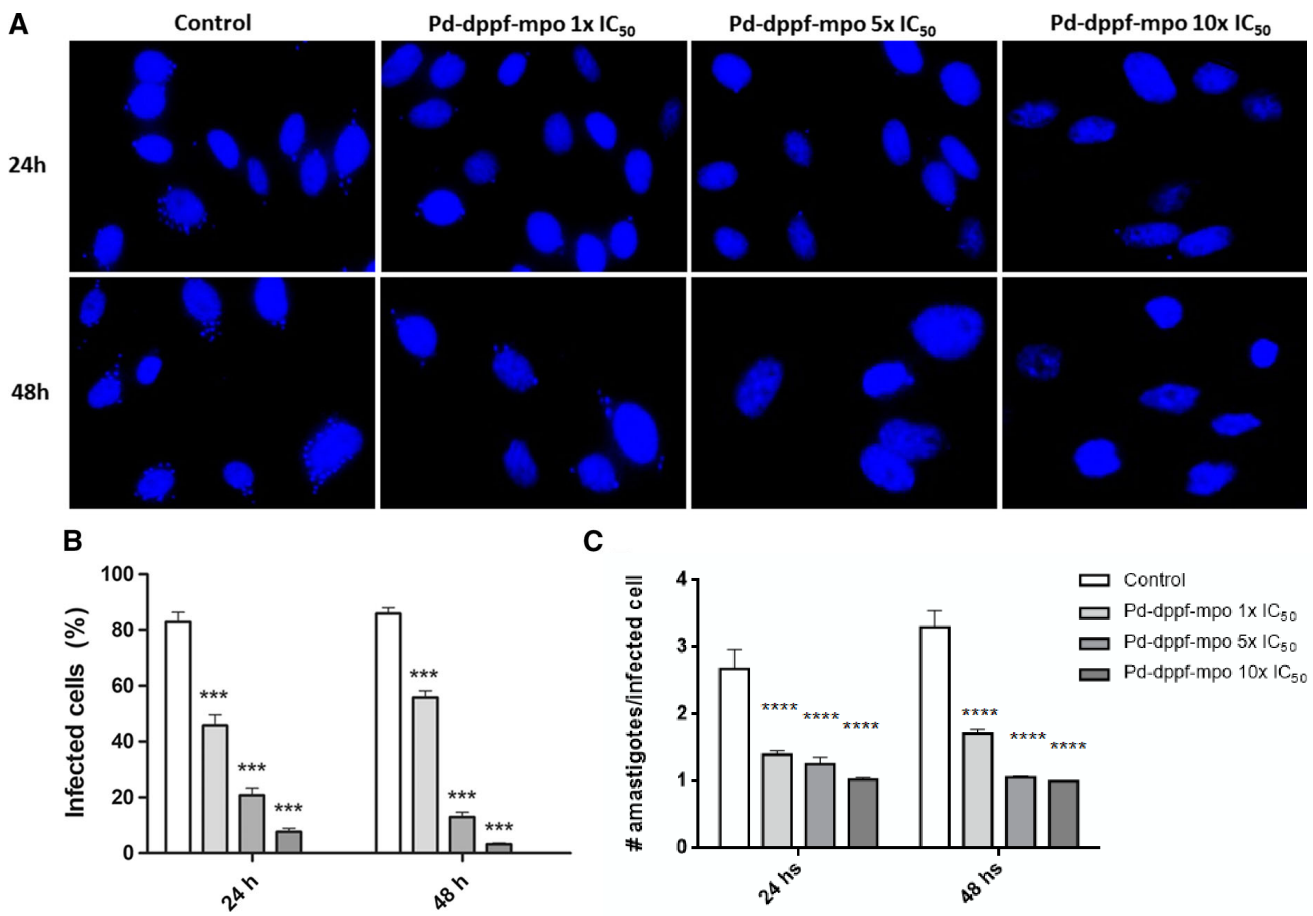

Fig. 9 Effect of Pd-dppf-mpo on the *T. cruzi* infection process. **a** Epifluorescence microscopy of the infection process with trypomastigotes pretreated with the indicated concentrations of Pd-dppf-mpo for 30 min. **b** Normalized number of infected cells using cell-derived trypomastigotes pretreated. Infected and non-infected cells were counted after 24 and 48 h post infection. Bars represent the percentage of infected cells using trypomastigotes incubated with the palladium compound at 1×, 5× and 10× IC_{50}. **c** Normalized number of amastigotes per cell post infection with pre-treated parasites after 24 and 48 h of drug incubation. Bars represent the number of amastigotes per cell treated with the palladium compound at 1×, 5× and 10× IC_{50}. Values were normalized against control untreated parasites. Two independent experiment were performed and at least 200 cells were counted per experiment. ANOVA test: ***$P < 0.001$

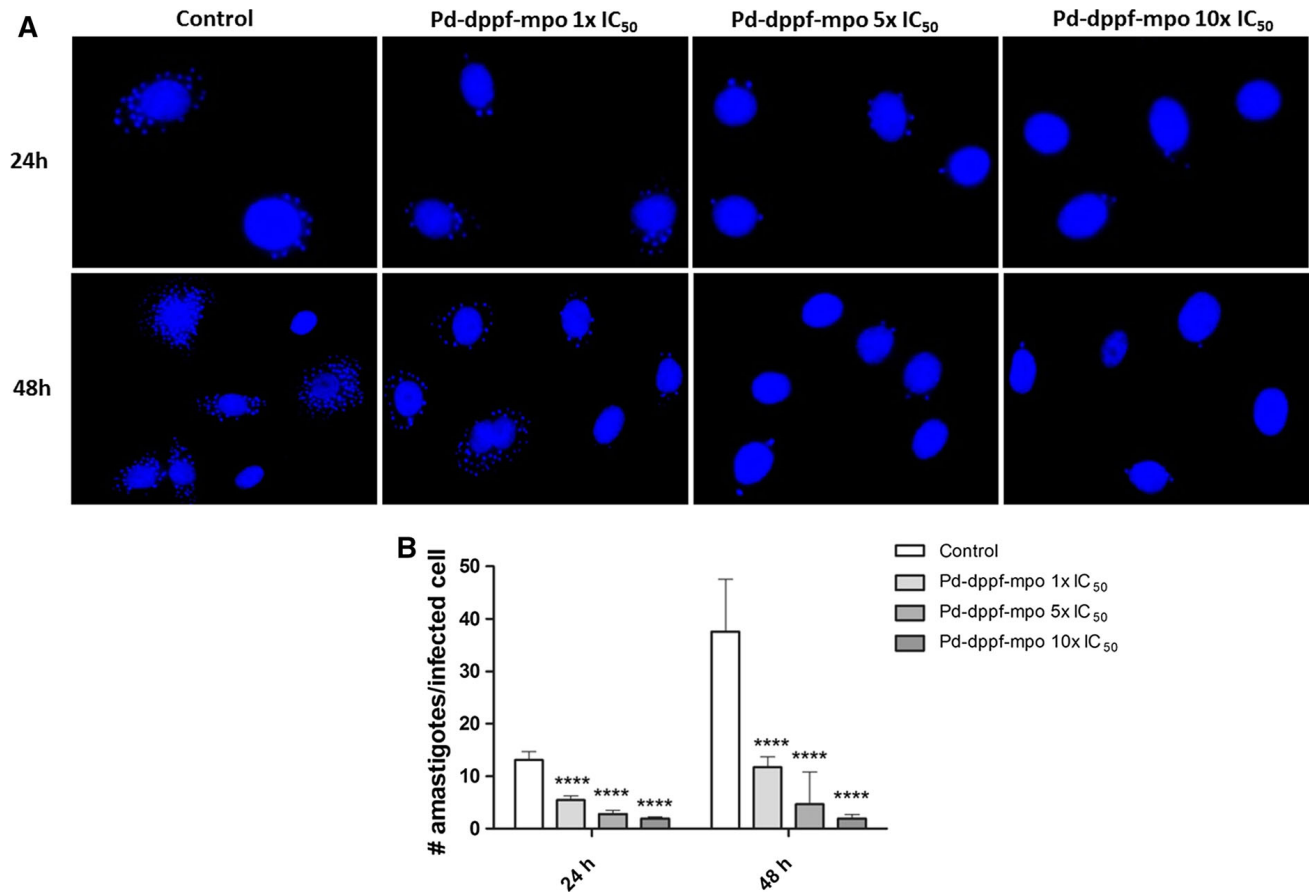

Fig. 10 Effect of Pd-dppf-mpo on the *T. cruzi* infection persistence. **a** Epifluorescence microscopy of the persistence in an established infection on VERO cell monolayers. **b** Number of amastigotes per cell on already infected cells incubated with different concentrations of Pd-dppf-mpo after 24 and 48 h of drug incubation. Bars represent the number of amastigotes per cell treated with the palladium compound at 1×, 5× and 10× IC_{50}. Values were normalized against control untreated parasites. Two independent experiment were performed. In each experiment, at least 200 cells were counted per experiment. ANOVA test: ****$P < 0.0001$

Fig. 9a, after 24 h post infection, a significative lower number of infected cells (less than 50%) were observed for parasites pretreated with the lowest assayed concentration of Pd-dppf-mpo (1× IC_{50}). Using a higher concentration (10× IC_{50}), the percentage of infected cells decrease to 10%. A similar pattern was observed after 48 h post infection. Besides the number of amastigotes per cell was significatively reduced for all the assayed concentrations either after 24 h or 48 h post-incubation in a dose dependent manner (Fig. 9b). These findings suggest that the treatment with Pd-dppf-mpo not only inhibits the infection process, but also the replication of these treated parasites inside the cell in a dose dependent manner.

The persistence of the parasite in an established infection was evaluated using drug free infected monolayers which were then challenged with different concentrations of Pd-dppf-mpo (Fig. 10). After 24 h of incubation, significative decreases of the number of intracellular parasites per cell were observed for all the assayed compound concentrations even for the 1× IC_{50}. This reduction in the number of intracellular amastigotes was more evident after 48 h post incubation comparing with the control infected monolayer without treatment. This finding suggest that the compound is able to reach intracellular parasites affecting their proliferation even at low concentration.

In conclusion, our findings support that Pd-dppf-mpo compound constitutes a promising anti-*Trypanosoma cruzi* compound effective on intracellular amastigotes with a fair SI. Its preferred association with DNA, the induction of necrosis after 24 h of treatment, together with the increase in esterase

activity, resembles the mode of action of the previously studied analogous metal-based compound Pt-dppf-mpo (Mosquillo et al. 2018).

Since these two compounds share the organic ligands it is tempting to hypothesize that there must be a strong contribution of the ligand in the here defined mechanisms of action although the differences in the IC_{50}, in the morphology of treated parasites, as well as in the uptake percentage of the compound, may be the result of the effect of the particular metal. Both metal compounds are structural analogues showing a similar stereochemistry that may conveniently expose the organic ligands but changing the metal center leads to different biological effects. Indeed, lower anti *T. cruzi* activity has been reported for the free mpo moiety (Na mpo IC_{50} 1.33 ± 0.08 μM) that significantly improves when this organic ligand is bound to the M-dppf organometallic moiety, where M = Pd(II) or Pt(II) (Rodriguez Arce et al. 2015). In addition, the inclusion of the ferrocene moiety (dppf ligand) improves the selectivity towards the parasite when compared to the previously reported $[M(mpo)_2]$ complexes (Rodriguez Arce et al. 2015; Vieites et al. 2008). While previous work determined the parasite fumarate reductase as a clear target for the mpo complexes (Merlino et al. 2014; Rodriguez Arce et al. 2015; Vieites et al. 2008) the work here presented suggests the existence of a more complex scenario probably due to the summing up and/or potentiation of the mechanism of action derived from the different moieties contribution. To further understand the implied mode of action and distinguish the peculiarities due to the metal counterpart of the complexes a deeper molecular analysis would be needed. Work is in progress to comparatively determine the transcriptomic and proteomic commonalities and differences exerted by the Pd-dppf-mpo and Pt dppf-mpo complexes on the parasite cells. Globally, the results here presented reinforce the importance of focusing on metal complexes for anti-Chagas drug discovery to fight against the still inefficiently treated chronical phase of the disease.

Acknowledgements This work was supported by Comisión Sectorial de Investigación Científica CSIC-Uruguay [Grant Number INI_2015_362]; Agencia Nacional de Investigación e Innovación ANII [Grant Number POS_FMV_2015_1_1005183]; and Programa de Desarrollo de Ciencias Básicas, Uruguay.

Compliance with ethical standards

Conflict of interest The authors declare that there is no conflict of interest.

References

Bermudez J, Davies C, Simonazzi A, Real JP, Palma S (2016) Current drug therapy and pharmaceutical challenges for Chagas disease. Acta Trop 156:1–16. https://doi.org/10.1016/j.actatropica.2015.12.017

Buckner FS, Navabi N (2010) Advances in Chagas disease drug development: 2009–2010. Curr Opin Infect Dis 23:609–616. https://doi.org/10.1097/QCO.0b013e3283402956

Coura JR (2015) The main sceneries of Chagas disease transmission. The vectors, blood and oral transmissions—a comprehensive review. Mem Inst Oswaldo Cruz 110:277–282. https://doi.org/10.1590/0074-0276140362

Demoro B et al (2013) Potential mechanism of the anti-trypanosomal activity of organoruthenium complexes with bioactive thiosemicarbazones. Biol Trace Elem Res 153:371–381. https://doi.org/10.1007/s12011-013-9653-4

Fadok VA, Bratton DL, Frasch SC, Warner ML, Henson PM (1998) The role of phosphatidylserine in recognition of apoptotic cells by phagocytes. Cell Death Differ 5:551–562. https://doi.org/10.1038/sj.cdd.4400404

Fernandez M et al (2013) A new series of heteroleptic oxidovanadium(IV) compounds with phenanthroline-derived co-ligands: selective *Trypanosoma cruzi* growth inhibitors. Dalton Trans 42:11900–11911. https://doi.org/10.1039/c3dt50512j

Hotez P, Raff S, Fenwick A, Richards F Jr, Molyneux DH (2007) Recent progress in integrated neglected tropical disease control. Trends Parasitol 23:511–514. https://doi.org/10.1016/j.pt.2007.08.015

Kessler RL, Soares MJ, Probst CM, Krieger MA (2013) *Trypanosoma cruzi* response to sterol biosynthesis inhibitors: morphophysiological alterations leading to cell death. PLoS ONE 8:e55497. https://doi.org/10.1371/journal.pone.0055497

Macedo AM, Machado CR, Oliveira RP, Pena SD (2004) *Trypanosoma cruzi*: genetic structure of populations and relevance of genetic variability to the pathogenesis of Chagas disease. Mem Inst Oswaldo Cruz 99:1–12

Manoel-Caetano Fda S, Silva AE (2007) Implications of genetic variability of *Trypanosoma cruzi* for the pathogenesis of Chagas disease. Cad Saude Publica 23:2263–2274

Merlino A, Vieites M, Gambino D, Coitino EL (2014) Homology modeling of *T. cruzi* and L. major NADH-dependent fumarate reductases: ligand docking, molecular dynamics validation, and insights on their binding modes. J Mol Graph Model 48:47–59. https://doi.org/10.1016/j.jmgm.2013.12.001

Molina I et al (2014) Randomized trial of posaconazole and benznidazole for chronic Chagas' disease. N Engl J Med 370:1899–1908. https://doi.org/10.1056/NEJMoa1313122

Morillo CA et al (2017) Benznidazole and posaconazole in eliminating parasites in asymptomatic *T. Cruzi* carriers: the

STOP-CHAGAS Trial. J Am Coll Cardiol 69:939–947. https://doi.org/10.1016/j.jacc.2016.12.023

Mosquillo MFB, Bilbao L, Hernández F, Tissot F, Gambino D, Garat B, Pérez-Díaz L (2018) *Trypanosoma cruzi* biochemical changes and cell death induced by an organometallic platinum based compound. Chem Biol Drug Des 92(3): 1657–1669. https://doi.org/10.1111/cbdd.13332

Munoz J et al (2009) Clinical profile of *Trypanosoma cruzi* infection in a non-endemic setting: immigration and Chagas disease in Barcelona (Spain). Acta Trop 111:51–55. https://doi.org/10.1016/j.actatropica.2009.02.005

Rassi A Jr, Rassi A, Marin-Neto JA (2010) Chagas disease. Lancet 375:1388–1402. https://doi.org/10.1016/S0140-6736(10)60061-X

Rodriguez Arce E et al (2015) Aromatic amine N-oxide organometallic compounds: searching for prospective agents against infectious diseases. Dalton Trans 44:14453–14464. https://doi.org/10.1039/c5dt00557d

Salomon CJ (2012) First century of Chagas' disease: an overview on novel approaches to nifurtimox and benzonidazole delivery systems. J Pharm Sci 101:888–894. https://doi.org/10.1002/jps.23010

Salvador F et al (2014) *Trypanosoma cruzi* infection in a non-endemic country: epidemiological and clinical profile. Clin Microbiol Infect 20:706–712. https://doi.org/10.1111/1469-0691.12443

Schmunis GA, Yadon ZE (2010) Chagas disease: a Latin American health problem becoming a world health problem. Acta Trop 115:14–21. https://doi.org/10.1016/j.actatropica.2009.11.003

Silva JJ et al (2010) Novel ruthenium complexes as potential drugs for Chagas's disease: enzyme inhibition and in vitro/in vivo trypanocidal activity. Br J Pharmacol 160:260–269. https://doi.org/10.1111/j.1476-5381.2009.00524.x

Soeiro Mde N, de Castro SL (2011) Screening of potential anti-trypanosoma cruzi candidates. in vitro and in vivo studies. Open Med Chem J 5:21–30. https://doi.org/10.2174/1874104501105010021

Traina MI et al (2017) Prevalence of chagas disease in a U.S. Population of Latin American immigrants with conduction abnormalities on electrocardiogram. PLoS Negl Trop Dis 11:e0005244. https://doi.org/10.1371/journal.pntd.0005244

Tyler KM, Engman DM (2001) The life cycle of *Trypanosoma cruzi* revisited. Int J Parasitol 31:472–481

Urbina JA (2010) Specific chemotherapy of Chagas disease: relevance, current limitations and new approaches. Acta Trop 115:55–68. https://doi.org/10.1016/j.actatropica.2009.10.023

Vieites M et al (2008) Potent in vitro anti-*Trypanosoma cruzi* activity of pyridine-2-thiol N-oxide metal complexes having an inhibitory effect on parasite-specific fumarate reductase. J Biol Inorg Chem 13:723–735. https://doi.org/10.1007/s00775-008-0358-7

Viotti R, Vigliano C, Lococo B, Alvarez MG, Petti M, Bertocchi G, Armenti A (2009) Side effects of benznidazole as treatment in chronic Chagas disease: fears and realities. Expert Rev Anti Infect Ther 7:157–163. https://doi.org/10.1586/14787210.7.2.157

WHO (2016) http://www.who.int/chagas/en/

Zhang Y, Chen X, Gueydan C, Han J (2018) Plasma membrane changes during programmed cell deaths. Cell Res 28:9–21. https://doi.org/10.1038/cr.2017.133

6 Capítulo III. Análisis transcriptómico y proteómico para el estudio de los compuestos M-dppf-mpo

Para comprender el mecanismo de acción molecular de los compuestos Pd-dppf-mpo y Pt-dppf-mpo contra *T. cruzi* se realizaron análisis de alto rendimiento a nivel del transcriptoma y del proteoma de los parásitos tratados. El análisis transcriptómico comparativo obtenido al incubar con cada compuesto, revela que los cambios en la expresión de ARNm de parásitos tratados vs parásitos control (Fold change, FC) son mayores luego del tratamiento con el compuesto de paladio, en comparación con su equivalente de platino. Se observaron 1076 genes sobreexpresados (10% del total detectado) y 1251 genes subexpresados (12%) luego del tratamiento con el compuesto de paladio. Para el compuesto de platino, dado que los cambios de FC eran menores, usando los parámetros establecidos (FC de $|1{,}5|$ y de FRD ≤ 0,01), menos genes cumplieron con los criterios de selección, detectándose sólo 82 (0,8%) y 119 genes (1%), sobre y subrepresentados, respectivamente. Los genes que presentaron una expresión modificada para el tratamiento con Pd-dppf-mpo y con Pt-dppf-mpo, mantenían su mismo comportamiento; es decir, no se encontraron genes aumentados para un tratamiento y disminuidos para el otro o viceversa. Por otro lado, fue empleado una aproximación proteómica analizando por separado las proteínas solubles e insolubles, para identificar proteínas y/o vías metabólicas involucradas. Si bien el RNA-Seq muestra que el número de transcritos y el cambio de su expresión fueron mayores para el tratamiento con paladio, el análisis proteómico revela que la cantidad de proteínas representadas diferencialmente fue similar luego de cada tratamiento (342 vs 411 para Pd y Pt, respectivamente). Para ambas fracciones, soluble e insoluble, se observa que el porcentaje de proteínas representadas diferencialmente constituye del 15% al 27% de las proteínas identificadas en el total de la fracción. Las correlaciones de datos transcriptómicos y proteómicos muestran que en el caso de Pt-dppf-mpo, el efecto es fundamentalmente a nivel proteómico, mientras que para Pd-dppf-mpo se observa efecto tanto a nivel de ARNm como de proteínas. El análisis global permitió obtener un modelo de los efectos celulares y potenciales objetivos moleculares para cada compuesto. En suma, nuestro análisis proporciona un repertorio integral de la respuesta molecular del parásito, que incluye objetivos farmacológicos que cumplen con los criterios de esencialidad, especificidad y/o drogabilidad, estableciendo así el escenario para futuras investigaciones.

Los resultados del estudio de los compuestos Pd-dppf-mpo y Pt-dppf-mpo se encuentran recopilados en el artículo titulado “Comparative high-throughput analysis of the *Trypanosoma cruzi* response to organometallic compounds” publicado en la revista Metallomics en el año 2020.

Metallomics

Integrated biometal science

Accepted Manuscript

This article can be cited before page numbers have been issued, to do this please use: M. F. Mosquillo, P. Smircich, M. Ciganda, A. Lima, D. Gambino, B. Garat and L. Pérez-Díaz, *Metallomics*, 2020, DOI: 10.1039/D0MT00030B.

ROYAL SOCIETY OF CHEMISTRY

rsc.li/metallomics

View Article Online
DOI: 10.1039/D0MT00030B

The manuscript “Comparative study of the mode of action of two organometallic compounds through high-throughput analysis” by Mosquillo *et al* addresses a long-standing problem in the field of molecular parasitology, namely the mode of action and potential targets of newly developed drugs, by carefully and systematically applying recently developed genome-wide analytical tools to the study of the global effects of two trypanocidal organometallic compounds on *Trypanosoma cruzi*. This parasite is the causative agent of Chagas disease, an ever-expanding pathology that remains part of the group of neglected diseases, and urgently needs attention from researchers and clinicians worldwide.

Comparative high-throughput analysis of the *Trypanosoma cruzi* response to organometallic compounds

M. Florencia Mosquillo[a], Pablo Smircich[a,b], Martín Ciganda[c], Analía Lima[b,d], Dinorah Gambino[e], Beatriz Garat[a], Leticia Pérez-Díaz[a*]

[a]Laboratorio de Interacciones Moleculares, Facultad de Ciencias, Universidad de la República, Montevideo, Uruguay
[b]Instituto de Investigaciones Biológicas Clemente Estable, Montevideo, Uruguay
[c]Department of Microbiology, University at Buffalo, USA
[d]Unidad de Bioquímica y Proteómica Analíticas, Institut Pasteur de Montevideo, Montevideo, Uruguay
[e]Área Química Inorgánica, Facultad de Química, Universidad de la República, Montevideo, Uruguay

*Corresponding author: Tel +598-25258618; fax +598-25258617

E-mail address: lperez@fcien.edu.uy

Abstract

There is an urgent need to develop new drugs against Chagas' disease In addition, the mechanisms of action of existing drugs have not been completely worked out at the molecular level. High throughput approaches have demonstrated to be powerful tools not only for understanding the basic biology of *Trypanosoma cruzi*, but also for the identification of drug targets such as proteins or pathways that are essential for parasite infection and survival within the mammalian host. Here, we have applied these tools towards the discovery of the effects of two organometallic compounds with trypanocidal activity, Pd-dppf-mpo and Pt-dppf-mpo, on the transcriptome and proteome of *T. cruzi* epimastigotes. These approaches have not yet been reported for any other prospective metal-based anti *T. cruzi* drug. We found differentially expressed transcripts and proteins in treated parasites. Pd-dppf-mpo treatment resulted in more modulated transcripts (2327 of 10785 identified transcripts) than Pt-dppf-mpo treatment (201 of 10773 identified transcripts) suggesting a mechanism of action for Pd-dppf-mpo at the transcriptome level. Similar number of differentially expressed proteins (342 and 411 for Pd-dppf-mpo and Pt-dppf-mpo respectively) were also observed. We further functionally categorized differentially expressed transcripts and identified cellular processes and pathways significantly impacted by treatment with the compounds. Transcripts involved in DNA binding, protein metabolism, transmembrane transport, oxidative defense, and the ergosterol pathways were found to be modulated by the presence of the compounds. Our transcriptomic dataset also contained previously validated essential genes. These data allowed us to hypothesize a multimodal mechanism of action for the trypanocidal activity of Pd-dppf-mpo and Pt-dppf-mpo, and a differential contribution of the metal moiety of each compound.

Introduction

View Article Online
DOI: 10.1039/D0MT00030B

Chagas disease (CD) is caused by the unicellular protozoan parasite of the kinetoplastida order named *Trypanosoma cruzi*. This parasite is transmitted by blood-sucking triatomines [1] and other routes such as congenital transmission [2], blood transfusion, and organ transplant [3]. Oral transmission [4] and sexual transmission in mice [5] have also been described. This devastating human infectious disease is considered endemic in 21 Latin American countries; about 8 million people are infected and nearly 100 million people are at risk of infection [6, 7]. In addition, because of migratory flows, CD has spread to non-endemic areas such as North America, Europe, and the Western Pacific.

CD has a variable clinical presentation which can be divided into an acute phase after the primary infection, with high parasitemia, and a chronic phase after a period of 4 to 8 weeks when parasitemia decreases. The acute phase is in most cases asymptomatic, however symptomatic manifestations such as prolonged fever, headache, myalgia, lymphadenitis, hepatomegaly, and splenomegaly can be observed. The infection remains silent during the chronic phase in most cases, although 30-40% of the initially asymptomatic patients can develop clinical manifestations including neurological, digestive (megacolon and megaesophagus syndromes), cardiac disorders, or both cardiac and digestive manifestations, which can lead to death [8, 9].

During its life cycle, the parasite goes through different stages. The proliferative epimastigote form in the midgut of the insect vector differentiates into non-dividing infective metacyclic trypomastigotes in the hindgut. This parasite form is released within the insect faeces and it can penetrate into the mammalian host invading a wide range of nucleated cell types [10]. Inside the mammalian cell, trypomastigotes give rise to dividing non-flagellated amastigotes which proliferate intracellularly until they differentiate into non-dividing cellular trypomastigotes that are released into the extracellular medium after host cell lysis. These cellular trypomastigotes can disseminate infection through invasion of new cells and migration through the lymphatic system and bloodstream [11].

Neglected Tropical Diseases (NTDs) affect more than one billion people living in poverty in tropical and subtropical areas, increasing their risk of morbidity and mortality and having marked economic repercussions [12-14]. CD has been classified by the WHO as one of the twenty NTDs comprising the group of 'the most neglected' diseases being ignored not just by the pharmaceutical industry but also by public-private partnerships [15].

There are no available vaccines to prevent CD or to block its transmission, and current treatment has been based on only two nitroaromatic drugs: Nifurtimox (Nfx) and Benznidazole (Bz). Both drugs are effective in the acute or congenital cases and in reactivation due to immunosuppression, however treatment is often discontinued due to important limitations in terms of safety, efficacy, administration, length of treatment, affordability, and parasite resistance [16, 17 18, 19].

In this context, the development of new antiparasitic agents effective against Chagas disease has become a major goal.

During the last decades, the use of metal complexes in different fields of medicine has gained impetus. Cisplatin is perhaps the most well-known anti-cancer metal-based drug. It induces apoptosis in cancer cells after its interaction with DNA [20-23]. Since metal complexes could act as antiproliferative agents through multiple mechanisms of action by a combination of the pharmacological actions of the metal and the ligand, their use in the area of NTD has also been proposed [24-28].

In previous work, our group has studied the biological effect of two novel compounds based on Pt and Pd synthetized as anti-trypanosomatid agents [29, 30]. In these

compounds, a Pt or Pd central ion was disposed in a nearly planar trapezoidal *cis* coordination bound to two bidentate ligands: a 1,1'-bis(diphenylphosphino)ferrocene (dppf) and a pyridine-2-thiolato-1-oxide (mpo). These ligands combine the anti-trypanosomatid activity of mpo [31], together with improved membrane permeability due to the dppf (Figure 1).

Both compounds under study are stable in solution, particularly in biological medium. Conductimetry measurements in DMSO solution and ^{1}H-NMR experiments [29] have verified their stability in such medium for days. Simultaneous quantification of internalized Fe and Pt or Pd by atomic absorption spectroscopy showed a stoichiometric 1:1 Fe to Pd or Pt relationship, in agreement with a high stability of the compounds in biological medium [27].

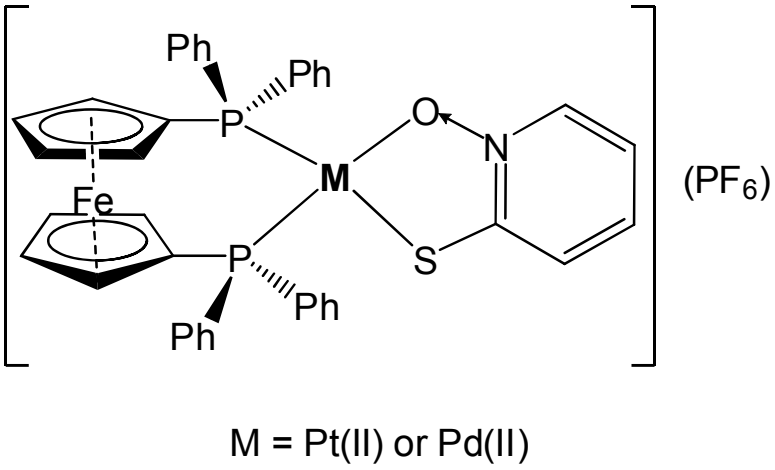

Figure 1: Chemical structure of Pd- and Pt-dppf-mpo compounds. M represents the coordinated central metal (Pd or Pt). The molecular weight of the compounds is 931,71 and 1020,37 for Pd-dppf-mpo and Pt-dppf-mpo respectively.

The aforementioned compounds displayed excellent IC_{50} values against *T. cruzi* epimastigotes (0.30 ± 0.03 μM and 0.06 ± 0.003 μM for Pd-dppf-mpo and Pt-dppf-mpo respectively), being also effective in both the infective and intracellular forms of the parasite in the mammalian host [29, 30]. Although these compounds showed a trypanocidal effect in epimastigotes, and led to parasite death through necrosis, their exact mechanism of action remains uncertain. Since both Pd-dppf-mpo and Pt-dppf-mpo showed a preferred association with DNA among other macromolecules tested, we sought to analyze the effect of these compounds on the general transcriptomic process itself. We used a high throughput approach to study whether specific transcripts were modified by the presence of the compounds.

In the last years RNA-seq has become a standard technique to study gene regulatory processes [32]. In *T. cruzi* this method has been used successfully to understand basic biological processes such as the progression of the infection process [33-35], the progression of the life and cellular cycles [36-38], regulatory mechanisms [39], pathogenesis [40] as well as the characterization of the response of the parasite's gene expression profile to the addition of antitrypanosomal drugs [41].

It is well accepted that gene expression exhibits some peculiarities in trypanosomatids, [42] including polycistronic transcription, the absence of classical promoters and control of

View Article Online
DOI: 10.1039/D0MT00030B

transcription initiation for protein coding genes, as well as extensive post-transcriptional regulation [43] mainly through mRNA stability and translational efficiency [37, 44]. Probably due to the apparent constitutive transcription, RNA and protein data correlate only poorly, thus many trypanosome research efforts have been devoted to the acquisition and analysis of proteomic data [45-49]. To identify putative target molecules that were potentially involved in the response to treatment with either Pd-dppf-mpo or Pt-dppf-mpo, a global proteomic analysis was also performed.

With the aim to deepen in the mode of action of these two promising organometallic compounds, high throughput transcriptomic and proteomic analysis were performed. Our comparative analysis led us to discriminate between transcripts/proteins specifically modified by Pd-dppf-mpo and Pt-dppf-mpo as well as between modified transcripts/proteins due to the dppf-mpo ligands alone and those modified specifically by the metal. Moreover, our data suggest that while the Pt-dppf-mpo compound has a global effect on protein abundance (411 modified of 1823 total detected proteins and only 201 modified of 10773 total detected transcripts), the Pd-dppf-mpo compound affects not only transcript (2327 out of 10785) but also protein (342 out of 2107). The identification of modified enzymes and/or metabolites present in the parasite, but absent in their mammalian host, constitute interesting targets for future rational drug design. This is the first report of a complete approach combining massive data at both transcriptomic and translatome levels to unravel the mechanism of action of anti-*T. cruzi* compounds.

Materials and Methods

Parasite culture

All parasite work was performed according to national and international guidelines for the handling of *T. cruzi*. The epimastigote form of the parasite, strain CL Brener was cultivated in a Biosafety Level 2 Laboratory. Parasites were grown in fresh BHI medium (Oxoid) supplemented with 10% Fetal Bovine Serum (Capricorn) and penicillin (100 units/mL) and streptomycin (100 μg/mL). Parasites were maintained at 28°C in mid-exponential growth phase ($2x10^7$ parasites/mL) through successive dilutions of the initial culture 1/10 each three days.

Compound preparation

Stock solutions were prepared by initial dissolution of compound in DMSO at 11.25 mM and further dilution with culture medium to a final concentration corresponding to 5x IC50 (1.5 and 0.3 μM for Pd-dppf-mpo and Pt-dppf-mpo respectively).

RNA extraction and evaluation

Total RNA was extracted from $1x10^9$/mL exponential phase epimastigotes using Trizol reagent (Life Technologies) as described by the manufacturer. RNA cleanup was performed using DNA-free kit (Life Technologies) according to the manufacturer's instructions. Purified RNA was quantified using Nanodrop by evaluating the absorbance at 260 and 280 nm and the quality and integrity of RNA was assessed through an Agilent RNA 6000 Nano Chip on Bioanalyzer 2100 (Agilent Technologies).

Transcriptomic assays and data analysis

View Article Online
DOI: 10.1039/D0MT00030B

For high throughput analysis, compound incubations were performed for a short period of time to focus our analysis on the early response triggered specifically by the compounds. Total RNA was isolated after 6 h of treatment with 5x IC_{50} of Pd or Pt-based compounds and from parasites without treatment (three independent replicas for each one). PoliA+ RNA pair-end sequencing was performed at Macrogen using Illumina TruSeq™ RNA Sample Preparation Kit v2 and HiSeq 2500 (www.macrogen.com).
Trimmomatic [50] was used to obtain good quality reads that were mapped to the non-Esmeraldo-like *T. cruzi* genome (version 29, http://tritrypdb.org) using bowtie2 in --very-sensitive mode [51]. The number of reads per gene was determined using htseq-count [52]. Differentially expressed genes between drug treated and control parasites were determined using the Deseq2 package available in R [53]. A double filter was applied to determine differentially expressed genes (DE), considering a fold change (FC) of |1.5| and a false discovery rate (FDR) less than 0.01. Enriched GO terms among DE gene products were established using TritrypDB tools (http://tritrypdb.org/) at a p-Adj value (Bonferroni correction) ≤ 0.05. For the analysis, pseudogenes and fragmented genes were excluded.

Real time PCR

For real time PCR, cDNA was synthesized from total RNA extracted from parasites incubated with each compound separately and from control untreated parasites. Two technical replicas were performed for each of the three biological replica. For retrotranscription, Superscript III (Life Technologies) was used with random primers following manufacturers' instructions. Primers for randomly selected up- and downregulated genes were designed with the OligoPerfect Primer Designer tool from Thermo Fisher Scientific (available at https://www.thermofisher.com). Reactions were performed in 10 µL using 10 ng/µL of total cDNA as a template, primers at a final concentration of 0.4 µM and the SensiFAST SYBR Hi-Rox Kit (Bioline). All quantitative measurements were normalized to the threonyl-tRNA synthetase gene, whose transcript level, according to transcriptome data, does not present variations between treated and untreated parasites. Annealing temperature was set to 60°C and a StepOnePlus Real-Time PCR System was used. The StepOnePlus™ Software v2.3 was used to process the data and the mRNA fold change was calculated by using the $2^{-\Delta\Delta CT}$ method [54].

Proteomic assays and data analysis

Three independent experiments were performed for both Pt-dppf-mpo and Pd-dppf-mpo treatments as well as for untreated control parasites. Total proteins from $1x10^9$ parasites, untreated and treated with 5x IC_{50} for 6 h, were isolated by incubation with lysis buffer (7 M urea, 2 M thiourea, 4% CHAPS) for 30 min at 4ºC, centrifuged at 4°C for 1 h at 20,000g to separate soluble from insoluble fractions, and analyzed by LC tandem-mass spectrometry (LC-MS/MS). Briefly, 20 µg of each sample were resolved in a pre-cast 4%-12% gradient gel (NuPAGE, MES System, Invitrogen) and each lane was cut, and processed for mass spectrometry analysis according to previously reported protocols [55]. Peptide samples were fractionated into a nano-HPLC system (EASY-nLC 1000, Thermo Scientific) equipped with a reverse-phase column (PepMap TM , RSLC, C18, 2 m, 100Å, 50 mm x 15 cm, Thermo Scientific) using a gradient from 50% to 100% of 0.1% formic acid in acetonitrile at a flow rate of 250 nL/min. Peptide analysis was performed in a LTQ Velos nano-ESI linear ion trap instrument (Thermo Scientific) operated in data dependent acquisition mode (top 10) with a dynamic exclusion list of 45s. Data analysis was carried

View Article Online
DOI: 10.1039/D0MT00030B

out using PatternLab for Proteomics software (version 4.0.0.84). Raw files were searched against a target-decoy database generated from *Trypanosoma cruzi* (strain CL Brener Esmeraldo and non-Esmeraldo like haplotypes) sequences downloaded from Uniprot (http://www.uniprot.org/proteomes/ on January 2017, 19239 entries) and applying the following parameters: trypsin as proteolytic enzyme with full specificity; methionine oxidation as variable modification; cysteine carbamidomethylation as fixed modification; and 800 ppm of tolerance from the measured precursor m/z. Identified peptides of more than six amino acids and proteins with a minimum of two spectrum matches and a FDR of 1% were filtered out [56]. Proteins found in at least two biological replicates from one of the conditions but missing in all replicates of the other conditions were considered as unique. PatternLab's T-Fold module was used to identify differential proteins appearing in both treated and untreated condition but at significantly different levels, determined by spectral counting.

Results and discussion

Transcriptomic and proteomic approaches

To understand the molecular mechanism of action of Pt- and Pd-dppf-mpo compounds against *T. cruzi*, high throughput analysis was performed comparing treated and control untreated parasites. To identify the immediate processes triggered specifically by the compounds, and to avoid general and/or late drug responses mechanisms, we analyzed transcriptome and proteome modifications in parasites 6 hours post treatment. After 6 hours of incubation with compound concentrations corresponding to 5x IC_{50} value, treated parasites showed evident morphological changes such as shortened cell bodies or rounded morphology with shortened flagellum in Pd-dppf-mpo and Pt-dppf-mpo treated parasites, respectively. Flow cytometry analysis using annexin V and propidium iodide labelling showed no evidence of increased necrosis in this condition, whereas after 24 hours necrosis process was evident [29, 30].

In the transcriptomic analysis, the total number of paired-end reads obtained after trimming ranged between 7 and 9 million for each condition (Table 1). Nearly 91% of the total reads were mapped to the reference genome, out of which an average of 50% mapped to CDS for each condition (around 4 million reads). Mapped data were analyzed through principal component analysis (PCA) and hierarchical clustering, showing the expected clustering (Figure S1). Transcriptomic data can be accessed at: https://dataview.ncbi.nlm.nih.gov/object/PRJNA609361?reviewer=9lckg3n61950gtslc8m218pk9d.

Table 1. Basic summary of sequence and sequencing reads mapping to reference genome. Reads of control and compound treated parasites are indicated.

Sample	Trimmed reads	Mapped reads	
		% genome	% CDS
Control 1	7256531	92.0	49.2
Control 2	7424503	91.9	49.1
Control 3	9061771	92.1	49.0
Pd-dppf-mpo1	8528457	91.4	48.9
Pd-dppf-mpo2	9481561	90.7	48.6
Pd-dppf-mpo3	8372978	90.9	48.7
Pt-dppf-mpo1	8421177	91.8	47.3

View Article Online
DOI: 10.1039/D0MT00030B

Pt-dppf-mpo2	7607366	91.7	50.4
Pt-dppf-mpo3	8261533	91.7	52.8

Global proteomic analyses of three independent assays were performed for each condition. Considering that reducing sample complexity would improve resolution and that a differential association between the insoluble and soluble fractions has been reported for both Pd and Pt-based compounds [29, 30], soluble and insoluble proteins were separately analyzed. An average of ~1900 proteins were detected in each sample (2107 and 1823 total proteins detected for Pd-dppf-mpo and Pt-dppf-mpo treatment respectively). The mass spectrometry proteomics data have been deposited to the ProteomeXchange Consortium via the PRIDE partner repository with the dataset identifier PXD018018. These results, although corresponding only to ~10% of all proteins encoded by the *T. cruzi* genome, are in good agreement with the 2784 [46], 4205 [45] or the 4920 [47] proteins identified in previous reported *T. cruzi* proteomic data.

Differentially expressed genes

From a total of 10785 genes detected in the case of the treatment with Pd-dppf-mpo, 2327 were differentially expressed (DE), being 1076 (10% of the total) and 1251 (12% of the total) up- and downregulated respectively (Figure 2A). Instead, less transcripts were differentially expressed after Pt-dppf-mpo treatment (201 out of the 10773 total genes detected), being 82 (0.8% of total genes) upregulated and 119 (1%) downregulated (Figure 2B). Table 2 lists the top 10 up- and downregulated transcripts. The greater number of modified transcripts obtained after treatment with Pd-dppf-mpo suggests the existence of an effect of the compound at the transcriptomic level that is not as evident in the case of treatment with Pt-dppf-mpo.

All DE genes after treatment are shown in Table S1. In the case of treatment with Pd-dppf-mpo, 69% of upregulated transcripts and 52% of downregulated transcripts correspond to hypothetical proteins. For cells treated with Pt-dppf-mpo, the percentage of upregulated and downregulated transcripts corresponding to hypothetical proteins were 46% and 52%, respectively.

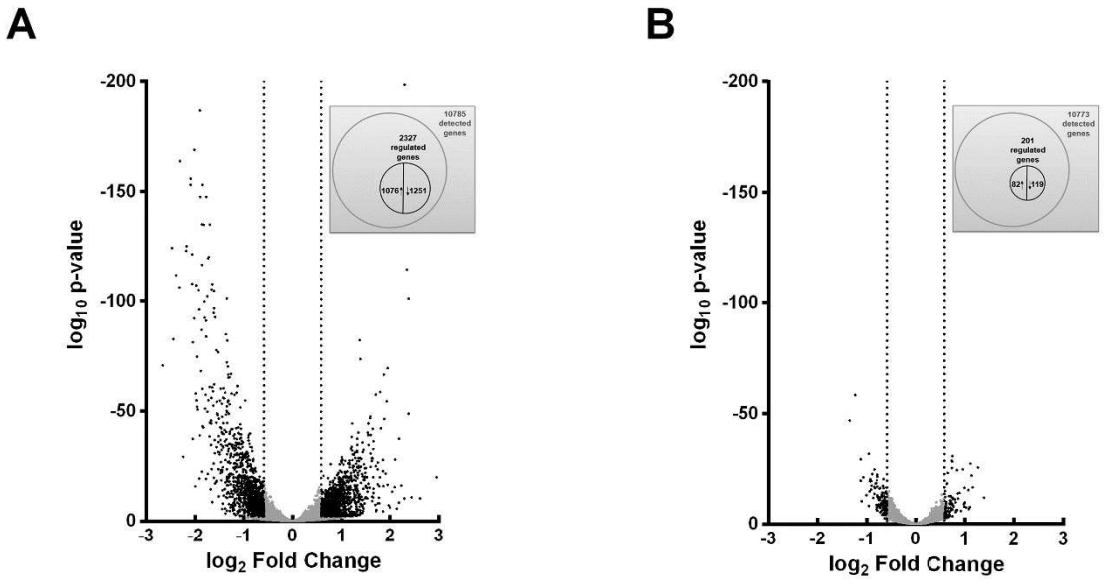

Figure 2. Volcano plot showing global transcriptional changes in Pd-dppf-mpo (A) and Pt-dppf-mpo (B) treated parasites vs untreated parasites. The log_2 fold change

View Article Online
DOI: 10.1039/D0MT00030B

in treated versus untreated parasites is represented on the x-axis. The y-axis shows the $\log_{10}$ of the p-value. Genes with fold change higher than 1.5 and lower than -1.5 are represented by black dots while genes with fold change between -1.5 and 1.5 are represented by gray dots. Diagram in the insets represents the number of mapped genes to the reference genome, the fraction of modulated genes and the number of up and down regulated transcripts identified.

Table 2. Differentially expressed genes in *T. cruzi* epimastigote after metal-dppf-mpo treatment. Only the 10 most regulated transcripts are shown. Transcripts coding for hypothetical proteins were excluded from the list. # Refers to the ordinal number in the list. FC: Fold Change. For the complete list see Table S2.

Pd-dppf-mpo treatment				
#	**Gene ID**	**FC**	**Padj**	**Product Description**
6	TcCLB.508701.20	4,905	4,268E-195	cation transporter, putative
9	TcCLB.509105.120	4,537	2,225E-36	protein kinase, putative
19	TcCLB.510581.20	3,686	3,818E-45	receptor-type adenylate cyclase, putative
20	TcCLB.511653.20	3,632	2,643E-15	dual-specificity protein phosphatase, putative
21	TcCLB.509937.130	3,620	2,064E-04	protein kinase, putative
22	TcCLB.508065.70	3,605	7,022E-27	protein associated with differentiation 8, putative
23	TcCLB.511649.100	3,604	6,134E-22	amino acid permease, putative
25	TcCLB.511277.200	3,435	6,338E-08	RNA-binding protein, putative
28	TcCLB.508231.190	3,359	1,107E-25	ATP-binding cassette protein subfamily G
30	TcCLB.511261.120	3,349	9,645E-23	pumilio/PUF RNA binding protein 2, putative
2	TcCLB.507913.20	-6,314	4,035E-69	phosphomevalonate kinase protein, putative
3	TcCLB.510947.50	-5,538	3,343E-122	cyclophilin, putative
5	TcCLB.509105.90	-5,219	1,523E-109	MRB1-associated protein, putative
6	TcCLB.511281.40	-4,980	3,809E-104	mevalonate-diphosphate decarboxylase, putative
7	TcCLB.510943.50	-4,943	2,945E-161	delta-1-pyrroline-5-carboxylate dehydrogenase, putative
8	TcCLB.509337.19	-4,736	2,892E-28	Mitochondrial pyruvate carrier 1
9	TcCLB.508501.250	-4,526	5,500E-121	UMP-CMP kinase, mitochondrial, putative
10	TcCLB.504045.60	-4,498	4,190E-123	thermostable carboxypeptidase 2, putative
11	TcCLB.506789.280	-4,245	2,174E-153	methylthioadenosine phosphorylase, putative
12	TcCLB.506201.39	-4,240	1,076E-150	25 kDa translation elongation factor 1-beta, putative
Pt-dppf-mpo treatment				
2	TcCLB.509161.10	2,412	2,858E-23	ubiquitin-conjugating enzyme E2, putative
3	TcCLB.510581.20	2,232	7,963E-15	receptor-type adenylate cyclase, putative
4	TcCLB.507063.70	2,200	8,992E-20	trans-sialidase, Group II, putative
8	TcCLB.506479.120	2,005	2,088E-08	cytidine triphosphate synthase, putative
9	TcCLB.508857.30	1,990	1,388E-14	trans-sialidase, Group I, putative
11	TcCLB.508859.118	1,976	7,457E-08	trans-sialidase, putative
12	TcCLB.506193.60	1,947	1,736E-22	ascorbate peroxidase, putative
13	TcCLB.511653.20	1,897	5,327E-05	dual-specificity protein phosphatase, putative
14	TcCLB.508799.270	1,792	3,737E-22	protein associated with differentiation 4, putative
15	TcCLB.508065.70	1,791	2,244E-05	protein associated with differentiation 8, putative
1	TcCLB.510947.50	-2,538	8,655E-44	cyclophilin, putative
2	TcCLB.511899.40	-2,350	5,167E-55	2-amino-3-ketobutyrate coenzyme A ligase, putative
3	TcCLB.507913.20	-2,172	9,913E-18	phosphomevalonate kinase protein, putative
4	TcCLB.511899.10	-2,170	7,370E-27	2-amino-3-ketobutyrate coenzyme A ligase, putative

View Article Online
DOI: 10.1039/D0MT00030B

6	TcCLB.507583.20	-2,096	3,813E-19	nucleolar protein, putative
8	TcCLB.503925.80	-1,937	3,707E-07	CDP-diacylglycerol--inositol 3-phosphatidyltransferase
9	TcCLB.505183.30	-1,936	3,179E-29	malic enzyme, putative
10	TcCLB.509253.30	-1,915	2,898E-13	3-β-hydroxysteroid- Δ(8), Δ(7)-isomerase, putative
11	TcCLB.509715.40	-1,908	1,441E-17	fibrillarin, putative
12	TcCLB.504839.50	-1,898	2,392E-18	nucleosome assembly protein-like protein, putative

At least 12 modulated transcripts were randomly selected for qRT-PCR validation. An excellent correlation between qRT-PCR and transcriptomic results for the selected set of genes was obtained (R Pearson 0.99 and 0.98, respectively) (Figure S2).

Functional enrichment analysis

To provide insights on the functional categories and pathways involved in the *T. cruzi* drug response, gene ontology (GO) enrichment analyses for DE transcripts were performed. The behavior of the DE genes after the treatment with the metal compounds follows the same pattern, that is, there are no genes whose expression is upregulated in one of the treatments and downregulated in the other. In spite of the high proportion of transcripts coding for hypothetical proteins, several functional terms were found to be significantly enriched for DE transcripts (Table 3 and Table S2).

Among GO enriched categories for Pd-dppf-mpo DE genes, we highlight DNA binding (GO: 0003677) with genes coding for histones (H4, H3, H2A, H2A variant z, H2B variant V, H3 variant V), helicases, topoisomerases and replication factor A protein 1, DNA repair protein and mismatch repair protein; transmembrane transport (GO: 0055085) including ABC transporters whose involvement in parasite drug resistance has been reported previously (Zingales, 2015) and protein metabolism with genes involved in ribosome biogenesis (GO: 0042254), cellular amino acid metabolic processes (GO: 0006520) and protein folding (GO: 0006457). All modified transcripts that belong to these categories are downregulated after treatment with Pd-dppf-mpo.

For Pt-dppf-mpo DE genes, the most relevant GO enriched category also is protein metabolism (ribosome biogenesis GO:0042254, protein folding GO:0006457 and unfolded protein binding GO:0051082). Transcripts for this category are also downregulated (Table S2).

The underrepresentation of gene transcripts encoding for proteins both involved in folding and associated with unfolded proteins (heat shock proteins, chaperones and chaperonins, and cyclophilin) could imply that cells treated with these compounds accumulate improperly folded or deficient protein products. The fact that both protein folding and ribosome biogenesis GO categories are downregulated DE after treatment either with Pd or Pt dppf-mpo suggests that this is not due to a metal-specific response.

Table 3. GO term enrichment analysis and KEGG. Complete list of significantly enriched GO terms and KEGG pathways (p-adj < 0.05). The most relevant GO terms are shown in bold and their corresponding transcripts are listed in Table S3.

Pd-dppf-mpo upregulated genes					
Term	ID	Name	Overlap	Fold enrichment	Bonferroni
BP	GO:0006464	cellular protein modification process	93/406	1,88	9,84E-09
MF	GO:0016301	kinase activity	83/301	2,26	2,77E-12

MF	GO:0043167	ion binding	177/1133	1,28	2,54E-03

Pd-dppf-mpo downregulated genes

Term	ID	Name	Result count	Fold enrichment	Bonferroni
BP	GO:0044281	small molecule metabolic process	113/330	2,17	4,88E-16
BP	GO:0006091	generation of precursor metabolites and energy	25/62	2,56	1,13E-04
BP	GO:0055085	transmembrane transport	40/129	1,97	3,88E-04
BP	GO:0042254	ribosome biogenesis	26/72	2,29	7,71E-04
BP	GO:0006520	cellular amino acid metabolic process	33/102	2,05	8,85E-04
BP	GO:0006790	sulfur compound metabolic process	16/35	2,90	1,13E-03
BP	GO:0051276	chromosome organization	30/91	2,09	1,39E-03
BP	GO:0006457	protein folding	34/118	1,83	9,05E-03
BP	GO:0065003	protein-containing complex assembly	20/59	2,15	1,86E-02
BP	GO:0022607	cellular component assembly	28/109	1,63	2,04E-01
BP	GO:0042592	homeostatic process	17/60	1,80	3,95E-01
CC	GO:0005739	Mitochondrion	231/825	1,77	3,78E-21
CC	GO:0005773	Vacuole	53/124	2,71	7,26E-12
CC	GO:0005634	Nucleus	294/1489	1,25	2,08E-05
CC	GO:0005783	endoplasmic reticulum	48/157	1,94	3,17E-05
CC	GO:0005777	Peroxisome	43/135	2,02	3,31E-05
MF	GO:0016491	oxidoreductase activity	69/236	1,85	2,78E-06
MF	GO:0003677	DNA binding	47/182	1,64	1,04E-02
MF	GO:0016829	lyase activity	20/59	2,15	1,68E-02
MF	GO:0022857	transmembrane transporter activity	38/144	1,67	2,49E-02
MF	GO:0016765	transferase activity, transferring alkyl or aryl	8/18	2,82	1,41E-01
KEGG	ec00720	Carbon fixation pathways in prokaryotes	19/36	3,12	9,51E-05
KEGG	ec00362	Benzoate degradation	17/33	3,05	5,81E-04
KEGG	ec00710	Carbon fixation in photosynthetic organisms	15/28	3,17	1,16E-03
KEGG	ec00260	Glycine, serine and threonine metabolism	17/39	2,58	9,39E-03
KEGG	ec00625	Chloroalkane and chloroalkene degradation	10/17	3,48	1,39E-02
KEGG	ec00640	Propanoate metabolism	14/32	2,59	3,96E-02

Pt-dppf-mpo upregulated genes

Term	ID	Name	Overlap	Fold enrichment	Bonferroni
BP	GO:0006950	response to stress	5/113	4,28	4,19E-02
MF	GO:0051082	unfolded protein binding	4/49	7,89	2,48E-02

Pt-dppf-mpo downregulated genes

Term	ID	Name	Overlap	Fold enrichment	Bonferroni
BP	GO:0042254	ribosome biogenesis	11/72	8,4	1,39E-06
BP	GO:0006457	protein folding	9/118	4,2	7,21E-03
BP	GO:0044281	small molecule metabolic process	16/330	2,67	7,32E-03
BP	GO:0006790	sulfur compound metabolic process	5/35	7,86	1,03E-02
CC	GO:0005829	Cytosol	12/144	4,58	1,28E-04
CC	GO:0005634	Nucleus	40/1489	1,48	4,72E-02
CC	GO:0005773	Vacuole	7/124	3,11	9,25E-02
MF	GO:0003723	RNA binding	23/423	2,99	4,26E-05
MF	GO:0019843	rRNA binding	5/13	21,16	6,23E-05
MF	GO:0008168	methyltransferase activity	8/72	6,11	1,26E-03
MF	GO:0051082	unfolded protein binding	6/49	6,74	6,99E-03
KEGG	ec00523	Polyketide sugar unit biosynthesis	9/53	6,72	4,46E-04
KEGG	ec00270	Cysteine and methionine metabolism	10/81	4,88	2,40E-03
KEGG	ec01057	Biosynthesis of type II polyketide products	10/85	4,65	3,70E-03

KEGG ec00950	Isoquinoline alkaloid biosynthesis	9/74	4,81	7,38E-03
KEGG ec00450	Selenocompound metabolism	7/43	6,44	7,83E-03
KEGG ec00627	Aminobenzoate degradation	8/67	4,72	2,24E-02
KEGG ec00333	Prodigiosin biosynthesis	7/51	5,43	2,40E-02
KEGG ec00624	Polycyclic aromatic hydrocarbon degradation	7/52	5,33	2,73E-02
KEGG ec00945	Stilbenoid, diarylheptanoid and gingerol biosynthesis	8/74	4,28	4,51E-02

The comparative transcriptomic analysis allowed us to discriminate between transcripts specifically modulated by each metal, and transcripts whose modulation could be due to the metal dppf-mpo, either Pd or Pt (Figure 3, Table S3). A total of 60 common transcripts are upregulated upon the treatment with both assayed metal compounds, representing 73% of the upregulated transcripts with Pt-dppf-mpo, but only 6% of the upregulated transcripts with Pd-dppf-mpo. In this later case a wide phenomenon due to the metal is suggested since 1016 transcripts (94%) are exclusively increased after Pd-dppf-mpo treatment. A similar trend is observed for the downregulated transcripts, being exclusive of the Pt-dppf-mpo treatment only 8% (9) whereas for the treatment with Pd-dppf-mpo, 91% (1141) of the downregulated transcripts are unshared with Pt-dppf-mpo transcripts and therefore considered specific for Pd.

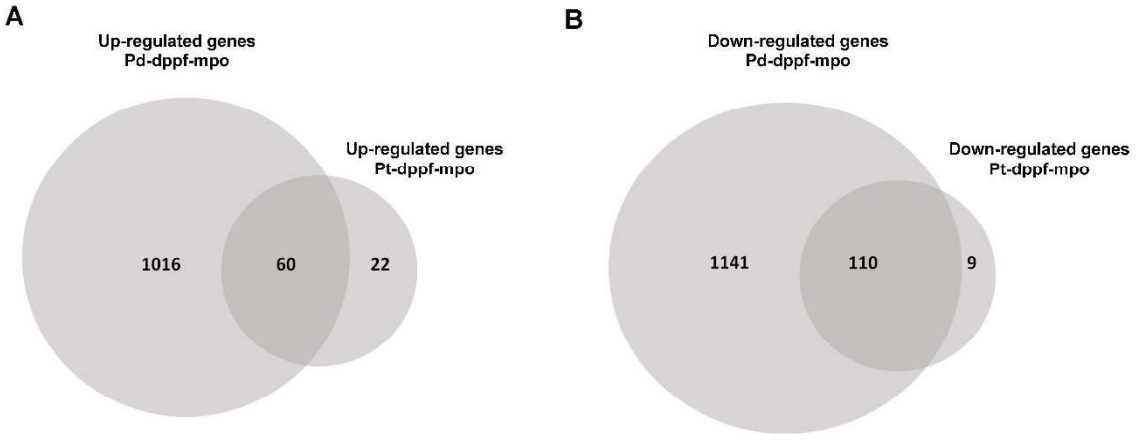

Figure 3. Venn diagram showing upregulated transcripts (> 1.5 fold; p-adj < 0.05) (A) and downregulated transcripts (< -1.5 fold; p-adj < 0.05) (B) in Pd-dppf-mpo and Pt-dppf-mpo treated parasites. Numbers indicate transcripts in each category, the intersection of the diagrams represents shared transcripts modulated in both treatments.

Differentially expressed proteins

Identified proteins were classified into over- and underrepresented protein groups, which, in turn, consisted of proteins whose abundance was altered due to treatment with the compounds (Table S4). After treatment with Pd-dppf-mpo, 180 out of 1167 soluble proteins (15.4%) were shown to be regulated. Fifty-five of these were overrepresented and 125 were underrepresented proteins. In the case of the insoluble fraction, 940 proteins were detected, and a similar percentage (162/940, i.e. 17.2%) was shown to be regulated. Seventy-three of these were overrepresented and 89 were underrepresented. After treatment with Pt-dppf-mpo, a higher percentage (314 out of 1158, i.e. 27%) of regulated soluble proteins was observed. Ninety-six of them were overrepresented and 218 were underrepresented. The insoluble regulated proteins also amounted to 15% of the total identified proteins (97/665). Eighty of these proteins were overrepresented and

View Article Online
DOI: 10.1039/D0MT00030B

only 17 were underrepresented insoluble proteins. All identified proteins as well as modulated proteins are listed in Table S5.

As for DE transcripts, modulated proteins common to both treatments and metal compound specific proteins were found. No specific pathway was identified neither in modulated proteins common to both treatments, nor in proteins specifically modulated by each metal compound. (Table S6).

It is worth noting that the proteins affected by the treatments do not correspond to the most modified transcripts in the aforementioned affected pathways (Table S2 and Table S7). Nevertheless, it has long been reported that MS-based protein identification is biased toward the detection of abundant proteins [57], a large subset of proteins being undetectable because their abundance levels are below the detection limit. Protein abundance quantification can also be affected by differential ion efficiencies, wide ranges in protein size, and differences in peptide solubility [58]. In addition, what we are presenting here is a snapshot of molecular changes after 6 hours of treatment. The observed changes in the abundance of transcripts may be reflected in proteomic changes at a later time point. Indeed, no correlation between proteomics (soluble and insoluble proteins) and transcriptomics was observed for Pd-dppf-mpo treatment (Figure 4A and B). The lack of correlation, together with the amount and abundance of altered transcripts and proteins, indicate that the mechanism of action is exerted at both mRNA and protein level. As mentioned above, in the case of treatment with Pt-dppf-mpo, no clear effect on transcript abundance was found (Figure 2B), and the mode of action was mainly seen at the protein level (Figure 4C and D). According to our previous studies, such difference cannot be attributable to different compound stability, since both are stable in biological media, or compound uptake, being the uptake of Pt-dppf-mpo almost 5 times greater than the one of Pd-dppf-mpo [29, 30].

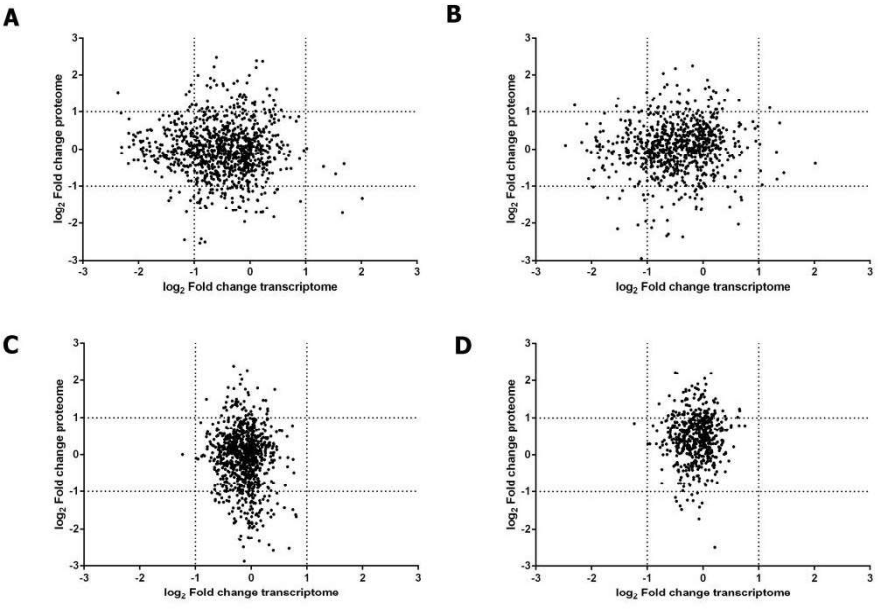

View Article Online
DOI: 10.1039/D0MT00030B

Figure 4. Correlation between proteomic and transcriptomic data in Pd-dppf-mpo (A and B) or Pt-dppf-mpo (C and D) treated parasites vs untreated parasites. Scatter plot of protein abundance ratios against corresponding transcript fold changes. Proteins with significant abundance alterations (FDR < 0.05) but no significant change in the corresponding transcript level are represented in the upper and lower central quadrant. Significant regulation (FDR < 0.05) only in the transcriptome but not in the proteome is represented by dots at the left and at the right of the middle quadrant. Shared regulation at both levels is depicted by dots in the corners. Soluble proteins are represented in panels A and C. Insoluble proteins are represented in panels B and D.

Although 269 (35.7%) of the 753 modulated proteins (Table S4 and S5) are uncharacterized proteins, STRING analysis [59] of the Pd-dppf-mpo modulated proteins showed significant predictive protein–protein interaction enrichment (p-value: 8.76e-3). The main clusters of functional interactions observed revealed their involvement in different metabolic pathways like the proteasome, oxidative phosphorylation, biosynthesis of secondary metabolites, purine metabolism and endocytosis. Significant interaction networks (p-value: 1.11e-16) were also observed for Pt-dppf-mpo-modulated proteins involved in biosynthesis of secondary metabolites, glycolysis/gluconeogenesis, pyruvate metabolism, citrate cycle, metabolism of amino acids (tryptophan, alanine, aspartate, glutamate, glycine, serine, threonine and histidine), degradation of amino acids (valine, leucine, isoleucine and lysine), aminoacyl-tRNA biosynthesis, glutathione metabolism, fatty acid metabolism and degradation, peroxisome, purine metabolism, sugar metabolism, and phagosome (Table S7).

Specific pathways and proteins

One of the prerequisites of a valuable drug target is that it be an essential molecule for cellular viability, at least in the parasite stage that coexists within the mammalian host. Recently, Jones et al have defined 16 essential genes validated through gene disruption in *T. cruzi* [60]. Keeping in mind that affected genes do not necessarily imply direct molecular targets of Pd-dppf-mpo or Pt-dppf-mpo, we interrogated our dataset for the effects of the compounds on the expression of these validated essential genes.

After Pd-dppf-mpo treatment, 4 of these 16 transcripts were downregulated: GPI alpha-mannosyltransferase (GPI10, involved in GPI-anchor biosynthesis), inositol 1,4,5-trisphosphate receptors (TcIP3Rb), and two copies of lanosterol 14-alpha-demethylase (CYP51, involved in ergosterol biosynthesis).

Dihydrofolate reductase-thymidylate synthase, DHFR-TS, is a bifunctional enzyme that catalyzes both the reduction of dihydrofolate to tetrahydrofolate, and the reductive methylation of deoxyuridine monophosphate (dUMP) to form thymidylate (dTMP). Tetrahydrofolate is the precursor of cofactors required for the synthesis of thymidylate, purine nucleotides, methionine, serine, and glycine for nucleic acid and protein synthesis [61]. Thymidylate (dTMP) is ultimately phosphorylated to thymidine triphosphate (dTTP) and used for DNA synthesis and repair [62]. The DHFR active site of the enzyme shows subtle differences compared with its human counterpart, the *dhfr-ts* gene being essential for parasite survival [60, 62, 63]. This enzyme has been chemically and genetically validated as a target in African trypanosomes [62].

Surprisingly, in Pd-dppf-mpo treated parasites, while the mRNA for DHFR-TS is decreased (1.28 fold), the protein is increased (2.18 fold). This discrepancy in the amount of mRNA and protein could be the result of a cellular compensatory mechanism (i.e.

View Article Online
DOI: 10.1039/D0MT00030B

through enhanced translatability) to produce more enzyme and achieve increased folate levels. In this sense, two folate/pteridine transporters (TcCLB.506149.10 and TcCLB.508027.40) are upregulated in the transcriptome data.

Only the gene encoding for GP10 was downregulated after Pt-dppf-mpo treatment (Table 4). The GPI-anchor represents the major carbohydrate modification of proteins on the cell surface of the parasite. Although the GPI core glycan is well conserved in all organisms, many differences in modifications of GPI structures and biosynthetic pathways have been reported [64]. Sugars and substrate analogues of the biosynthetic pathway resulted in the inhibition of both parasite and mammalian enzymes. In this context, there is a need to find inhibitors that affect GPI synthesis in trypanosomatids without affecting the mammalian enzymes [65].

TcIP3Rb is a Ca^{2+} channel. When its expression level is reduced to less than one-half of that in wild-type (wt) cells, parasite growth is impaired [66]. In addition, antisense targeting of the TcIP3Rb mRNA, inhibits trypomastigote invasion of host cells [67].

Table 4. List of modulated essential *T. cruzi* genes after treatment. Essentiality criteria as defined by Jones et al. [60]. S and P stand for Esmeraldo and non-Esmeraldo haplotypes

Haplo-type	Gene ID	Protein	FC Pd-dppf-mpo	FC Pt-dppf-mpo
S	TcCLB.503527.40	GPI10 GPI alpha-mannosyltransferase	-2.24	-1.62
P	TcCLB.511481.40	GPI12 N-Acetyl-Dglucosaminylphosphatidylinositol de-N-acetylase	1.42	1.06
S	TcCLB.503419.30	TC52 Thioredoxin-glutaredoxin like	-1.11	1.23
S	TcCLB.507091.40	DHOD Dihydroorotate dehydrogenase	-1.24	-1.09
S	TcCLB.506811.190	GALE UDP-glucose 4′-epimerase Galactose metabolism	1.31	-1.03
S	TcCLB.509153.90	DHFR-TS Dihyrofolate reductase—thymidylate synthase	-1.28	1.03
S	TcCLB.507547.40	ECH1 Enoyl-coenzyme A (CoA) hydratase 1	-1.04	1.01
P	TcCLB.508319.40	SUB2b RNA helicase DEAD-box protein	-1.47	-1.29
P	TcCLB.511277.450	GPI8 Cysteine peptidase, Clan CD, family C13	-1.24	-1.24
S	TcCLB.509011.40	CRT Calreticulin	-1.36	1.01
P	TcCLB.509461.90	IP3Rb Inositol 1,4,5-trisphosphate receptors	-2.14	-1.26
P	TcCLB.510821.50	RPA2 Replication protein A	-1.16	1.02
S	TcCLB.509757.30	STI1 Stress-inducible protein 1	-1.16	-1.11
P	TcCLB.511283.90	NMT N-myristoyltransferase	1.25	1.10
S	TcCLB.511353.30	Triose-phosphate transporter	-1.02	-1.11
S	TcCLB.510101.50	CYP51 Lanosterol 14-alpha-demethylase	-2.33	-1.04
P	TcCLB.506297.260	CYP51 Lanosterol 14-alpha-demethylase	-2.10	1.10

Drugs of current use for the treatment of Chagas disease and diseases caused by other trypanosomatids seem to have several modes of action [12]. Two essential pathways have been exploited for drug design in trypanosomes: ergosterol synthesis and antioxidant defense mechanisms, since many of their components are absent in mammals [68, 69]. However, the molecular targets of these drugs remain unclear.

Since *T. cruzi* is entirely dependent on endogenously produced sterols for survival and proliferation, this pathway constitutes an especially attractive target for antichagasic drug

View Article Online
DOI: 10.1039/D0MT00030B

design [68, 70-73]. Sterols are essential for several processes, including the organization and function of cell membranes, ergosterol being the main sterol component of the parasite. In *T. cruzi,* the *de novo* ergosterol biosynthesis pathway is similar to that in fungi, differing in several key steps from the mammalian cholesterol biosynthesis pathway. When ergosterol synthesis is blocked, there is no way for the parasite to compensate for this effect since it is unable to use the supply of host cholesterol, and there are no appreciable amounts of ergosterol in either host cells or growth media [74].

After treatment with Pd-dppf-mpo, transcripts encoding for 13 of the 20 steps of the isoprenoid and sterol biosynthesis pathways turned out to be significantly downregulated: 3-hydroxy-3-methylglutaryl-CoA synthase, 3-hydroxy-3-methylglutaryl-CoA reductase, mevalonate kinase, phosphomevalonate kinase protein, mevalonate-diphosphate decarboxylase, farnesyl pyrophosphate synthase, isopentenyl-diphosphate delta-isomerase, squalene synthase, squalene monooxygenase, lanosterol 14-alpha demethylase (CYP51), C-14 sterol reductase, C-5 sterol desaturase, and NAD(P)-dependent steroid dehydrogenase protein. In addition, four of the five enzymes involved in the last steps of the pathway converting zymosterol in ergosterol, were also significantly downregulated (FDR < 0.01) but with FCs values that do not satisfy our cutoff criteria (FC < -1.5) (Figure 5). Some of the downregulated genes were absent in the KEGG metabolic map, and two of them (TcCLB.408799.19 and TcCLB.510873.10) were annotated in the *T. cruzi* genome database as truncated genes (fragments), which could be the reason why this pathway was not enriched in our analysis (Table S2).

In *T. brucei*, the lack of the first two enzymes of the sterol pathway (squalene synthase, squalene monooxygenase) resulted not only in the depletion of cellular sterol intermediates and final products, but also in impaired cell growth, DNA fragmentation, modifications in mitochondrial function, and aberrant cell morphologies [75]. In *T. cruzi,* morphophysiological alterations leading to cell death were observed in response to sterol biosynthesis inhibitors [76]. Similarly, treatment of *T. cruzi* with Pd-dppf-mpo resulted in a reduction of the size of the cell body [29].

Phosphomevalonate kinase also participates in the biosynthesis of ergosterol, catalyzing the phosphorylation of phosphomevalonate into diphosphomevalonate. Its mRNA levels are drastically reduced after treatment with both compounds (FC -6.31 and -2.17 for Pd-dppf-mpo and Pt-dppf-mpo, respectively). The phosphomevalonate kinases of pathogenic bacteria, fungi, and trypanosomes are attractive targets for the design of selective inhibitors, because the same phosphorylation reaction in humans and other animals is catalyzed by a non-orthologous enzyme [73, 77]. Remarkably, after Pd-dppf-mpo treatment, the Lanosterol 14-alpha demethylase (CYP51) mRNA levels are decreased by more than twofold (FC T -2.11) and the protein is no longer detected. Azoles, which are inhibitors of the activity of CYP51 and highly effective antifungal drugs, have been assayed against *T. cruzi* activity *in vitro* and *in vivo* [71]. Although two promising azoles, posaconazole and ravuconazole, were ineffective in the treatment of chronic Chagas disease in humans, others such as VNI, VNV, and VT-1161 may not be yet discarded as they were shown to be safe, highly efficient, as well as selective in the eradication of *T. cruzi* infections from murine models [78-81].

View Article Online
DOI: 10.1039/D0MT00030B

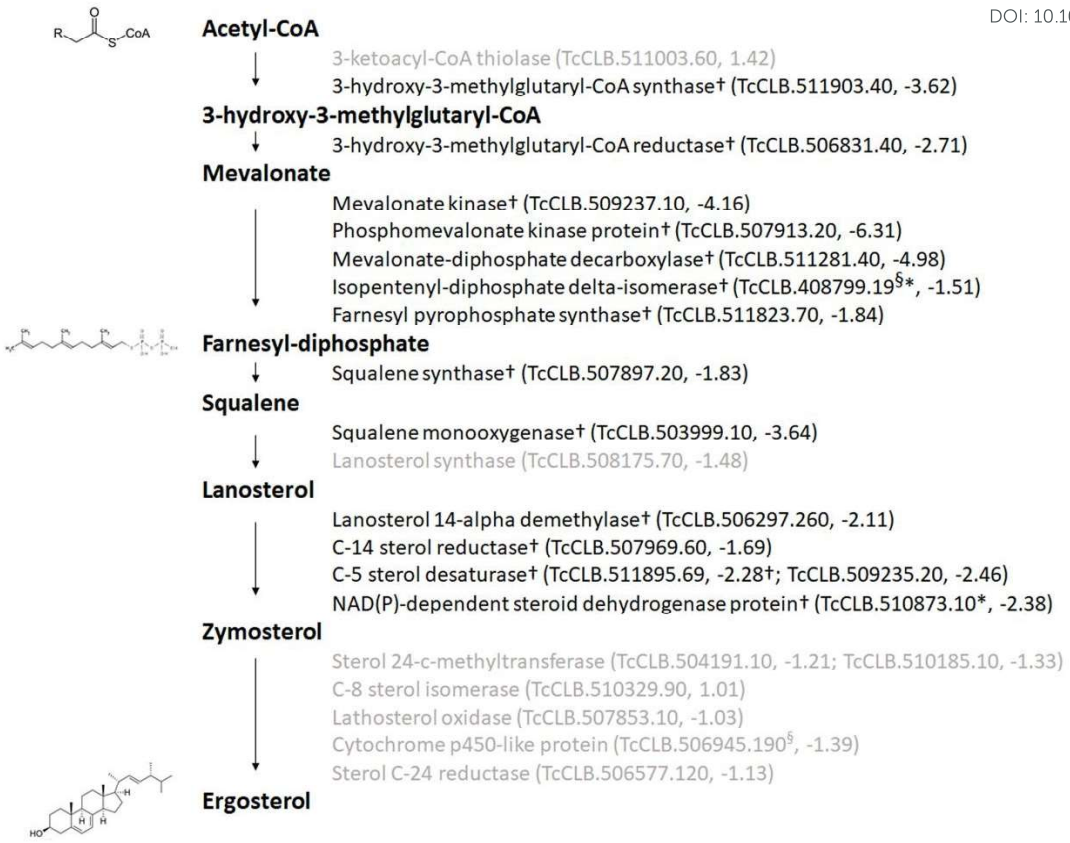

Figure 5. Simplified ergosterol biosynthesis pathway in *T. cruzi* Enzyme gene names are shown on the right with their current annotation in the TriTrypDB followed by the fold change after Pd-dppf-mpo treatment. Gene names in light gray represent transcripts whose abundance was either not modulated or was poorly modulated (between -1.5 and 1.5 fold). (†) Enzymes whose transcripts are significantly downregulated; (*) gene in TrytripDB is annotated as fragment; (§) Gene belonging to the Esmeraldo haplotype, the other genes are Non-Esmeraldo.

Since *T. cruzi* is an intracellular parasite with a digenetic life cycle, it has to deal with a variety of host environments contributing several sources of oxidative stress, not only from reactive oxygen species (ROS) produced by its own aerobic metabolism, but also from ROS generated by the host immune system. To face these variable sources of oxidative stress, the parasite has developed a complex antioxidant system which includes specific detoxification enzymes which are absent in mammals, as well as low molecular weight compounds containing thiol groups such as glutathione (GSH) and trypanothione (Try(SH)2) [82]. The iron superoxide dismutases (Fe-SOD), which have been proposed as promising drug targets [83], reduce the superoxide anions giving rise to hydrogen peroxide and molecular oxygen. Catalase and ascorbate peroxidase can then reduce hydrogen peroxide to water. Highly reactive hydroperoxides (ROOH) can be reduced by tryparedoxin peroxidases (TryXP). $Try(SH)_2$ non-enzymatically reduces tryparedoxin ($TryX(S)_2$). The process is assisted by $TryX(S)_2$ (tryparedoxin: TryX1 y TryX2). The oxidized form of $TryX(S)_2$ is returned back to $TryX(SH)_2$ by the enzyme trypanothione reductase (TR), a reaction that requires NADPH. TryX1, TR and trypanothione synthetase (TS) are absent in human hosts and are essential for parasite

View Article Online
DOI: 10.1039/D0MT00030B

survival fulfilling two of the prerequisites for a promising drug target [84-86] (Figure 6). Previous reports have shown that organometallic compounds irreversibly inactivate *T. cruzi* TR [87].

As a consequence of Pd-dppf-mpo treatment, parasites showed reduced levels of mRNA encoding Fe-SOD and enzymes of the trypanothione pathway (TryX1, TR and TS). Since the trypanosome thiol-based redox control system was downregulated after treatment with Pd-dppf-mpo, we speculate that an increase in the levels of oxidative stress is at least partially responsible for parasite death as previously reported [29].

After Pt-dppf-mpo treatment, we detected a down-regulation of TS, and an up-regulation of the enzyme ascorbate peroxidase, an antioxidant enzyme that is also absent in the mammalian host, but it has been shown to be dispensable for the parasite. *T. cruzi* null mutants for this enzyme had no defects on cell growth and were able to complete their life cycle in vivo [88].

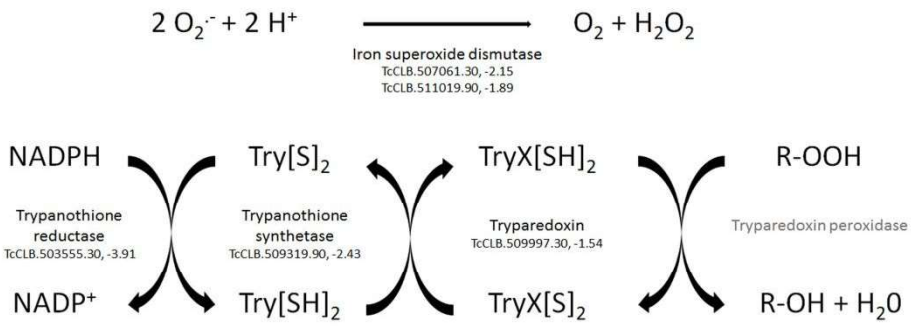

Figure 6. Simplified defense system against oxidative stress in *T. cruzi.* Enzyme gene names are shown with their current ID annotation in the TriTrypDB followed by the fold change after Pd-dppf-mpo treatment. Gene name in light gray represents transcripts whose abundance was either not modulated or was only poorly modulated (between -1.5 and 1.5 fold). Genes from Non-Esmeraldo haplotype are shown.

Cyclophilin (TcCLB.510947.50), also known as rotamase, not only participates in the response to oxidative stress, but also has protein folding activity [41]. In previous reports, cyclophilin has been found to be positively regulated in parasites resistant to drugs such as Benznidazole, [41, 49, 89]. In Pd-dppf-mpo and Pt-dppf-mpo-treated parasites, cyclophilin mRNA levels are downregulated (FC T -5.54 and -2.54). However, protein levels do not change in treated and untreated parasites after Pd-dppf-mpo incubation (FC 1.07). Although we cannot rule out the existence of a cellular mechanism to counteract this decrease in mRNA levels (perhaps through protein stabilization), it should be kept in mind that effects on protein abundance may not be detectable until a later time point.

NADH-dependent fumarate reductase (FRD, TcCLB.503849.60)) is the enzyme responsible for the conversion of fumarate to succinate in a NADH-dependent reaction. This protein is expressed all along the parasite's life cycle and it is absent in the human host. In previous work, the inhibitory effect of related compounds against FRD was predicted by molecular docking studies and experimentally confirmed on *T. cruzi* protein extracts [31]. After Pt-dppf-mpo treatment, mRNA levels were slightly decreased (FC T -1.23). However, protein levels were increased by more than 3 fold (FC 3.27). This finding

View Article Online
DOI: 10.1039/D0MT00030B

leads us to hypothesize that FRD activity may be impaired in Pt-dppf-mpo-treated parasites, and that the observed increased protein level may be part of a response mechanism triggered to overcome this impaired FRD activity.

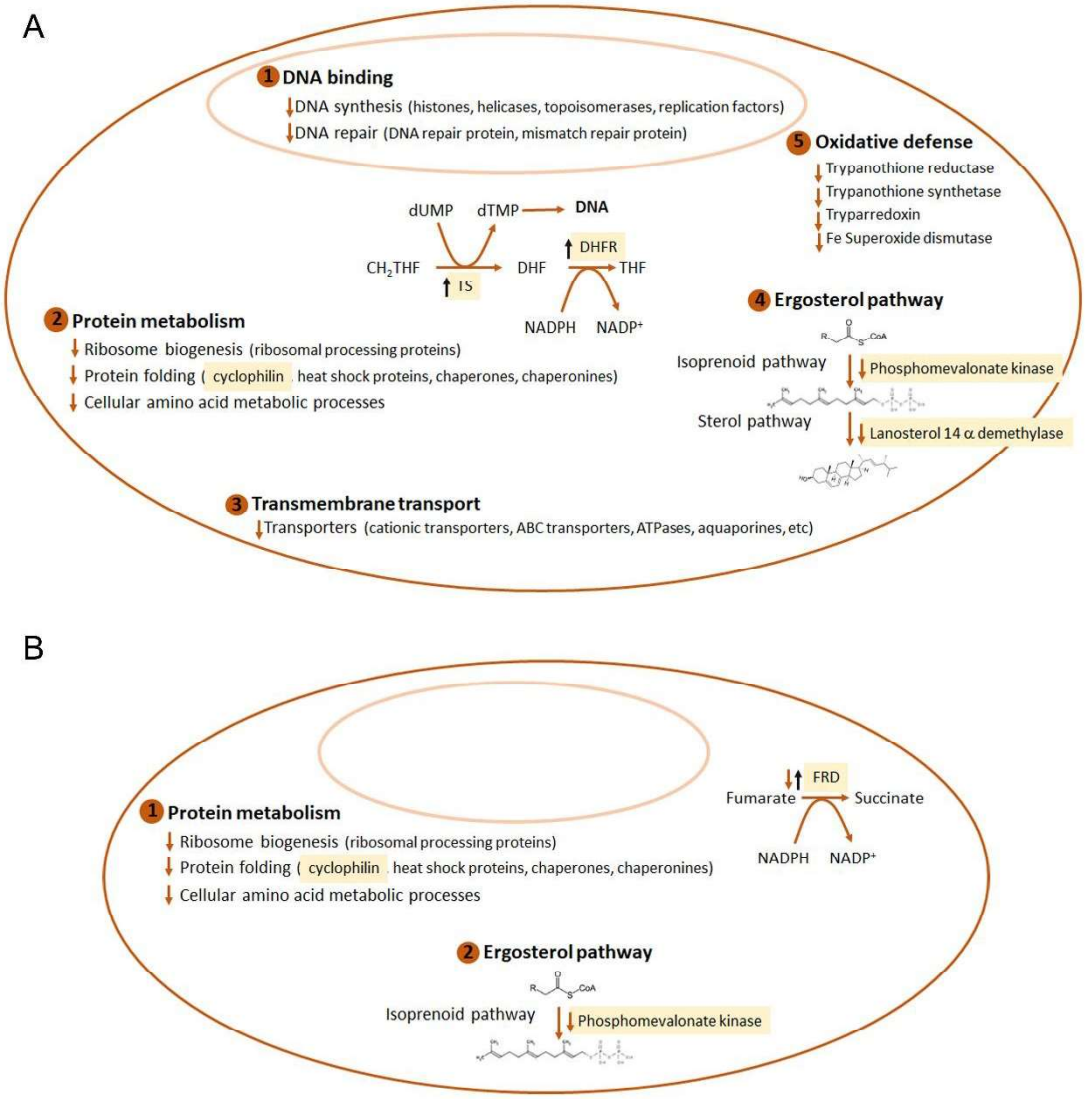

Figure 7. Schematic model of cellular effects and potential targets of Pd-dppf-mpo (A) and Pt-dppf-mpo (B) on treated parasites. Altered pathways and essential genes are represented. Orange arrows indicate regulated transcripts in treated parasites (up or down) whereas black arrows represent regulated proteins. **A)** Altered pathways and relevant enzymes after treatment with Pd-dppf-mpo. **(1)** Proteins involved in DNA synthesis (histones, helicases, topoisomerases, replication factors) and DNA repair are downregulated. **(2)** Proteins involved in ribosome biogenesis, protein folding and related to cellular amino acid processes. **(3)** Pd-dppf-mpo treatment also affect transmembrane transport and **(4)** Ergosterol synthesis pathway in which almost all participating enzymes are downregulated. **(5)** Several enzymes involved in response to oxidative stress are altered, also suggesting that Pd-dppf-mpo acts on the Oxidative defense pathway. Essential enzymes that can be considered promising drug target proteins are represented in yellow: Cyclophilin is involved in protein folding and abundance, and its mRNA is underrepresented; phosphomevalonate kinase and lanosterol-14-a-

demethylase are essential and important enzymes in the ergosterol pathway whose mRNA is also decreased in treated parasites. In *T. cruzi*, dihydropholate reductase and thymidylate synthase activities are together in a unique bifunctional enzyme. TS participates in the *de novo* synthesis of dTMP for DNA synthesis and DHFR takes the produced dihydrofolate to produce tetrahydrofolate used for one carbon unit transfer reactions in several biochemical processes, including thymidylate, purine, and amino acid biosynthesis. Proteomic data reveals that this bifunctional protein is increased after treatment. **B)** Altered pathways and relevant enzymes after treatment with Pt-dppf-mpo. **(1)** This treatment also affects proteins involved in ribosome biogenesis, protein folding and pathways related to cellular amino acid processes. Essential enzymes considered good drug targets are also represented in yellow. **(2)** As with Pd-dppf-mpo, expression of mRNA coding for phosphomevalonate kinase is decreased. Fumarate reductase is the enzyme responsible for the conversion of fumarate into succinate, a highly important step in microbial metabolism as part of anaerobic respiration. Its mRNA levels are decreased whereas its protein levels are increased after treatment, suggesting the existence of a cellular mechanism that responds to low mRNA levels by increasing protein translation or stability, therefore compensating for low transcript levels after Pt-dppf-mpo treatment.

Concluding remarks

In this study, we have taken an in-depth, comparative look at the effects of two structurally related organometallic Pd and Pt compounds on the global gene expression pattern of *T. cruzi* epimastigotes. Twenty-two percent of *T. cruzi* detected genes were modulated at the transcript level by treatment with Pd-dppf-mpo. Fewer than 2% of detected genes were modulated at the transcript level by treatment with Pt-dppf-mpo. A relatively low correlation between transcriptome and proteome expression values has been highlighted before for *T. cruzi,* where transcriptional initiation is not considered to be a significant point of regulation. Treatment with Pd-dppf-mpo seems to have both a transcriptomic and a proteomic effect. (Figure 4, panels A and B). In the case of Pt-dppf-mpo, where a lower percentage of transcripts were differentially expressed after treatment with the drug, we observed a clear effect of the compound at the proteome level (Figure 4, Panels C and D), strongly suggesting translational and post-translational modulation attributable to Pt-dppf-mpo. Transcripts modulated by both drugs invariably changed in the same direction. Our approach allowed us to tease out the effects that were specific to the metal (Pt or Pd) and the effects that were likely attributable to the ligand moiety shared by both drugs. Functional enrichment analysis of the *T. cruzi* transcriptome modified by incubation with these organometallic compounds yielded categories such as DNA binding, protein metabolism, and transmembrane transport (Table 3). Cell death is likely not the result of the action of a compound on a single pathway or target and our studies have indeed identified several potential modes of action of Pt-dppf-mpo and Pd-dppf-mpo. We queried our dataset for the presence of a set of previously defined and validated essential gene products in *T. cruzi*, and we found that 25% (4 out of 16) of them are downregulated after treatment with Pd-dppf-mpo and one is downregulated after treatment with Pt-dppf-mpo (Table 4). It is important to highlight that our approach revealed that these metal compounds impact the levels of transcripts encoding enzymes that belong to pathways which are either parasite-specific, essential, or both (Figure 7). Transcripts whose products belong to relevant pathways,

including those related to ergosterol synthesis and antioxidant defense, were downregulated after treatment. In particular, transcripts that code for products considered to be appropriate targets for pharmacological intervention were decreased by incubation with our compounds (Figure 7, highlighted in yellow). Further research is needed to ascertain the mechanism of action through which these targets are affected by Pd-dppf-mpo or Pt-dppf-mpo. We additionally included proteomic data to strengthen our model. As noted above, many genes affected at the transcript level were unaffected at the protein level. This may reflect either compensatory mechanisms or differential kinetics of the effect of the compounds on RNA and protein. In the case of DHFR-TS, even though transcript levels are partially depleted by treatment, proteins levels actually increase (Figure 7, black arrows), strongly implicating mechanisms at the level of translational efficiency or protein turnover to maintain an adequate supply of this essential enzyme. The protein levels of FRD, an enzyme whose activity was previously shown to be inhibited by related compounds [31], is increased after treatment with Pt-dppf-mpo (possibly as a compensatory mechanism), making it an attractive target for further studies. In sum, our analysis expanded on our knowledge of the mechanism of action of two organometallic compounds on *T. cruzi* providing a comprehensive repertoire of the parasite molecular response including pharmacological targets that meet the criteria of essentiality, specificity, and/or drugability, thereby setting the stage for future research.

Acknowledgement
This research was supported by Agencia Nacional de Investigación e Innovación, ANII (grant POS_FMV_2015_1_1005183) and Comisión Sectorial de Investigación Científica, CSIC (grant CSIC_POS_362).

Conflicts of interest
There are no conflicts of interest to declare

References

1. Guarner, J. (2019) Chagas disease as example of a reemerging parasite, *Semin Diagn Pathol 36*, 164-169.
2. Bustos, P. L., Milduberger, N., Volta, B. J., Perrone, A. E., Laucella, S. A., and Bua, J. (2019) Trypanosoma cruzi Infection at the Maternal-Fetal Interface: Implications of Parasite Load in the Congenital Transmission and Challenges in the Diagnosis of Infected Newborns, *Front Microbiol 10*, 1250.
3. Benvenuti, L. A., Roggerio, A., Cavalcanti, M. M., Nishiya, A. S., and Levi, J. E. (2017) An autopsy-based study of Trypanosoma cruzi persistence in organs of chronic chagasic patients and its relevance for transplantation, *Transpl Infect Dis 19*.
4. Santana, R. A. G., Guerra, M., Sousa, D. R., Couceiro, K., Ortiz, J. V., Oliveira, M., Ferreira, L. S., Souza, K. R., Tavares, I. C., Morais, R. F., Silva, G. A. V., Melo, G. C., Vergel, G. M., Albuquerque, B. C., Arcanjo, A. R. L., Monteiro, W. M., Ferreira, J., Lacerda, M. V. G., Silveira, H., and Guerra, J. A. O. (2019) Oral Transmission of Trypanosoma cruzi, Brazilian Amazon, *Emerg Infect Dis 25*, 132-135.
5. Ribeiro, M., Nitz, N., Santana, C., Moraes, A., Hagstrom, L., Andrade, R., Rios, A., Sousa, A., Dallago, B., Gurgel-Goncalves, R., and Hecht, M. (2016) Sexual transmission of Trypanosoma cruzi in murine model, *Exp Parasitol 162*, 1-6.

6. Paucar, R., Moreno-Viguri, E., and Perez-Silanes, S. (2016) Challenges in Chagas Disease Drug Discovery: A Review, *Curr Med Chem 23*, 3154-3170.
7. Sales Junior, P. A., Molina, I., Fonseca Murta, S. M., Sanchez-Montalva, A., Salvador, F., Correa-Oliveira, R., and Carneiro, C. M. (2017) Experimental and Clinical Treatment of Chagas Disease: A Review, *Am J Trop Med Hyg 97*, 1289-1303.
8. Prata, A. (2001) Clinical and epidemiological aspects of Chagas disease, *Lancet Infect Dis 1*, 92-100.
9. Rassi, A., Rezende, J., Ostermayer, A., and Rassi Jr, A. (2010) *Clinical Phases and Forms of Chagas Disease.* , First edition ed., Elsevier.
10. Rassi, A., Jr., Rassi, A., and Marin-Neto, J. A. (2010) Chagas disease, *Lancet 375*, 1388-1402.
11. Tyler K.M., O. C. L., ; Engman D.M. (2003) *The Life Cycle Of Trypanosoma Cruzi.*, Vol. 7.
12. Field, M. C., Horn, D., Fairlamb, A. H., Ferguson, M. A. J., Gray, D. W., Read, K. D., De Rycker, M., Torrie, L. S., Wyatt, P. G., Wyllie, S., and Gilbert, I. H. (2017) Anti-trypanosomatid drug discovery: an ongoing challenge and a continuing need, *Nature reviews. Microbiology 15*, 447.
13. Barrett, M. P., Burchmore, R. J., Stich, A., Lazzari, J. O., Frasch, A. C., Cazzulo, J. J., and Krishna, S. (2003) The trypanosomiases, *Lancet 362*, 1469-1480.
14. WHO, W. H. O. (2020) http://www.who.int/chagas/en/.
15. WHO, W. H. O. (2020) https://www.who.int/neglected_diseases/diseases/en/.
16. Nunes, M. C., Dones, W., Morillo, C. A., Encina, J. J., Ribeiro, A. L., and Council on Chagas Disease of the Interamerican Society of, C. (2013) Chagas disease: an overview of clinical and epidemiological aspects, *J Am Coll Cardiol 62*, 767-776.
17. Apt, W. (2017) Treatment of Chagas disease, *American Trypanosomiasis Chagas Disease (Second Edition) One Hundred Years of Research*, 751-771.
18. Ribeiro, V., Dias, N., Paiva, T., Hagstrom-Bex, L., Nitz, N., Pratesi, R., and Hecht, M. (2019) Current trends in the pharmacological management of Chagas disease, *International journal for parasitology. Drugs and drug resistance 12*, 7-17.
19. Barrett, M. P., Kyle, D. E., Sibley, L. D., Radke, J. B., and Tarleton, R. L. (2019) Protozoan persister-like cells and drug treatment failure, *Nature reviews. Microbiology 17*, 607-620.
20. Komeda, S., and Casini, A. (2012) Next-generation anticancer metallodrugs, *Curr Top Med Chem 12*, 219-235.
21. de Almeida, A., Oliveira, B. L., Correia, J. D. G., Soveral, G., and Casini, A. (2013) Emerging protein targets for metal-based pharmaceutical agents: An update., *Coordination Chemistry Reviews. 257*, 2689-2704.
22. Mjos, K. D., and Orvig, C. (2014) Metallodrugs in medicinal inorganic chemistry, *Chem Rev 114*, 4540-4563.
23. Medici, S., Peana, M., Marin Nurchi, V., Lachowicz, J. I., Crisponi, G., and Zoroddu, M. A. (2015) Noble metals in medicine: Latest advances, *Coordination Chemistry Reviews 284*, 329-350.
24. Sanchez-Delgado, R. A., and Anzellotti, A. (2004) Metal complexes as chemotherapeutic agents against tropical diseases: trypanosomiasis, malaria and leishmaniasis, *Mini Rev Med Chem 4*, 23-30.
25. Navarro, M., Gabbiani, C., Messori, L., and Gambino, D. (2010) Metal-based drugs for malaria, trypanosomiasis and leishmaniasis: recent achievements and perspectives, *Drug Discov Today 15*, 1070-1078.
26. Gambino, D., and Otero, L. (2012) Perspectives on what ruthenium-based compounds could offer in the development of potential antiparasitic drugs, *Inorganica Chimica Acta 393*, 103-114.

27. Gambino, D., and Otero, L. (2018) Design of prospective antiparasitic metal-based compounds including selected organometallic cores, *Inorganica Chimica Acta 472*, 58-75.
28. Glisic, B. D., and Djuran, M. I. (2014) Gold complexes as antimicrobial agents: an overview of different biological activities in relation to the oxidation state of the gold ion and the ligand structure, *Dalton Trans 43*, 5950-5969.
29. Mosquillo, M. F., Bilbao, L., Hernandez, F., Machado, I., Gambino, D., Garat, B., and Perez-Diaz, L. (2018) Effect of a new anti-T. cruzi metallic compound based on palladium, *Biometals 31*, 961-974.
30. Mosquillo, M. F., Bilbao, L., Hernandez, F., Tissot, F., Gambino, D., Garat, B., and Perez-Diaz, L. (2018) Trypanosoma cruzi biochemical changes and cell death induced by an organometallic platinum-based compound, *Chem Biol Drug Des 92*, 1657-1669.
31. Rodriguez Arce, E., Mosquillo, M. F., Perez-Diaz, L., Echeverria, G. A., Piro, O. E., Merlino, A., Coitino, E. L., Maringolo Ribeiro, C., Leite, C. Q., Pavan, F. R., Otero, L., and Gambino, D. (2015) Aromatic amine N-oxide organometallic compounds: searching for prospective agents against infectious diseases, *Dalton Trans 44*, 14453-14464.
32. Mortazavi, A., Williams, B. A., McCue, K., Schaeffer, L., and Wold, B. (2008) Mapping and quantifying mammalian transcriptomes by RNA-Seq, *Nat Methods 5*, 621-628.
33. Li, Y., Shah-Simpson, S., Okrah, K., Belew, A. T., Choi, J., Caradonna, K. L., Padmanabhan, P., Ndegwa, D. M., Temanni, M. R., Corrada Bravo, H., El-Sayed, N. M., and Burleigh, B. A. (2016) Transcriptome Remodeling in Trypanosoma cruzi and Human Cells during Intracellular Infection, *PLoS Pathog 12*, e1005511.
34. Oliveira, A. E. R., Grazielle-Silva, V., Ferreira, L. R. P., and Teixeira, S. M. R. (2020) Close encounters between Trypanosoma cruzi and the host mammalian cell: Lessons from genome-wide expression studies, *Genomics 112*, 990-997.
35. Berna, L., Chiribao, M. L., Greif, G., Rodriguez, M., Alvarez-Valin, F., and Robello, C. (2017) Transcriptomic analysis reveals metabolic switches and surface remodeling as key processes for stage transition in Trypanosoma cruzi, *PeerJ 5*, e3017.
36. Chavez, S., Eastman, G., Smircich, P., Becco, L. L., Oliveira-Rizzo, C., Fort, R., Potenza, M., Garat, B., Sotelo-Silveira, J. R., and Duhagon, M. A. (2017) Transcriptome-wide analysis of the Trypanosoma cruzi proliferative cycle identifies the periodically expressed mRNAs and their multiple levels of control, *PLoS One 12*, e0188441.
37. Smircich, P., Eastman, G., Bispo, S., Duhagon, M. A., Guerra-Slompo, E. P., Garat, B., Goldenberg, S., Munroe, D. J., Dallagiovanna, B., Holetz, F., and Sotelo-Silveira, J. R. (2015) Ribosome profiling reveals translation control as a key mechanism generating differential gene expression in Trypanosoma cruzi, *BMC Genomics 16*, 443.
38. Avila, C. C., Mule, S. N., Rosa-Fernandes, L., Viner, R., Barison, M. J., Costa-Martins, A. G., Oliveira, G. S., Teixeira, M. M. G., Marinho, C. R. F., Silber, A. M., and Palmisano, G. (2018) Proteome-Wide Analysis of Trypanosoma cruzi Exponential and Stationary Growth Phases Reveals a Subcellular Compartment-Specific Regulation, *Genes (Basel) 9*.
39. Pastro, L., Smircich, P., Di Paolo, A., Becco, L., Duhagon, M. A., Sotelo-Silveira, J., and Garat, B. (2017) Nuclear Compartmentalization Contributes to Stage-Specific Gene Expression Control in Trypanosoma cruzi, *Front Cell Dev Biol 5*, 8.
40. Belew, A. T., Junqueira, C., Rodrigues-Luiz, G. F., Valente, B. M., Oliveira, A. E. R., Polidoro, R. B., Zuccherato, L. W., Bartholomeu, D. C., Schenkman, S., Gazzinelli, R. T., Burleigh, B. A., El-Sayed, N. M., and Teixeira, S. M. R. (2017) Comparative transcriptome profiling of virulent and non-virulent Trypanosoma

cruzi underlines the role of surface proteins during infection, *PLoS Pathog 13*, e1006767.
41. Garcia-Huertas, P., Mejia-Jaramillo, A. M., Gonzalez, L., and Triana-Chavez, O. (2017) Transcriptome and Functional Genomics Reveal the Participation of Adenine Phosphoribosyltransferase in Trypanosoma cruzi Resistance to Benznidazole, *J Cell Biochem 118*, 1936-1945.
42. Clayton, C. E. (2016) Gene expression in Kinetoplastids, *Curr Opin Microbiol 32*, 46-51.
43. De Gaudenzi, J. G., Noe, G., Campo, V. A., Frasch, A. C., and Cassola, A. (2011) Gene expression regulation in trypanosomatids, *Essays Biochem 51*, 31-46.
44. Parsons, M., and Myler, P. J. (2016) Illuminating Parasite Protein Production by Ribosome Profiling, *Trends Parasitol 32*, 446-457.
45. Lucena, A. C. R., Amorim, J. C., de Paula Lima, C. V., Batista, M., Krieger, M. A., de Godoy, L. M. F., and Marchini, F. K. (2019) Quantitative phosphoproteome and proteome analyses emphasize the influence of phosphorylation events during the nutritional stress of Trypanosoma cruzi: the initial moments of in vitro metacyclogenesis, *Cell Stress Chaperones 24*, 927-936.
46. Atwood, J. A., 3rd, Weatherly, D. B., Minning, T. A., Bundy, B., Cavola, C., Opperdoes, F. R., Orlando, R., and Tarleton, R. L. (2005) The Trypanosoma cruzi proteome, *Science 309*, 473-476.
47. de Godoy, L. M., Marchini, F. K., Pavoni, D. P., Rampazzo Rde, C., Probst, C. M., Goldenberg, S., and Krieger, M. A. (2012) Quantitative proteomics of Trypanosoma cruzi during metacyclogenesis, *Proteomics 12*, 2694-2703.
48. Queiroz, R. M., Charneau, S., Motta, F. N., Santana, J. M., Roepstorff, P., and Ricart, C. A. (2013) Comprehensive proteomic analysis of Trypanosoma cruzi epimastigote cell surface proteins by two complementary methods, *J Proteome Res 12*, 3255-3263.
49. Andrade, H. M., Murta, S. M., Chapeaurouge, A., Perales, J., Nirde, P., and Romanha, A. J. (2008) Proteomic analysis of Trypanosoma cruzi resistance to Benznidazole, *J Proteome Res 7*, 2357-2367.
50. Bolger, A. M., Lohse, M., and Usadel, B. (2014) Trimmomatic: a flexible trimmer for Illumina sequence data, *Bioinformatics 30*, 2114-2120.
51. Langmead, B., and Salzberg, S. L. (2012) Fast gapped-read alignment with Bowtie 2, *Nat Methods 9*, 357-359.
52. Anders, S., Pyl, P. T., and Huber, W. (2015) HTSeq--a Python framework to work with high-throughput sequencing data, *Bioinformatics 31*, 166-169.
53. Love, M. I. H., W.; Anders, S. (2014) Moderated estimation of fold change and dispersion for RNA-seq data with DESeq2, *Genome Biol 15*, 550.
54. Livak, K. J., and Schmittgen, T. D. (2001) Analysis of relative gene expression data using real-time quantitative PCR and the 2(-Delta Delta C(T)) Method, *Methods 25*, 402-408.
55. Rossello, J., Lima, A., Gil, M., Rodriguez Duarte, J., Correa, A., Carvalho, P. C., Kierbel, A., and Duran, R. (2017) The EAL-domain protein FcsR regulates flagella, chemotaxis and type III secretion system in Pseudomonas aeruginosa by a phosphodiesterase independent mechanism, *Sci Rep 7*, 10281.
56. Carvalho, P. C., Fischer, J. S., Xu, T., Cociorva, D., Balbuena, T. S., Valente, R. H., Perales, J., Yates, J. R., 3rd, and Barbosa, V. C. (2012) Search engine processor: Filtering and organizing peptide spectrum matches, *Proteomics 12*, 944-949.
57. Ghaemmaghami, S., Huh, W. K., Bower, K., Howson, R. W., Belle, A., Dephoure, N., O'Shea, E. K., and Weissman, J. S. (2003) Global analysis of protein expression in yeast, *Nature 425*, 737-741.
58. Lundgren, D. H., Hwang, S. I., Wu, L., and Han, D. K. (2010) Role of spectral counting in quantitative proteomics, *Expert Rev Proteomics 7*, 39-53.

59. Szklarczyk, D., Gable, A. L., Lyon, D., Junge, A., Wyder, S., Huerta-Cepas, J., Simonovic, M., Doncheva, N. T., Morris, J. H., Bork, P., Jensen, L. J., and Mering, C. V. (2019) STRING v11: protein-protein association networks with increased coverage, supporting functional discovery in genome-wide experimental datasets, *Nucleic Acids Res 47*, D607-D613.
60. Jones, N. G., Catta-Preta, C. M. C., Lima, A., and Mottram, J. C. (2018) Genetically Validated Drug Targets in Leishmania: Current Knowledge and Future Prospects, *ACS Infect Dis 4*, 467-477.
61. McGuire, J. J. (2003) Anticancer antifolates: current status and future directions, *Curr Pharm Des 9*, 2593-2613.
62. Sienkiewicz, N., Jaroslawski, S., Wyllie, S., and Fairlamb, A. H. (2008) Chemical and genetic validation of dihydrofolate reductase-thymidylate synthase as a drug target in African trypanosomes, *Mol Microbiol 69*, 520-533.
63. Beck, J. T., and Ullman, B. (1990) Nutritional requirements of wild-type and folate transport-deficient Leishmania donovani for pterins and folates, *Mol Biochem Parasitol 43*, 221-230.
64. Cardoso, M. S., Junqueira, C., Trigueiro, R. C., Shams-Eldin, H., Macedo, C. S., Araujo, P. R., Gomes, D. A., Martinelli, P. M., Kimmel, J., Stahl, P., Niehus, S., Schwarz, R. T., Previato, J. O., Mendonca-Previato, L., Gazzinelli, R. T., and Teixeira, S. M. (2013) Identification and functional analysis of Trypanosoma cruzi genes that encode proteins of the glycosylphosphatidylinositol biosynthetic pathway, *PLoS Negl Trop Dis 7*, e2369.
65. de Macedo, C. S., Shams-Eldin, H., Smith, T. K., Schwarz, R. T., and Azzouz, N. (2003) Inhibitors of glycosyl-phosphatidylinositol anchor biosynthesis, *Biochimie 85*, 465-472.
66. Hashimoto, M., Enomoto, M., Morales, J., Kurebayashi, N., Sakurai, T., Hashimoto, T., Nara, T., and Mikoshiba, K. (2013) Inositol 1,4,5-trisphosphate receptor regulates replication, differentiation, infectivity and virulence of the parasitic protist Trypanosoma cruzi, *Mol Microbiol 87*, 1133-1150.
67. Hashimoto, M., Nara, T., Hirawake, H., Morales, J., Enomoto, M., and Mikoshiba, K. (2014) Antisense oligonucleotides targeting parasite inositol 1,4,5-trisphosphate receptor inhibits mammalian host cell invasion by Trypanosoma cruzi, *Sci Rep 4*, 4231.
68. Osorio-Mendez, J. F., and Cevallos, A. M. (2018) Discovery and Genetic Validation of Chemotherapeutic Targets for Chagas' Disease, *Front Cell Infect Microbiol 8*, 439.
69. Nagle, A. S., Khare, S., Kumar, A. B., Supek, F., Buchynskyy, A., Mathison, C. J., Chennamaneni, N. K., Pendem, N., Buckner, F. S., Gelb, M. H., and Molteni, V. (2014) Recent developments in drug discovery for leishmaniasis and human African trypanosomiasis, *Chem Rev 114*, 11305-11347.
70. Silva, D. T., de Nazareth, S. L. d. M. M., Almeida, D., Urbina, J. A., and Pereira, M. C. (2006) Cytoskeleton reassembly in cardiomyocytes infected by Trypanosoma cruzi is triggered by treatment with ergosterol biosynthesis inhibitors, *Int J Antimicrob Agents 27*, 530-537.
71. Lepesheva, G. I., Villalta, F., and Waterman, M. R. (2011) Targeting Trypanosoma cruzi sterol 14alpha-demethylase (CYP51), *Adv Parasitol 75*, 65-87.
72. Buckner, F. S., and Urbina, J. A. (2012) Recent Developments in Sterol 14-demethylase Inhibitors for Chagas Disease, *International journal for parasitology. Drugs and drug resistance 2*, 236-242.
73. Cosentino, R. O., and Aguero, F. (2014) Genetic profiling of the isoprenoid and sterol biosynthesis pathway genes of Trypanosoma cruzi, *PLoS One 9*, e96762.
74. Urbina, J. A. (2009) Ergosterol biosynthesis and drug development for Chagas disease, *Mem Inst Oswaldo Cruz 104 Suppl 1*, 311-318.

75. Perez-Moreno, G., Sealey-Cardona, M., Rodrigues-Poveda, C., Gelb, M. H., Ruiz-Perez, L. M., Castillo-Acosta, V., Urbina, J. A., and Gonzalez-Pacanowska, D. (2012) Endogenous sterol biosynthesis is important for mitochondrial function and cell morphology in procyclic forms of Trypanosoma brucei, *Int J Parasitol 42*, 975-989.
76. Kessler, R. L., Soares, M. J., Probst, C. M., and Krieger, M. A. (2013) Trypanosoma cruzi response to sterol biosynthesis inhibitors: morphophysiological alterations leading to cell death, *PLoS One 8*, e55497.
77. Houten, S. M., and Waterham, H. R. (2001) Nonorthologous gene displacement of phosphomevalonate kinase, *Mol Genet Metab 72*, 273-276.
78. Villalta, F., Dobish, M. C., Nde, P. N., Kleshchenko, Y. Y., Hargrove, T. Y., Johnson, C. A., Waterman, M. R., Johnston, J. N., and Lepesheva, G. I. (2013) VNI cures acute and chronic experimental Chagas disease, *J Infect Dis 208*, 504-511.
79. Lepesheva, G. I., Hargrove, T. Y., Rachakonda, G., Wawrzak, Z., Pomel, S., Cojean, S., Nde, P. N., Nes, W. D., Locuson, C. W., Calcutt, M. W., Waterman, M. R., Daniels, J. S., Loiseau, P. M., and Villalta, F. (2015) VFV as a New Effective CYP51 Structure-Derived Drug Candidate for Chagas Disease and Visceral Leishmaniasis, *J Infect Dis 212*, 1439-1448.
80. Hoekstra, W. J., Hargrove, T. Y., Wawrzak, Z., da Gama Jaen Batista, D., da Silva, C. F., Nefertiti, A. S., Rachakonda, G., Schotzinger, R. J., Villalta, F., Soeiro Mde, N., and Lepesheva, G. I. (2016) Clinical Candidate VT-1161's Antiparasitic Effect In Vitro, Activity in a Murine Model of Chagas Disease, and Structural Characterization in Complex with the Target Enzyme CYP51 from Trypanosoma cruzi, *Antimicrob Agents Chemother 60*, 1058-1066.
81. Guedes-da-Silva, F. H., Batista, D. G., Da Silva, C. F., De Araujo, J. S., Pavao, B. P., Simoes-Silva, M. R., Batista, M. M., Demarque, K. C., Moreira, O. C., Britto, C., Lepesheva, G. I., and Soeiro, M. N. (2017) Antitrypanosomal Activity of Sterol 14alpha-Demethylase (CYP51) Inhibitors VNI and VFV in the Swiss Mouse Models of Chagas Disease Induced by the Trypanosoma cruzi Y Strain, *Antimicrob Agents Chemother 61*.
82. Krauth-Siegel, R. L., and Comini, M. A. (2008) Redox control in trypanosomatids, parasitic protozoa with trypanothione-based thiol metabolism, *Biochim Biophys Acta 1780*, 1236-1248.
83. Turrens, J. F. (2004) Oxidative stress and antioxidant defenses: a target for the treatment of diseases caused by parasitic protozoa, *Mol Aspects Med 25*, 211-220.
84. Colotti, G., Baiocco, P., Fiorillo, A., Boffi, A., Poser, E., Chiaro, F. D., and Ilari, A. (2013) Structural insights into the enzymes of the trypanothione pathway: targets for antileishmaniasis drugs, *Future Med Chem 5*, 1861-1875.
85. Leroux, A. E., and Krauth-Siegel, R. L. (2016) Thiol redox biology of trypanosomatids and potential targets for chemotherapy, *Mol Biochem Parasitol 206*, 67-74.
86. Ilari, A., Fiorillo, A., Genovese, I., and Colotti, G. (2017) Polyamine-trypanothione pathway: an update, *Future Med Chem 9*, 61-77.
87. Krauth-Siegel, R. L., Bauer, H., and Schirmer, R. H. (2005) Dithiol proteins as guardians of the intracellular redox milieu in parasites: old and new drug targets in trypanosomes and malaria-causing plasmodia, *Angew Chem Int Ed Engl 44*, 690-715.
88. Taylor, M. C., Lewis, M. D., Fortes Francisco, A., Wilkinson, S. R., and Kelly, J. M. (2015) The Trypanosoma cruzi vitamin C dependent peroxidase confers protection against oxidative stress but is not a determinant of virulence, *PLoS Negl Trop Dis 9*, e0003707.
89. Rego, J. V., Duarte, A. P., Liarte, D. B., de Carvalho Sousa, F., Barreto, H. M., Bua, J., Romanha, A. J., Radis-Baptista, G., and Murta, S. M. (2015)

Molecular characterization of Cyclophilin (TcCyP19) in Trypanosoma cruzi populations susceptible and resistant to benznidazole, *Exp Parasitol 148*, 73-80.

View Article Online
DOI: 10.1039/D0MT00030B

Supplementary Figures and Tables

Figure S1. Principal component analysis (PCA) plot of *T. cruzi* transcriptomic data. Trends exhibited by the expression profiles of control untreated parasites (red dots), Pd-dppf-mpo (upper panel, green dots) and Pt-dppf-mpo treated parasites (lower panel, green dots). Each dot represents an independent sample.

Figure S2. Validation of RNA-Seq results. (A) Relative mRNA quantification of randomly selected modified transcripts identified by RNA-Seq through quantitative real-time PCR (qRT-PCR). For relative quantification the threonyl-tRNA synthetase transcript was used as a reference gene since its abundance was not affected by compound incubation. Upper and lower panels represent Pd-dppf-mpo and Pt-dppf-mpo modified transcripts respectively. **(B)** Correlation between qRT-PCR and RNA-Seq data is shown for Pd-dppf-mpo treatment (upper plot) and Pt-dppf-mpo treatment (lower plot). Comparison of $\log_2$ fold change of randomly selected genes obtained by RNA-seq and RT-qPCR. Statistically significant Pearson correlation is shown between the expression levels measured using both approaches (boxed number).

Table S1. Complete list of detected and regulated genes in Pd-dppf-mpo, Pt-dppf-mpo treated and untreated *T. cruzi* epimastigotes.

Table S2. Complete Gene ontology and KEGG up- and down- regulated in transcriptomic assay.

Table S3. Common and specific genes modulated after Pd-dppf-mpo and Pt-dppf-mpo treatment.

Table S4. Modulated proteins after treatment. The number of regulated soluble and insoluble proteins is shown for each treatment. Overrepresented proteins comprise proteins detected only in treated samples (Unique) and proteins found in both treated and untreated condition but increased to significantly different levels after treatment (Augmented). Underrepresented proteins comprise proteins detected only in control parasites (Unique) and proteins found in both treated and untreated conditions but increased to significantly different levels in untreated condition (Diminished).

Table S5. List of detected and regulated proteins after Pd-dppf-mpo and Pt-dppf-mpo treatment.

Table S6. List of common proteins to both compounds and specific to each central metal ion

Table S7. Metabolic Pathway enrichment analysis of proteomic data through STRING

7 Capítulo IV. Efecto de los compuestos M-dppf-mpo sobre los potenciales blancos moleculares seleccionados

Con el objetivo de comenzar a validar los modelos de acción propuestos para los compuestos M-dppf-mpo, fue estudiado particularmente el efecto sobre la vía del ergosterol y sobre blancos moleculares a distintos niveles de la misma. A través de la determinación de los niveles de esteroles por HPLC en parásitos tratados comparados con parásitos sin tratar, fue cuantificada la disminución de la producción del producto final ergosterol, confirmando que esta vía se encuentra afectada en respuesta al tratamiento con los compuestos basados en Pd y Pt. Se seleccionaron dos enzimas de la vía como dianas moleculares para su posterior análisis: fue evaluada la participación en la respuesta a los compuestos de la enzima fosfomevalonato quinasa (PMK), que participa en la vía isoprenoide, y la enzima lanosterol 14-α demetilasa (CYP51), de la vía de biosíntesis de esteroles. Estas enzimas cumplen con criterios fundamentales como esencialidad, selectividad y/o drogabilidad. Avanzando en intentar comprender el nivel molecular en el que participan estos compuestos, en colaboración con el grupo de la Dra. Paulino del Departamento de Experimentación y Teoría de la Estructura de la Materia y sus Aplicaciones (DETEMA) se realizaron procesos de *docking* molecular donde se encontraron potenciales sitios de interacción de los compuestos con las enzimas PMK y CYP51. Fueron generados parásitos que las sobreexpresan, los cuales se verificaron mediante RT-qPCR, citometría y microscopía confocal. Se avanzó hacia la validación de estas enzimas como participantes del mecanismo de acción, evaluando como impactan en la producción de ergosterol, y de los intermediarios escualeno y lanosterol. En conjunto, los resultados presentados confirman que el mecanismo de acción de los compuestos Pd-dppf-mpo y Pt-dppf-mpo consiste principalmente en la inhibición de la enzima CYP51 de la vía del ergosterol, lo que conduce a una disminución de la cantidad de este metabolito en la célula, esencial para la sobrevida del parásito. Cabe recordar que el modelo propuesto es multi-blanco, por lo que no se descarta la participación de más blancos moleculares actuando en paralelo y se requiere más investigación para completar el conocimiento del mecanismo de acción de estos compuestos.

Los resultados se encuentran recopilados en el manuscrito titulado “Treatment with Pt and Pd based compounds impairs ergosterol pathway in *Trypanosoma cruzi*”, enviado para su revisión por pares en la revista científica European Journal of Medicinal Chemistry.

European Journal of Medicinal Chemistry

Treatment with Pt and Pd based compounds impairs ergosterol pathway in Trypanosoma cruzi

--Manuscript Draft--

Manuscript Number:	
Article Type:	Full Paper
Keywords:	ergosterol biosynthesis; Trypanosoma cruzi; metal-based drugs
Corresponding Author:	Leticia Perez Diaz, PhD Facultad de Ciencias Montevideo, Montevideo URUGUAY
First Author:	Florencia Mosquillo
Order of Authors:	Florencia Mosquillo
	Gonzalo Scalese
	Rodrigo Moreira
	Pablo A Denis
	Ignacio Machado
	Margot Paulino
	Dinorah Gambino
	Leticia Perez Diaz, PhD
Abstract:	Current treatment for Chagas' disease is based on two drugs, Nifurtimox and Benznidazol, which have limitations, contraindications, and side effects that reduce the effectiveness and continuity of treatment, thus there is an urgent need to develop new safe and effective drugs. Metal-based complexes have shown to be a promising approach against parasitic diseases and this study aims to advance the search for effective compounds. In previous work, two new metal-based compounds with trypanocidal activity, Pd-dppf-mpo and Pt-dppf-mpo, were fully characterized. To unravel the whole mechanism of action of these two analogous metal-based drugs, high throughput omics studies on T. cruzi were performed. A multimodal mechanism of action was postulated with the selection of several candidates for molecular targets. In this work, we validated the ergosterol biosynthesis pathway as a target of action of these compounds. Ergosterol is essential for providing structure and function of parasite membranes and it is absent in mammalians. Through the determination of sterol levels in treated parasites we determined that this pathway is affected by the action of the compounds. Moving forward in the attempt to understand the molecular level at which these compounds participate, two enzymes that met eligibility criteria at different levels in the pathway were selected for further studies: phosphomevalonate kinase (PMK) and lanosterol 14-α demethylase (CYP51). Molecular docking processes were carried out to search for potential sites of interaction for both enzymes. To validate these candidates, a gain-of-function strategy was used, through the generation of overexpressing PMK and CYP51 parasites. Altogether, results here presented confirm that the mechanism of action of Pd-dppf-mpo and Pt-dppf-mpo compounds involves the inhibition of both enzymes PMK and CYP51, leading to a decrease in the amount of ergosterol in treated cells.
Suggested Reviewers:	Samuel Meier-Menches University of Vienna samuel.meier@univie.ac.at Expertise in metal compounds, drug discovery, ómics analysis
	Omar Triana-Chavez Universidad de Antioquia omar.triana@udea.edu.co expertise in drug discovery, host-parasite interaction, Trypanosoma cruzi

	Carolina Mascayano Universidad de Santiago de Chile carolina.mascayano@usach.cl Expertise in in silico studies and biochemistry

Cover Letter

Facultad de Ciencias
Sección Genómica Funcional

UNIVERSIDAD DE LA REPÚBLICA
URUGUAY

FACULTAD DE
CIENCIAS
UDELAR | fcien.edu.uy

December 21, 2022

Dr. Herve Galons
Editor-in-Chief.
EUROPEAN JOURNAL OF MEDICINAL CHEMISTRY
Dear Dr. Galons,

We are here submitting our manuscript entitled "Treatment with Pt and Pd based compounds impairs ergosterol pathway in *Trypanosoma cruzi*" for your review and consideration for publication in The European Journal of Medicinal Chemistry.

In this work, through the determination of sterol levels in treated parasites we determined that this pathway is affected by the action of synthetized Pd-dppf-mpo and Pt-dppf-mpo compounds. To deepen in the molecular level at which these compounds participate, two enzymes that met eligibility criteria at different levels in the pathway were selected for further studies. Molecular docking processes were carried out to search for potential sites of interaction for both enzymes: phosphomevalonate kinase (PMK) and lanosterol 14-α demethylase (CYP51). A gain-of-function strategy was used through the generation of overexpressing PMK and CYP51 parasites to validate these enzymes as targets of both compounds. Altogether, results here presented confirm that the mechanism of action of Pd-dppf-mpo and Pt-dppf-mpo compounds involves the inhibition of both enzymes PMK and CYP51, leading to a decrease in the amount of ergosterol in treated cells.

For the last 50 years, treatment of Chagas disease caused by *T. cruzi* has been solely based on two drugs that exhibit severe side effects, especially in children and immunosuppressed patients. Therefore, development of new effective and nontoxic drugs is urgent. In this context, we believe that the study of the mode of action of these new effective anti-*T. cruzi* compounds contributes new information in this field and may be of interest to the readers of the European Journal of Medicinal Chemistry.

We are confident that our manuscript will meet the high standards required by and expected from the journal, and we thank you in advance for your careful consideration.

Yours sincerely,

Leticia Pérez-Díaz, PhD
Facultad de Ciencias, Montevideo, Uruguay
E-mail: lperez@fcien.edu.uy

Sección Genómica Funcional
Iguá 4225, 11400
Tel: (5982) 2525 8618 # 7237
Fax (5982) 2525 86 17

Sección Genómica Funcional
Iguá 4225, 11400
Tel: (5982) 2525 8618 # 7237
Fax (5982) 2525 86 17

Graphical Abstract (for review)

Click here to access/download;Graphical Abstract (for review);GraphicalAbstract.tif

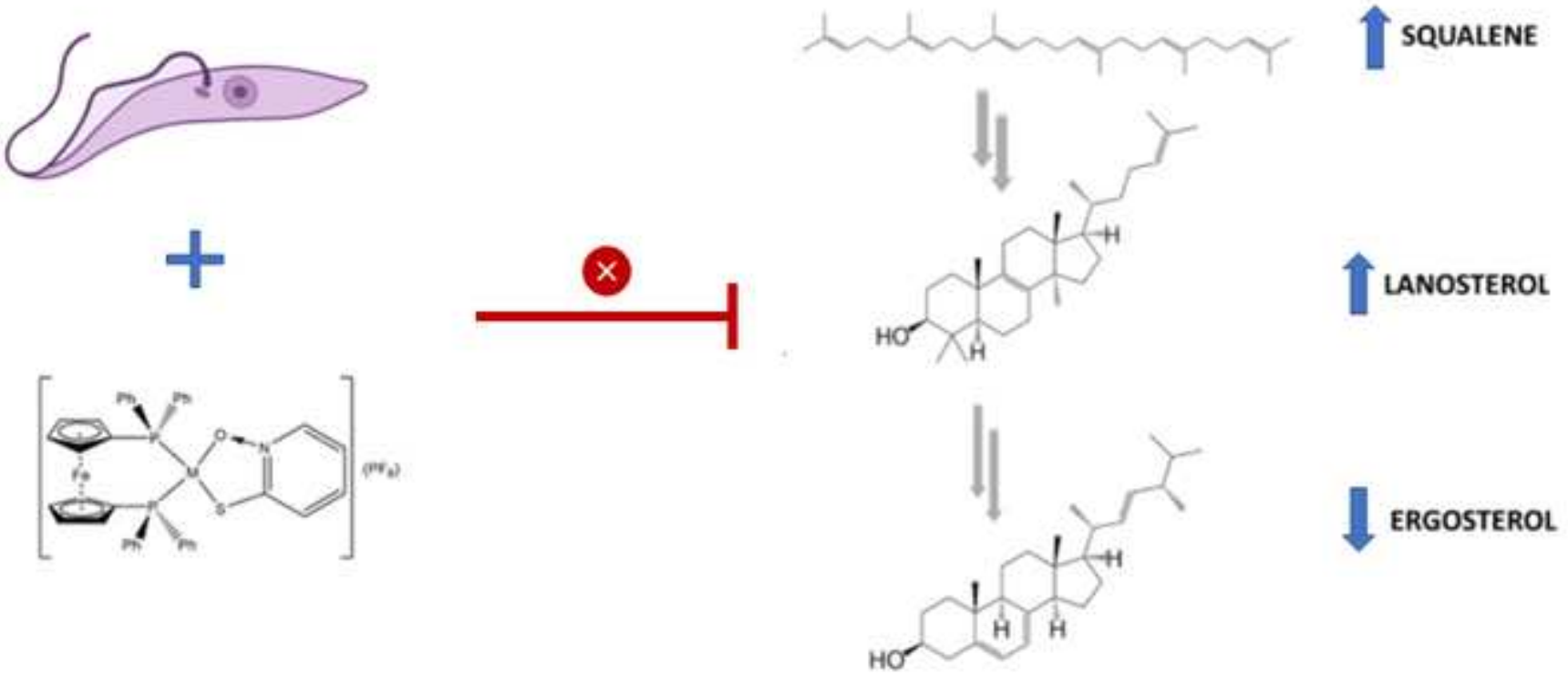

Treatment with Pt and Pd based compounds impairs ergosterol pathway in *Trypanosoma cruzi*

Florencia Mosquillo[1], Gonzalo Scalese[1,2], Rodrigo Moreira[2], Pablo A. Denis[3], Ignacio Machado[4], Margot Paulino[5], Dinorah Gambino[2], Leticia Pérez-Díaz[1*]

[1] Sección Genómica Funcional, Instituto de Química Biológica, Facultad de Ciencias, Universidad de la República, Uruguay.

[2] Área Química Inorgánica, DEC, Facultad de Química, Universidad de la República, Uruguay.

[3] Computational Nanotechnology, DETEMA, Facultad de Química, Universidad de la República, Uruguay.

[4] Área Química Analítica, DEC, Facultad de Química, Universidad de la República, Uruguay.

[5] Centro de Bioinformática, Facultad de Química, Universidad de la República, Uruguay.

*Address for correspondence to: Sección Genómica Funcional, Instituto de Química Biológica, Facultad de Ciencias, Universidad de la República, Igua 4225, Montevideo, Uruguay. lperez@fcien.edu.uy

Abstract

Current treatment for Chagas' disease is based on two drugs, Nifurtimox and Benznidazol, which have limitations, contraindications, and side effects that reduce the effectiveness and continuity of treatment. Thus there is an urgent need to develop new safe and effective drugs. Metal-based compounds have shown to be a promising approach against parasitic diseases and this study aims to advance the search for effective antitrypanosomal compounds. In previous work, two new metal-based compounds with trypanocidal activity, Pd-dppf-mpo and Pt-dppf-mpo, were fully characterized. To unravel the whole mechanism of action of these two analogous metal-based drugs, high throughput *omics* studies on *T. cruzi* were performed. A multimodal mechanism of action was postulated with several candidates as molecular targets. In this work, we validated the ergosterol biosynthesis pathway as a target of action of these compounds. Ergosterol is essential for providing structure and function of parasite membranes and it is absent in mammalians. Through the determination of sterol levels in treated parasites we determined that this pathway is affected by the action of the compounds. Moving forward in the attempt to understand the molecular level at which these compounds participate, two enzymes that met eligibility criteria at different levels in the pathway were selected for further studies: phosphomevalonate kinase (PMK) and lanosterol 14-α demethylase (CYP51). Molecular docking processes were carried out to search for potential sites of interaction for both enzymes. To validate these candidates, a gain-of-function strategy was used, through the generation of overexpressing PMK and CYP51 parasites. Altogether, results here presented confirm that the mechanism of action of Pd-dppf-mpo and Pt-dppf-mpo compounds involves the inhibition of both enzymes PMK and CYP51, leading to a decrease in the amount of ergosterol in treated cells.

Keywords: ergosterol biosynthesis; Trypanosoma cruzi; metal-based drugs

Introduction

Chagas disease (American Trypanosomiasis) is an ancient disease, discovered and described for the first time more than 100 years ago by the Brazilian scientist Carlos Chagas [1]. It is endemic in 21 Latin American countries, but the disease has spread across Europe, Australia, Japan and North America due to the growing number of people moving across borders [2, 3].

The disease is caused by the protozoan parasite *Trypanosoma cruzi* (*T. cruzi*). It is mainly transmitted to the mammalian host by the bite of infected blood-sucking triatomine bugs, but also through organ transplant and blood transfusion from unknowingly infected people, from infected pregnant woman to fetus and, less commonly, by consumption of uncooked food contaminated with feces from infected triatomine bugs.

It is estimated that 6-7 million people are currently infected, more than 10,000 people die every year on account of the infection and 25 million people are at risk of infection. Chagas disease is classified as a neglected tropical disease (NTD) by the World Health Organization WHO, mainly due to low pharmaceutical industry investment in drug research because of the low associated revenue [4-6].

In fact, there is an urgent need for more efficient and less toxic chemotherapy for this disease. Available chemotherapy is based on two drugs developed more than 60 years ago, Benznidazole and Nifurtimox. Both drugs produce significant side effects, show low efficacy for the chronic phase of the disease and poor tolerability, and require long treatments that often develop drug resistance. Even though in the last years different efforts have pushed forward the drug discovery research, no new drugs have entered the clinic in the last decades [7].

In the past years, our group has contributed to demonstrate that the rational design of metal-based drugs with different metal ions or organometallic centers could be a successful strategy for the development of new prospective agents against *T. cruzi* [8, 9] [10] [11, 12].

In particular, platinum(II) and palladium(II) classical coordination complexes or organometallic compounds have been designed as multifunctional agents joining,

in a single molecule, different chemical species that could affect different parasitic targets [8].

Among others, we developed at a first stage promising Pt(I) or Pd(II) homoleptic compounds, [M(mpo)$_2$], with pyridine-2-thiol *N*-oxide (2-mercaptopyridine *N*-oxide, Hmpo) as bioactive ligand. Mpo had shown a high anti-*T. cruzi* activity against all forms of the parasite and no unspecific toxicity on mammalian cells. In order to further address the therapeutic potential of palladium and platinum compounds with this bioactive ligand, we included a ferrocene moiety in the structure which led to [M(dppf)(L)](PF_6) compounds, where dppf = 1,1'-bis(dipheny1phosphino) ferrocene [13].

Both ferrocenyl compounds showed IC_{50} values in the nanomolar range on *T. cruzi* epimastigotes as well as low cytotoxicity on mammalian cells, leading to good selectivity towards the parasite**.** The complexes were about 10–20 times more active than the antitrypanosomal drug Nifurtimox. Both complexes also affected the parasite infection process as well as the number of intracellular parasites per cell [14, 15].

Identification of molecular targets and understanding of the mode of action of drug candidates are essential data for their clinical development. In previous work, high throughput *omic* studies on *T. cruzi* for both analogous compounds were performed to unravel their whole mechanism of action. Proteomic and transcriptomic analyses allowed to identify differentially expressed transcripts and proteins after 6 hours of treatment with concentrations corresponding to 5x the calculated IC_{50} values for each compound.

Differentially expressed transcripts were functionally categorized allowing the identification of cellular processes and pathways that were affected by the treatment with each compound. Among the affected pathways, the biosynthesis of ergosterol was found to be modulated by the compounds [14-16].

Ergosterol is essential for providing structure and function of parasite membranes and is required for parasite multiplication. It is synthesized through a two-step biosynthetic pathway, the isoprenoid pathway (from Acetyl-CoA to farnesyl diphosphate) and the sterol pathway (from farnesyl-diphosphate to sterols). The parasite is entirely dependent on endogenously produced sterols for survival and

proliferation. Since the enzymes involved in this metabolic pathway are different to their counterparts in the mammalian host, the sterol biosynthesis and, particularly, the set of enzymes that participate in the pathway are recognized as attractive targets for antichagasic drugs discovery [17, 18].

In this work, through sterols levels determination we confirmed the involvement of this pathway in the response to both Pd and Pt based compounds under study. Two enzymes of the pathway were selected as Pd- and Pd-dppf-mpo molecular targets for further analysis: phosphomevalonate kinase (PMK) and lanosterol 14α–demethylase (CYP51). Structure preparation for both enzymes, charge assignments of all atoms of ferrocenyl compounds under study by crystallography and optimization by quantum mechanics, and further molecular docking, suggested a energetically favorable interaction of the compounds with CYP51 and PMK and also a putative competitive inhibition for PMK. The involvement of PMK and CYP51 was experimentally evaluated in the parasites' response to the selected compounds through the generation of PMK and CYP51 overexpressing parasites. Altogether, results here presented confirm that the mechanism of action of Pd-dppf-mpo and Pt-dppf-mpo compounds involves the inhibition of both enzymes PMK and CYP51, leading to a decrease in the amount of ergosterol in the cell.

Materials and methods

Compounds and dilutions

Stock solutions of Pd-dppf-mpo and Pt-dppf-mpo compounds were prepared in DMSO and diluted in Brain Heart Infusion-tryptose (BHI) medium (Capricorn) to obtain the stock drug concentration of 100 µg/mL. The final concentration of each compound was prepared adding BHI-tryptose medium.

Trypanosoma cruzi culture

T. cruzi epimastigotes of the CL Brener strain were maintained in exponential growth at 28°C in BHI-glucose medium complemented with 10 % (v/v) fetal bovine serum inactivated (FBS). For transfectant populations, 500 µg/mL of G-418 was added to the culture medium.

Squalene, lanosterol and ergosterol determination

Epimastigotes of *T. cruzi* at a density of 9×10^7 parasites/mL were incubated for 6 h at 28°C with both Pd-dppf-mpo and Pd-dppf-mpo at concentrations corresponding to 1x, 5x and 10x IC_{50} value previously determined (0.3, 1.5 and 3 µM for Pd-dppf-mpo and 0.06, 0.3 and 0.6 µM for Pt-dppf-mpo). Untreated parasites were used as negative control and treatment with the drug Clotrimazole was used as positive control in a concentration of 5.39 µM. Membrane sterols were extracted from the parasites as described following. After incubation time, parasites were centrifugated at 3000 rpm for 10 min, washed with PBS and resuspended in 1 mL of a chloroform: methanol (2:1) mixture. The obtained suspension was then kept at 4 °C for 12 h. Next, 2 mL of saturated NaCl solution was added and the mixture was extracted with 1 mL of chloroform, taking special care to avoid collecting any aqueous phase. This step was repeated twice to achieve a quantitative extraction [19, 20].

The obtained organic phase was evaporated under nitrogen and redissolved in 1 mL of acetonitrile for the subsequent determination by liquid chromatography coupled to diode array detection (HPLC-DAD). The chromatographic system used consisted of a C8 stationary phase (250 × 4.6 mm, 5 µm) and 100% acetonitrile was used as the mobile phase, at a flow rate of 0.9 mL/min. Detection was performed at 210 nm [19, 21].

Cloning and overexpression of phosphomevalonate kinase (PMK) and Lanosterol 14α-demethylase (CYP51) in T. cruzi

The PMK and CYP51 (TcCLB.507913.20 and TcCLB.506297.260, respectively) open reading frames (ORF) were PCR amplified and cloned into the XbaI and HindIII restriction sites of pTREX-nGFP vector [22]. XbaI site and c-Myc tag sequence were included in the forward primer sequence in phase with the ORF of each molecular target. HindIII site sequence was included in the reverse primer (**Table 1**).

Table 1. Primers used to amplify and clone PMK and CYP51 genes into pTREX-nGFP vector. XbaI and HindIII restriction sites are represented in italics and c-Myc sequence in lower case.

PMK forward primer	5'*TCTAGA*atggagcagaagctgatttcagaggaggacctgATGGATACTGCTATTGCGACTACGAG 3'
PMK reverse primer	5'*AAGCTT*CCTTCTCTTCAGAAAAAAGAAGTCCAGCG 3'
CYP51 forward primer	5'*TCTAGA*atggagcagaagctgatttcagaggaggacctgATGTTCATTGAAGCCATTGTATTGGG 3'
CYP51 reverse primer	5'*AAGCTT*CCGAGGGCAATTTCTTCTTGC 3'

PCR reactions were performed with the enzyme DreamTaq DNA Polymerase (Thermo Fisher Scientific) following manufacturers' instructions, using *T. cruzi* genomic DNA as template. The expression vector and PCR products were linearized with the enzymes XbaI and HindIII and ligated with T4 Ligase (Thermo Scientific). For control experiments pTREX-cMyc-nGFP vector was constructed by hybridization of complementary sequences coding for c-Myc tag (requested as 5' phosphorylated primers containing XbaI and HindIII restriction sites) and ligation in the linearized pTREX-nGFP vector. All primers were synthetized in Macrogen, Korea and plasmid constructions were verified by Sanger sequencing.

Recombinant plasmids were purified from 100 mL bacterial cultures using the PureLink™ HiPure Plasmid Midiprep Kit (Invitogen) and resuspended in 100 µL of Tb-BSF electroporation buffer (50 mM Hepes, 0.15 mM $CaCl_2$, 5 mM KCl, 90 mM phosphate buffer, pH 7.2). Epimastigotes in exponential phase were washed with PBS 1X, centrifuged, and resuspended in Tb-BSF buffer at a final concentration of $1x10^8$ parasites/mL. For electroporation, $2x10^7$ epimastigotes were incubated with 30 µg of plasmid DNA according to established protocols [23]. A mock control transfection without plasmid was included. The mixture was transferred to 2 mm cuvettes and electroporated with the X-014 program in an Amaxa Nucleofector™ 2b (Lonza). The recovery of the parasites was carried out immediately by incubating the mixture with 2 mL of BHI-tryptose medium supplemented with 10 % FBS at 28ºC. After 24 hours of transfection, the selection process was performed by adding 250 µg/mL of G-418 to the culture medium. The strain selection process was carried out maintaining the antibiotic pressure at 500 µg/mL.

Analysis of overexpressing parasites

The overexpression of PMK and CYP51 in transfected parasites was evaluated by Quantitative Real Time PCR (qPCR) and confocal microscopy.

qPCR was performed using SensiFAST SYBR Hi-ROX Kit (Bioline). cDNA was obtained by retrotranscription from total RNA of each transfected population using random hexamers and Superscript IV (Life Technologies). Specific primers (**Table 2**) were designed with the OligoPerfect Primer Designer tool from Thermo Fisher Scientific (https://www.thermofisher.com). Relative quantifications were performed using the threonyl-tRNA synthetase as a reference internal control, since its transcript level does not present variations between treated and control parasites according to previous transcriptomic data [16]. The reactions were carried out according to the manufacturer's instructions in a volume of 10 µL using 2 µL of cDNA diluted 1/16 and 0.4 µM of each primer in a two-step cycling protocol at 60°C in a StepOnePlus Real-Time PCR System. All reactions were performed in four replicates.

Table 2. Primers used for qPCR. ThrRS: threonyl-tRNA synthetase (ID: TcCLB.508299.80).

ThrRS forward	5' ACCGCATACGCCACGAAAGT 3'
ThrRS reverse	5' CTTGTCCAATGTCGGTTGC 3'
GFP forward	5' GGTGATGTTAATGGGCACAA 3'
GFP reverse	5' TCTCGCAAAGCATTGAACAC 3'

To evaluate target proteins overexpression confocal microscopy was performed. Confocal microscopy was performed in a Confocal Zeiss LSM 800 (Institut Pasteur de Montevideo). Parasites ($2x10^7$) were fixed in 4% PFA for 15 minutes, washed twice with PBS and deposited in slides with 80% glycerol. Fiji software was used for image analysis [24].

Parasites viability assay

$1x10^7$ parasites per well were seeded in black 96 well plates in BHI-tryptose medium with concentrations corresponding to 1x, 5x and 10x the IC_{50} value

previously determined on wild type epimastigotes of CL Brener strain [14, 15] for 6 h. Parasites viability was tested using resazurin, which is reduced to highly fluorescent resorufin product by mitochondrion of viable cells. 50 µL of Resazurin solution (2 mg/mL in BHI) were added to each well and incubated for 4 h at 28°C [25]. Fluorescence (excitation 530 nm/emission 590 nm) was measured in a Thermo Scientific Varioskan® Flash Multimode plate spectrofluorimeter instrument. The results are presented as % viability ± SD (standard deviation) of two independent biological replicates.

Modelling and parametrization of Pd-dppf-mpo and Pt-dppf-mpo compounds

The structures of both compounds were previously obtained by single crystal X-Ray diffraction methods [13] and quantum mechanical evaluation performed at the B3LYP level, and the ultrafine grid was selected [26, 27]. The basis set employed for C, N, O, S and H was the 6-311G* [28, 29] while the LANL2TZ was used for the metal atoms [30]. Atomic charges were derived from Mulliken analysis. All calculations were carried out using Gaussian 09 [31].

The 2D and 3D pictures of resulting structure (from Gaussian View module (GaussView, Version 6, Dennington, Roy; Keith, Todd A.; Millam, John M. Semichem Inc., Shawnee Mission, KS, 2016.)) are shown in **Figure 1**. Mulliken charges assigned to the structure are described in **Tables S1** and **S2**.

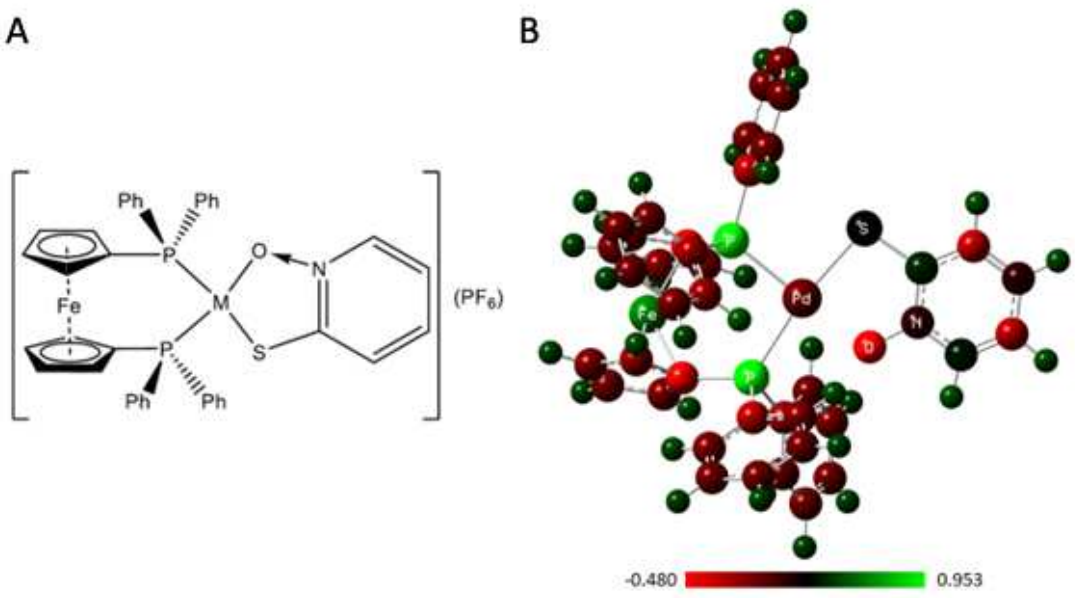

Figure 1. A. 2D view of resulting molecular models of Pd-dppf-mpo and Pt-dppf-mpo compounds. M = Pd or Pt. **B.** 3D balls and sticks view of Pd complex (PF_6^- is omitted) with all atoms´ names labeled inside balls.

Molecular docking studies

The calculations were done running the Molecular Operating Environment suite on Windows [32], using a workstation with an eight-core processor Hyperthread equipped.

The *T. cruzi* CYP51 crystallographic structure (PDB: 3K1O) of 2.89 Å resolution was used and further modelling of 217-220 residues Trp_{217}-Leu-Leu-Arg_{220} was made. The last 478-487 amino acids (Lys_{478}-Leu-Pro-His-His-His-His-His-His_{487}) were not included in the model. Charges were adjusted to pH 7.4 environment. The final model was energy minimized using the force field Amber14-EHT inside MOE suite. The co-crystallized CYP51-POZ (POZ, pozoconazole) was analyzed separately, and further docking was made to re-localize it as validation step using the Triangle Matcher as placement and the London dG algorithms as scoring function. Further re-scoring with the GBVI/WSA ΔG was performed [33]. In all cases a Rigid Receptor selection was used for the treatment of protein structure. After verifying a RMSD (root mean square deviation) of 3 Å (average of three posed structures) between crystallographic and re-docked POZ structure, the docking strategy was considered valid and all molecular docking after this step were performed with identical procedure.

For PMK analysis, an Alphafold model of the *T. cruzi* PMK enzyme was used (AF-A0A2V2W7P9)[34], The crystallographic structure from *Streptococcus pneumoniae* R6 (PDB id 3GON) was used as a template of catalytic site components where a molecule of phosphomevalonate (PMV, the endogenous substrate), and a modified ATP molecule (phospho amino phosphonic acid adenylate ester – ANP) were placed. From the final modelled structures, Ramachandran plot was obtained. Graphical analyses are shown in **Figure S1A** and **S1B** for CYP51 and PMK, respectively**.**

To elucidate all putative binding sites in CYP51 and PMK a Site Finder (Module Site Finder inside MOE suite [32]) was performed with the following parameters:

two Probe radius 1: 1.4 and 1.8 Å; Isolated donor/acceptor: 3; Connection distance: 2.5 Å; Minimum site size: 3 and Radius: 2 Å.

Statistical analysis

All the graphs, calculations, and statistical analyses were performed using GraphPad Prism software version 6.0 for Windows (GraphPad Software, San Diego, CA, USA). A bifactorial analysis by two-way ANOVA test was performed followed by Bonferroni's multiple comparisons test p-values: **** <0.0001, *** <0.001, ** <0.01, * <0.1.

Results and discussion

Ergosterol pathway constitutes an encouraging target for drug design not only because it is an essential molecule for parasitic growth and viability, but also it is absent in mammalian host cells which may result in higher selectivities and less toxicity of the drug. Previous transcriptomic and proteomic analysis revealed that most genes coding for enzymes involved in ergosterol pathway resulted downregulated after Pd-dppf-mpo and Pt-dppf-mpo treatment [16].

Sterols determination in Pd-dppf-mpo and Pt-dppf-mpo treated parasites

To evaluate the effect of Pd and Pt based compounds in the ergosterol synthesis pathway, ergosterol, lanosterol and squalene concentrations were determined by HPLC in *T. cruzi* parasites treated with Pd-dppf-mpo and Pt-dppf-mpo in concentrations corresponding to 1, 5 and 10x the calculated IC_{50} [14, 15]. Treatment with both metal compounds resulted in the accumulation of intermediate sterols (lanosterol and squalene) and in a decrease of the final product ergosterol in a dose dependent manner (**Figure 2**). This result is in accordance with a damped function of intermediate enzymes of the ergosterol pathway of Pd-dppf-mpo and Pt-dppf-mpo treated parasites since the low levels of ergosterol could be explained by the inability of some intermediate enzyme to metabolize lanosterol causing its accumulation while decreasing the levels of the ergosterol as a final product. Since squalene and lanosterol levels are increased after Pd-dppf-mpo and Pt-dppf-mpo treatment in a dose dependent manner, we can hypothesize that the compounds mainly affect the sterol pathway in a step after lanosterol synthesis. Moreover, parasites treated with Clotrimazole, an

inhibitor of the ergosterol pathway that inhibits CYP51 enzyme (**Figure 3**) displayed a similar behavior with lanosterol and squalene accumulation and a decrease in the amount of ergosterol. In all cases, the reduced levels of ergosterol could also trigger an increase in the synthesis of squalene and lanosterol as a precursor.

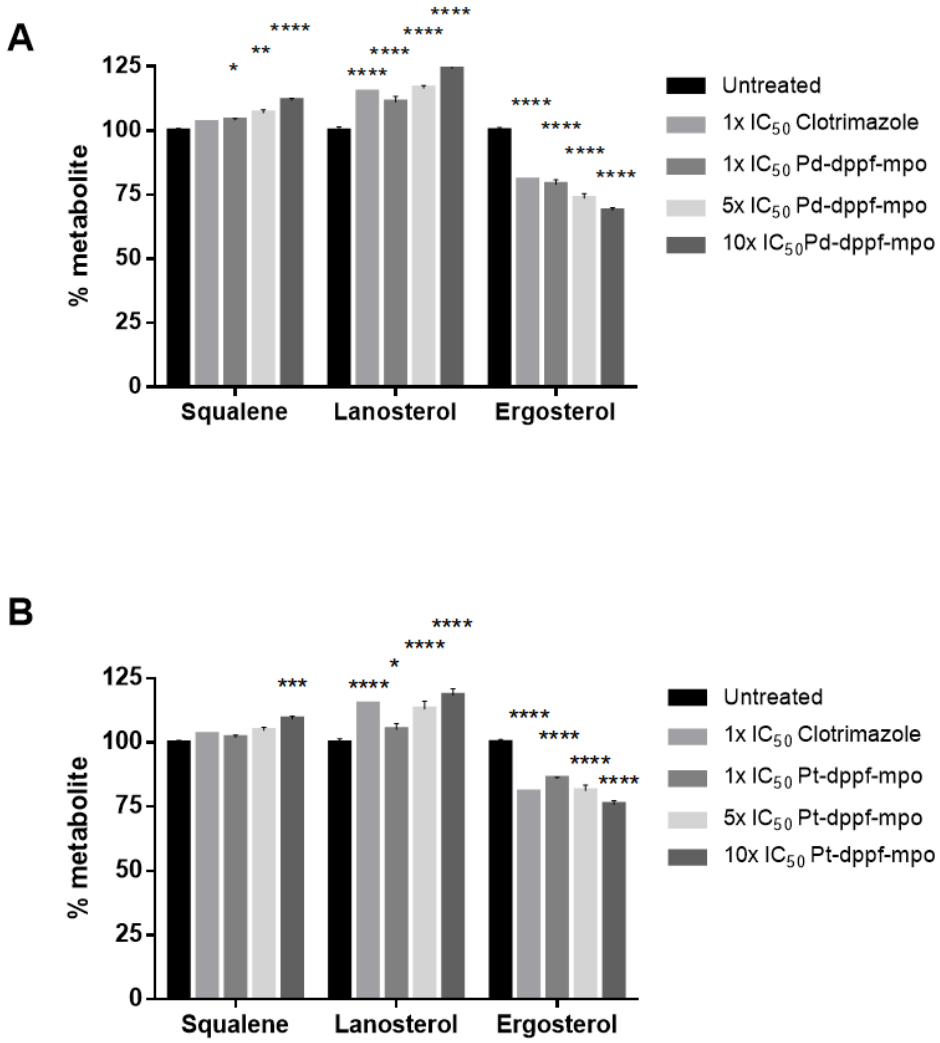

Figure 2. Percentage of the metabolites squalene, lanosterol and ergosterol after 6 hours of treatment with different concentrations of Pd-dppf-mpo (**A**) and Pt-dppf-mpo (**B**). Parasites treated with Clotrimazole were included as a control. The results are presented as averages ± SD (standard deviation) of two biological replicates. To compare treated against untreated parasites, two-way ANOVA test

followed by Bonferroni's multiple comparisons test was performed. p-values: **** <0.0001, *** <0.001, ** < 0.01, * <0.1.

Docking studies

To deepen in the study of the effect of Pd-dppf-mpo and Pt-dppf-mpo compounds over the ergosterol pathway, we selected two enzymes of the pathway for further analysis (**Figure 3**). The enzyme phosphomevalonate kinase (PMK) constitutes an essential glycosomal protein involved in early steps of the isoprenoid biosynthesis and it has been previously considered an attractive target for rational drug design since the same phosphorylation reaction in the host is catalyzed by a non-orthologous enzyme [35]. Previous research revealed that PMK transcript levels decreased 6 and 2-fold after Pd-dppf-mpo and Pt-dppf-mpo treatment respectively and the coded protein was absent in treated parasites comparing with control untreated parasites [16]. CYP51 is a P-450-containing monooxygenase enzyme which participates in one of the earliest steps in the lanosterol pathway. It is an essential enzyme characterized by a high druggability, and it has been reported as a target of azole antifungal drugs with demonstrated anti-*T. cruzi* activity [36-40]. Like PMK, CYP51 also showed reduced transcript levels in treated parasites (2 and 1-fold after Pd-dppf-mpo and Pt-dppf-mpo treatment, respectively) and no protein was detected in treated parasites by proteomic studies [16]. In addition to being highly druggable enzymes essential for the survival of the parasite, both proteins are expressed throughout the entire life cycle of the parasite [41].

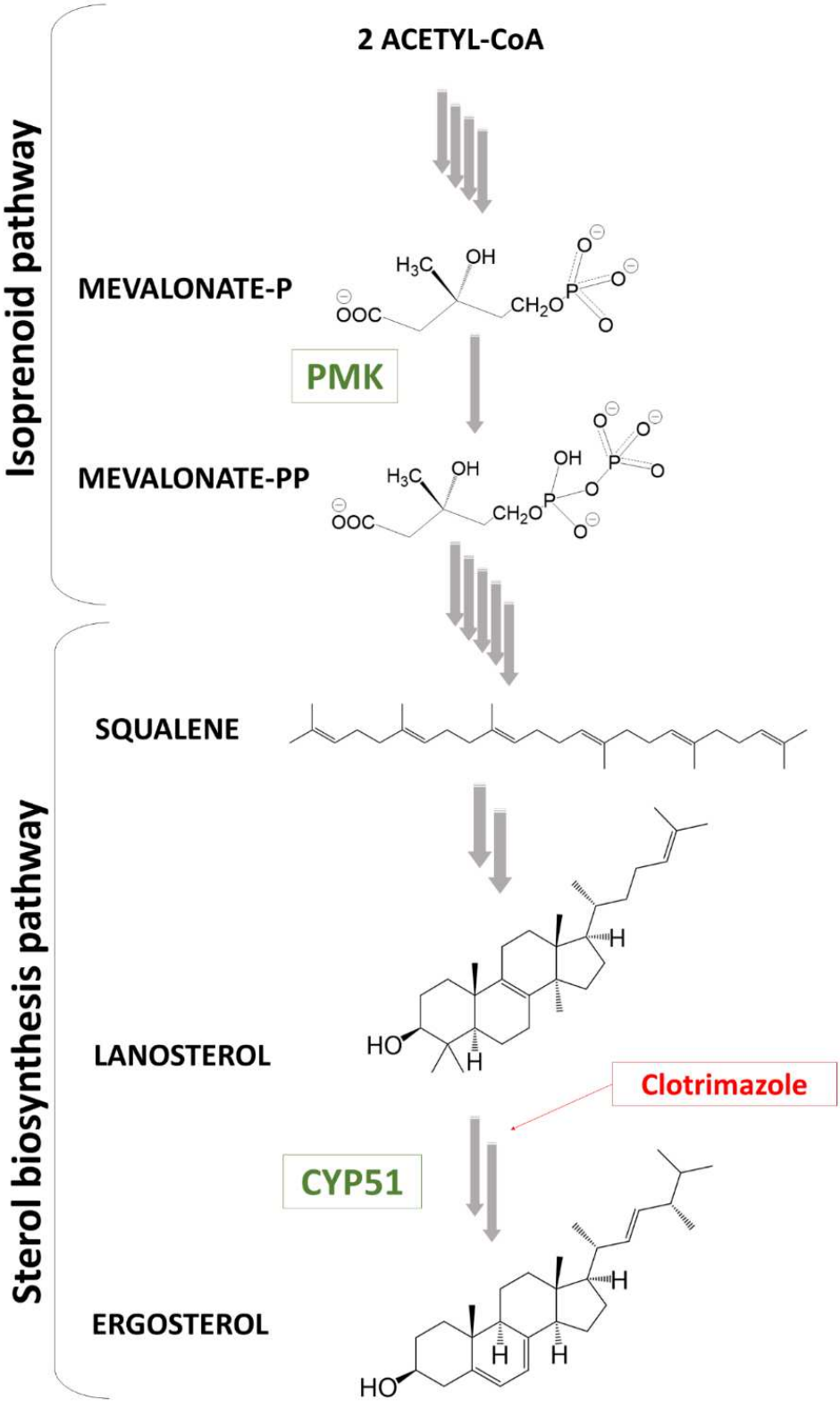

Figure 3. Ergosterol biosynthesis pathway in *T. cruzi.* Selected enzymes are shown in green. PMK is a kinase involved in early steps of the isoprenoid

biosynthesis. CYP51 participates in one of the last steps of the ergosterol pathway. Clotrimazole is an antifungal inhibitor of CYP51 [42].

To predict putative sites in the CYP51 and PMK enzymes, Site Finder analysis was performed. **Table S3** and **Figure 4A** show the putative sites found for CYP51 and the putative sites for PMK are shown in **Table S4** and **Figure 4B**. For PMK, the substrate of the enzyme resulted placed inside then Site 2, confirming the localization of the catalytic *T. cruzi* site (**Figure 4B**).

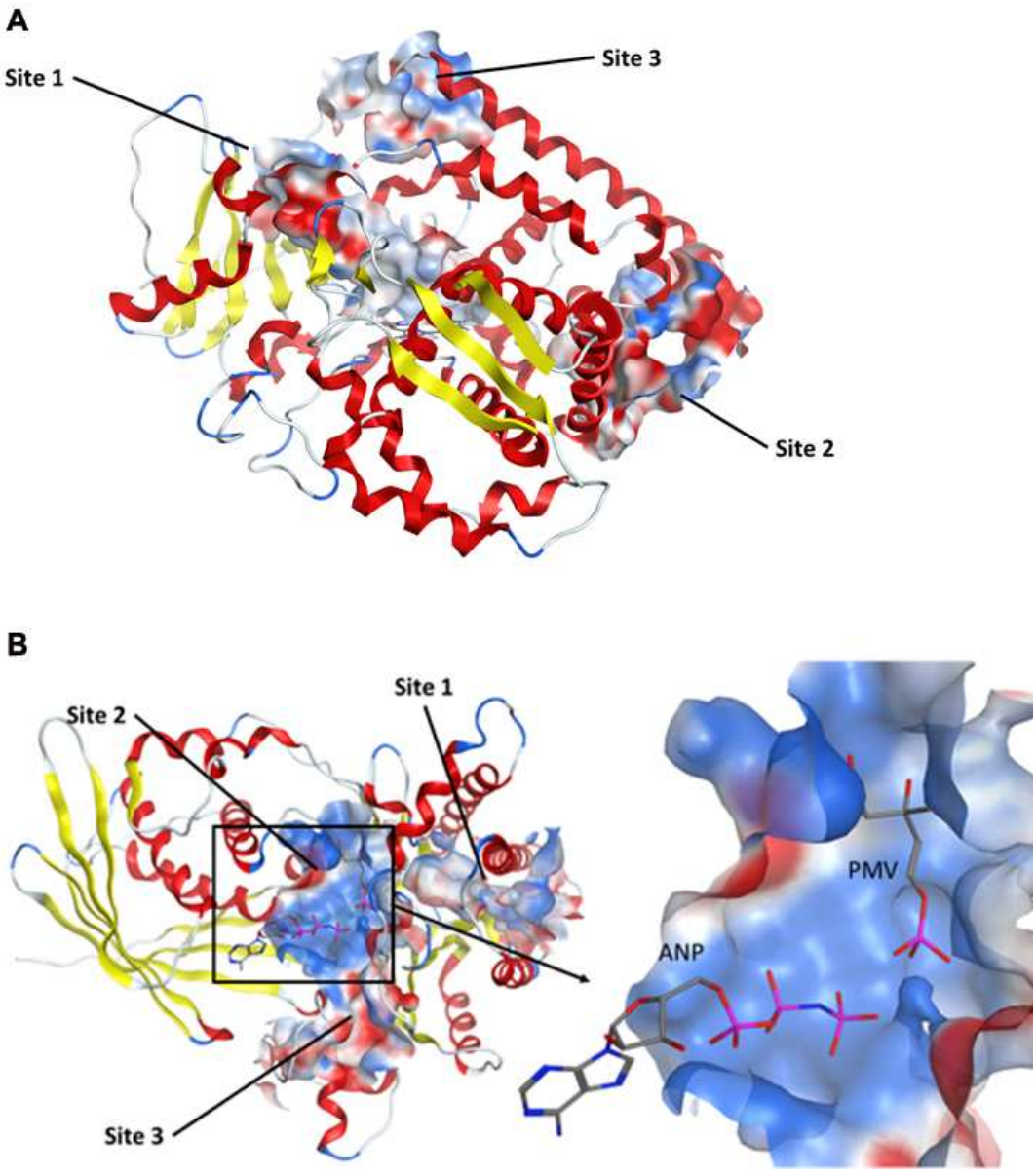

Figure 4. Putative sites found for CYP51 and PMK through Site Finder module. (**A**) The three sites found for CYP51 are shown as surfaces. (**B**) Sites found for PMK with the substrate PMV (phosphomevalonate) and ANP (phoshoaminophosphonic acid-adenylate ester) ligands. The electrostatic colored surface found surrounding Site 2 is shown magnified in the right. Positive charged residues are shown in blue, negative charged residues in red and neutral charge in white.

To validate the strategy, docking calculations made in Site 1 were performed on CYP51 with the drug Posaconazole (POZ), a known inhibitor of the enzyme [43]. The –10.9 Kcal/mol score for POZ docking over the center of mass of crystallographic pose of POZ together with the good correlation in both crystallographic and docked POZ poses, with an average RMSD of 3 Å, revealed a good interaction (**Figure 5A** and **Table S5).**

After CYP51-POZ docking interaction, we performed the analysis on the enzyme outfacing Pd-dppf-mpo and Pt-dppf-mpo compounds using two strategies: blind docking and POZ site. The scoring interaction energies were very similar for both compounds (**Table S6**), and also, the predicted sites were the same. It could also be observed that their preferred site in the enzyme is placed at the entrance of the catalytic site whereas the POZ preferred site is inside the catalytic site (**Figure 5B-C**). Although the same site was found for both compounds, the mode of interaction seems to be different.

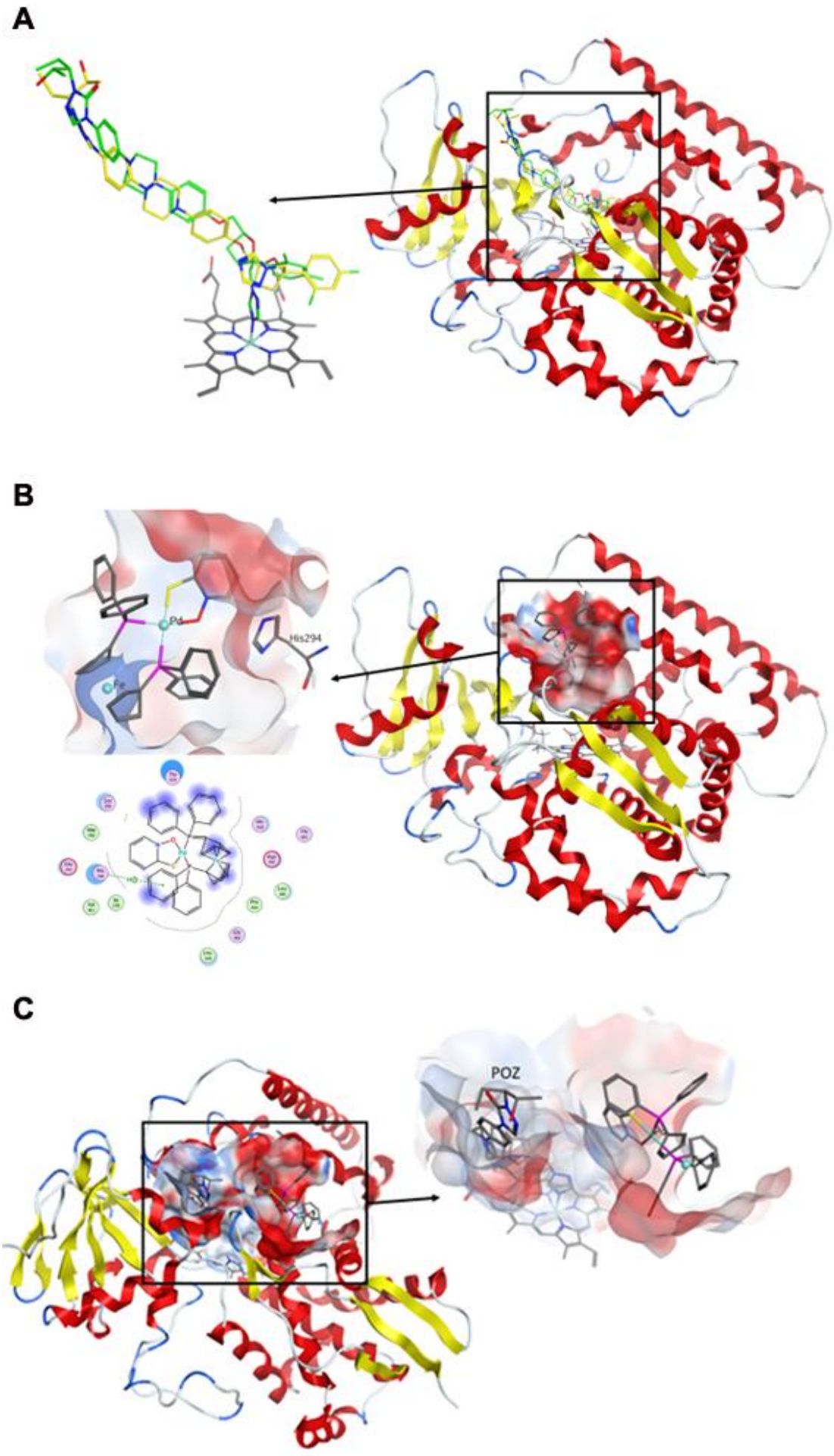
A
B
Pd
Fe
His294
C
POZ

Figure 5. (**A**) View of POZ docked in the active site of CYP51. On the left, the crystallographic (green) and docked (yellow) POZ overlapped structures is shown. On the right, the alpha/beta global structure of CYP51 is shown with docked POZ in Site 1. (**B**) The CYP51 catalytic surface with docked Pd-dppf-mpo compound is shown. (**C**) Ribbon description of CYP51 crystallographic structure, together with POZ and docked Pd-dppf-mpo structures. The same surface with a near view of POZ and Pd-dppf-mpo is shown on the right. Positive charged amino acids are shown in blue, negative charged in red and neutral in white.

PMK docking site was defined from Alphafold modelling (**Figura 4B**). Finally, the molecular docking was performed under the same settings as designed for CYP51. The graphical and scoring results are shown in the **Figure 6** and **Table S7**. The score of –7 kcal/mol obtained together with the structural position found of both putative ligands allow us to propose the inhibition as competitive.

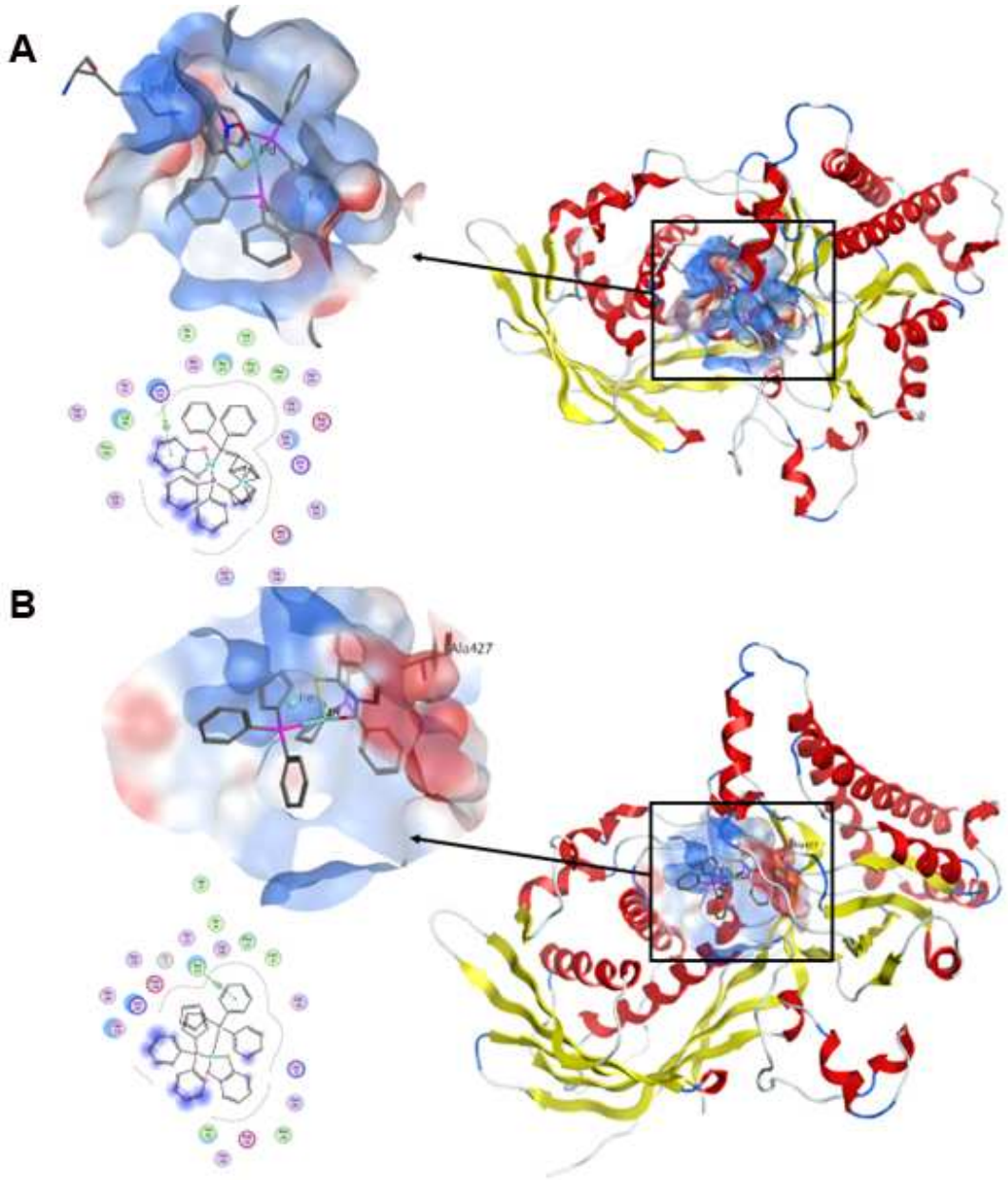

Figure 6. (**A**) PMK surface with docked Pd-dppf-mpo compound. (**B**) PMK surface with docked Pt-dppf-mpo compound. Electrostatic colored code: positive charged in blue, negative charged in red and neutral charge in white.

Since docking studies revealed a good score interaction of Pt-dppf-mpo and Pd-dppf-mpo with both enzymes (**Table S6** and **S7**), PMK and CYP51, we selected these proteins to experimentally validate their involvement in the mode of action of Pt- and Pd-dppf-compounds.

Antiproliferative activity of Pd-dppf-mpo and Pt-dppf-mpo in PMK and CYP51 overexpressing parasites

It is expected that the overexpression of a drug's molecular target can lead to increased drug resistance. We employed this strategy for target validation using PMK and CYP51 overexpressing parasites. Genes coding for PMK and CYP51 were cloned into the pTREX-nGFP expression vector. The resulting constructs pTREX-PMK-nGFP and pTREX-CYP51-nGFP were sequenced and no sequence mutations were found. After parasite transfection and selection with G-418, the overexpression of both genes was confirmed by qRT-PCR using -specific primers (**Figure 7A**).

According to previous transcriptomic analysis of wild type parasites, the expression of PMK and CYP51 relative to the threonyl-tRNA synthetase reference gene in epimastigotes is 0.9 and 1.1-fold respectively (**Table S8**). Since overexpressing parasites showed a 413 and 20-fold transcript increase for PMK and CYP51, respectively, relative to the internal reference gene (**Figure 7B**), we determined an overexpression of 458 and 18 for PMK and CYP genes in transfected parasites. Western blot analysis using anti-cMyc antibody and total extracts of PMK and CYP51 overexpressing parasites, also confirmed the ectopic expression of both proteins, being PMK expressed in higher levels than CYP51 (data not shown).

Confocal microscopy analysis of PMK and CYP51 overexpressing parasites not only confirmed the ectopic expression of GFP-fused PMK and CYP51, but also revealed a location of GFP-fused PMK all over the whole parasite, whereas GFP-CYP51 appears concentrated in discrete foci presented in the anterior portion of the parasite. Microscopic analysis also corroborated a higher expression of GFP-PMK compared to GFP-CYP51 (**Figure 7C**).

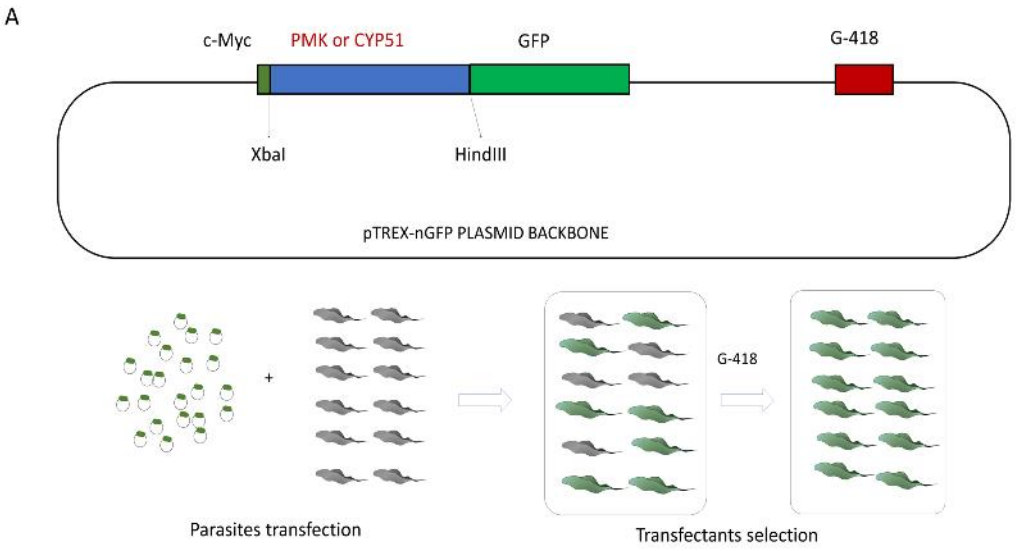
A
c-Myc
PMK or CYP51
GFP
G-418
XbaI
HindIII
pTREX-nGFP PLASMID BACKBONE
+
G-418
Parasites transfection
Transfectants selection

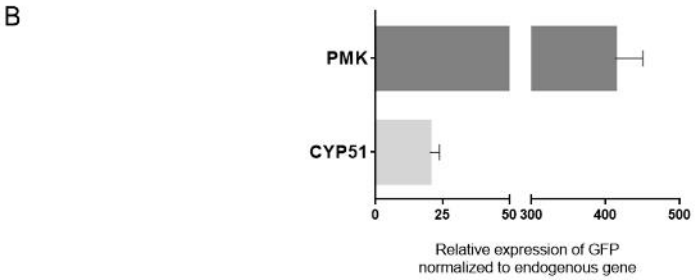
B
PMK
CYP51
0
25
50 300
400
500
Relative expression of GFP
normalized to endogenous gene

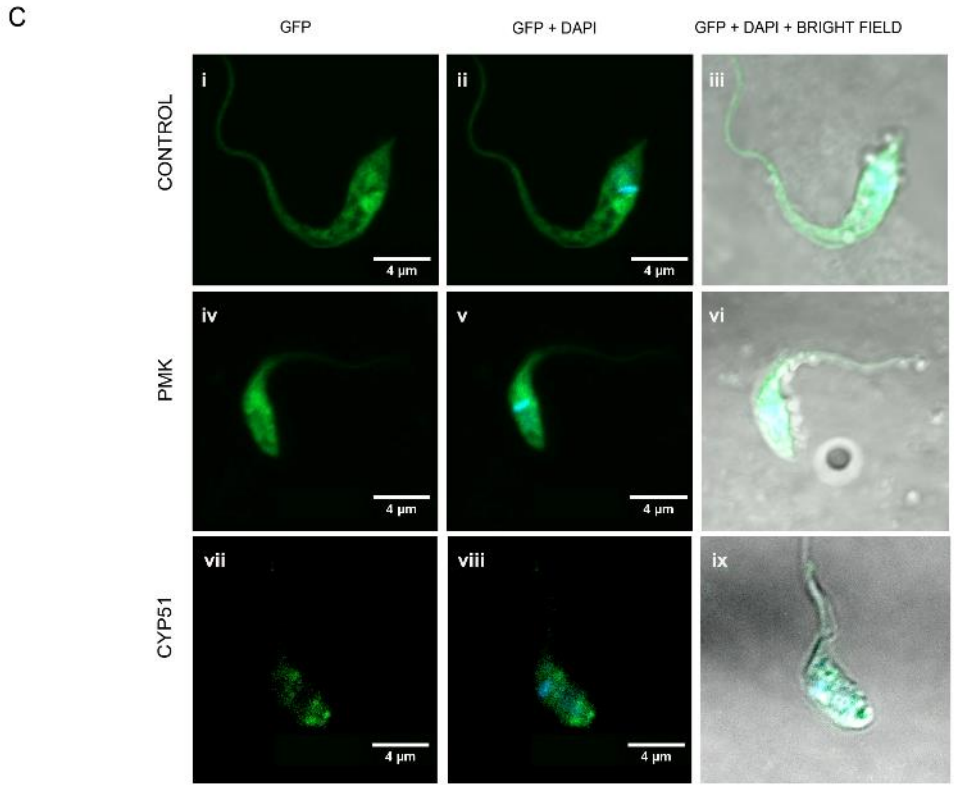
C
GFP
GFP + DAPI
GFP + DAPI + BRIGHT FIELD
CONTROL
PMK
CYP51
i
ii
iii
iv
v
vi
vii
viii
ix
4 µm

Figure 7. (**A**) Schematic representation (not in scale) of the overexpression of pTREX-nGFP containing genes coding for PMK or CYP51 fragment. Parasites were electroporated and the transfected parasites were selected through resistance to G-418, stably expressed from the backbone. (**B**) qRT-PCR quantification of PMK and CYP51 overexpression. Relative expression of GFP normalized to an endogenous gene is shown. (**C**) Fluorescence confocal microscopy images of control GFP transfected parasites (i, ii, and iii) and parasites expressing PMK-GFP fusion protein (iv, v, and vi) and CYP51-GFP fusion proteins (vii, viii, and ix) from an episomal expression vector. Left panels: GFP control protein or GFP fusion proteins localization (green). Center panels: merged images of GFP expression and DAPI nuclear stain (blue). Right panels: merged images GFP, DAPI and brightfield.

To assess if PMK and CYP51 overexpression confers resistance to Pd and Pt based compounds, we studied their effect on viability comparing with wild type and with control transfected parasites.

A significant increase in the viability of CYP51 overexpressing parasites was observed using Pt-dppf-mpo concentrations corresponding to 1x and 5x IC_{50} and for all tested Pd-dppf-mpo concentrations (**Figure 8**). The overexpression of CYP51 parasites exerts a protective effect after compounds treatment, reaching viability percentages similar to untreated parasites. This increase in viability of transfected parasites can be explained by a resistance to growth-inhibitory drugs conferred by the overexpression of CYP51, and thus highlighting the involvement of this enzyme in the mechanism of action of Pt and Pd based drugs.

Regarding PMK, for Pd-dppf-mpo treatment, only a slight but significant increase in the percentage of viability was observed in overexpressing parasites treated with 1x IC_{50} value. Likewise, for Pt-dppf-mpo treatment an increase in viability was observed only with treatment using 5x IC_{50} (**Figure 8**). It is worth to notice that 98% of the parasite population overexpressing PMK used for these assays is positive for GFP (**Figure S2**), therefore it is ruled out that their behavior is due to a loss of PMK overexpression due to parasite adaptation.

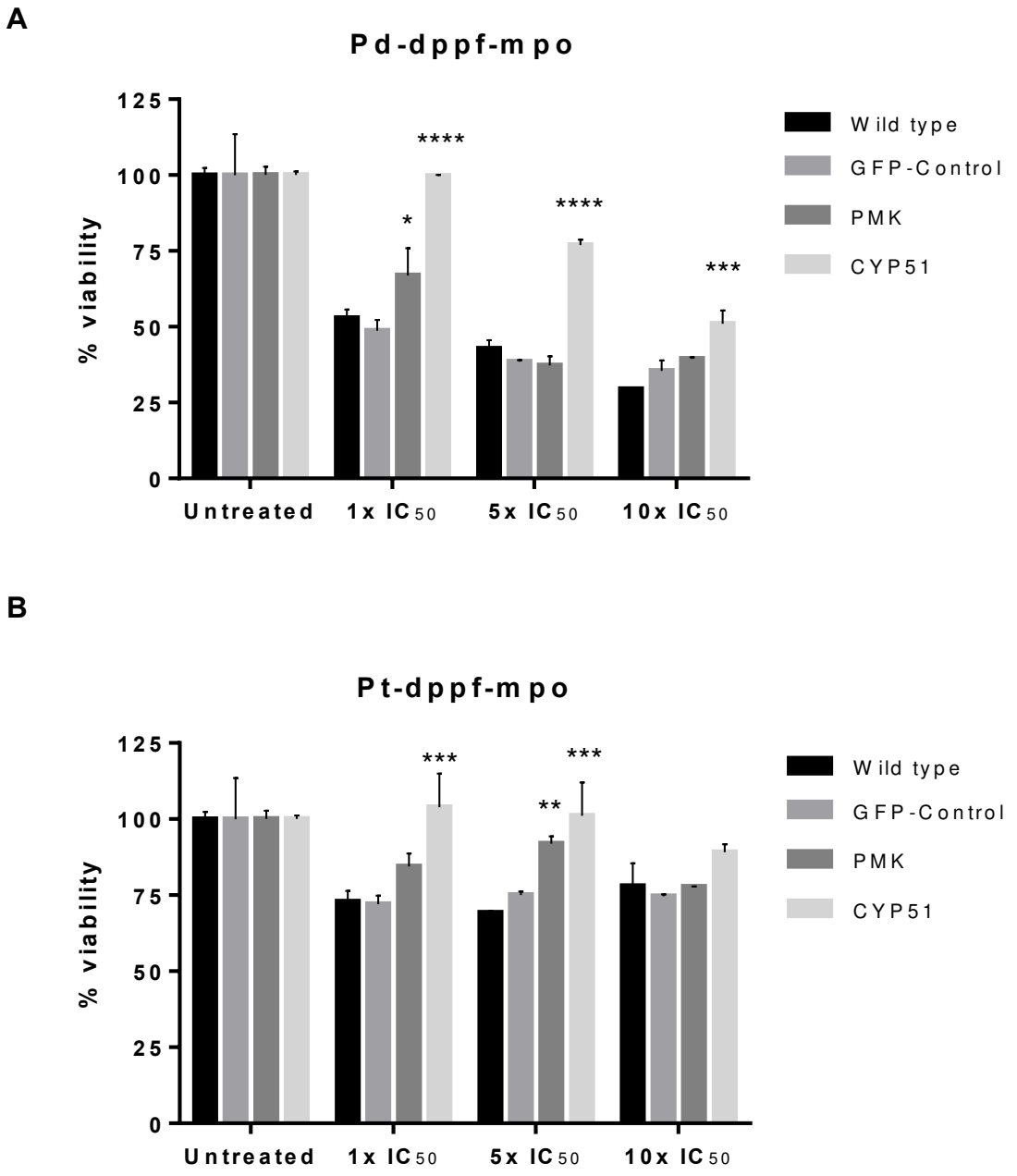

Figure 8. Viability of wild type, GFP-control, PMK transfectants and CYP51 transfectants parasites after 6 hours of incubation with 1x, 5x and 10x IC_{50} of Pd-dppf-mpo (**A**) and Pt-dppf-mpo (**B**). Untreated parasites were used as a control. To compare treated transfectants against wild type treated parasites, two-way ANOVA test followed by Bonferroni's multiple comparisons test was performed. p-values: **** <0.0001, *** <0.001, ** <0.01, * <0.1.

It is worth to mention, that even with lower levels of overexpression compared with PMK transfectants, the rescue effect of CYP51 is stronger than the effect exerted by PMK overexpression (**Figure 8 and 9**). This finding is in accordance with sterols levels variations in treated wild type parasites (**Figure 2**), where an accumulation of squalene and lanosterol intermediates and a decrease of the final product suggest a main effect of the compound in a step of ergosterol, rather than the isoprenoid pathway.

Sterols determination in Pd-dppf-mpo and Pt-dppf-mpo treated PMK and CYP51 overexpressing parasites

To further analyze the involvement of PMK and CYP51 in the mechanism of action of Pd-dppf-mpo compounds, we determined the amount of ergosterol pathway intermediates in overexpressing parasites treated with Pt-dppf-mpo and Pt-dppf-mpo for 6 hours with concentrations equivalent to the 5x the calculated IC_{50} value.

We observed that in parasites overexpressing CYP51, the accumulation of lanosterol detected in treated wild type parasites is reverted and the amount of the final product of the pathway, ergosterol, increases (**Figure 9**). This result was also observed when using compounds concentrations of 1x and 10x IC_{50} in a dose dependent manner (**Figure S3**). These findings are consistent with an unblocking of the pathway at this point with the concomitant conversion of lanosterol into ergosterol. For PMK overexpressing parasites, although its transcript and protein levels result highly downregulated in treated parasites [16], this protective effect cannot be observed, since intermediate metabolite levels and the final product ergosterol do not differ significatively with treated wild type parasites. These results are in agreement with the viability assays (**Figure 8**), where the overexpression of PMK did not result in an improvement in the viability of the parasites, generating a protective effect after treatment with the compounds as observed after CYP51 overexpression (**Figure 8**). A possible explanation to describe why the overexpression of PMK does not increase the resistance of the parasites to the compounds, could be the fact that PMK is fused to GFP in the transfectants, so, this enzyme could not adopt an adequate conformation and therefore the enzyme could not be functional. In this case, a misfolded non-functional enzyme would not allow the rescue of the phenotype.

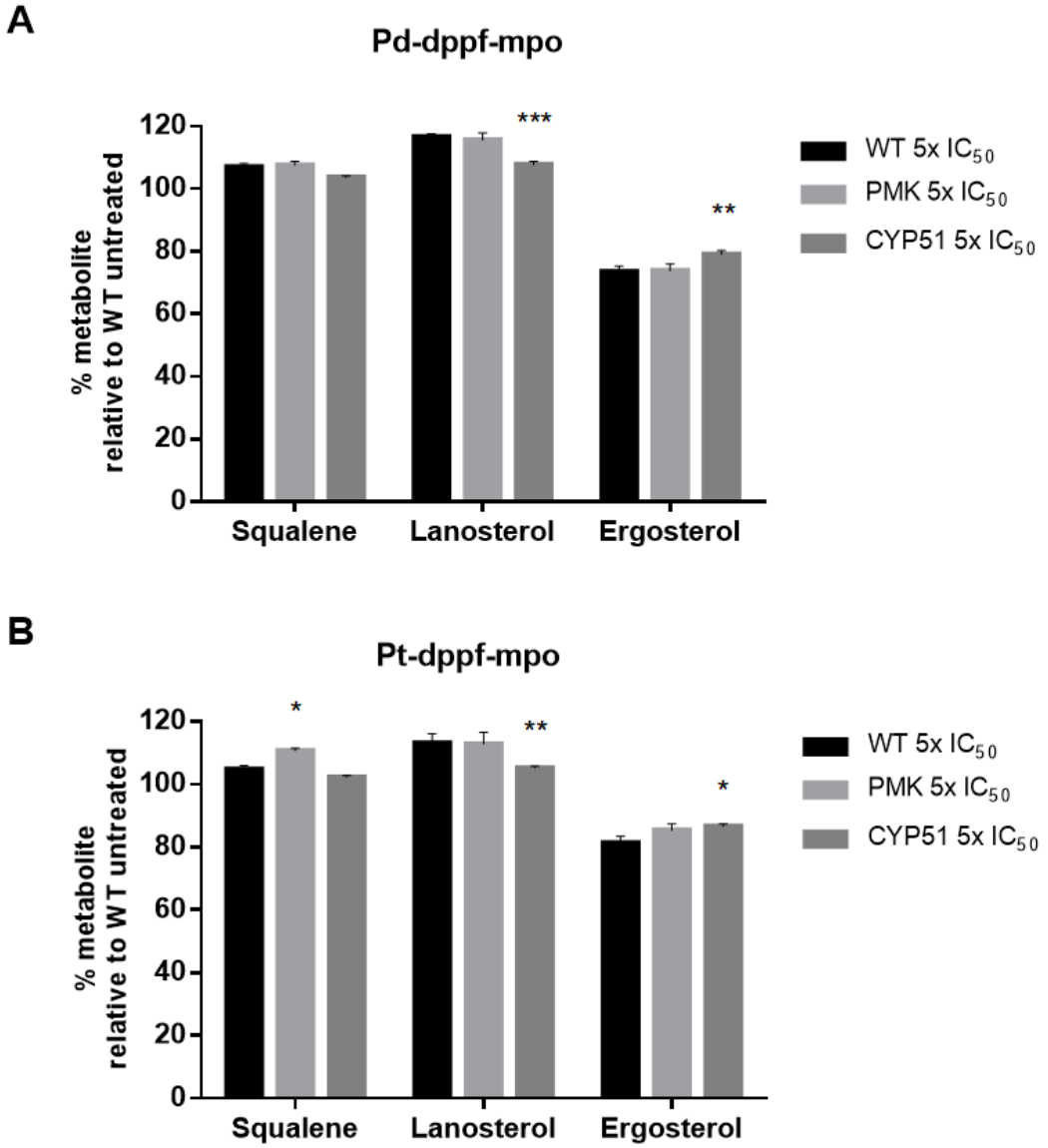

Figure 9. Percentage of the metabolites squalene, lanosterol and ergosterol in wild type, PMK and CYP51 overexpressing parasites after 6 hours of treatment with 5x IC_{50} of Pd-dppf-mpo (**A**) and Pt-dppf-mpo (**B**). The results are presented as averages ± SD (standard deviation) of two biological replicates. To compare 5x IC_{50} treated transfectants against 5x IC_{50} treated wild type parasites, two-way ANOVA test followed by Bonferroni's multiple comparisons test was performed. p-values: **** <0.0001, *** <0.001, ** <0.01, * <0.1.

Concluding remarks

Identifying the mechanism of action and molecular targets of compounds is necessary to improve effectiveness and compound selectivity. Determining the molecular targets of active compounds can be challenging, however, in previous work, using high throughput omic approaches, we identified several enzymes of the ergosterol pathway as promising candidates. In this paper, we validated the involvement of PMK and mainly CYP51 as molecular targets of Pd-dppf-mpo and Pt-dppf-mpo.

We found a dose dependent accumulation of the intermediate metabolites squalene and lanosterol together with a decrease of the final product of the pathway, ergosterol, in treated parasites. These results suggest that after treatment, the pathway is mainly blocked in a step after lanosterol production and before ergosterol synthesis. Through an overexpression gain-of-function strategy, we observed a slight increase in the viability of PMK overexpressing parasites for some compound concentration. Moreover, for CYP51 overexpressing parasites higher viability percentages, accompanied with a decrease in lanosterol accumulation levels driving to higher ergosterol production comparing to treated wild type parasites were observed. Altogether, we propose the involvement of CYP51 and PMK in the mechanism of action of the palladium and platinum compounds since the addback of both enzymes led to a partial rescue of the phenotype.

Since the ergosterol pathway is also essential in other trypanosomatids, our compounds could also be promising against other related parasites like *Leishmania* sp. and *Trypanosoma brucei*.

Declaration of competing interests

Authors have no competing interests to declare.

Author contributions

FM, GS, DG, LPD: conceptualization, methodology, investigation, writing original draft; IM: ergosterol determinations by HPLC; MP, PD, RM: computational

studies; FM, GS, LPD: formal analysis, investigation; DG, LPD: supervision, resources.

Acknowledgements

Authors acknowledge Dr. Marcelo Comini for enabling to use the Nucleofector device at the Institut Pasteur de Montevideo. Authors would like to thank Dra. Marcela Díaz for assistance in using confocal microscopy. This research was supported by Programa de Desarrollo de las Ciencias Básicas (PEDECIBA), Comisión académica de Posgrados (CAP-UdelaR) FM: AP_2019_63 and CAP_2022_36.

References

1. Chagas, C., *Nova tripanozomiase humana. Estudos sobre a morfolojia e o ciclo evolutivo do Schizotrypanum cruzi n. gen. n. sp., ajente etiolojico de nova entidade mórbida do homem.* Memorias do Instituto Oswaldo Cruz, 1909. **1**: p. 159-218.
2. Traina, M.I., et al., *Prevalence of Chagas Disease in a U.S. Population of Latin American Immigrants with Conduction Abnormalities on Electrocardiogram.* PLoS Negl Trop Dis, 2017. **11**(1): p. e0005244.
3. Park, S., et al., *The Prevalence of Chagas Disease Among Latin American Immigrants with Pacemakers in Los Angeles, California.* Am J Trop Med Hyg, 2017. **96**(5): p. 1139-1142.
4. Chatelain, E. and J.R. Ioset, *Phenotypic screening approaches for Chagas disease drug discovery.* Expert Opin Drug Discov, 2018. **13**(2): p. 141-153.
5. Santos, S.S., et al., *Searching for drugs for Chagas disease, leishmaniasis and schistosomiasis: a review.* Int J Antimicrob Agents, 2020. **55**(4): p. 105906.
6. WHO, W.H.O. *Neglected tropical diseases. https://www.who.int/news-room/q-a-detail/neglected-tropical-diseases accesed december 2022.* 2022.
7. de Oliveira, R.G., et al., *Chagas Disease Drug Discovery in Latin America-A Mini Review of Antiparasitic Agents Explored Between 2010 and 2021.* Front Chem, 2021. **9**: p. 771143.
8. Gambino, D. and L. Otero, *Facing Diseases Caused by Trypanosomatid Parasites: Rational Design of Pd and Pt Complexes With Bioactive Ligands.* Front Chem, 2022. **9**: p. 816266.
9. Gambino, D., Otero, L., *Design of prospective antiparasitic metal-based compounds including selected organometallic cores.* Inorganica Chimica Acta, 2018. **472**: p. 58-75.
10. Gambino, D., Otero, L., *Perspectives on what ruthenium-based compounds could offer in the development of potential antiparasitic drugs.* Inorganica Chimica Acta, 2012. **393**: p. 103-114.

11. Gambino, D., *Potentiality of vanadium compounds as anti-parasitic agents.* Coordination Chemistry Reviews, 2011. **255**: p. 2193-2203.
12. Pessoa, J.C., S. Etcheverry, and D. Gambino, *Vanadium compounds in medicine.* Coord Chem Rev, 2015. **301**: p. 24-48.
13. Rodriguez Arce, E., et al., *Aromatic amine N-oxide organometallic compounds: searching for prospective agents against infectious diseases.* Dalton Trans, 2015. **44**(32): p. 14453-64.
14. Mosquillo, M.F., et al., *Effect of a new anti-T. cruzi metallic compound based on palladium.* Biometals, 2018. **31**(6): p. 961-974.
15. Mosquillo, M.F., et al., *Trypanosoma cruzi biochemical changes and cell death induced by an organometallic platinum-based compound.* Chem Biol Drug Des, 2018. **92**(3): p. 1657-1669.
16. Mosquillo, M.F., et al., *Comparative high-throughput analysis of the Trypanosoma cruzi response to organometallic compounds.* Metallomics, 2020. **12**(5): p. 813-828.
17. Villalta, F. and G. Rachakonda, *Advances in preclinical approaches to Chagas disease drug discovery.* Expert Opin Drug Discov, 2019. **14**(11): p. 1161-1174.
18. Urbina, J.A., *Ergosterol biosynthesis and drug development for Chagas disease.* Mem Inst Oswaldo Cruz, 2009. **104 Suppl 1**: p. 311-8.
19. Gerpe, A., et al., *5-Nitrofuranes and 5-nitrothiophenes with anti-Trypanosoma cruzi activity and ability to accumulate squalene.* Bioorg Med Chem, 2009. **17**(21): p. 7500-9.
20. Santivanez-Veliz, M., et al., *Development, validation and application of a GC-MS method for the simultaneous detection and quantification of neutral lipid species in Trypanosoma cruzi.* J Chromatogr B Analyt Technol Biomed Life Sci, 2017. **1061-1062**: p. 225-232.
21. Bavisetty, S.C. and B. Narayan, *An improved RP-HPLC method for simultaneous analyses of squalene and cholesterol especially in aquatic foods.* J Food Sci Technol, 2015. **52**(9): p. 6083-9.
22. Vazquez, M.P. and M.J. Levin, *Functional analysis of the intergenic regions of TcP2beta gene loci allowed the construction of an improved Trypanosoma cruzi expression vector.* Gene, 1999. **239**(2): p. 217-25.
23. Pacheco-Lugo, L., et al., *Effective gene delivery to Trypanosoma cruzi epimastigotes through nucleofection.* Parasitol Int, 2017. **66**(3): p. 236-239.
24. Schindelin, J., et al., *Fiji: an open-source platform for biological-image analysis.* Nat Methods, 2012. **9**(7): p. 676-82.
25. Scalese, G., et al., *Heteroleptic Oxidovanadium(V) Complexes with Activity against Infective and Non-Infective Stages of Trypanosoma cruzi.* Molecules, 2021. **26**(17).
26. Becke, A.D., *A new inhomogeneity parameter in density-functional theory.* The Journal of Chemical Physics, 1998. **109**(6): p. 2092-2098.
27. Lee, C., W. Yang, and R.G. Parr, *Development of the Colle-Salvetti correlation-energy formula into a functional of the electron density.* Phys Rev B Condens Matter, 1988. **37**(2): p. 785-789.
28. McLean, A.D. and G.S. Chandler, *Contracted Gaussian basis sets for molecular calculations. I. Second row atoms, Z=11–18.* The Journal of Chemical Physics, 1980. **72**(10): p. 5639-5648.

29. Krishnan, R., et al., *Self-consistent molecular orbital methods. XX. A basis set for correlated wave functions.* The Journal of Chemical Physics, 1980. **72**(1): p. 650-654.
30. Roy, L.E., P.J. Hay, and R.L. Martin, *Revised Basis Sets for the LANL Effective Core Potentials.* Journal of Chemical Theory and Computation, 2008. **4**: p. 1029-1031.
31. Frisch, M.J., et al., *Gaussian 09, Revision A.02*. 2016: Inc., Wallingford CT.
32. (MOE), M.O.E. 2019, 1010 Sherbooke St. West, Suite #910, Montreal, QC, Canada, H3A 2R7: Chemical Computing Group ULC.
33. Naïm, M., et al., *Solvated Interaction Energy (SIE) for Scoring Protein−Ligand Binding Affinities. 1. Exploring the Parameter Space.* Journal of Chemical Information and Modeling, 2007. **47**(1): p. 122-133.
34. Jumper, J., et al., *Highly accurate protein structure prediction with AlphaFold.* Nature, 2021. **596**(7873): p. 583-589.
35. Cosentino, R.O. and F. Aguero, *Genetic profiling of the isoprenoid and sterol biosynthesis pathway genes of Trypanosoma cruzi.* PLoS One, 2014. **9**(5): p. e96762.
36. Urbina, J.A., et al., *Alteration of lipid order profile and permeability of plasma membranes from Trypanosoma cruzi epimastigotes grown in the presence of ketoconazole.* Mol Biochem Parasitol, 1988. **30**(2): p. 185-95.
37. Buckner, F.S. and J.A. Urbina, *Recent Developments in Sterol 14-demethylase Inhibitors for Chagas Disease.* Int J Parasitol Drugs Drug Resist, 2012. **2**: p. 236-242.
38. Osorio-Mendez, J.F. and A.M. Cevallos, *Discovery and Genetic Validation of Chemotherapeutic Targets for Chagas' Disease.* Front Cell Infect Microbiol, 2018. **8**: p. 439.
39. Liendo, A., et al., *Sterol composition and biosynthesis in Trypanosoma cruzi amastigotes.* Mol Biochem Parasitol, 1999. **104**(1): p. 81-91.
40. Soeiro, M.N. and S.L. de Castro, *Trypanosoma cruzi targets for new chemotherapeutic approaches.* Expert Opin Ther Targets, 2009. **13**(1): p. 105-21.
41. Li, Y., et al., *Transcriptome Remodeling in Trypanosoma cruzi and Human Cells during Intracellular Infection.* PLoS Pathog, 2016. **12**(4): p. e1005511.
42. Warrilow, A.G., et al., *Clotrimazole as a potent agent for treating the oomycete fish pathogen Saprolegnia parasitica through inhibition of sterol 14alpha-demethylase (CYP51).* Appl Environ Microbiol, 2014. **80**(19): p. 6154-66.
43. Chen, C.K., et al., *Structural characterization of CYP51 from Trypanosoma cruzi and Trypanosoma brucei bound to the antifungal drugs posaconazole and fluconazole.* PLoS Negl Trop Dis, 2010. **4**(4): p. e651.

Supplementary Figures

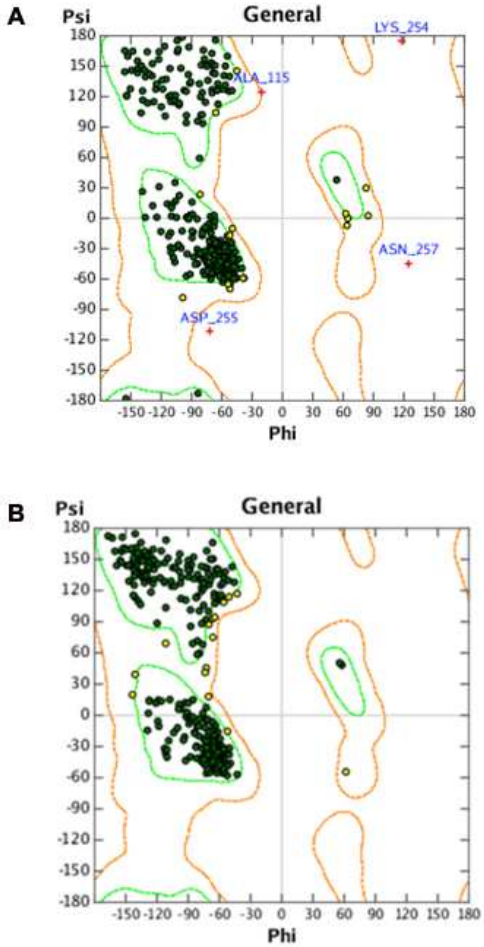

Supplementary figure S1. (**A**) Ramachandran plot of crystallographic *T. cruzi* CYP51 protein. (**B**) Ramachandran plot of modelled *T. cruzi* PMK protein.

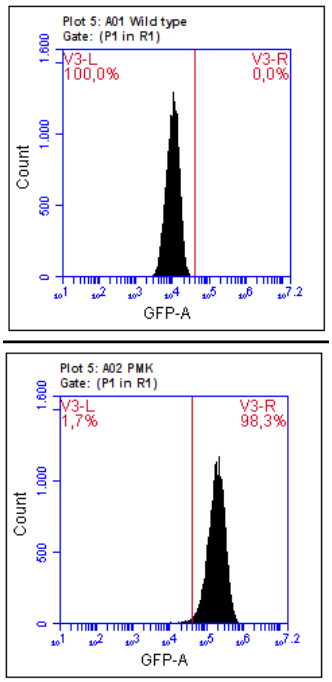

Supplementary figure S2. Analysis of PMK transfected parasites by flow cytometry. Control non transfected parasites are shown in the upper panel and PMK-GFP transfected parasites are shown in the lower panel. 10,000 events were acquired in the gated region previously identified as corresponding to epimastigotes in a BD Accuri C6 (BD Biosciences).

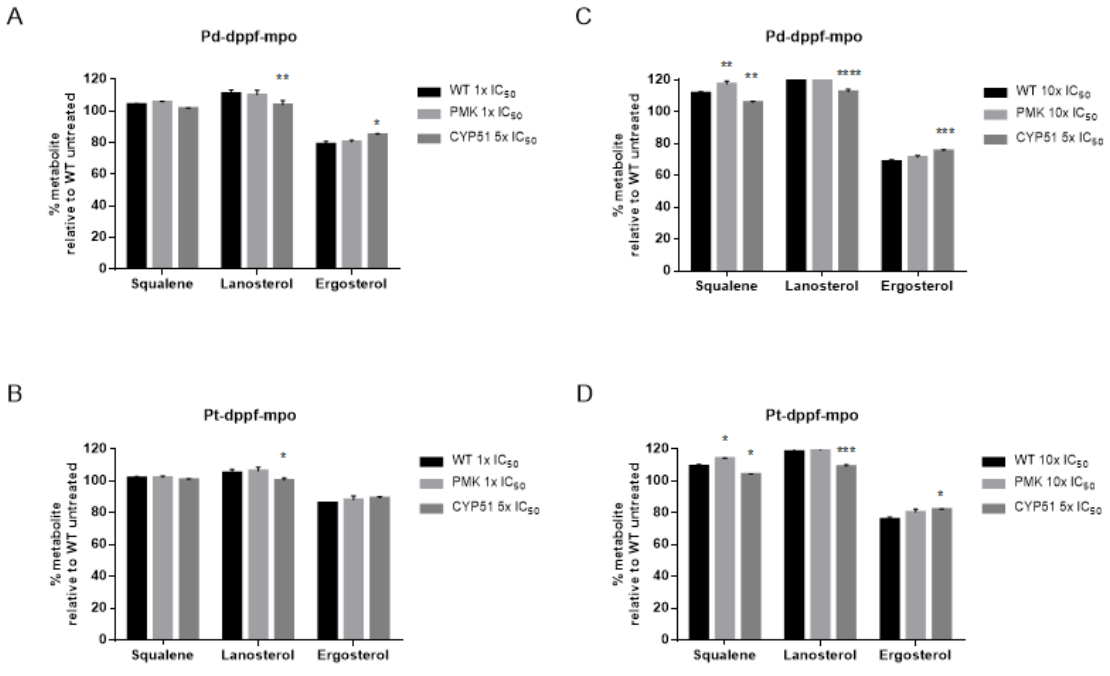

Supplementary figure S3. Percentage of the metabolites squalene, lanosterol and ergosterol in wild type, PMK and CYP51 overexpressing parasites after 6 hours of treatment with 1x IC_{50} of Pd-dppf-mpo (**A**) and Pt-dppf-mpo (**B**), and with 10x IC_{50} of Pd-dppf-mpo (**C**) and Pt-dppf-mpo (**D**). The results are presented as averages ± SD (standard deviation) of two biological replicates. To compare treated transfectants against treated wild type parasites, two-way ANOVA test followed by Bonferroni's multiple comparisons test was performed. p-values: **** <0.0001, *** <0.001, ** <0.01, * <0.1.

Supplementary Tables

Table S1. Mulliken charges of all atoms after energy minimization for the Pd-dppf-mpo complex.

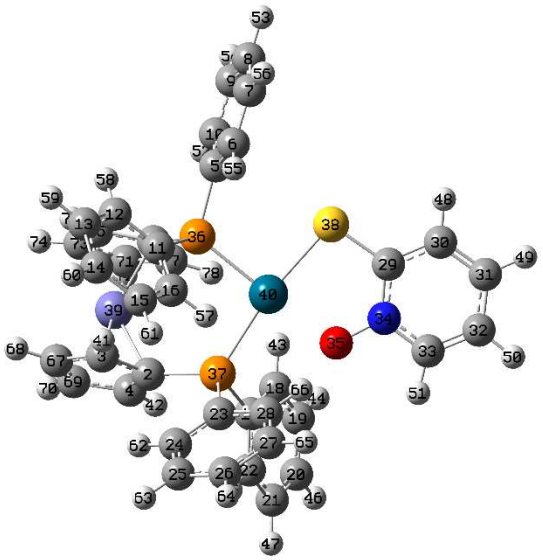

Atom		Charge	Atom		Charge	Atom		Charge
1	C	-0.40718	27	C	-0.182876	53	H	0.216914
2	C	-0.411364	28	C	-0.209905	54	H	0.213922
3	C	-0.242663	29	C	0.123505	55	H	0.226915
4	C	-0.197637	30	C	-0.327439	56	H	0.214323
5	C	-0.304664	31	C	-0.075828	57	H	0.290803
6	C	-0.189005	32	C	-0.306622	58	H	0.2292
7	C	-0.176359	33	C	0.074529	59	H	0.219966
8	C	-0.179251	34	N	-0.079705	60	H	0.220866
9	C	-0.176884	35	O	-0.48007	61	H	0.217152
10	C	-0.187799	36	P	0.926197	62	H	0.236422
11	C	-0.26306	37	P	0.953071	63	H	0.215715
12	C	-0.181306	38	S	0.027373	64	H	0.21821

13	C	-0.184087	39	Fe	0.451063	65	H	0.212828
14	C	-0.17535	40	Pd	-0.185592	66	H	0.257303
15	C	-0.190911	41	H	0.248001	67	C	-0.201686
16	C	-0.244125	42	H	0.232327	68	H	0.219322
17	C	-0.262992	43	H	0.225657	69	C	-0.198713
18	C	-0.180859	44	H	0.210358	70	H	0.222971
19	C	-0.193521	45	H	0.223975	71	C	-0.215268
20	C	-0.183744	46	H	0.21723	72	H	0.220911
21	C	-0.187323	47	H	0.215717	73	C	-0.196156
22	C	-0.174681	48	H	0.243928	74	H	0.223714
23	C	-0.311371	49	H	0.234686	75	C	-0.196205
24	C	-0.19906	50	H	0.236583	76	H	0.214166
25	C	-0.18146	51	H	0.264153	77	C	-0.22016
26	C	-0.183863	52	H	0.225519	78	H	0.221248

Table S2. Mulliken charges of all atoms after energy minimization for the Pt-dppf-mpo complex.

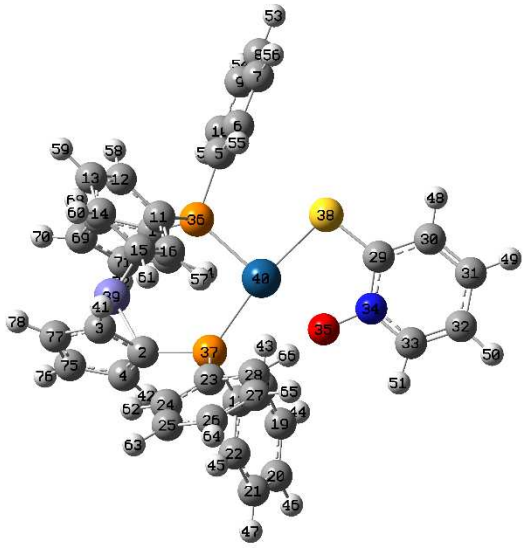

Atom		Charge	Atom		Charge	Atom		Charge
1	C	-0.402356	27	C	-0.182516	53	H	0.216383
2	C	-0.419324	28	C	-0.205464	54	H	0.21354
3	C	-0.238143	29	C	0.126898	55	H	0.226363
4	C	-0.196295	30	C	-0.329621	56	H	0.213768
5	C	-0.30768	31	C	-0.075989	57	H	0.305482
6	C	-0.186376	32	C	-0.306172	58	H	0.229651
7	C	-0.177888	33	C	0.079032	59	H	0.21926
8	C	-0.179107	34	N	-0.083652	60	H	0.220098
9	C	-0.177591	35	O	-0.517768	61	H	0.215823
10	C	-0.18612	36	P	0.940948	62	H	0.236858
11	C	-0.258696	37	P	0.951595	63	H	0.216057
12	C	-0.183079	38	S	0.071116	64	H	0.218215
13	C	-0.184842	39	Fe	0.448104	65	H	0.212766

14	C	-0.174762	40	Pt	-0.25463	66	H	0.257117
15	C	-0.190539	41	H	0.248045	67	C	-0.193508
16	C	-0.245964	42	H	0.231891	68	H	0.215653
17	C	-0.266658	43	H	0.235968	69	C	-0.19708
18	C	-0.178788	44	H	0.210211	70	H	0.223035
19	C	-0.19499	45	H	0.225523	71	C	-0.214942
20	C	-0.181591	46	H	0.216985	72	H	0.22033
21	C	-0.192407	47	H	0.215313	73	C	-0.218837
22	C	-0.171918	48	H	0.245008	74	H	0.229643
23	C	-0.307129	49	H	0.236219	75	C	-0.197986
24	C	-0.19866	50	H	0.238421	76	H	0.222575
25	C	-0.180476	51	H	0.265918	77	C	-0.201988
26	C	-0.183204	52	H	0.225693	78	H	0.219232

Table S3. Putative CYP51 sites found with Site Finder module. Size: number of alpha spheres comprising the site, PLB: propensity for ligand binding, Hyd: number of hydrophobic contact atoms in the receptor

Site	Size	PLB	Hyd	
1	155	4.29	73	(ILE45 PHE48 GLY49 PRO52 ILE72 TYR103 ILE105 MET106 PHE110 ALA115 TYR116 LEU127 LEU130 PRO210 ALA211 VAL213 PHE214 ALA287 ALA288 PHE290 ALA291 GLY292 GLN293 HIS294 THR295 PRO355 LEU356 LEU357 MET358 VAL359 MET360 TYR457 HIS458 THR459 MET460 VAL461 VAL462)2:(HEM488)
2	183	3.13	34	GLU133 ALA137 LYS138 GLN140 ASN141 PHE142 PRO144 ALA145 HIS148 GLN181 CYS182 LEU183 PHE184 GLY185 GLU186 ASP187 ARG189 ARG247 GLU248 GLU250 GLU251 ALA252 SER253 LYS254 ASP255 ASN256 ASN257 THR258 SER259 ASP260 LEU261 GLY263
3	59	1.06	30	ILE105 PRO108 SER207 LEU208 ILE209 ALA212 LEU218 LEU219 ARG220 LEU221 PRO222 LEU223 GLN225 SER226 CYS229 ARG230

Table S4. Putative PMK sites found with Site Finder module. Size: number of alpha spheres comprising the site, PLB: propensity for ligand binding, Hyd: number of hydrophobic contact atoms in the receptor

Site	Size	PLB	Hyd	
1	155	4.29	73	(ILE45 PHE48 GLY49 PRO52 ILE72 TYR103 ILE105 MET106 PHE110 ALA115 TYR116 LEU127 LEU130 PRO210 ALA211 VAL213 PHE214 ALA287 ALA288 PHE290 ALA291 GLY292 GLN293 HIS294 THR295 PRO355 LEU356 LEU357 MET358 VAL359 MET360 TYR457 HIS458 THR459 MET460 VAL461 VAL462)2:(HEM488)
2	183	3.13	34	GLU133 ALA137 LYS138 GLN140 ASN141 PHE142 PRO144 ALA145 HIS148 GLN181 CYS182 LEU183 PHE184 GLY185 GLU186 ASP187 ARG189 ARG247 GLU248 GLU250 GLU251 ALA252 SER253 LYS254 ASP255 ASN256 ASN257 THR258 SER259 ASP260 LEU261 GLY263
3	59	1.06	30	ILE105 PRO108 SER207 LEU208 ILE209 ALA212 LEU218 LEU219 ARG220 LEU221 PRO222 LEU223 GLN225 SER226 CYS229 ARG230

Table S5. CYP51- POZ docking scores (kcal/mol).

	Score	rmsd_refine	E_conf	E_place	E_score1	E_refine	E_score2
	-10.940316	1.5433674	83.285828	-115.17203	-12.939788	-53.155125	-10.940316
	-10.686852	1.1773831	96.574661	-138.15756	-12.093087	-55.371719	-10.686852
	-10.673535	1.7766356	92.139328	-111.12427	-10.875208	-58.004139	-10.673535
	-10.458047	2.2843845	105.31147	-158.09682	-11.950311	-48.643242	-10.458047
	-10.392945	3.1578598	88.986099	-101.51168	-12.172669	-42.686264	-10.392945
Mean	-10.630339	1.98792608	93.259477	-124.81247	-12.006212	-51.572098	-10.630339
SD	0.21632487	0.7674452	8.29504593	22.9628564	0.73978279	6.03842879	0.21632487

Table S6. CYP51 Pd-dppf-mpo and Pt-dppf-mpo docking scores (kcal/mol). * value not included for the mean calculation

Pd-dppf-mpo							
	Score	rmsd_refine	E_conf	E_place	E_score1	E_refine	E_score2
	-6.630682	3.4687738	878.07208	-25.473139	-4.7524948	-33.264717	-6.630682
	-5.9541073	1.5324298	886.75525	-4.409276	-5.3224163	-26.378717	-5.9541073
	-5.9368792	0.96233362	881.40381	-16.547628	-6.6223254	-27.446678	-5.9368792
	-5.8228583	3.9457266	877.29291	-37.696068	-5.0617938	-34.122536	-5.8228583
	-5.7538123	4.7777739	878.18689	-43.270348	-5.8153296	-25.237322	-5.7538123
Mean	-6.01966782	2.93740754	880.342188	-25.4792918	-5.51487198	-29.289994	-6.01966782
SD	0.31429401	1.45333308	3.50289028	14.0676332	0.65425772	3.67285674	0.31429401
Pt-dppf-mpo							
	Score	rmsd_refine	E_conf	E_place	E_score1	E_refine	E_score2
	-6.5139918	2.5208039	791.70862	-17.364498	-8.802001	-34.436138	-6.5139918

	-6.488112	1.6864315	787.15399	-56.238148	-8.2905846	-35.335846	-6.488112
	-6.378098	2.709944	788.12488	-16.372377	-6.1494813	-30.783268	-6.378098
	-6.3137879	2.5554321	789.27319	-33.23774	-9.3500624	-31.276436	-6.3137879
	-6.2530317	2.4511271	798.12231	2.0723453*	-7.5933156	-25.455833	-6.2530317
Mean	-6.38940428	2.38474772	790.876598	-30.8031908	-8.03708898	-31.4575042	-6.38940428
SD	0.09970799	0.35929064	3.92920558	16.1377735	1.10754207	3.47624026	0.09970799

Table S7. PMK Pd-dppf-mpo and Pt-dppf-mpo docking scores (kcal/mol). * value not included for the mean calculation

Pd-dppf-mpo							
	Score	rmsd_refine	E_conf	E_place	E_score1	E_refine	E_score2
	-6.7430925	1.3337919	882.01141	-2.4837584*	-10.233498	-43.606136	-6.7430925
	-6.7221484	2.0357306	875.36194	-39.401211	-10.959346	-42.836227	-6.7221484
	-6.6946316	2.0741041	898.62402	-26.803722	-9.7030792	-39.037994	-6.6946316
	-6.6577544	1.9699802	887.49603	4.5698967*	-10.887565	-29.67708	-6.6577544
	-6.4463143	2.2757843	880.36542	-29.574938	-11.370107	-33.813545	-6.4463143
Mean	-6.65278824	1.93787822	884.771764	-31.9266237	-10.630719	-37.7941964	-6.65278824
SD	0.10711929	0.31883034	7.93582801	5.40505944	0.58973898	5.33818155	0.10711929
Pt-dppf-mpo							
	S	rmsd_refine	E_conf	E_place	E_score1	E_refine	E_score2
	-7.7756844	2.6181996	778.58801	-35.219135	-10.368558	-42.476456	-7.7756844
	-7.6836891	2.2090101	796.6571	-51.475647	-9.7841597	-41.026878	-7.6836891
	-7.3847041	2.3056695	784.9079	-37.916164	-9.6980228	-37.386398	-7.3847041
	-7.1561542	1.5266721	789.58881	-48.057507	-10.602125	-3.1532404	-7.1561542
	-6.9944615	1.8058484	803.36127	-24.512594	-10.103442	-25.770691	-6.9944615
Mean	-7.39893866	2.09307994	790.620618	-39.4362094	-10.1112615	-29.9627327	-7.39893866
SD	0.29858629	0.38411055	8.68615863	9.61335926	0.34204427	14.6317564	0.29858629

Table S8. *T. cruzi* gene log-transformed quantile-normalized count per million (CPM) expression values [41].

Gen	ID Non-Esmeraldo like	ID Esmeraldo like	Epi log_2 CPM ± SD	Relative expression against reference gene
PMK	TcCLB.507913.20	TcCLB.508277.140	7.997 ± 0.030	0.946
CYP51	TcCLB.506297.260	TcCLB.510101.50	9.209 ± 0.038	1.089
Thr-tRNA synthetase	TcCLB.508299.80	TcCLB.511181.80	8.455 ± 0.039	

Declaration of Interest Statement

Declaration of interests

☒The authors declare that they have no known competing financial interests or personal relationships that could have appeared to influence the work reported in this paper.

☐The authors declare the following financial interests/personal relationships which may be considered as potential competing interests:

8 Discusión general

Los principales resultados obtenidos de los nuevos compuestos en estudio se encuentran recopilados en la Tabla 2 para facilitar su análisis y comparación. En primer lugar, los valores de IC_{50} reportados para los compuestos $V^{IV}O$(5Brsal)(aminofén), Pd-dppf-mpo y Pt-dppf-mpo sobre epimastigotas de la cepa CL Brener, se encuentran en el rango micromolar, exhibiendo una alta capacidad citotóxica contra el parásito. Para discernir si la potencialidad de estos compuestos es específica, se realizaron ensayos de citotoxicidad sobre células normales de mamífero. Para el compuesto de vanadio, el valor de IC_{50} se encuentra reportado en la bibliografía sobre macrófagos J-774 (Fernandez, 2013b) y para los restantes compuestos, el valor de IC_{50} fue determinado sobre células VERO. El Índice de Selectividad (IS), calculado como el IC_{50} *T. cruzi* / IC_{50} células mamífero, permite evaluar si la actividad citotóxica sobre el parásito afecta también a las células normales de mamífero. Actualmente, son aceptados los criterios propuestos por la *Drugs for Neglected Diseases initiative* (DNDi) para el desarrollo de nuevos compuestos, los cuales implican que éstos presenten una eficacia considerable (IC_{50} < 10 µM) y sean selectivos contra el parásito (>10 veces sobre células de mamífero) (Katsuno, 2015). En todos los casos, los compuestos de este trabajo cumplen con los criterios, destacándose la actividad del compuesto Pt-dppf-mpo por presentar una eficacia en el rango nanomolar y un excelente IS.

Tabla 2. Resumen de los principales resultados obtenidos para los compuestos $V^{IV}O$(5Brsal)(aminofén), Pd-dppf-mpo y Pt-dppf-mpo.

Ensayo		$V^{IV}O$(5Brsal)(aminofén)	Pd-dppf-mpo	Pt-dppf-mpo
IC_{50} Brener *T. cruzi*		3,76 ± 0,08 µM	0,300 ± 0,030 µM	0,060 ± 0,003 µM
IC_{50} Células mamífero		50 ± 2 µM [b]	24,5 ± 12,2 µM	5,1 ± 3,3 µM
Indice de selectividad		13	83	85
% incorporación a 24 h	1x IC_{50}	0,50 nmol/15 nmol (3,33%)	0,012 µM/0,300 µM (4%)	0,045 µM/0,060 µM (75%)
	5x IC_{50}	1,18 nmol/75 nmol (1,57%)	0,180 µM/1,500 µM (12%)	0,140 µM/0,30 µM (48%)
	10x IC_{50}	3,51 nmol/150 nmol (2,34%)	0,480 µM/3,000 µM (16%)	0,110 µM/0,60 µM (19%)
Asociación preferencial a macromoleculas (6 h)	5x IC_{50}	Fracción insoluble (96%)	ADN (75%)	ADN (62%)
	10x IC_{50}	ND	ADN (61%)	ADN (71%)
Tripanostático/tripanocida (4 h incubación/72 h observación)	1x IC_{50}	Tripanostático	Tripanostático	Tripanostático
	5x IC_{50}	Tripanostático	Tripanocida	Tripanostático
	10x IC_{50}	Tripanostático	Tripanocida	Tripanocida
Tipo de muerte celular inducido (3, 6 y 24 h)	1x IC_{50}	Apoptosis/necrosis no detectadas a 3, 6 y 24 h	Apoptosis/necrosis no detectadas a 3, 6 y 24 h	Apoptosis/necrosis no detectadas a 3, 6 y 24 h
	5x IC_{50}	Apoptosis/necrosis no detectadas a 3, 6 y 24 h	Necrosis a 24 h (17,5%)	Apoptosis/necrosis no detectadas a 3, 6 y 24 h
	10x IC_{50}	Apoptosis/necrosis no detectadas a 3, 6 y 24 h	Necrosis a 24 h (55,7%)	Necrosis a 24 h (10,6%)
Efecto en el proceso de infección (% células infectadas a 24 h | 48 h)	Control	ND	83% | 86%	100% | 100%
	1x IC_{50}	ND	46% | 56%	97% | 85%
	5x IC_{50}	ND	21% | 13%	92% | 62%
	10x IC_{50}	ND	8% | 3%	66% | 31%
Efecto en una infección establecida (n° amastigotas/célula infectada a 24 h | 48 h)	Control	ND	13 | 38	4 | 30
	1x IC_{50}	ND	5 | 12	4 | 19
	5x IC_{50}	ND	3 | 5	3 | 12
	10x IC_{50}	ND	2 | 2	3 | 8
Transcritos modificados (6 h)	5x IC_{50}	88/10951	2327/10785	201/10773
Proteínas modificadas (6 h)	5x IC_{50}	523/3638	342/2107	411/1823

[b] (Fernández, 2013)

El análisis metalómico de los compuestos permite determinar la cantidad, localización e identidad de las especies metálicas dentro del parásito unicelular (Scalese, 2022). Los porcentajes de incorporación varían notablemente entre compuestos, incluso entre los compuestos M-dppf-mpo, de naturaleza similar. Esta variación en los porcentajes se debe a la cantidad de compuesto incorporada al sistema, que se calcula de acuerdo al valor de IC_{50} determinado. Por esto es mejor observar los valores de incorporación en moles o concentración, los cuales aumentan en todos los casos de manera dosis dependiente, excepto para el compuesto Pt-dppf-mpo a la mayor concentración, lo cual podría deberse a cierta saturación del sistema o al eflujo del compuesto (Brandon, 2006).

El estudio de la asociación de los distintos compuestos con diferentes macromoléculas, determina que el compuesto de vanadio presenta una mayor asociación con la fracción insoluble, incluyendo principalmente membranas y proteínas insolubles, a pesar del diseño racional que incluye el ligando con capacidad intercalante en el ADN (Fernandez, 2013b). Por su parte, los compuestos M-dppf-mpo, fueron también diseñados para tener una mayor afinidad con los ácidos nucleicos, efecto que se comprueba en este trabajo, y que demuestra que la asociación se da preferencialmente con ácidos desoxirribonucleicos, y en menor porcentaje, con las proteínas del parásito. Además, fueron cuantificados en cada fracción los moles de los metales Pd y Fe o Pt y Fe, y pudo determinarse una relación estequiométrica de 1:1, sugiriendo la integridad del complejo al alcanzar cualquiera de las macromoléculas.

En la bibliografía se encuentra descrito que, si un compuesto actúa de forma tripanocida, apenas 4 horas de incubación son suficientes para desencadenar los mecanismos de muerte celular de forma irreversible (Kessler, 2013). El comportamiento tripanocida o tripanostático de los distintos compuestos en las diferentes concentraciones, correlaciona con los datos obtenidos sobre el mecanismo de muerte celular analizado mediante citometría de flujo con Anexina V y Ioduro de propidio, luego de 24 horas de incubación con los compuestos. El efecto tripanocida está, en todos los casos detectados, vinculado a necrosis celular y no a apoptosis, aunque no pueden ser descartados otros mecanismos de muerte celular. Los menores tiempos de incubación de 3 y 6 horas demuestran que no hay marcación inicial con Anexina V, descartando apoptosis temprana, igualmente, sería recomendable realizar incubaciones a 12, 16 o 20 horas para realizar un mejor seguimiento en el tiempo del proceso de muerte celular. De todas maneras, nuestro grupo demostró que esta técnica permite identificar correctamente la apoptosis como tipo de muerte celular luego de 24 horas de tratamiento, ya que durante la puesta a punto se trabajó en paralelo con otros compuestos de oxidovanadio(IV), identificándose apoptosis como tipo de muerte celular inducido (Scalese, 2017). En el caso del compuesto de vanadio, ninguna de las concentraciones ensayadas presentó un efecto tripanocida, lo cual podría ser explicado por los magros porcentajes de incorporación por parte del parásito; ya sea por falta de lipofilia o por

mayor eflujo ya que no se encontraron cantidades significativas del compuesto en los parásitos. De todas maneras, el valor de 2,4% obtenido en promedio es similar al de otros compuestos metálicos como el cisplatino. Cabe recordar que este compuesto no cuenta con la inclusión de la esfera de ferroceno, dppf, para una mejor permeabilidad de la membrana, como sí presentan los M-dppf-mpo. Por otro lado, dado que el compuesto fue diseñado para interaccionar con el ADN, y su mayor asociación se encontró con la fracción insoluble, podría ser posible hipotetizar que el compuesto no ejerce efecto tripanocida por su incapacidad de ingresar de forma eficaz al parásito, alcanzando su presunta molécula diana, el ADN. No obstante, el efecto tripanostático del compuesto de vanadio podría explicarse por la ocurrencia de dormancia en los parásitos. Este estado de latencia se presenta como una forma de resistencia a condiciones ambientales no óptimas, en el que las células arrestan su crecimiento (Resende, 2020). Estos parásitos persistentes o dormantes, se definen fenotípicamente como una subpoblación transitoria que es menos susceptible al tratamiento de fármacos debido a diferentes grados de inactividad metabólica. Si la célula no se divide, o se divide muy lentamente, los fármacos que tienen como objetivo la replicación del ADN o la división celular pueden no ser eficaces. También hay indicios de cambios en la regulación de los transportadores que pueden afectar los niveles de fármaco en el patógeno, al modificar ya sea captación o salida. Sin embargo, los mecanismos moleculares precisos que definen a estas poblaciones persistentes aún no son bien conocidos (De Rycker, 2022). Para *T. cruzi*, se demostró que los amastigotas detenidos no son capaces de incorporar el análogo de nucleótido 5-etinil-2'-desoxiuridina (EdU), pero pueden realizar la diferenciación a tripomastigotas. Curiosamente, esos parásitos latentes fueron resistentes a dosis de Benznidazol 50 veces más altas que la dosis IC_{50} normal (Sanchez-Valdez, 2018). Particularmente, en ensayos a 6 días se ha observado que las cepas híbridas, como CL Brener, exhiben una mayor capacidad de entrar en latencia a lo largo del tiempo, y que tienen la habilidad de recuperar la duplicación celular en condiciones de cultivo fresco (Resende, 2020). Sería entonces interesante caracterizar los parásitos tratados, para evaluar la existencia o no de dormancia durante el tratamiento.

El análisis de los compuestos continúa con el estudio de su efecto sobre tripomastigotas celulares, la forma infectiva del parásito. Para estudiar si los compuestos M-dppf-mpo pueden afectar el proceso de infección por parte de los tripomastigotas, éstos fueron pretratados con 1x, 5x y 10x el valor IC_{50} determinado para epimastigotas durante 30 minutos y se utilizaron para infectar células VERO. El porcentaje de células infectadas con parásitos pretratados y con parásitos control sin pretratar fue determinado comparativamente después de 24 y 48 horas. Un número de células infectadas significativamente menor fue observado para parásitos pretratados luego 48 horas para todas las concentraciones empleadas, con un descenso en la infección dependiente de la dosis. También fue cuantificada la presencia de amastigotas en esas células

infectadas, observándose una reducción dosis dependiente en el número de amastigotas por célula incluso después de 24 horas de incubación. Este efecto resulta más evidente a las 48 horas. Este hallazgo sugiere que la preincubación de tripomastigotas celulares con los compuestos no afecta sólo el proceso de infección, sino también la replicación de estos parásitos tratados dentro de la célula. Asimismo, fue estudiando el rol de los compuestos en la persistencia del parásito en un proceso de infección ya establecido, empleando monocapas de células VERO infectadas en ausencia de compuesto y posteriormente tratadas con las distintas concentraciones de los compuestos. En este caso, fue observada una disminución significativa en el número de amastigotas por célula después de 24 y 48 horas de incubación. Este hallazgo sugiere que los compuestos son capaces de alcanzar parásitos intracelulares, promoviendo su muerte o afectando su proliferación en manera dosis dependiente.

Considerando que las aproximaciones “ómicas” constituyen una estrategia conveniente para identificar vías metabólicas o posibles dianas moleculares para comprender el mecanismo de acción de un compuesto, se procedió a la identificación de los ARN mensajeros totales (RNA-*Seq*) y a la identificación de las proteínas totales (*Shotgun proteomics)*, de los parásitos tratados con cada uno de los compuestos y de parásitos control sin tratar (Van den Kerkhof, 2020). De acuerdo con los resultados de ensayos previos y con el fin de estudiar la respuesta temprana del parásito frente al compuesto, identificando genes y vías metabólicas participantes en el mecanismo de inhibición del crecimiento antes de que se inicien los mecanismos de muerte celular, se procedió a realizar los ensayos con parásitos incubados con 5 veces el valor IC_{50} calculado para epimastigotas, durante 6 horas. Es interesante destacar que los tres compuestos en estudio presentaron diferentes perfiles a nivel transcriptómico, por un lado, el compuesto de vanadio fue capaz de modificar un bajo porcentaje de los transcritos del parásito, y el compuesto de paladio presenta 10 veces más transcritos modificados que su homólogo de platino. Por su parte, a nivel proteómico todos presentan niveles similares de proteínas con expresión alterada. Estos resultados son esperables para el compuesto de vanadio, ya que su principal asociación a macromoléculas fue encontrada con la fracción insoluble. Por su parte, los compuestos de la serie dppf-mpo presentan una asociación preferencial con el ADN, aunque también se detectan menores niveles de asociación con otras macromoléculas. A pesar de las mejoras en las técnicas proteómicas, muchas proteínas no son identificadas en esos estudios, ya sea por sensibilidad o por sesgos de las tecnologías, generando que este nivel de expresión no sea bien evaluado (Chang, 2014). Aunque la cantidad de proteínas detectadas es comparable a la encontrada en trabajos recientes (3262 proteínas con un FDR < 1% en (de Castro Andreassa, 2021)), sería interesante complementar estos resultados empleando una técnica más sensible para proteómica comparativa, como lo es 2D-DIGE (2D-*Difference gel electrophoresis*) que permite un análisis preciso de las diferencias en la abundancia de proteínas entre las muestras, previa marcación

fluorescente de las muestras antes de la separación (Ohlendieck, 2018).

Con la información transcriptómica y proteómica recabada se elaboraron los posibles modelos de acción multi-blanco, y se seleccionaron y analizaron potenciales candidatos a blancos moleculares de los compuestos M-dppf-mpo, relevantes para el parásito. El tratamiento con Pd-dppf-mpo impacta fuertemente en la vía del ergosterol, la cual ha sido muy estudiada como blanco terapéutico contra todos los tripanosomátidos (Beltran-Hortelano, 2022; Osorio-Mendez, 2018). Este tratamiento afecta de forma estadísticamente significativa a 13 de los 20 transcriptos que codifican para las enzimas involucradas en toda la vía, disminuyendo en todos los casos su abundancia. En el caso del compuesto de platino, al presentarse cambios de FC menores, muchos genes no superaron el umbral de $|1{,}5,|$ pero si compartieron el mismo patrón de comportamiento a la baja o no presentaron cambios. Fue seleccionada para su estudio la enzima **fosfomevalonato quinasa** (PMK: TcCLB.507913.20), cuyos valores a nivel transcriptómico disminuyeron 6,3 y 2,2 veces luego de incubar con Pd-dppf-mpo y Pt-dppf-mpo, respectivamente en comparación con parásitos control sin tratar. Más, aún, luego de los tratamientos la proteína no es detectada. Además, se seleccionó el gen esencial que codifica para la enzima **lanosterol 14-α demetilasa** (CYP51: TcCLB.506297.260), que participa en la misma ruta. Luego del tratamiento con Pd-dppf-mpo los niveles del ARNm que codifica para esta enzima bajan 2,1 veces y los niveles de proteína no son detectados en proteómica. Asimismo, también fue seleccionado para su estudio, la **dihidrofolato reductasa-timidilato sintasa** (DHFR-TS: TcCLB.509153.90) que, siendo esencial, muestra una desproporción entre nivel de ARNm (disminución de 1,3 veces con el tratamiento de Pd y sin cambios con el compuesto de Pt) y proteína (aumento de 2,2 y 1,7 veces luego del tratamiento con Pd-dppf-mpo y Pt-dppf-mpo, respectivamente) que podría ser el resultado de un mecanismo compensatorio celular. Esta enzima resulta particularmente interesante no sólo por su rol en la producción de folato, precursor de cofactores necesarios para la síntesis ácidos nucleicos y proteínas, sino porque se ha observado que tiene porciones de baja homología con su contraparte en mamíferos (Juarez-Saldivar, 2020; Senkovich, 2009). A partir de los datos de Pt-dppf-mpo, fue seleccionado el gen que codifica para la enzima **fumarato reductasa dependiente de NADH** (FRD: TcCLB.503849.60), una enzima presente en todas las etapas del ciclo de vida, pero ausente en el hospedero mamífero, que produce succinato a partir de fumarato y está involucrada en el mantenimiento del balance redox intracelular (Campos-Fernandez, 2022). En este caso también se observa una desproporción entre niveles de ARNm (disminución de 1,2 veces) y proteína (aumento de 3,3 veces). Los valores transcriptómicos y proteómicos de cada uno de los potenciales blancos moleculares se encuentran resumidos en la Tabla 3. Es importante destacar que los productos proteicos no detectados, no estuvieron representados en ninguna réplica de ninguna de las muestras analizadas (tratado o control), por

lo que no puede ser descartada la falta de representación por sesgos o limitaciones de la técnica proteómica.

Tabla 3. Resumen de los resultados de transcriptómica y proteómica para los productos génicos candidatos a dianas moleculares de los compuestos Pd-dppf-mpo y Pt-dppf-mpo.

Producto génico	ID	FC Transcriptoma		FC Proteoma	
		Pd-dppf-mpo	Pt-dppf-mpo	Pd-dppf-mpo	Pt-dppf-mpo
Fosfomevalonato quinasa	TcCLB.507913.20	-6,314	-2,172	N/D	N/D
Lanosterol 14α-demetilasa	TcCLB.506297.260	-2,105	-1,026	N/D	N/D
Dihidrofolato reductasa-timidilato sintasa	TcCLB.509153.90	-1,281	1,026	2,177	1,732
Fumarato reductasa dependiente de NADH	TcCLB.503849.60	-1,429	-1,236	-1,473	3,268

Para estos genes diferencialmente expresados de acuerdo con los estudios ómicos, se procedió a estudiar si cumplían los criterios de elegibilidad presentados en la Introducción de este trabajo. Los datos de esencialidad son escasos en *T. cruzi*, por lo que no fue considerado un criterio eliminatorio (Osorio-Mendez, 2018). En cuanto a la drogabilidad, con la información disponible se seleccionaron blancos con índices en el entorno de drogable y altamente drogable (Tabla 4).

Tabla 4. Características de los genes seleccionados. Se detallan el tamaño del CDS y el peso molecular de la proteína, así como la esencialidad en *T. cruzi* y el índice de drogabilidad reportado por la base de datos TDR Targets. Este índice se mide en una escala que va del 0 al 1 y se divide en cuatro categorías: no drogable (≤0,2), poco drogable (0,2-0,5), drogable (0,5-0,7) y altamente drogable (>0,7).

Gen	Código	Tamaño CDS (pb)	Peso molecular (Da)	Esencialidad	Drogabilidad
Fosfomevalonato quinasa	PMK	1431	51568	ND	ND
Lanosterol 14α-demetilasa	CYP51	1446	54669	SÍ (1KO obtenido CRISPR-CAS9 + Sensibilidad aumentada a Posaconazol)	0,8
Dihidrofolato reductasa-timidilato sintasa	DHFR-TS	1566	58853	SÍ (Falló recombinación 2KO)	0,8
Fumarato reductasa dependiente de NADH	FRD	2370	85491	ND	0,5

Posteriormente, se analizaron los valores de expresión a lo largo del ciclo de vida de *T. cruzi* a nivel transcriptómico de los genes de interés, usando los datos publicados en el trabajo de Li, *et al*, 2016 (Li, 2016). El análisis del set de genes candidatos indica que todos son de expresión constitutiva en todas las etapas del ciclo de vida del parásito, y que registran niveles de expresión que superan la media del conjunto de genes. Las distribuciones de los niveles de expresión a nivel transcriptómico se observan en la Figura 5, y los valores específicos de expresión de cada uno se encuentran recopilados en la Tabla 5.

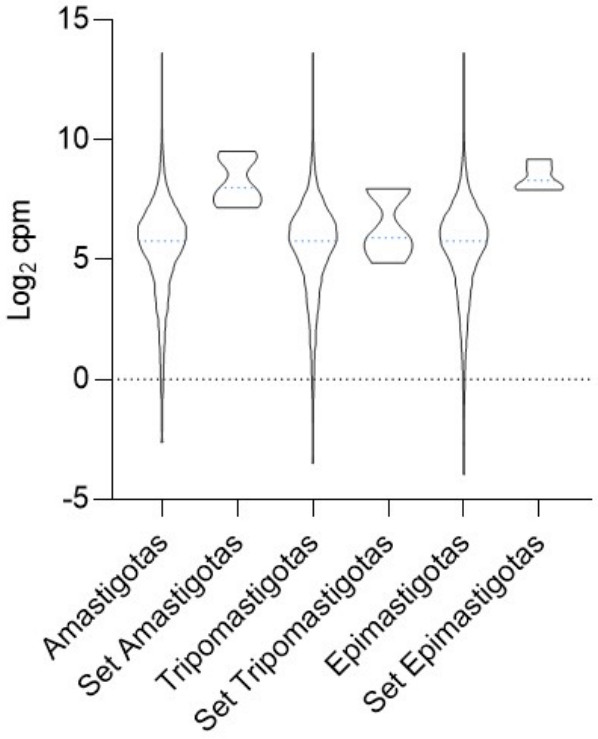

Figura 5. Distribución de la expresión a nivel transcriptómico del conjunto total de genes de cada estadio, así como del set de genes seleccionados, en cada etapa del ciclo de vida de *T. cruzi*. Log_2 CPM: log_2 de conteos por millón. El estadio tripomastigota hace referencia a tripomastigotas extracelulares (Li, 2016).

Tabla 5. Expresión a nivel transcriptómico de los genes seleccionados en el ciclo de vida de *T. cruzi*. Log_2 CPM: log_2 de conteos por millón; SD: desviación estándar. Ama: amastigotas. Try: tripomastigotas extracelulares. Epi: epimastigotas. Datos extraídos de (Li, 2016).

Gen	ID Non-Esmeraldo like	ID Esmeraldo like	Ama log_2 CPM ± SD	Try log_2 CPM ± SD	Epi log_2 CPM ± SD
PMK	TcCLB.507913.20	TcCLB.508277.140	7,181 ± 0,190	5,913 ± 0,116	7,997 ± 0,030
DHFR-TS	TcCLB.510303.320	TcCLB.509153.90	9,100 ± 0,042	7,866 ± 0,282	8,771 ± 0,034
CYP51	TcCLB.506297.260	TcCLB.510101.50	9,531 ± 0,080	9,404 ± 0,132	9,209 ± 0,038
FRD	TcCLB.503849.60	TcCLB.508535.10	7,526 ± 0,448	7,975 ± 0,094	8,305 ± 0,042
		TcCLB.510215.10	8,009 ± 0,107	7,958 ± 0,239	7,916 ± 0,017

Se han publicado hasta la fecha distintos proteomas de *T. cruzi* con diversas aproximaciones y para diversos enfoques como el estudio de modificaciones postraduccionales tales como fosforilaciones (Marchini, 2011), SUMOilaciones (Bayona, 2011), acetilaciones (Moretti, 2018), fracciones subcelulares de reservosomas (Sant'Anna, 2009) y vacuola contráctil (Ulrich, 2011), proteínas de membrana solubilizadas (Cordero, 2009), proteínas de superficie (Queiroz, 2013), proteínas en el ciclo celular (Chavez, 2021; Santos Junior, 2021) y durante el proceso de metaciclogénesis (de Godoy, 2012). Una característica común de todos los trabajos publicados, es que los ensayos proteómicos no se realizan en todos los estadios del ciclo de vida del parásito. El estadio más representado es el epimastigota y en menor medida los

tripomastigotas metacíclicos. El trabajo pionero que reúne los datos de expresión de proteínas en todos los estadios es el de Atwood de 2005 (Atwood, 2005), pero las limitaciones de la técnica, no permitieron obtener los valores de expresión de todas las proteínas de interés para este trabajo. La única proteína con evidencia de expresión de acuerdo con ese estudio es FRD. Por su parte, para CYP51 también se encontró evidencia de expresión en todos los estadios del parásito (Lepesheva, 2011a). De acuerdo con el comportamiento de los genes en los ensayos ómicos, a su drogabilidad y a su expresión constitutiva en todos los estadios del ciclo de vida del parásito, los genes seleccionados avanzaron a la etapa de validación por genómica funcional mediante sobreexpresión de los potenciales blancos moleculares.

La selección del método de validación estuvo basada en diferentes aspectos, por un lado, al tratarse de productos génicos validados como esenciales o con funciones fundamentales para la sobrevida del parásito, fue descartada la opción de generar parásitos *knock out* para los blancos moleculares. Este enfoque de función reducida presenta dificultades para encontrar el blanco de acción de un fármaco, ya que éstos a menudo actúan inhibiendo las enzimas, y la sustracción del blanco molecular puede ser letal incluso en ausencia de fármaco, aumentando la probabilidad de que no pudiera establecerse una línea celular KO (Begolo, 2014). Por lo tanto, las metodologías alternativas, basadas en enfoques de ganancia de función, son mucho más apropiadas para la determinación directa de los blancos moleculares de los compuestos (Alsford, 2013). La sobreexpresión de la proteína de interés fue la estrategia de elección, verificando la participación del blanco seleccionado en la respuesta al compuesto sin excluir otras vías de respuesta activándose en paralelo. La sobreexpresión para revelar mecanismos de acción ha demostrado ser útil desde procariotas hasta eucariotas, incluyendo tripanosomátidos, tanto para compuestos citostáticos como citocidas, pero su interpretación no es siempre sencilla (Begolo, 2014; Palmer, 2014; Prelich, 2012). Si un fármaco antitripanosomátido inhibe la función de una proteína, la sobreexpresión de esa proteína o de un fragmento que contenga el sitio de unión del fármaco podría aumentar la resistencia al fármaco (Ranade, 2013). No obstante, otras variaciones pueden revelar cómo los compuestos afectan a sus blancos moleculares, por ejemplo, sin presentar cambios a pesar de la sobreexpresión, debido a que se desvía el flujo metabólico en lugar de inhibirlo, o que a pesar de la sobreexpresión aumente la sensibilidad al fármaco, lo cual puede deberse a la inducción de reacciones dañinas catalizadas por el blanco molecular (Palmer, 2014; Prelich, 2012). En este caso, fue realizada la sobreexpresión empleando un vector de expresión diseñado para *T. cruzi*, que permite la fusión con la proteína GFP para una fácil evaluación mediante microscopía o citometría de flujo. Una vez establecida la selección y validados los modelos se procede a los ensayos *in vitro*.

El ensayo de viabilidad celular realizado sobre cada una de las poblaciones sobreexpresantes (Anexo I), incubando durante 6 horas con los distintos tratamientos, demuestra

que las poblaciones que sobreexpresan los blancos CYP51, DHFR-TS y FRD tienen menos sensibilidad al compuesto de paladio en todas las concentraciones ensayadas, y se observa poco efecto cuando es sobreexpresada la enzima PMK. Un efecto similar se observa para el compuesto de platino para las concentraciones 1x y 5x IC_{50} (Figura 6). El aumento del porcentaje de viabilidad puede explicarse por una disminución de la sensibilidad a los compuestos conferida principalmente por la sobreexpresión de CYP51, DHFR-TS y FRD, sugiriendo la implicación de estas enzimas en el mecanismo de acción de los complejos basados en Pd y Pt.

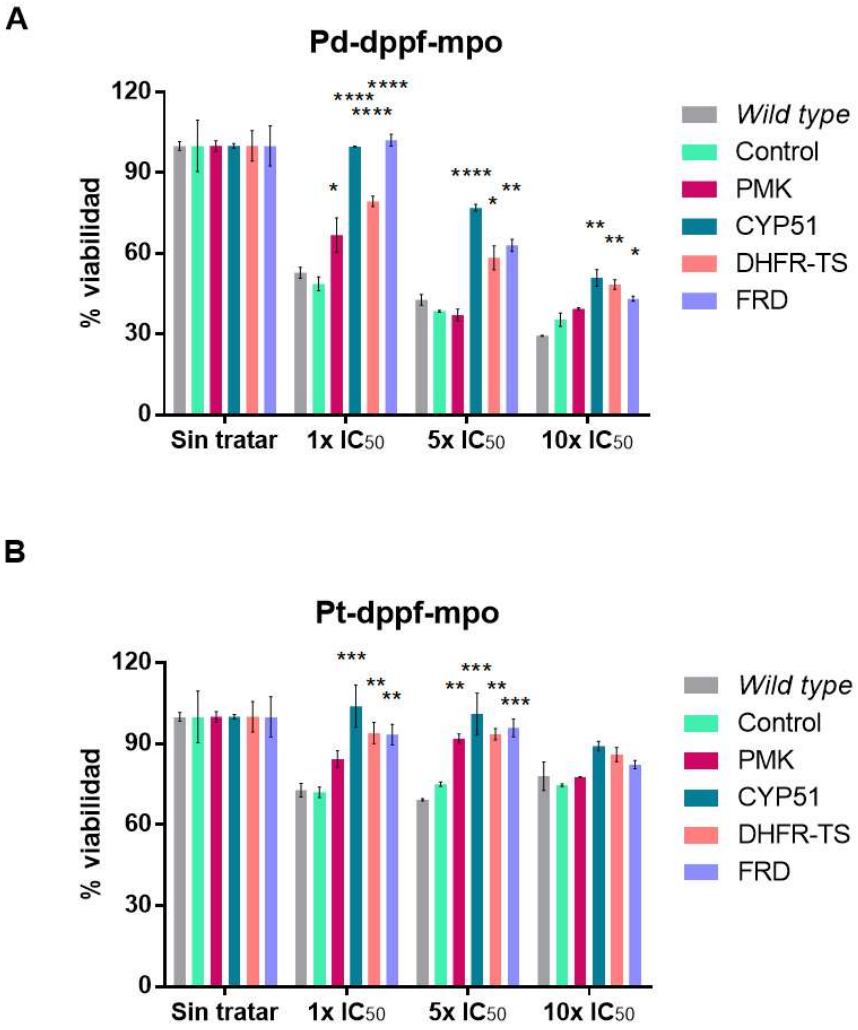

Figura 6. Porcentaje de viabilidad de las poblaciones *Wild type*, control y transfectantes al ser incubadas con los complejos M-dppf-mpo. Los resultados se presentan como promedios ± SD de dos réplicas biológicas. Estadística realizada transfectantes vs. *Wild type*. 2-*way* ANOVA test seguido de Bonferroni para múltiples comparaciones. p-valores: ****p < 0,0001; ***p < 0,001; **p < 0,01; *p < 0,1.

Con los transfectantes PMK y CYP51 se avanzó hacia su validación como participantes del mecanismo de acción, evaluando como impacta el tratamiento con los compuestos en la producción de ergosterol, y de los intermediarios escualeno y lanosterol. La acumulación de

escualeno y lanosterol se mantiene al comparar los valores de parásitos PMK con los parásitos salvajes, pero se observa una significativa disminución de lanosterol cuando se compara parásitos CYP51 con parásitos salvajes, a todas las concentraciones ensayadas para Pd-dppf-mpo y a las mayores concentraciones para Pt-dppf-mpo. En cuanto a la producción de ergosterol, se observa un aumento en la producción en parásitos que sobreexpresan CYP51 con respecto a parásitos salvajes, nuevamente a todas las concentraciones empleadas de Pd-dppf-mpo y a las mayores de Pt-dppf-mpo. En cuanto a los sobreexpresantes de PMK, no lograron producir más ergosterol que los parásitos salvajes tratados. Estos resultados sugieren que el mayor efecto sobre la vía del ergosterol esta dado por la presencia/actividad de la enzima CYP51.

Actualmente, seguimos trabajando en la validación de los potenciales blancos moleculares FRD y DHFR-TS, sin descartar la evaluación de otros posibles blancos que surjan, para continuar comprendiendo el modo de acción de estos compuestos. La optimización y el desarrollo de nuevos fármacos se ven facilitados en gran medida por el conocimiento de su mecanismo de acción y de sus blancos moleculares. En ese contexto, los resultados de este trabajo han contribuido con valiosos aportes para avanzar en mejorar el estado actual del tratamiento contra la Enfermedad de Chagas.

9 Conclusiones

El efecto de los compuestos metálicos **$V^{IV}O$(5Brsal)(aminofén)**, **Pd-dppf-mpo** y **Pt-dppf-mpo** fue estudiado a través del análisis del metaloma, transcriptoma y proteoma de epimastigotas tratados en comparación con parásitos control sin tratar:

- Todos los compuestos presentan de aceptables a excelentes valores de IC_{50} e índice de selectividad y se determinó en qué condiciones actúan como agentes tripanostáticos o tripanocidas.
- Mediante metalómica se determinaron la cantidad, localización e identidad de las especies metálicas dentro del parásito unicelular.
- Se determinó el tipo de muerte celular que induce cada compuesto, observándose una prevalencia de necrosis.
- Para los compuestos de paladio y platino se comprobó que tienen la capacidad de afectar a los estadios relevantes en el hospedero.
- Los compuestos de vanadio y platino ejercen su efecto principalmente a nivel proteómico, y el compuesto de paladio tanto a nivel proteómico como transcriptómico.

El análisis del metaloma, el transcriptoma y el proteoma de parásitos tratados con los compuestos de paladio y platino permitió identificar y seleccionar candidatos a blancos moleculares y validarlos mediante expresión ectópica en sistema homólogo:

- La sobreexpresión de las enzimas CYP51, DHFR-TS y FRD disminuye la sensibilidad de los parásitos a los compuestos de paladio y platino. Un efecto menor se observa para la sobreexpresión de PMK.
- El mayor efecto sobre la vía del ergosterol está dado sobre la enzima CYP51, cuya sobreexpresión recupera la producción de la vía metabólica, demostrando que esta enzima tiene un rol en el mecanismo de acción de los compuestos.

10 Perspectivas

Validar potenciales blancos moleculares propuestos para el compuesto de vanadio.

Complementar los ensayos ómicos con una aproximación de metabolómica que permita estudiar los procesos metabólicos que se inducen o reprimen por acción de los compuestos.

Realizar una transfección estable con el plásmido lineal de todas las construcciones para su incorporación en el genoma de *T. cruzi*.

Realizar análisis celulares del efecto de los compuestos en parásitos sobreexpresando las proteínas candidatas a blancos de acción en epimastigotas y en estadios del parásito presentes en el hospedero mamífero (amastigotas y tripomastigotas celulares).

Realizar estudios *in vivo* infectando ratones con parásitos control y transfectantes para estudiar el efecto de los compuestos en un modelo animal.

11 Anexo: Obtención de parásitos de *T. cruzi* sobreexpresando los blancos moleculares

El vector de expresión empleado en este trabajo fue pTREX-nGFP. El vector de expresión pTREX-n fue inicialmente diseñado para *T. cruzi,* reteniendo de su predecesor, el pRIBOTEX, el gen *neo* que otorga resistencia a neomicina como marcador de selección de los parásitos transfectantes (Vazquez, 1999). Los sitios XbaI y HindIII permiten el clonado direccional en fase con GFP que se encuentra adyacente y que formará parte del C-terminal del producto proteico. El sitio HX1 y la región intergénica de GAPDH funcionan como regiones reguladoras para el correcto procesamiento del ARNm maduro. La generación del vector de expresión para la sobreexpresión de la enzima CYP51 fue parte del trabajo de final de carrera de la Licenciatura en Bioquímica de la Bach. Antonela Bosch, finalizado en el año 2022, del cual fui orientadora junto a la co-orientación de la Dra. Leticia Pérez-Díaz. Por su parte, la enzima FRD fue objeto de estudio de mi tesis de grado de la Licenciatura en Bioquímica, que consistió en la expresión heteróloga de la proteína recombinante en bacterias. Asimismo, fue parte de un proyecto del Programa de Apoyo a la Investigación Estudiantes (PAIE), en el año 2014, que implicó la generación de una herramienta para producción homóloga de la proteína recombinante. Esa herramienta era el vector pTREX-nGFP clonado con el gen de la enzima, el cuál fue conservado en el laboratorio y pudo ser incluido en este trabajo.

Para los restantes blancos moleculares seleccionados para su validación (PMK y DHFR-TS), fue amplificado mediante reacción de PCR el marco abierto de lectura de cada gen empleando la enzima DreamTaq DNA Polymerase (Thermo Fisher Scientific). Para ello, se incluyeron los sitios de restricción XbaI (5'T↓CTAGA3') y HindIII (5'A↓AGCTT3') en los cebadores directo y reverso, respectivamente, para que sean compatibles con el clonado en fase con GFP en el vector de expresión de destino. Fue incluida además la secuencia correspondiente al *tag* C-myc en el primer directo de manera que quede en fase con el marco de lectura abierto de cada blanco molecular. Esta secuencia que codifica para 11 aminoácidos se encuentra optimizada para el uso de codones en *T. cruzi* (ATG GAG CAG AAG CTG ATT TCA GAG GAG GAC CTG). En el extremo 5' fueron añadidas seis bases extra simplemente con el fin de que funcionen de anclaje para las enzimas de restricción y poder realizar la digestión directa del producto de PCR sin emplear un vector de clonado. En el primer reverso se eliminaron las últimas tres bases codificantes para el codón de finalización y se agregó una base extra para que coincida el marco abierto de lectura con el de GFP, y así obtener un producto fusionado. La secuencia de cada cebador se encuentra disponible en la Tabla A1.

Tabla A1. Lista de cebadores empleados en las reacciones de PCR. En negrita se marca el sitio de restricción y en negrita e itálica la secuencia correspondiente al *tag c-myc*. En los cebadores reversos se incluyó una base adicional adyacente al sitio de restricción para su clonado en fase con el tag GFP. En la última columna se específica la T_m de la porción del cebador que hibrida con el molde.

Cebador	Secuencia 5' → 3'	T_m (°C)
PMK_FW_XbaI_CMYC	TCTCTC **TCTAGA *ATGGAGCAGAAGCTGATTTCAGAGGAGGACCTG*** ATGGATACTGCTATTGCGACTACGAG	58,0
PMK_REV_HindIII_PTREX	TCTCTC **AAGCTT** C CTTCTCTTCAGAAAAAAGAAGTCCAGCG	57,8
DHFR-TS FW_XbaI_CMYC	TCTCTC **TCTAGA *ATGGAGCAGAAGCTGATTTCAGAGGAGGACCTG*** ATGTCGCTGTTTAAGATCCGCATG	57,8
DHFR-TS REV_HindIII_PTREX	TCTCTC **AAGCTT** C AACCGCCATCTTCATGGAGATG	57,4

Para la puesta a punto de la reacción de PCR se realizó la amplificación mediante PCR en gradiente variando las temperaturas para determinar la temperatura óptima de hibridación de cada par de primers, obteniendo temperaturas óptimas de hibridación para PMK y DHFR-TS de 56ºC Y 57ºC, respectivamente. En la Figura A1 A se muestra el resultado de la reacción de PCR, donde se observa la presencia de productos únicos en cada reacción. Los productos de PCR fueron directamente digeridos con las enzimas de restricción XbaI y HindIII, con la posterior inactivación térmica de las enzimas, para generar los extremos cohesivos compatibles con los sitios en el vector de expresión de destino, pTREX-nGFP. Este último también se digirió con las mismas enzimas de restricción, se verificó que cada una de ellas corte correctamente el vector y se procedió a la doble digestión, con posterior desfosforilación de los extremos empleando fosfatasa alcalina (FastAP Thermosensitive Alkaline Phosphatase de ThermoFisher Scientific) (Figura A1 B).

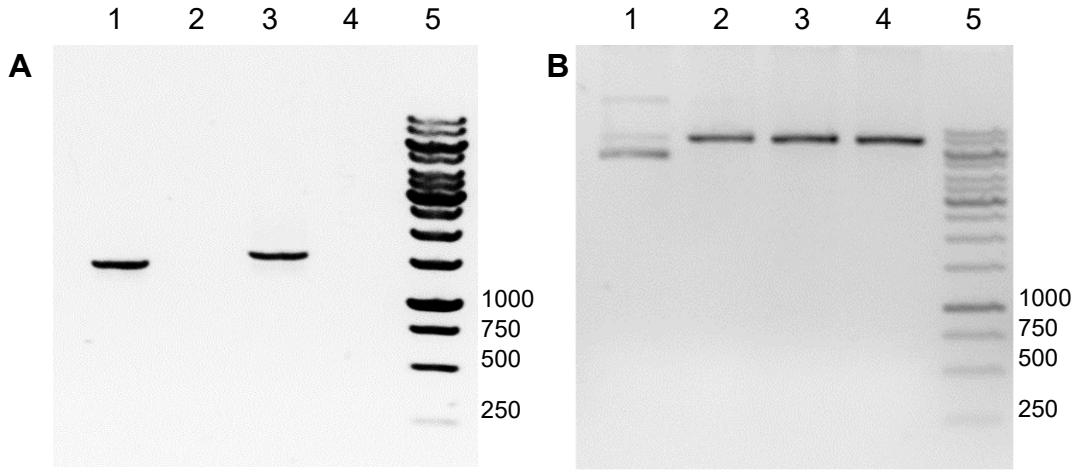

Figura A1. A. Gel de agarosa 1% donde se visualiza la amplificación por PCR de los productos PMK y DHFR-TS. Carriles: 1. Amplificación de PMK (1431 pb); 2. Control negativo de PMK; 3. Amplificación de DHFR-TS (1566 pb); 4. Control negativo de DHFR-TS; 5. Marcador de peso molecular (MPM) GeneRuler 1 kb DNA (Thermo Fisher Scientific). **B.** Gel de agarosa 1% donde se observa el vector pTREX sin digerir, las digestiones con enzimas de restricción individuales y la doble digestión. Carriles: 1. pTREX+buffer; 2. pTREX+XbaI; 3. pTREX+HindIII; 4. pTREX+XbaI+HindIII; 5. MPM 1kb.

Luego de la ligación y la transformación de células competentes *E. coli* TOP10, se obtuvieron colonias de las cuales fue aislado el ADN plasmídico por el método de lisis alcalina (Sambrook, 1989). Para verificar la presencia del inserto previo a la secuenciación, se realizó la digestión del vector pTREX con las enzimas XbaI y XhoI, obteniéndose los fragmentos de tamaño esperado (2300 pb para PMK y 2400 pb para DHFR-TS), además del vector linealizado. En el caso de DHFR-TS pudo corroborarse la identidad del inserto porque la secuencia presenta el sitio de restricción para XhoI, y se observa la digestión que rinde fragmentos de 2000 y 400 pb y también una banda equivalente a la suma de esos tamaños (2400 pb), producto de la digestión parcial (Figura A2).

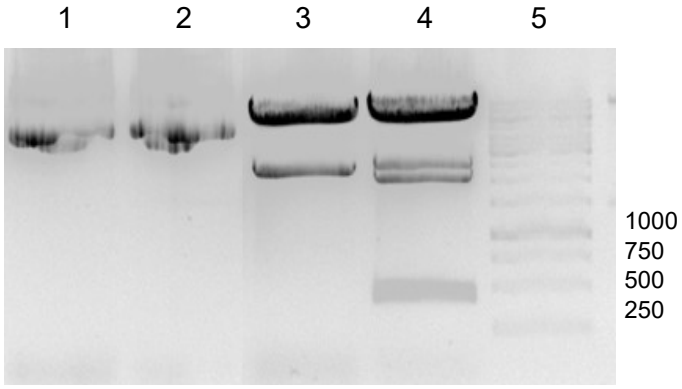

Figura A2. Midiprepraciones de ADN plasmídico y digestiones de los plásmidos pTREX-nGFP conteniendo los blancos moleculares. Carriles: 1. Midipreparación de pTREX-PMK-nGFP; 2. Midipreparación de pTREX-DHFR-TS-nGFP. 3. Doble digestión con XbaI/XhoI de ADN plasmídico de pTREX-PMK-nGFP; 4. Doble digestión con XbaI/XhoI de ADN plasmídico de pTREX-DHFR-TS-nGFP. 5. MPM 1 kb.

Luego de la verificación por digestión, se procedió a realizar la secuenciación de los clones positivos. El marco abierto de lectura clonado perteneciente a la enzima PMK presenta 21 SNPs ya reportadas en la base de datos TriTrypDB, y una mutación sinónima en la posición 678 que cambia una T → C en la tercera base del codón, codificando igualmente para una glicina (GGT → GGC). Todas las variantes se encuentran detalladas en la Tabla A2.

Tabla A2. Variantes nucleotídicas halladas en el marco abierto de lectura de PMK.

Posición	Variante	Frecuencia alélica
486	C → A	0.33/0.67
542	C → T	0.33/0.67
560	C → G	0.67/0.33
571	A → C	0.67/0.33
574	A → G	0.33/0.67
584	A → C	0.33/0.67
586	G → A	0.67/0.33
597	A → C	0.33/0.67
696	G → A	0.67/0.33

733	A → C	0.75/0.25
783	A → G	0.67/0.33
843	T → C	0.33/0.67
882	G → T	0.67/0.33
894	T → C	0.67/0.33
906	A → G	0.33/0.67
975	A → G	0.33/0.67
984	A → G	0.33/0.67
1035	A → T	0.33/0.67
1239	C → G	0.67/0.33
1281	G → A	0.33/0.67
1384	T → C	0.33/0.67

En el caso de la enzima DHFR-TS, se observan 12 SNPs, los cuales ya han sido reportados, y se detallan en la Tabla A3. Además, se observan 3 mutaciones sinónimas en las bases 408, 1248 y 1296, donde en todos los casos se sustituyó una G por una A, T y A, respectivamente. En las primeras dos ubicaciones se modificó el codón que codifica para leucina y en el último el codificante de prolina. Debido entonces a la ausencia de mutaciones de cambio de aminoácido en las secuencias para ambas proteínas, se procedió entonces a utilizar estos plásmidos recombinantes para posteriormente expresar las proteínas de interés en *T. cruzi.*

Tabla A3. Variantes nucleotídicas halladas en el marco abierto de lectura de DHFR-TS.

Posición	Variante	Frecuencia alélica
153	T → C	0.33/0.67
163	T → G	0.33/0.67
195	A → G	0.67/0.33
222	T → C	0.67/0.33
288	C → T	0.67/0.33
294	T → C	0.33/0.67
324	C → G	0.33/0.67
410	G → A	0.33/0.67
522	C → T	0.67/0.33
1095	T → G	0.75/0.25
1125	G → A	0.67/0.33
1158	A → C	0.33/0.67

Se empleó como control un vector pTREX-nGFP fusionado a c-myc. Debido al pequeño tamaño de este *tag*, se realizó una hibridación de secuencias complementarias, sintetizadas como cebadores fosforilados en 5', incluyendo el sitio de restricción complementario al del vector de destino digerido con las enzimas XbaI y HindIII (Macrogen). Fue empleada una concentración 100 µM de cada uno de los oligos y un protocolo de hibridación de tipo *touchdown,* con una

desnaturalización inicial a 95°C por 5 minutos, y luego reduciendo la temperatura gradualmente (1°C/min) hasta la Tm de hibridación de las secuencias, incubando 30 minutos a esa temperatura, para finalizar bajando la temperatura (1°C/min) hasta llegar a temperatura ambiente. Se procedió a ligar el fragmento obtenido con el vector de expresión linealizado, usando la enzima T4 Ligasa como se describió anteriormente. La secuenciación de este vector permitió confirmar que la secuencia se encuentra correctamente en fase con GFP.

Los parásitos fueron transfectados con las construcciones obtenidas y con el vector de expresión control, mediante electroporación con un equipo Amaxa Nucleofector™ 2b (Lonza) siguiendo lo reportado por Pacheco-Lugo *et al.*, quienes al comparar distintos tampones, concentraciones de ADN y protocolos en el programa del Nucleofector obtuvieron el método de transfección más eficiente (Pacheco-Lugo, 2017). En concordancia con lo reportado en dicho trabajo, los parásitos mostraron una tasa de sobrevivencia mayor al 90% luego de 24 horas de electroporados. Los mismos fueron seleccionados durante 21 días con 500 µg/mL de G-418 (Silva-Gomes, 2020), período de tiempo en el cual murió la población del *mock* (parásitos control transfectados sin plásmido). Luego de seleccionados, se mantuvieron siempre con la presión selectiva del antibiótico para prevenir la pérdida del plásmido, hasta ser empleados en los ensayos *in vitro*.

12 Referencias bibliográficas

Akopyants NS, Matlib RS, Bukanova EN, Smeds MR, Brownstein BH, Stormo GD and Beverley SM (2004) Expression profiling using random genomic DNA microarrays identifies differentially expressed genes associated with three major developmental stages of the protozoan parasite Leishmania major. *Molecular and biochemical parasitology* 136:71-86.

Alberca LN, Sbaraglini ML, Balcazar D, Fraccaroli L, Carrillo C, Medeiros A, Benitez D, Comini M and Talevi A (2016) Discovery of novel polyamine analogs with anti-protozoal activity by computer guided drug repositioning. *Journal of computer-aided molecular design* 30:305-321.

Alsford S, Kelly JM, Baker N and Horn D (2013) Genetic dissection of drug resistance in trypanosomes. *Parasitology* 140:1478-1491.

Alvarez G, Martinez J, Aguirre-Lopez B, Cabrera N, Perez-Diaz L, de Gomez-Puyou MT, Gomez-Puyou A, Perez-Montfort R, Garat B, Merlino A, Gonzalez M and Cerecetto H (2014) New chemotypes as Trypanosoma cruzi triosephosphate isomerase inhibitors: a deeper insight into the mechanism of inhibition. *Journal of enzyme inhibition and medicinal chemistry* 29:198-204.

Alves LR and Goldenberg S (2016) RNA-binding proteins related to stress response and differentiation in protozoa. *World journal of biological chemistry* 7:78-87.

Annoura T, Nara T, Makiuchi T, Hashimoto T and Aoki T (2005) The origin of dihydroorotate dehydrogenase genes of kinetoplastids, with special reference to their biological significance and adaptation to anaerobic, parasitic conditions. *Journal of molecular evolution* 60:113-127.

Aphasizhev R and Aphasizheva I (2014) Mitochondrial RNA editing in trypanosomes: small RNAs in control. *Biochimie* 100:125-131.

Atwood JA, 3rd, Weatherly DB, Minning TA, Bundy B, Cavola C, Opperdoes FR, Orlando R and Tarleton RL (2005) The Trypanosoma cruzi proteome. *Science* 309:473-476.

Bahia MT, Nascimento AF, Mazzeti AL, Marques LF, Goncalves KR, Mota LW, Diniz Lde F, Caldas IS, Talvani A, Shackleford DM, Koltun M, Saunders J, White KL, Scandale I, Charman SA and Chatelain E (2014) Antitrypanosomal activity of fexinidazole metabolites, potential new drug candidates for Chagas disease. *Antimicrobial agents and chemotherapy* 58:4362-4370.

Bangs JD, Crain PF, Hashizume T, McCloskey JA and Boothroyd JC (1992) Mass spectrometry of mRNA cap 4 from trypanosomatids reveals two novel nucleosides. *The Journal of biological chemistry* 267:9805-9815.

Barbosa da Silva E, Dall E, Briza P, Brandstetter H and Ferreira RS (2019) Cruzain structures: apocruzain and cruzain bound to S-methyl thiomethanesulfonate and implications for drug design. *Acta crystallographica Section F, Structural biology communications* 75:419-427.

Bartel LC, Montalto de Mecca M, de Castro CR, Bietto FM and Castro JA (2010) Metabolization of nifurtimox and benznidazole in cellular fractions of rat mammary tissue. *Human & experimental toxicology* 29:813-822.

Batista CM, Kessler RL, Eger I and Soares MJ (2015) Trypanosoma cruzi Intracellular Amastigotes Isolated by Nitrogen Decompression Are Capable of Endocytosis and Cargo Storage in Reservosomes. *PloS one* 10:e0130165.

Bayona JC, Nakayasu ES, Laverriere M, Aguilar C, Sobreira TJ, Choi H, Nesvizhskii AI, Almeida IC, Cazzulo JJ and Alvarez VE (2011) SUMOylation pathway in Trypanosoma cruzi: functional characterization and proteomic analysis of target proteins. *Molecular & cellular proteomics : MCP* 10:M110 007369.

Begolo D, Erben E and Clayton C (2014) Drug target identification using a trypanosome overexpression library. *Antimicrobial agents and chemotherapy* 58:6260-6264.

Beltran-Hortelano I, Alcolea V, Font M and Perez-Silanes S (2020) The role of imidazole and benzimidazole heterocycles in Chagas disease: A review. *European journal of medicinal chemistry* 206:112692.

Beltran-Hortelano I, Alcolea V, Font M and Perez-Silanes S (2022) Examination of multiple Trypanosoma cruzi targets in a new drug discovery approach for Chagas disease. *Bioorganic & medicinal chemistry* 58:116577.

Beltran-Hortelano I, Perez-Silanes S and Galiano S (2017) Trypanothione Reductase and Superoxide Dismutase as Current Drug Targets for Trypanosoma cruzi: An Overview of Compounds with Activity against Chagas Disease. *Current medicinal chemistry* 24:1066-1138.

Benitez J, Becco L, Correia I, Leal SM, Guiset H, Pessoa JC, Lorenzo J, Tanco S, Escobar P, Moreno V, Garat B and Gambino D (2011) Vanadium polypyridyl compounds as potential antiparasitic and antitumoral agents: new achievements. *Journal of inorganic biochemistry* 105:303-312.

Benz C, Nilsson D, Andersson B, Clayton C and Guilbride DL (2005) Messenger RNA processing sites in Trypanosoma brucei. *Molecular and biochemical parasitology* 143:125-134.

Berenstein AJ, Falk N, Moscatelli G, Moroni S, Gonzalez N, Garcia-Bournissen F, Ballering G, Freilij H and Altcheh J (2021) Adverse Events Associated with Nifurtimox Treatment for Chagas Disease in Children and Adults. *Antimicrobial agents and chemotherapy* 65.

Bermudez J, Davies C, Simonazzi A, Real JP and Palma S (2016) Current drug therapy and pharmaceutical challenges for Chagas disease. *Acta tropica* 156:1-16.

Berna L, Greif G, Pita S, Faral-Tello P, Diaz-Viraque F, Souza RCM, Vallejo GA, Alvarez-Valin F and Robello C (2021) Maxicircle architecture and evolutionary insights into Trypanosoma cruzi complex. *PLoS neglected tropical diseases* 15:e0009719.

Berna L, Rodriguez M, Chiribao ML, Parodi-Talice A, Pita S, Rijo G, Alvarez-Valin F and Robello C (2018) Expanding an expanded genome: long-read sequencing of Trypanosoma cruzi. *Microbial genomics* 4.

Bouton J, Ferreira de Almeida Fiuza L, Cardoso Santos C, Mazzarella MA, Soeiro MNC, Maes L, Karalic I, Caljon G and Van Calenbergh S (2021) Revisiting Pyrazolo[3,4-d]pyrimidine Nucleosides as Anti-Trypanosoma cruzi and Antileishmanial Agents. *Journal of medicinal chemistry* 64:4206-4238.

Brandon EF, Bosch TM, Deenen MJ, Levink R, van der Wal E, van Meerveld JB, Bijl M, Beijnen JH, Schellens JH and Meijerman I (2006) Validation of in vitro cell models used in drug metabolism and transport studies; genotyping of cytochrome P450, phase II enzymes and drug transporter polymorphisms in the human hepatoma (HepG2), ovarian carcinoma (IGROV-1) and colon carcinoma (CaCo-2, LS180) cell lines. *Toxicology and applied pharmacology* 211:1-10.

Brener Z, Cancado JR, Galvao LM, da Luz ZM, Filardi Lde S, Pereira ME, Santos LM and Cancado CB (1993) An experimental and clinical assay with ketoconazole in the treatment of Chagas disease. *Memorias do Instituto Oswaldo Cruz* 88:149-153.

Breniere SF, Waleckx E and Barnabe C (2016) Over Six Thousand Trypanosoma cruzi Strains Classified into Discrete Typing Units (DTUs): Attempt at an Inventory. *PLoS neglected tropical diseases* 10:e0004792.

Brennand A, Rico E and Michels PA (2012) Autophagy in trypanosomatids. *Cells* 1:346-371.

Buckner FS and Urbina JA (2012) Recent Developments in Sterol 14-demethylase Inhibitors for Chagas Disease. *International journal for parasitology Drugs and drug resistance* 2:236-242.

Burle-Caldas GA, Dos Santos NSA, de Castro JT, Mugge FLB, Grazielle-Silva V, Oliveira AER, Pereira MCA, Reis-Cunha JL, Dos Santos AC, Gomes DA, Bartholomeu DC, Moretti NS, Schenkman S, Gazzinelli RT and Teixeira SMR (2022) Disruption of Active Trans-Sialidase Genes Impairs Egress from Mammalian Host Cells and Generates Highly Attenuated Trypanosoma cruzi Parasites. *mBio*:e0347821.

Burle-Caldas Gde A, Grazielle-Silva V, Laibida LA, DaRocha WD and Teixeira SM (2015) Expanding the tool box for genetic manipulation of Trypanosoma cruzi. *Molecular and biochemical parasitology* 203:25-33.

Callejon-Leblic B, Arias-Borrego A, Pereira-Vega A, Gomez-Ariza JL and Garcia-Barrera T (2019) The Metallome of Lung Cancer and its Potential Use as Biomarker. *International journal of molecular sciences* 20.

Campos-Fernandez L, Ortiz-Muniz R, Cortes-Barberena E, Mares-Samano S, Garduno-Juarez R and Soriano-Correa C (2022) Imidazole and nitroimidazole derivatives as NADH-fumarate reductase inhibitors: Density functional theory studies, homology modeling, and molecular docking. *Journal of computational chemistry* 43:1573-1595.

Canavaci AM, Bustamante JM, Padilla AM, Perez Brandan CM, Simpson LJ, Xu D, Boehlke CL and Tarleton RL (2010) In vitro and in vivo high-throughput assays for the testing of anti-Trypanosoma cruzi compounds. *PLoS neglected tropical diseases* 4:e740.

Clayton C (2019) Regulation of gene expression in trypanosomatids: living with polycistronic transcription. *Open biology* 9:190072.

Clayton CE (2016) Gene expression in Kinetoplastids. *Current opinion in microbiology* 32:46-51.

Cordero EM, Nakayasu ES, Gentil LG, Yoshida N, Almeida IC and da Silveira JF (2009) Proteomic analysis of detergent-solubilized membrane proteins from insect-developmental forms of Trypanosoma cruzi. *Journal of proteome research* 8:3642-3652.

Coura JR (2015) The main sceneries of Chagas disease transmission. The vectors, blood and oral transmissions--a comprehensive review. *Memorias do Instituto Oswaldo Cruz* 110:277-282.

Crul M, van Waardenburg RC, Beijnen JH and Schellens JH (2002) DNA-based drug interactions of cisplatin. *Cancer treatment reviews* 28:291-303.

Chagas C (1909) Nova tripanozomiaze humana. Estudos sobre a morfologia e o ciclo evolutivo do Schizotrypanum cruzi, agente etiologico da nova entidade mórbida do homen. *Mem Inst Oswaldo Cruz* 1:159-219.

Chang C, Li L, Zhang C, Wu S, Guo K, Zi J, Chen Z, Jiang J, Ma J, Yu Q, Fan F, Qin P, Han M, Su N, Chen T, Wang K, Zhai L, Zhang T, Ying W, Xu Z, Zhang Y, Liu Y, Liu X, Zhong F, Shen H, Wang Q, Hou G, Zhao H, Li G, Liu S, Gu W, Wang G, Wang T, Zhang G, Qian X, Li N, He QY, Lin L, Yang P, Zhu Y, He F and Xu P (2014) Systematic analyses of the transcriptome, translatome, and proteome provide a global view and potential strategy for the C-HPP. *Journal of proteome research* 13:38-49.

Chatelain E (2015) Chagas disease drug discovery: toward a new era. *Journal of biomolecular screening* 20:22-35.

Chatelain E and Ioset JR (2018) Phenotypic screening approaches for Chagas disease drug discovery. *Expert opinion on drug discovery* 13:141-153.

Chavez S, Urbaniak MD, Benz C, Smircich P, Garat B, Sotelo-Silveira JR and Duhagon MA (2021) Extensive Translational Regulation through the Proliferative Transition of Trypanosoma cruzi Revealed by Multi-Omics. *mSphere* 6:e0036621.

Cheleski J, Rocha JR, Pinheiro MP, Wiggers HJ, da Silva AB, Nonato MC and Montanari CA (2010) Novel insights for dihydroorotate dehydrogenase class 1A inhibitors discovery. *European journal of medicinal chemistry* 45:5899-5909.

Chen YJ, Tan BC, Cheng YY, Chen JS and Lee SC (2010) Differential regulation of CHOP translation by phosphorylated eIF4E under stress conditions. *Nucleic acids research* 38:764-777.

Chitnumsub P, Yuvaniyama J, Chahomchuen T, Vilaivan T and Yuthavong Y (2009) Crystallization and preliminary crystallographic studies of dihydrofolate reductase-thymidylate synthase from Trypanosoma cruzi, the Chagas disease pathogen. *Acta crystallographica Section F, Structural biology and crystallization communications* 65:1175-1178.

da Fonseca LM, da Costa KM, Chaves VS, Freire-de-Lima CG, Morrot A, Mendonca-Previato L, Previato JO and Freire-de-Lima L (2019) Theft and Reception of Host Cell's Sialic Acid: Dynamics of Trypanosoma Cruzi Trans-sialidases and Mucin-Like Molecules on Chagas' Disease Immunomodulation. *Frontiers in immunology* 10:164.

da Silva Augusto L, Moretti NS, Ramos TC, de Jesus TC, Zhang M, Castilho BA and Schenkman S (2015) A membrane-bound eIF2 alpha kinase located in endosomes is regulated by heme and controls differentiation and ROS levels in Trypanosoma cruzi. *PLoS pathogens* 11:e1004618.

de Castro Andreassa E, Santos M, Wassmandorf R, Wippel HH, Carvalho PC, Fischer J and Souza T (2021) Proteomic changes in Trypanosoma cruzi epimastigotes treated with the proapoptotic compound PAC-1. *Biochimica et biophysica acta Proteins and proteomics* 1869:140582.

de Freitas Nascimento J, Kelly S, Sunter J and Carrington M (2018) Codon choice directs constitutive mRNA levels in trypanosomes. *eLife* 7.

De Gaudenzi JG, Carmona SJ, Aguero F and Frasch AC (2013) Genome-wide analysis of 3'-untranslated regions supports the existence of post-transcriptional regulons controlling gene expression in trypanosomes. *PeerJ* 1:e118.

de Godoy LM, Marchini FK, Pavoni DP, Rampazzo Rde C, Probst CM, Goldenberg S and Krieger MA (2012) Quantitative proteomics of Trypanosoma cruzi during metacyclogenesis. *Proteomics* 12:2694-2703.

De Rycker M, Wyllie S, Horn D, Read KD and Gilbert IH (2022) Anti-trypanosomatid drug discovery: progress and challenges. *Nature reviews Microbiology* 21:35-50.

Deeks ED (2019) Fexinidazole: First Global Approval. *Drugs* 79:215-220.

Docampo R, de Souza W, Miranda K, Rohloff P and Moreno SN (2005) Acidocalcisomes - conserved from bacteria to man. *Nature reviews Microbiology* 3:251-261.

Durrant JD, Keranen H, Wilson BA and McCammon JA (2010) Computational identification of uncharacterized cruzain binding sites. *PLoS neglected tropical diseases* 4:e676.

El-Sayed NM, Myler PJ, Bartholomeu DC, Nilsson D, Aggarwal G, Tran AN, Ghedin E, Worthey EA, Delcher AL, Blandin G, Westenberger SJ, Caler E, Cerqueira GC, Branche C, Haas B, Anupama A, Arner E, Aslund L, Attipoe P, Bontempi E, Bringaud F, Burton P, Cadag E, Campbell DA, Carrington M, Crabtree J, Darban H, da Silveira JF, de Jong P, Edwards K, Englund PT, Fazelina G, Feldblyum T, Ferella M, Frasch AC, Gull K, Horn D, Hou L, Huang Y, Kindlund E, Klingbeil M, Kluge S, Koo H, Lacerda D, Levin MJ, Lorenzi H, Louie T, Machado CR, McCulloch R, McKenna A, Mizuno Y, Mottram JC, Nelson S, Ochaya S, Osoegawa K, Pai G, Parsons M, Pentony M, Pettersson U, Pop M, Ramirez JL, Rinta J, Robertson L, Salzberg SL, Sanchez DO, Seyler A, Sharma R, Shetty J, Simpson AJ, Sisk E, Tammi MT, Tarleton R, Teixeira S, Van Aken S, Vogt C, Ward PN, Wickstead B, Wortman J, White O, Fraser CM, Stuart KD and Andersson B (2005a) The genome sequence of Trypanosoma cruzi, etiologic agent of Chagas disease. *Science* 309:409-415.

El-Sayed NM, Myler PJ, Blandin G, Berriman M, Crabtree J, Aggarwal G, Caler E, Renauld H, Worthey EA, Hertz-Fowler C, Ghedin E, Peacock C, Bartholomeu DC, Haas BJ, Tran AN, Wortman JR, Alsmark UC, Angiuoli S, Anupama A, Badger J, Bringaud F, Cadag E, Carlton JM, Cerqueira GC, Creasy T, Delcher AL, Djikeng A, Embley TM, Hauser C, Ivens AC, Kummerfeld SK, Pereira-Leal JB, Nilsson D, Peterson J, Salzberg SL, Shallom J, Silva JC, Sundaram J, Westenberger S, White O, Melville SE, Donelson JE, Andersson B, Stuart KD and Hall N (2005b) Comparative genomics of trypanosomatid parasitic protozoa. *Science* 309:404-409.

Elias MC, Marques-Porto R, Freymuller E and Schenkman S (2001) Transcription rate modulation through the Trypanosoma cruzi life cycle occurs in parallel with changes in nuclear organisation. *Molecular and biochemical parasitology* 112:79-90.

Fernandez M, Becco L, Correia I, Benitez J, Piro OE, Echeverria GA, Medeiros A, Comini M, Lavaggi ML, Gonzalez M, Cerecetto H, Moreno V, Pessoa JC, Garat B and Gambino D (2013a) Oxidovanadium(IV) and dioxidovanadium(V) complexes of tridentate salicylaldehyde semicarbazones: searching for prospective antitrypanosomal agents. *Journal of inorganic biochemistry* 127:150-160.

Fernandez M, Varela J, Correia I, Birriel E, Castiglioni J, Moreno V, Costa Pessoa J, Cerecetto H, Gonzalez M and Gambino D (2013b) A new series of heteroleptic oxidovanadium(IV)

compounds with phenanthroline-derived co-ligands: selective Trypanosoma cruzi growth inhibitors. *Dalton transactions* 42:11900-11911.

Ferreira LG and Andricopulo AD (2017) Targeting cysteine proteases in trypanosomatid disease drug discovery. *Pharmacology & therapeutics* 180:49-61.

Francisco AF, Jayawardhana S, Lewis MD, White KL, Shackleford DM, Chen G, Saunders J, Osuna-Cabello M, Read KD, Charman SA, Chatelain E and Kelly JM (2016) Nitroheterocyclic drugs cure experimental Trypanosoma cruzi infections more effectively in the chronic stage than in the acute stage. *Scientific reports* 6:35351.

Freire KA, Torres MT, Lima DB, Monteiro ML, Bezerra de Menezes R, Martins AMC and Oliveira VX, Jr. (2020) Wasp venom peptide as a new antichagasic agent. *Toxicon : official journal of the International Society on Toxinology* 181:71-78.

Gambino D and Otero L (2017) Design of prospective antiparasitic metal-based compounds including selected organometallic cores. *Inorganica Chimica Acta*.

Gilinger G and Bellofatto V (2001) Trypanosome spliced leader RNA genes contain the first identified RNA polymerase II gene promoter in these organisms. *Nucleic acids research* 29:1556-1564.

Gomez C, Esther Ramirez M, Calixto-Galvez M, Medel O and Rodriguez MA (2010) Regulation of gene expression in protozoa parasites. *Journal of biomedicine & biotechnology* 2010:726045.

Goos C, Dejung M, Wehman AM, E MN, Schmidt J, Sunter J, Engstler M, Butter F and Kramer S (2019) Trypanosomes can initiate nuclear export co-transcriptionally. *Nucleic acids research* 47:266-282.

Hall BS and Wilkinson SR (2012) Activation of benznidazole by trypanosomal type I nitroreductases results in glyoxal formation. *Antimicrobial agents and chemotherapy* 56:115-123.

Hannaert V, Bringaud F, Opperdoes FR and Michels PA (2003) Evolution of energy metabolism and its compartmentation in Kinetoplastida. *Kinetoplastid biology and disease* 2:11.

Hargrove TY, Wawrzak Z, Fisher PM, Child SA, Nes WD, Guengerich FP, Waterman MR and Lepesheva GI (2018) Binding of a physiological substrate causes large-scale conformational reorganization in cytochrome P450 51. *The Journal of biological chemistry* 293:19344-19353.

Hasne MP, Coppens I, Soysa R and Ullman B (2010) A high-affinity putrescine-cadaverine transporter from Trypanosoma cruzi. *Molecular microbiology* 76:78-91.

Hernandez M, Wicz S, Santamaria MH and Corral RS (2018) Curcumin exerts anti-inflammatory and vasoprotective effects through amelioration of NFAT-dependent endothelin-1

production in mice with acute Chagas cardiomyopathy. *Memorias do Instituto Oswaldo Cruz* 113:e180171.

Herreros-Cabello A, Callejas-Hernandez F, Girones N and Fresno M (2020) Trypanosoma Cruzi Genome: Organization, Multi-Gene Families, Transcription, and Biological Implications. *Genes* 11.

Iantorno SAD, C.; Khan, A.; Sanders, M. J.; Beverley, S. M.; Warren, W. C.; Berriman, M.; Sacks, D. L.; Cotton, J. A.; Grigg, M. E. (2017) Gene Expression in Leishmania Is Regulated Predominantly by Gene Dosage. *mBio* 8.

Inaoka DK, Iida M, Hashimoto S, Tabuchi T, Kuranaga T, Balogun EO, Honma T, Tanaka A, Harada S, Nara T, Kita K and Inoue M (2017) Design and synthesis of potent substrate-based inhibitors of the Trypanosoma cruzi dihydroorotate dehydrogenase. *Bioorganic & medicinal chemistry* 25:1465-1470.

Inaoka DK, Iida M, Tabuchi T, Honma T, Lee N, Hashimoto S, Matsuoka S, Kuranaga T, Sato K, Shiba T, Sakamoto K, Balogun EO, Suzuki S, Nara T, Rocha JR, Montanari CA, Tanaka A, Inoue M, Kita K and Harada S (2016) The Open Form Inducer Approach for Structure-Based Drug Design. *PloS one* 11:e0167078.

Jeacock L, Faria J and Horn D (2018) Codon usage bias controls mRNA and protein abundance in trypanosomatids. *eLife* 7.

Jones NG, Catta-Preta CMC, Lima A and Mottram JC (2018) Genetically Validated Drug Targets in Leishmania: Current Knowledge and Future Prospects. *ACS infectious diseases* 4:467-477.

Juarez-Saldivar A, Schroeder M, Salentin S, Haupt VJ, Saavedra E, Vazquez C, Reyes-Espinosa F, Herrera-Mayorga V, Villalobos-Rocha JC, Garcia-Perez CA, Campillo NE and Rivera G (2020) Computational Drug Repositioning for Chagas Disease Using Protein-Ligand Interaction Profiling. *International journal of molecular sciences* 21.

Katsuno K, Burrows JN, Duncan K, Hooft van Huijsduijnen R, Kaneko T, Kita K, Mowbray CE, Schmatz D, Warner P and Slingsby BT (2015) Hit and lead criteria in drug discovery for infectious diseases of the developing world. *Nature reviews Drug discovery* 14:751-758.

Kessler RL, Soares MJ, Probst CM and Krieger MA (2013) Trypanosoma cruzi response to sterol biosynthesis inhibitors: morphophysiological alterations leading to cell death. *PloS one* 8:e55497.

Kolev NG, Tschudi C and Ullu E (2011) RNA interference in protozoan parasites: achievements and challenges. *Eukaryotic cell* 10:1156-1163.

Kramer S (2021) Nuclear mRNA maturation and mRNA export control: from trypanosomes to opisthokonts. *Parasitology* 148:1196-1218.

Kratz JM, Garcia Bournissen F, Forsyth CJ and Sosa-Estani S (2018) Clinical and pharmacological profile of benznidazole for treatment of Chagas disease. *Expert review of clinical pharmacology* 11:943-957.

Kurkcuoglu Z, Ural G, Demet Akten E and Doruker P (2011) Blind Dockings of Benzothiazoles to Multiple Receptor Conformations of Triosephosphate Isomerase from Trypanosoma cruzi and Human. *Molecular informatics* 30:986-995.

LaCount DJ, Barrett B and Donelson JE (2002) Trypanosoma brucei FLA1 is required for flagellum attachment and cytokinesis. *The Journal of biological chemistry* 277:17580-17588.

Lander N, Li ZH, Niyogi S and Docampo R (2015) CRISPR/Cas9-Induced Disruption of Paraflagellar Rod Protein 1 and 2 Genes in Trypanosoma cruzi Reveals Their Role in Flagellar Attachment. *mBio* 6:e01012.

Lascano F, Garcia Bournissen F and Altcheh J (2020) Review of pharmacological options for the treatment of Chagas disease. *British journal of clinical pharmacology*.

Lepesheva GI, Ott RD, Hargrove TY, Kleshchenko YY, Schuster I, Nes WD, Hill GC, Villalta F and Waterman MR (2007a) Sterol 14alpha-demethylase as a potential target for antitrypanosomal therapy: enzyme inhibition and parasite cell growth. *Chemistry & biology* 14:1283-1293.

Lepesheva GI, Seliskar M, Knutson CG, Stourman NV, Rozman D and Waterman MR (2007b) Conformational dynamics in the F/G segment of CYP51 from Mycobacterium tuberculosis monitored by FRET. *Archives of biochemistry and biophysics* 464:221-227.

Lepesheva GI, Villalta F and Waterman MR (2011a) Targeting Trypanosoma cruzi sterol 14alpha-demethylase (CYP51). *Advances in parasitology* 75:65-87.

Lepesheva GI and Waterman MR (2011b) Sterol 14alpha-demethylase (CYP51) as a therapeutic target for human trypanosomiasis and leishmaniasis. *Current topics in medicinal chemistry* 11:2060-2071.

Li H, Wang R and Sun H (2019) Systems Approaches for Unveiling the Mechanism of Action of Bismuth Drugs: New Medicinal Applications beyond Helicobacter Pylori Infection. *Accounts of chemical research* 52:216-227.

Li Y, Shah-Simpson S, Okrah K, Belew AT, Choi J, Caradonna KL, Padmanabhan P, Ndegwa DM, Temanni MR, Corrada Bravo H, El-Sayed NM and Burleigh BA (2016) Transcriptome Remodeling in Trypanosoma cruzi and Human Cells during Intracellular Infection. *PLoS pathogens* 12:e1005511.

Lima ARJ, de Araujo CB, Bispo S, Patane J, Silber AM, Elias MC and da Cunha JPC (2021) Nucleosome landscape reflects phenotypic differences in Trypanosoma cruzi life forms. *PLoS pathogens* 17:e1009272.

Lima L, Espinosa-Alvarez O, Ortiz PA, Trejo-Varon JA, Carranza JC, Pinto CM, Serrano MG, Buck GA, Camargo EP and Teixeira MM (2015) Genetic diversity of Trypanosoma cruzi in bats, and multilocus phylogenetic and phylogeographical analyses supporting Tcbat as an independent DTU (discrete typing unit). *Acta tropica* 151:166-177.

Lopez-Barea J and Gomez-Ariza JL (2006) Environmental proteomics and metallomics. *Proteomics* 6 Suppl 1:S51-62.

Macias F, Lopez MC and Thomas MC (2016) The Trypanosomatid Pr77-hallmark contains a downstream core promoter element essential for transcription activity of the Trypanosoma cruzi L1Tc retrotransposon. *BMC genomics* 17:105.

Mair G, Shi H, Li H, Djikeng A, Aviles HO, Bishop JR, Falcone FH, Gavrilescu C, Montgomery JL, Santori MI, Stern LS, Wang Z, Ullu E and Tschudi C (2000) A new twist in trypanosome RNA metabolism: cis-splicing of pre-mRNA. *Rna* 6:163-169.

Marchini FK, de Godoy LM, Rampazzo RC, Pavoni DP, Probst CM, Gnad F, Mann M and Krieger MA (2011) Profiling the Trypanosoma cruzi phosphoproteome. *PloS one* 6:e25381.

Martin-Escolano R, Moreno-Viguri E, Santivanez-Veliz M, Martin-Montes A, Medina-Carmona E, Paucar R, Marin C, Azqueta A, Cirauqui N, Pey AL, Perez-Silanes S and Sanchez-Moreno M (2018) Second Generation of Mannich Base-Type Derivatives with in Vivo Activity against Trypanosoma cruzi. *Journal of medicinal chemistry* 61:5643-5663.

Martinez-Mayorga K, Byler KG, Ramirez-Hernandez AI and Terrazas-Alvares DE (2015) Cruzain inhibitors: efforts made, current leads and a structural outlook of new hits. *Drug discovery today* 20:890-898.

Matthews KR, Tschudi C and Ullu E (1994) A common pyrimidine-rich motif governs trans-splicing and polyadenylation of tubulin polycistronic pre-mRNA in trypanosomes. *Genes & development* 8:491-501.

Mazzeti AL, Diniz LF, Goncalves KR, WonDollinger RS, Assiria T, Ribeiro I and Bahia MT (2019) Synergic Effect of Allopurinol in Combination with Nitroheterocyclic Compounds against Trypanosoma cruzi. *Antimicrobial agents and chemotherapy* 63.

McGuire JJ (2003) Anticancer antifolates: current status and future directions. *Current pharmaceutical design* 9:2593-2613.

Messenger LA, Miles MA and Bern C (2015) Between a bug and a hard place: Trypanosoma cruzi genetic diversity and the clinical outcomes of Chagas disease. *Expert review of anti-infective therapy* 13:995-1029.

Mesu V, Kalonji WM, Bardonneau C, Mordt OV, Blesson S, Simon F, Delhomme S, Bernhard S, Kuziena W, Lubaki JF, Vuvu SL, Ngima PN, Mbembo HM, Ilunga M, Bonama AK, Heradi JA, Solomo JLL, Mandula G, Badibabi LK, Dama FR, Lukula PK, Tete DN, Lumbala C, Scherrer B, Strub-Wourgaft N and Tarral A (2018) Oral fexinidazole for late-stage African

Trypanosoma brucei gambiense trypanosomiasis: a pivotal multicentre, randomised, non-inferiority trial. *Lancet* 391:144-154.

Michaeli S (2011) Trans-splicing in trypanosomes: machinery and its impact on the parasite transcriptome. *Future microbiology* 6:459-474.

Michels PA, Hannaert V and Bringaud F (2000) Metabolic aspects of glycosomes in trypanosomatidae - new data and views. *Parasitology today* 16:482-489.

Minning TA, Weatherly DB, Atwood J, 3rd, Orlando R and Tarleton RL (2009) The steady-state transcriptome of the four major life-cycle stages of Trypanosoma cruzi. *BMC genomics* 10:370.

Molina I, Gomez i Prat J, Salvador F, Trevino B, Sulleiro E, Serre N, Pou D, Roure S, Cabezos J, Valerio L, Blanco-Grau A, Sanchez-Montalva A, Vidal X and Pahissa A (2014) Randomized trial of posaconazole and benznidazole for chronic Chagas' disease. *The New England journal of medicine* 370:1899-1908.

Moraes CB, Giardini MA, Kim H, Franco CH, Araujo-Junior AM, Schenkman S, Chatelain E and Freitas-Junior LH (2014) Nitroheterocyclic compounds are more efficacious than CYP51 inhibitors against Trypanosoma cruzi: implications for Chagas disease drug discovery and development. *Scientific reports* 4:4703.

Moretti NS, Cestari I, Anupama A, Stuart K and Schenkman S (2018) Comparative Proteomic Analysis of Lysine Acetylation in Trypanosomes. *Journal of proteome research* 17:374-385.

Morillo CA, Waskin H, Sosa-Estani S, Del Carmen Bangher M, Cuneo C, Milesi R, Mallagray M, Apt W, Beloscar J, Gascon J, Molina I, Echeverria LE, Colombo H, Perez-Molina JA, Wyss F, Meeks B, Bonilla LR, Gao P, Wei B, McCarthy M, Yusuf S and Investigators S-C (2017) Benznidazole and Posaconazole in Eliminating Parasites in Asymptomatic T. Cruzi Carriers: The STOP-CHAGAS Trial. *Journal of the American College of Cardiology* 69:939-947.

Mosquillo MF, Bilbao L, Hernandez F, Tissot F, Gambino D, Garat B and Perez-Diaz L (2018) Trypanosoma cruzi biochemical changes and cell death induced by an organometallic platinum-based compound. *Chemical biology & drug design* 92:1657-1669.

Moyersoen J, Choe J, Fan E, Hol WG and Michels PA (2004) Biogenesis of peroxisomes and glycosomes: trypanosomatid glycosome assembly is a promising new drug target. *FEMS microbiology reviews* 28:603-643.

Nara T, Kamei Y, Tsubouchi A, Annoura T, Hirota K, Iizumi K, Dohmoto Y, Ono T and Aoki T (2005) Inhibitory action of marine algae extracts on the Trypanosoma cruzi dihydroorotate dehydrogenase activity and on the protozoan growth in mammalian cells. *Parasitology international* 54:59-64.

Navarro M, Gabbiani C, Messori L and Gambino D (2010) Metal-based drugs for malaria, trypanosomiasis and leishmaniasis: recent achievements and perspectives. *Drug discovery today* 15:1070-1078.

Neuditschko B, Legin AA, Baier D, Schintlmeister A, Reipert S, Wagner M, Keppler BK, Berger W, Meier-Menches SM and Gerner C (2021) Interaction with Ribosomal Proteins Accompanies Stress Induction of the Anticancer Metallodrug BOLD-100/KP1339 in the Endoplasmic Reticulum. *Angewandte Chemie* 60:5063-5068.

Noe G, De Gaudenzi JG and Frasch AC (2008) Functionally related transcripts have common RNA motifs for specific RNA-binding proteins in trypanosomes. *BMC molecular biology* 9:107.

Ohlendieck K (2018) Comparative DIGE Proteomics. *Methods in molecular biology* 1664:17-24.

Olivares-Illana V, Rodriguez-Romero A, Becker I, Berzunza M, Garcia J, Perez-Montfort R, Cabrera N, Lopez-Calahorra F, de Gomez-Puyou MT and Gomez-Puyou A (2007) Perturbation of the dimer interface of triosephosphate isomerase and its effect on Trypanosoma cruzi. *PLoS neglected tropical diseases* 1:e1.

Olivier M, Asmis R, Hawkins GA, Howard TD and Cox LA (2019) The Need for Multi-Omics Biomarker Signatures in Precision Medicine. *International journal of molecular sciences* 20.

OMS (2002) Organización mundial de la Salud. Control of Chagas disease: second report of the WHO expert committee, WHO Expert Committee on the Control of Chagas Disease (2000: Brasilia, Brazil) & World Health Organization.

OMS (2021a) Organización Mundial de la Salud: La enfermedad de Chagas (tripanosomiasis americana).

OMS (2021b) Organización mundial de la Salud: Poner fin a la desatención para alcanzar los objetivos de desarrollo sostenible.

OPS (2022) Organización Panamericana de la Salud: Enfermedad de Chagas.

Osorio-Mendez JF and Cevallos AM (2018) Discovery and Genetic Validation of Chemotherapeutic Targets for Chagas' Disease. *Frontiers in cellular and infection microbiology* 8:439.

Pacheco-Lugo L, Diaz-Olmos Y, Saenz-Garcia J, Probst CM and DaRocha WD (2017) Effective gene delivery to Trypanosoma cruzi epimastigotes through nucleofection. *Parasitology international* 66:236-239.

Padilla-Mejia NE, Florencio-Martinez LE, Figueroa-Angulo EE, Manning-Cela RG, Hernandez-Rivas R, Myler PJ and Martinez-Calvillo S (2009) Gene organization and sequence analyses of transfer RNA genes in Trypanosomatid parasites. *BMC genomics* 10:232.

Palmer AC and Kishony R (2014) Opposing effects of target overexpression reveal drug mechanisms. *Nature communications* 5:4296.

Park S, Sanchez DR, Traina MI, Bradfield JS, Hernandez S, Ufion AJA, Dufani J, Bergin P, Wachsner RY and Meymandi SK (2017) The Prevalence of Chagas Disease Among Latin American Immigrants with Pacemakers in Los Angeles, California. *The American journal of tropical medicine and hygiene* 96:1139-1142.

Pastro L, Smircich P, Di Paolo A, Becco L, Duhagon MA, Sotelo-Silveira J and Garat B (2017) Nuclear Compartmentalization Contributes to Stage-Specific Gene Expression Control in Trypanosoma cruzi. *Frontiers in cell and developmental biology* 5:8.

Paucar R, Martín-Escolano R, Moreno-Viguri E, Cirauqui N, Marín C, Sánchez-Moreno M and Pérez-Silanes S (2019) Antichagasic profile of a series of Mannich base-type derivatives: design, synthesis, in vitro evaluation, and computational studies involving iron superoxide dismutase. *Chemistry Select* 4:8112-8121.

Perez-Mazliah DE, Alvarez MG, Cooley G, Lococo BE, Bertocchi G, Petti M, Albareda MC, Armenti AH, Tarleton RL, Laucella SA and Viotti R (2013) Sequential combined treatment with allopurinol and benznidazole in the chronic phase of Trypanosoma cruzi infection: a pilot study. *The Journal of antimicrobial chemotherapy* 68:424-437.

Perez-Molina JA and Molina I (2018) Chagas disease. *Lancet* 391:82-94.

Pessoa JC, Etcheverry S and Gambino D (2015) Vanadium compounds in medicine. *Coordination chemistry reviews* 301:24-48.

Pez D, Leal I, Zuccotto F, Boussard C, Brun R, Croft SL, Yardley V, Ruiz Perez LM, Gonzalez Pacanowska D and Gilbert IH (2003) 2,4-Diaminopyrimidines as inhibitors of Leishmanial and Trypanosomal dihydrofolate reductase. *Bioorganic & medicinal chemistry* 11:4693-4711.

Portman N and Gull K (2010) The paraflagellar rod of kinetoplastid parasites: from structure to components and function. *International journal for parasitology* 40:135-148.

Prelich G (2012) Gene overexpression: uses, mechanisms, and interpretation. *Genetics* 190:841-854.

Preusser C, Jae N and Bindereif A (2012) mRNA splicing in trypanosomes. *International journal of medical microbiology : IJMM* 302:221-224.

Queiroz RM, Charneau S, Motta FN, Santana JM, Roepstorff P and Ricart CA (2013) Comprehensive proteomic analysis of Trypanosoma cruzi epimastigote cell surface proteins by two complementary methods. *Journal of proteome research* 12:3255-3263.

Radio S, Garat B, Sotelo-Silveira J and Smircich P (2020) Upstream ORFs Influence Translation Efficiency in the Parasite Trypanosoma cruzi. *Frontiers in genetics* 11:166.

Ramirez JD, Hernandez C, Montilla M, Zambrano P, Florez AC, Parra E and Cucunuba ZM (2014) First report of human Trypanosoma cruzi infection attributed to TcBat genotype. *Zoonoses and public health* 61:477-479.

Ranade RM, Gillespie JR, Shibata S, Verlinde CL, Fan E, Hol WG and Buckner FS (2013) Induced resistance to methionyl-tRNA synthetase inhibitors in Trypanosoma brucei is due to overexpression of the target. *Antimicrobial agents and chemotherapy* 57:3021-3028.

Rassi A, Jr., Rassi A and Marin-Neto JA (2010a) Chagas disease. *Lancet* 375:1388-1402.

Rassi A, Luquetti AO, Rassi A, Jr., Rassi GG, Rassi SG, IG DAS and Rassi AG (2007) Specific treatment for Trypanosoma cruzi: lack of efficacy of allopurinol in the human chronic phase of Chagas disease. *The American journal of tropical medicine and hygiene* 76:58-61.

Rassi A, Rezende J, Ostermayer A and Rassi Jr A (2010b) *Clinical Phases and Forms of Chagas Disease.* , Elsevier.

Read LK, Lukes J and Hashimi H (2016) Trypanosome RNA editing: the complexity of getting U in and taking U out. *Wiley interdisciplinary reviews RNA* 7:33-51.

Rehder D (2012) The potentiality of vanadium in medicinal applications. *Future medicinal chemistry* 4:1823-1837.

Resende BC, Oliveira ACS, Guanabens ACP, Repoles BM, Santana V, Hiraiwa PM, Pena SDJ, Franco GR, Macedo AM, Tahara EB, Fragoso SP, Andrade LO and Machado CR (2020) The Influence of Recombinational Processes to Induce Dormancy in Trypanosoma cruzi. *Frontiers in cellular and infection microbiology* 10:5.

Respuela P, Ferella M, Rada-Iglesias A and Aslund L (2008) Histone acetylation and methylation at sites initiating divergent polycistronic transcription in Trypanosoma cruzi. *The Journal of biological chemistry* 283:15884-15892.

Ribeiro V, Dias N, Paiva T, Hagstrom-Bex L, Nitz N, Pratesi R and Hecht M (2020) Current trends in the pharmacological management of Chagas disease. *International journal for parasitology Drugs and drug resistance* 12:7-17.

Rivas F, Medeiros A, Quiroga C, Benitez D, Comini M, Rodriguez-Arce E, Machado I, Cerecetto H and Gambino D (2021) New Pd-Fe ferrocenyl antiparasitic compounds with bioactive 8-hydroxyquinoline ligands: a comparative study with their Pt-Fe analogues. *Dalton transactions* 50:1651-1665.

Rodriguez Arce E, Mosquillo MF, Perez-Diaz L, Echeverria GA, Piro OE, Merlino A, Coitino EL, Maringolo Ribeiro C, Leite CQ, Pavan FR, Otero L and Gambino D (2015) Aromatic amine N-oxide organometallic compounds: searching for prospective agents against infectious diseases. *Dalton transactions* 44:14453-14464.

Rodriques Coura J and de Castro SL (2002) A critical review on Chagas disease chemotherapy. *Memorias do Instituto Oswaldo Cruz* 97:3-24.

Rohloff P and Docampo R (2008) A contractile vacuole complex is involved in osmoregulation in Trypanosoma cruzi. *Experimental parasitology* 118:17-24.

Romanha AJ, Castro SL, Soeiro Mde N, Lannes-Vieira J, Ribeiro I, Talvani A, Bourdin B, Blum B, Olivieri B, Zani C, Spadafora C, Chiari E, Chatelain E, Chaves G, Calzada JE, Bustamante JM, Freitas-Junior LH, Romero LI, Bahia MT, Lotrowska M, Soares M, Andrade SG, Armstrong T, Degrave W and Andrade Zde A (2010) In vitro and in vivo experimental models for drug screening and development for Chagas disease. *Memorias do Instituto Oswaldo Cruz* 105:233-238.

Salvador F, Trevino B, Sulleiro E, Pou D, Sanchez-Montalva A, Cabezos J, Soriano A, Serre N, Gomez IPJ, Pahissa A and Molina I (2014) Trypanosoma cruzi infection in a non-endemic country: epidemiological and clinical profile. *Clinical microbiology and infection : the official publication of the European Society of Clinical Microbiology and Infectious Diseases* 20:706-712.

Sambrook J, Fritsch EF and Maniatis T (1989) *Molecular Cloning: A Laboratory Manual*.

Sanchez-Valdez FJ, Padilla A, Wang W, Orr D and Tarleton RL (2018) Spontaneous dormancy protects Trypanosoma cruzi during extended drug exposure. *eLife* 7.

Sant'Anna C, Nakayasu ES, Pereira MG, Lourenco D, de Souza W, Almeida IC and Cunha ESNL (2009) Subcellular proteomics of Trypanosoma cruzi reservosomes. *Proteomics* 9:1782-1794.

Santi AMM, Ribeiro JM, Reis-Cunha JL, Burle-Caldas GA, Santos IFM, Silva PA, Resende DM, Bartholomeu DC, Teixeira SMR and Murta SMF (2022) Disruption of multiple copies of the Prostaglandin F2alpha synthase gene affects oxidative stress response and infectivity in Trypanosoma cruzi. *PLoS neglected tropical diseases* 16:e0010845.

Santos Junior A, Melo RM, Ferreira BVG, Pontes AH, Lima CMR, Fontes W, Sousa MV, Lima BD and Ricart CAO (2021) Quantitative proteomics and phosphoproteomics of Trypanosoma cruzi epimastigote cell cycle. *Biochimica et biophysica acta Proteins and proteomics* 1869:140619.

Santos Souza HF, Rocha SC, Damasceno FS, Rapado LN, Pral EMF, Marinho CRF and Silber AM (2019) The effect of memantine, an antagonist of the NMDA glutamate receptor, in in vitro and in vivo infections by Trypanosoma cruzi. *PLoS neglected tropical diseases* 13:e0007226.

Scalese G, Kostenkova K, Crans DC and Gambino D (2022) Metallomics and other omics approaches in antiparasitic metal-based drug research. *Current opinion in chemical biology* 67:102127.

Scalese G, Mosquillo MF, Rostan S, Castiglioni J, Alho I, Perez L, Correia I, Marques F, Costa Pessoa J and Gambino D (2017) Heteroleptic oxidovanadium(IV) complexes of 2-

hydroxynaphtylaldimine and polypyridyl ligands against Trypanosoma cruzi and prostate cancer cells. *Journal of inorganic biochemistry* 175:154-166.

Scarim CB, Jornada DH, Chelucci RC, de Almeida L, Dos Santos JL and Chung MC (2018) Current advances in drug discovery for Chagas disease. *European journal of medicinal chemistry* 155:824-838.

Schenkman S, Pascoalino Bdos S and Nardelli SC (2011) Nuclear structure of Trypanosoma cruzi. *Advances in parasitology* 75:251-283.

Schmunis GA and Yadon ZE (2010) Chagas disease: a Latin American health problem becoming a world health problem. *Acta tropica* 115:14-21.

Senkovich O, Bhatia V, Garg N and Chattopadhyay D (2005) Lipophilic antifolate trimetrexate is a potent inhibitor of Trypanosoma cruzi: prospect for chemotherapy of Chagas' disease. *Antimicrobial agents and chemotherapy* 49:3234-3238.

Senkovich O, Schormann N and Chattopadhyay D (2009) Structures of dihydrofolate reductase-thymidylate synthase of Trypanosoma cruzi in the folate-free state and in complex with two antifolate drugs, trimetrexate and methotrexate. *Acta crystallographica Section D, Biological crystallography* 65:704-716.

Shirokikh NE and Preiss T (2018) Translation initiation by cap-dependent ribosome recruitment: Recent insights and open questions. *Wiley interdisciplinary reviews RNA* 9:e1473.

Siegel TN, Hekstra DR, Kemp LE, Figueiredo LM, Lowell JE, Fenyo D, Wang X, Dewell S and Cross GA (2009) Four histone variants mark the boundaries of polycistronic transcription units in Trypanosoma brucei. *Genes & development* 23:1063-1076.

Siegel TN, Hekstra DR, Wang X, Dewell S and Cross GA (2010) Genome-wide analysis of mRNA abundance in two life-cycle stages of Trypanosoma brucei and identification of splicing and polyadenylation sites. *Nucleic acids research* 38:4946-4957.

Sienkiewicz N, Jaroslawski S, Wyllie S and Fairlamb AH (2008) Chemical and genetic validation of dihydrofolate reductase-thymidylate synthase as a drug target in African trypanosomes. *Molecular microbiology* 69:520-533.

Silva-Gomes NL, Rampazzo RCP, Moreira C, Porcino GN, Dos Santos CMB, Krieger MA, Vasconcelos EG, Fragoso SP and Moreira OC (2020) Knocking Down TcNTPDase-1 Gene Reduces in vitro Infectivity of Trypanosoma cruzi. *Frontiers in microbiology* 11:434.

Simoes-Silva MR, De Araujo JS, Peres RB, Da Silva PB, Batista MM, De Azevedo LD, Bastos MM, Bahia MT, Boechat N and Soeiro MNC (2019) Repurposing strategies for Chagas disease therapy: the effect of imatinib and derivatives against Trypanosoma cruzi. *Parasitology* 146:1006-1012.

Simpson L, Sbicego S and Aphasizhev R (2003) Uridine insertion/deletion RNA editing in trypanosome mitochondria: a complex business. *Rna* 9:265-276.

Singh V and Verma K (2018) Metals from cell to environment: Connecting Metallomics with other omics. *Open Journal of Plant Science* 3:001-014.

Smircich P, Eastman G, Bispo S, Duhagon MA, Guerra-Slompo EP, Garat B, Goldenberg S, Munroe DJ, Dallagiovanna B, Holetz F and Sotelo-Silveira JR (2015) Ribosome profiling reveals translation control as a key mechanism generating differential gene expression in Trypanosoma cruzi. *BMC genomics* 16:443.

Smith M, Blanchette M and Papadopoulou B (2008) Improving the prediction of mRNA extremities in the parasitic protozoan Leishmania. *BMC bioinformatics* 9:158.

Soares FGN, Goethel G, Kagami LP, das Neves GM, Sauer E, Birriel E, Varela J, Goncalves IL, Von Poser G, Gonzalez M, Kawano DF, Paula FR, de Melo EB, Garcia SC, Cerecetto H and Eifler-Lima VL (2019) Novel coumarins active against Trypanosoma cruzi and toxicity assessment using the animal model Caenorhabditis elegans. *BMC pharmacology & toxicology* 20:76.

Sosa A, Salamanca Capusiri E, Amaya S, Bardon A, Gimenez-Turba A, Vera N and Borkosky S (2020) Trypanocidal activity of South American Vernonieae (Asteraceae) extracts and its sesquiterpene lactones. *Natural product research*:1-5.

Sosa EJ, Burguener G, Lanzarotti E, Defelipe L, Radusky L, Pardo AM, Marti M, Turjanski AG and Fernandez Do Porto D (2018) Target-Pathogen: a structural bioinformatic approach to prioritize drug targets in pathogens. *Nucleic acids research* 46:D413-D418.

Srivastava A, Badjatia N, Lee JH, Hao B and Gunzl A (2018) An RNA polymerase II-associated TFIIF-like complex is indispensable for SL RNA gene transcription in Trypanosoma brucei. *Nucleic acids research* 46:1695-1709.

Takashima E, Inaoka DK, Osanai A, Nara T, Odaka M, Aoki T, Inaka K, Harada S and Kita K (2002) Characterization of the dihydroorotate dehydrogenase as a soluble fumarate reductase in Trypanosoma cruzi. *Molecular and biochemical parasitology* 122:189-200.

Taylor MC and Kelly JM (2010) Iron metabolism in trypanosomatids, and its crucial role in infection. *Parasitology* 137:899-917.

Thomas S, Green A, Sturm NR, Campbell DA and Myler PJ (2009) Histone acetylations mark origins of polycistronic transcription in Leishmania major. *BMC genomics* 10:152.

Thompson KH, Lichter J, LeBel C, Scaife MC, McNeill JH and Orvig C (2009) Vanadium treatment of type 2 diabetes: a view to the future. *Journal of inorganic biochemistry* 103:554-558.

Torrico F, Gascon J, Ortiz L, Alonso-Vega C, Pinazo MJ, Schijman A, Almeida IC, Alves F, Strub-Wourgaft N, Ribeiro I and Group ES (2018) Treatment of adult chronic indeterminate Chagas disease with benznidazole and three E1224 dosing regimens: a proof-of-concept, randomised, placebo-controlled trial. *The Lancet Infectious diseases* 18:419-430.

Trochine A, Creek DJ, Faral-Tello P, Barrett MP and Robello C (2014) Benznidazole biotransformation and multiple targets in Trypanosoma cruzi revealed by metabolomics. *PLoS neglected tropical diseases* 8:e2844.

Tyler K.M. OCL, ; Engman D.M. (2003) *The Life Cycle Of Trypanosoma Cruzi.*

Ulrich PN, Jimenez V, Park M, Martins VP, Atwood J, 3rd, Moles K, Collins D, Rohloff P, Tarleton R, Moreno SN, Orlando R and Docampo R (2011) Identification of contractile vacuole proteins in Trypanosoma cruzi. *PloS one* 6:e18013.

Uran Landaburu L, Berenstein AJ, Videla S, Maru P, Shanmugam D, Chernomoretz A and Aguero F (2020) TDR Targets 6: driving drug discovery for human pathogens through intensive chemogenomic data integration. *Nucleic acids research* 48:D992-D1005.

Van den Kerkhof M, Sterckx YG, Leprohon P, Maes L and Caljon G (2020) Experimental Strategies to Explore Drug Action and Resistance in Kinetoplastid Parasites. *Microorganisms* 8.

Vazquez MP and Levin MJ (1999) Functional analysis of the intergenic regions of TcP2beta gene loci allowed the construction of an improved Trypanosoma cruzi expression vector. *Gene* 239:217-225.

Veas R, Rojas-Pirela M, Castillo C, Olea-Azar C, Moncada M, Ulloa P, Rojas V and Kemmerling U (2020) Microalgae extracts: Potential anti-Trypanosoma cruzi agents? *Biomedicine & pharmacotherapy = Biomedecine & pharmacotherapie* 127:110178.

Vela A, Coral-Almeida M, Sereno D, Costales JA, Barnabe C and Breniere SF (2021) In vitro susceptibility of Trypanosoma cruzi discrete typing units (DTUs) to benznidazole: A systematic review and meta-analysis. *PLoS neglected tropical diseases* 15:e0009269.

Vilar-Pereira G, Carneiro VC, Mata-Santos H, Vicentino AR, Ramos IP, Giarola NL, Feijo DF, Meyer-Fernandes JR, Paula-Neto HA, Medei E, Bozza MT, Lannes-Vieira J and Paiva CN (2016) Resveratrol Reverses Functional Chagas Heart Disease in Mice. *PLoS pathogens* 12:e1005947.

Villalta F and Rachakonda G (2019) Advances in preclinical approaches to Chagas disease drug discovery. *Expert opinion on drug discovery* 14:1161-1174.

Villar JC, Perez JG, Cortes OL, Riarte A, Pepper M, Marin-Neto JA and Guyatt GH (2014) Trypanocidal drugs for chronic asymptomatic Trypanosoma cruzi infection. *The Cochrane database of systematic reviews*:CD003463.

Wang H, Zhou Y, Xu X, Li H and Sun H (2020) Metalloproteomics in conjunction with other omics for uncovering the mechanism of action of metallodrugs: Mechanism-driven new therapy development. *Current opinion in chemical biology* 55:171-179.

Wang Y, Li H and Sun H (2019) Metalloproteomics for Unveiling the Mechanism of Action of Metallodrugs. *Inorganic chemistry* 58:13673-13685.

Watson JA, Strub-Wourgraft N, Tarral A, Ribeiro I, Tarning J and White NJ (2019) Pharmacokinetic-Pharmacodynamic Assessment of the Hepatic and Bone Marrow Toxicities of the New Trypanoside Fexinidazole. *Antimicrobial agents and chemotherapy* 63.

Willsky GR, Chi LH, Godzala M, 3rd, Kostyniak PJ, Smee JJ, Trujillo AM, Alfano JA, Ding W, Hu Z and Crans DC (2011) Anti-diabetic effects of a series of vanadium dipicolinate complexes in rats with streptozotocin-induced diabetes. *Coordination chemistry reviews* 255:2258-2269.

Zamudio JR, Mittra B, Campbell DA and Sturm NR (2009) Hypermethylated cap 4 maximizes Trypanosoma brucei translation. *Molecular microbiology* 72:1100-1110.

Zarate-Perez F, Chanez-Cardenas ME and Vazquez-Contreras E (2008) The folding pathway of triosephosphate isomerase. *Progress in molecular biology and translational science* 84:251-267.

Zeiner GM, Sturm NR and Campbell DA (2003) The Leishmania tarentolae spliced leader contains determinants for association with polysomes. *The Journal of biological chemistry* 278:38269-38275.

Zingales B, Miles MA, Moraes CB, Luquetti A, Guhl F, Schijman AG, Ribeiro I, Drugs for Neglected Disease I and Chagas Clinical Research Platform M (2014) Drug discovery for Chagas disease should consider Trypanosoma cruzi strain diversity. *Memorias do Instituto Oswaldo Cruz* 109:828-833.

Zuccotto F, Martin AC, Laskowski RA, Thornton JM and Gilbert IH (1998) Dihydrofolate reductase: a potential drug target in trypanosomes and leishmania. *Journal of computer-aided molecular design* 12:241-257.